RUSSIAN ACADEMY OF SCIENCES
SCIENTIFIC COUNCIL ON PROBLEMS OF BIOLOGICAL PHYSICS
PUSHCHINO SCIENTIFIC CENTER OF BIOLOGICAL RESEARCH
INSTITUTE OF THEORETICAL AND EXPERIMENTAL BIOPHYSICS
INSTITUTE OF CELL BIOPHYSICS

BIOLOGICAL MOTILITY

FUNDAMENTAL AND APPLIED SCIENCE

Pushchino • 2012

УДК 577+61
ББК 28.071
Б633

Biological Motility: Fundamental and Applied Science. – Pushchino: Foton-Vek – 2012. – 284 p.

This volume contains the presentations that were made during the International Symposium "Biological motility: Fundamental and Applied Science ". It took place in Pushchino, Moscow region and was devoted to new ashievements and perspectives in this area of knowledge.
Materials of the Symposium are of interest for biologists, medical and other specialists.

The materials are presented as the author's versions.

Support of the Symposium by the following sponsors is gratefully acknowledged:

- Presidium of Russian Academy of Sciences
- Scientific Council on problems of biological physics of Russian Academy of Sciences
- Russian Foundation for Basic Research

Responsible for the issue S.N. Udaltsov

ISBN 978-5-90378-926-9

THE NEGATIVE INOTROPIC EFFECT OF HYDROGEN SULFIDE ON FROG MYOCARDIUM AFTER INHIBITION OF PHOSPHODIESTERASES AND ACTIVATION OF BETA-ADRENERGIC RECEPTORS

D.R. Akhmetshina, N.N. Khaertdinov, A.V. Yakovlev., G.F. Sitdikova

Kazan Federal University, 18, Kremlevskii str., Kazan, 420008, Russia

Hydrogen sulfide (H_2S) is an endogenously synthesized gaseous molecule which induces the number of effects in the cardiovascular system in almost all species of vertebrates. In the myocardium of the frog H_2S exerts a negative inotropic effect which is partially mediated by activation of ATP-dependent potassium channels (Sitdikova et al, 2011). Among the possible targets of the H_2S in cardiomyocytes is the cAMP-dependent system (Yong et al, 2008). It is known that myocardial contractility is directly regulated by the adrenergic system. Activation of β-adrenergic receptors leads to increased contractility of cardiomyocytes by elevation of cAMP level. The purpose of the present study was to study the role of cAMP system in the effects of H_2S on myocardial contractility of frog *Rana ridibunda.*

Methods

Experiments were held on isolated strips of heart ventricle using 4-channel myographic apparatus (Biopac, USA). Preparations were stimulated through two silver-plated electrodes by electric impulses with duration of 5 ms, amplitude 10 V with frequency 0,1 Hz. Muscle contractions were recorded by isometric force transducers sensitivity of 0–50 g. Processing and analyzing of the results were performed using an original programs Elf and Origin. The effects to application of the investigated compounds were calculated as a percentage of the initial value of contraction. In addition, the effect of H_2S on the rate of Ca^{2+}-signals in the atrial cardiomyocytes was investigated using the fluorescent dye fluo-4, AM (Molecular Probes, USA) at a concentration of 2 mkM. In the experiments atrium was stretched with the needles in the bath which had a working volume of 2 ml. To register the staining AxioCam camera (Carl Zeiss, Germany) was used. For image processing ImageJ program was used. The intensity of the fluorescence was estimated in relative units (r.u.), which corresponds to the value of the brightness of a pixel. The intensity of the Ca^{2+}-signals in control was taken as 100%. Sodium hydrogen sulfide (NaHS) used as a donor of H2S (Sigma, USA). 3-isobutyl-1-methylxanthine (IBMX), 8BrcAMP, 8-(4-Chlorophenylthio)adenosine 3',5'-cyclic monophosphate sodium salt (pCPTcAMP), DL-Isoproterenol hemisulfate (ISO) (Sigma, USA) also were used in the experiments.

Results

Bath application of NaHS in concentration 100 mkM decreased the amplitude of contraction of isolated ventricle stripes by 66±6% ($n=14$, $p<0.05$) of control (figure).

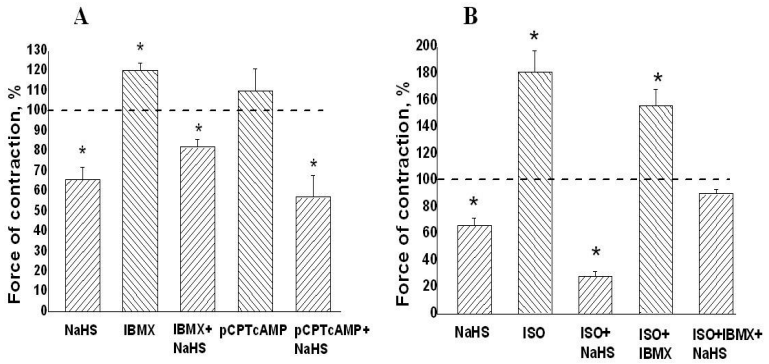

The role of cAMP system in the effect of NaHS on heart contractility of the frog. **A** - The amplitude of contraction of the myocardium under the action of NaHS (100 mkM) in control, IBMX (200 mkM), pCPTcAMP (100 mkM) and NaHS on the background of these agents. **B** - The amplitude of contraction of the myocardium under the action of NaHS (100 mkM) in control, ISO (1 mkM), IBMX (200 mkM) and NaHS on the background of these agents. * - $p<0.05$

In the nervous system of the mammals and cardiomyocytes H2S effects may be mediated through the changes in the level of cAMP (Yong et al, 2008, Kimura, 2000). The elevation of cAMP level is the mechanism of regulation of myocardial contractility in response to activation of β-adrenergic receptors followed by the increase of the voltage-dependent Ca^{2+}-channels through phosphorylation of channels by cAMP-dependent protein kinases.

To increase the concentration of cAMP cell permeable analogs – 8BrcAMP (100 mkM) and pCPTcAMP (100 mkM) were used. Application of 8BrcAMP or pCPTcAMP did not lead to significant changes in the amplitude of contractions. Addition of NaHS (100 mkM) on the background of 8BrcAMP decreased contractility of strips to 70±6% ($n=5$, $p<0.05$) and to 57±11% ($n=5$, $p<0.05$) respectively (figure, A). Thus the effect of NaHS after application of cAMP analogs was the same as in control conditions. The inhibition of phosphodiesterases with a nonspecific blocker of IBMX resulted in the increase of contraction to 120±4% ($n=7$, $p<0.05$) by 8 min of applications which appears to be associated with the accumulation of cAMP in cardiomyocytes (figure, A). Under these conditions, addition of NaHS (100 mkM) reduced the force of contraction of myocardium strips to 82±4% ($n=5$, $p<0.05$) (figure, A). This effect was significantly smaller than the effect of NaHS in control.

Thus the effect of H2S is completely maintained after increase of the intracellular level of cAMP by analogs but was partially prevented after inhibition of phosphodiesterases. This may indicate on the activation of phosphodiesterases by H2S.

In ventricular cardiomyocytes of frog Ca^{2+}-current is regulated by a local

increase in cAMP level near the plasma membrane. Phosphodiesterases provide the compartmentation of cAMP preventing its diffusion along the length of cardiomyocyte. It is known that β-adrenergic receptors provide a local increase in cAMP level near the Ca^{2+}-channels which leads to their phosphorylation and increase inward Ca^{2+}-current (Kamp et al, 2000).

To activate the β-adrenergic receptors in cardiomyocytes ISO at a concentration 1 mkM was used. Application of ISO induced the increase of force of myocardium contraction up to 181±16 (n=11, $p<0.05$) (fig. 1 B). Effect of NaHS (100 mkM) after pre-activation of β-adrenergic receptors with ISO was 28±4% (n=5, $p<0.05$) which was significantly greater than the effect of NaHS in the control (figure, B). Apparently this indicates the involvement of intracellular systems which initiated by the activation of β-adrenergic receptors in the effects of H_2S. To confirm the hypothesis of the involvement of phosphodiesterases in the effects of NaHS used simultaneously application of ISO (1 mkM) and IBMX (200 mkM). Under these conditions, the negative inotropic effect of NaHS did not developed and the amplitude of contractions was 90±3% (n=5, $p>0.05$) (fig. 1B).

Analysis of the intensity of the Ca^{2+}-signals in cardiomyocytes showed that in the control it was 1,32±0,40 r.u. (n=6, $p<0.05$). The addition of NaHS (100 mkM) reduced the intensity of the Ca^{2+}-waves to 0,56±0,10 r.u. (n=3, $p<0.05$) by 10 min of application. The effect of NaHS was reversible. On the background of activation of β-adrenergic receptors with ISO (1 mkM) application of NaHS (100 mkM) reduced the intensity of the Ca^{2+}-waves to 0,38±0,16 r.u. by 10 min (n=3, $p<0.05$). Thus along with a decrease in contractility NaHS also caused the reduction of Ca^{2+}-concentration in cardiomyocytes which indirectly indicates the decrease of inward Ca2+-current into the cell.

The obtained data suggests that cAMP system is one of the target of H2S action in frog myocardium and activation of phosphodiesterases may mediate the reduction of cAMP level and decrease the Ca^{2+}-concentration in cardiomyocites.

This study was funded by RFBR and Leading Scientific School № SS-4670.2012.4.

References

Sitdikova G. F., Khaertdinov N. N., Zefirov A. L. Role of Calcium and Potassium Channels in Effects of Hydrogen Sulfide on Frog Myocardial Contractility // Bulletin of Experimental Biology and Medicine. Volume 151, Issue 2 (2011), Page 163-166.

Yong Q., Pan T., Hu L., Bian J. 2008. Negative regulation of β-adrenergic function by hydrogen sulfide in the rat hearts. J. Mol. Cell Cardiol. 44 (4), 701–710.

Kimura H. 2000. Hydrogen Sulfide Induces Cyclic AMP and Modulates the NMDA Receptor. Biochem. Biophys. Res. Commun.. 267, 129–133.

Kamp T., Hell J. 2000. Regulation of Cardiac L-Type Calcium Channels by Protein Kinase A and Protein Kinase C. Circ Res. 87, 1095-1102.

ORNITHINE DECARBOXYLASE OF HEART AND SKELETAL MUSCLES DURING THE HIBERNATION OF GROUND SQUIRREL *SPERMOPHILUS UNDULATUS* AND ARTIFICAL HYPOBIOSIS OF RAT *WISTAR*

G.E. Aksyonova, L.A. Fialkovskaya, N.M. Zakharova, I.K. Kolomiytseva

Institute of Cell Biophysics RAS, 3 Institutskaya st., Pushchino, Moscow redion, 142290, Russia

Ornithine decarboxylase (ODC, E.C. 4.1.1.17) is a rapidly exchanging, short-lived and very highly regulated enzyme of the biosynthesis of polyamines (putrescine, spermidine, spermine). ODC induction is one of the earliest molecular effects of activated metabolism in cell getting ready for growth and division, differentiation or active realization of special-purpose function. On the organism's level, the hormonal regulation of physiological functions of different organs is associated with changes in the activity of its ODC. Due to the fact that the ODC activity in organs and tissues is sensitive to both the central neuroendocrine and paracrine influences, it can serve as a functional biochemical test to study systemic adaptive responses of an organism to external influences, including hypobiosis. Natural (hibernation) and artificial rodent hypobiosis are characterized by reduced ODC activity in many organs [1-4]. In contrary, high absolute values of ODC activity (measured at 37 ºC) was observed in skeletal muscular tissue of active and torpid ground squirrel S. undulatus with no reliable variations [5]. Skeletal muscles play a large role during arousal of torpor producing more than 60% of heat by nonshivering and shivering thermogenesis [6]. Functional load on the heart muscle is growing during arousal too due to the sharp increase in heart rate. It is of a great interest to compare the ODC activity in heart and skeletal muscles adapting to hypobiosis in hibernating and nonhibernating species.

The studies were performed on ground squirrels Spermophilus undulatus and Wistar rats. All procedures with animals were carried out in the accordance with institutional and international standards (European Convention for the Protection of Vertebrate Animals used for Experimental and other Scientific Purposes 1986 86/609/EEC). The male and female ground squirrels with mass of 500–800 g were used in summer ("summer" animals) as well as during a season of hibernation ("winter" animals). "Winter" ground squirrels were divided into two groups: 1) torpid – animals, which were decapitated at body temperature of 1–7 ºC; 2) active winter ground squirrels –interbout active animals, (body temperature 37 ºC) were decapitated in 12-24 h after an arousal. The state of artificial hypobiosis in male Wistar rats weighted 180-220 g was got by the method of closed vessel. Rats were kept in individual 5 dm3 hermetic glass chambers at the temperature of 1-2°C for 3-3.5 hours; under conditions of hypoxia–hypercapnia, increasing with respiration, resulted in the state of cold anesthesia or hypobiosis. After removing the rats from the chambers and replacing them under standard conditions their rectal body temperature was 16.2 ± 0.2°C on average compared to the normal 38°C; heart rate (HR) was 60 ± 3 bpm compared to the normal rate

340-360 bpm. Upon replacing under standard conditions, the rats recovered to normothermia themselves within 3-4 hours and manifested no changes in their behavior later on. For biochemical assays, the animals were decapitated in a state of hypobiosis (immediately after removing from the chambers. Control rats (without treatment) were decapitated at the same time as the experimental ones. A piece of skeletal musculature of a thigh (m. quadriceps femoris) and a heart was withdrawn and immediately frozen in liquid nitrogen and was stored for analysis of enzyme activity. ODC activity was determined by the radioisotope method measuring release of 14CO2 from [1–14C]ornithine. The protein concentration in samples was determined by the method of Lowry. Statistical significance of the difference in ODC between the groups was calculated by Student's t-test. The results were represented as the mean ± standard error.

The functional and metabolic depression in organs and tissues of ground squirrels S. undulatus in torpid state correlated with reducing of its ODC activity (liver, kindey, spleen, intestine mucosa, bone marrow were studed). The mean values of ODC activity in these organs didn't exceed 10 pmol CO2 × (mg protein × hour)-1 in torpid state [2,3]. On the contrary, the heart and skeletal muscles kept very high values of the enzyme activity in torpor (table 1). The results should be discussed in the context of the functioning of these tissues in the course of hibernation. The isolated rat heart becomes arhythmogenic and fails between 17 ºC and 12 ºC, whereas ground squirrel heart continues to pump at temperatures as low as 5 ºC. When the hibernator enters torpor, heart rate and cardiac output falls, but stroke volume increases. Surprisingly, coronary blood flow was not reduced as temperature fell in the isolated ground squirrel heart and in vivo in the woodchuck (Marmota monax) despite a lower cardiac output. Maintenance of coronary blood flow during hibernation is in direct contrast to the fall in blood flow to visceral organs (kidney, intestines, spleen and stomach) and brain. Stabilization of resting cell membrane potential with decreasing temperature and improved Ca^{2+} handling were shown in cardiomyocytes isolated from the ground squirrel or hedgehog, rat myocytes were less stable [7]. The activation of energy metabolism enzymes was shown in the heart of torpid animals [8]. Thus, some functional and metabolic parameters of heart revealed a resistance to torpor and even the activation. This phenomenon was observed for the ODC activity in muscular tissues of hibernating ground squirrels (table 1). For comparison, the ODC activity of a rat heart in artificial hypobiosis state reliable decreased ($p<0,05$) (table 2).

Physiological role of active muscular ODC storing may be concerned with functional load on skeletal musculature in fast arousal after torpor (non-shivering and shivering thermogenesis). Skeletal musculature can also serve as a contributor of polyamines for other organs and tissues realizing the transmembrane transport of polyamines in addition to the endogenous synthesis. In rats, the muscles with a predominance of oxidative red fibers have a much higher ODC activity then with a predominance of glycolytic white ones [9].

Table 1. The ODC activity of heart and skeletal muscle of ground squirrels *S. undulates* in summer and during the hibernation season.

Organ	ODC activity, pmol CO_2 × (mg protein × hour)$^{-1}$		
	"Summer" animals	"Winter" animals	
		Active	Torpid
heart	141±9 (n=4)	129±25 (n=4)	180,0±15,4 (n=4)
m. quadriceps femoris	326±44 (n=3)	228±38 (n=4)	226,9±112,3 (n=4)

Table 2. The influence of artificial hypobiosis of rat on heart and skeletal muscle ODC activity.

Organ	ODC activity, pmol CO_2 × (mg protein × hour)$^{-1}$	
	Control	Artifical hypobiosis state
heart	180,4±11,0 (n=5)	115,0±5,7*(n=3)
m. quadriceps femoris	30,1±5,3 (n=3)	23,5±1,9 (n=3)

The role of red muscle fibers is seems to increase in ground squirrels, which explains the high activity of ODC in m. quadriceps femoris in comparison with rats one. The preferential atrophy of white muscle fibers is observed during hibernation [8]; this is in agreement with the suppression of glycolis.

The high activity of ODC in the heart and skeletal muscles of ground squirrel S. undulatus, continuing in the torpid state, is apparently a component of the adaptation of these tissues to hypobiosis and fast reworming. These data are also important to study the metabolism of short-lived proteins during hibernation.

References

1. Aksyonova G.E, Logvinovich O.S., Fialkovskaya L.A., Afanasyev V.N., Ignat'ev D.A., Kolomiytseva I.K. // Biochemistry (Mosc).–2010–V.75(9); P.1126.
2. Logvinovich O.S., Aksyonova G.E., Fialkovskaya L.A., Afanasyev V.N., Ignat'ev D.A., Kolomiytseva I.K., Fesenko E,E. // Dokl. Biochem. Biophys.–2010–V.433; P.216-218.
3. Logvinovich O.S., The activity of ornithine decarboxylase in the organs and tissues of mammals in hibernation mode and artificial hypobiosis. The thesis of candidate of biological sciences. - Pushchino, 2010. 122p.
4. Melnichuk D.O., Mikhailovsky V.O., Melnichuk C.D. //Ukr. Biokhim. Zh.–2000–V.72(4-5); P.70-80. [in Ukrainian].
5.. Aksyonova G.E, Logvinovich O.S., Fialkovskaya L.A., Ignat'ev D.A., Kolomiytseva I.K. // Biological motility: from fundamental achievements to nanotechnologies. – Pushchino: Synchrobook. 2010. P.5-7.
6. Lyman C.P., Willis J.S., Malan A., Wang L.C.H. Hibernation and torpor in mammals and birds // Academic press, INC (London), LTD. 1982. 303p.
7. Dobson G.P. // Comp. Biochem. Physiol. Pt.B.–2004.–V.139; P.469–485.
8. Wickler S.J., I-Ioyt D.F., van Breukelen F. // Am. J. Physiol.–1991–V. 261(5 Pt 2); P.1214-1217.
9. Chideckel E.W., Belur E.B. // Endocrinology.–1980.–V.107; P.918-923.

THE FLUCTUATION OF ANIMAL CELLULAR VOLUME UNDER THE MELAFEN – PLANT GROWTH REGULATOR, ACTION

O.M. Alekseeva [1], E.A. Yagolnik [2], Yu. A. Kim [3]

[1]*Emanuel Institute of Biochemical Physics, Russian Academy of Sciences, 119334, Moscow, st. Kosygin d.4; (495) 939-74-09, olgavek@yandex.ru*

[2]*Tula State University*

[3]*Institute of Cell Biophysics, Russian Academy of Sciences, Pushchino*

Melafen (a melamine salt of bis (hydroxymethyl) phosphinic acid) is a hydrophilic polifunction substance (Fig. 1). There are the acid, phosphoric, oxymethyl groups at Melafen molecule, potentially pointed at the certain targets at the biological cells. The pre-treatment of crop seeds by aqueous solutions of melafen at concentration 10^{-11} – 10^{-9} M increased the yield of plant production by 11% or more due to the increasing of plants stress tolerance under the bed environment. The increasing of the concentration of melafen to 10^{-8}, 10^{-7} M inhibits the growth of plants completely. Therefore, our studies were carried out in a wide range of concentrations (10^{-21} M–10^{-2} M). The main purpose was to determine how the aqueous solutions

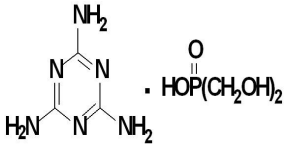

Fig.1. Melafen.

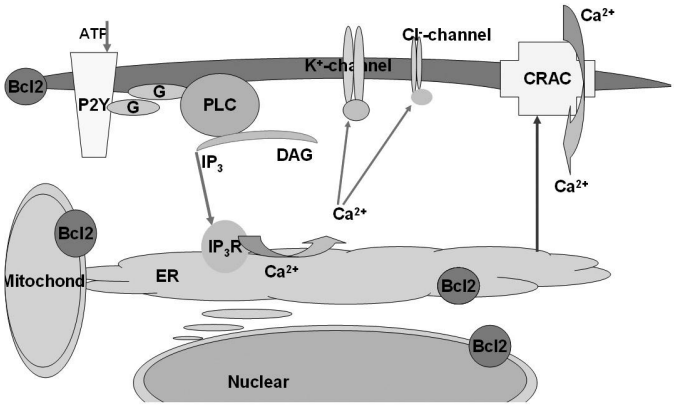

Fig. 2. Scheme of P2Y –related system of signal transduction.

of melafen in a wide range of concentrations influence to the function of animal cells.

The using of light scattering method allowed us to investigate the overall cellular answer to the Melafen additions. Thanks to presented method we tested the action of Melafen to the animal cells and its components under a wide range of concentrations.

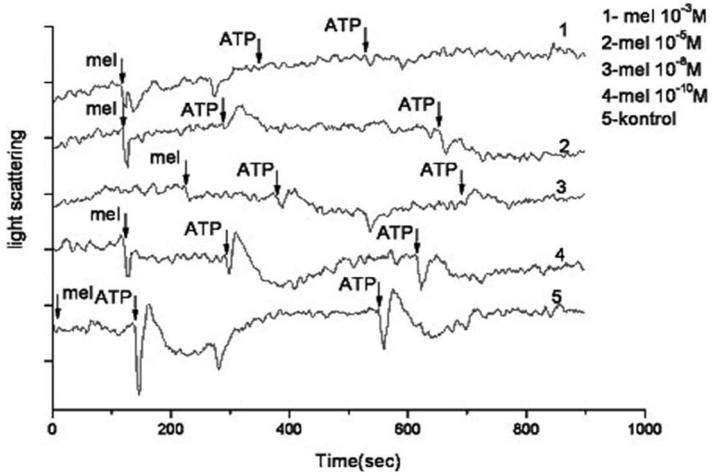

Fig. 3. The influence of melafen to the first (A) and second (B) cellular answer of EAC cells. Kinetic curves of light scattering the cell suspension.

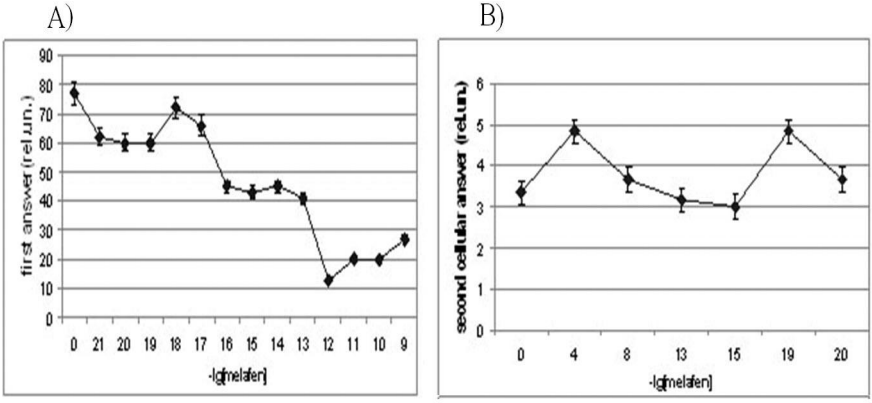

Fig.4. The influence of melafen to the first (A) and second (B) cellular answer of rat thymocytes. The amplitude of light scattering rising after the ATP addition to the cell suspension on the dependence of melafen concentration.

The 3 cellular objects were used, as the solute cells cellular suspension: ascetic Ehrlich carcinoma (EAC) cells - transformed cells with uncontrolled growth (Fig. 3), and normal cells thymocytes (Fig. 4) and lymphocytes (the white fraction of blood without the platelets and erythrocytes) (Fig. 5).

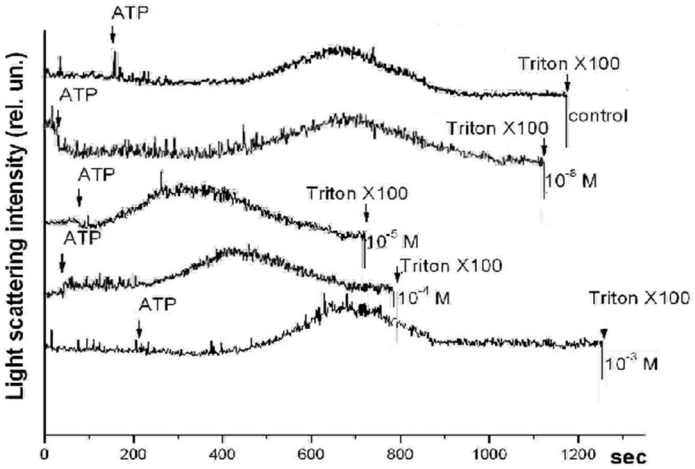

Fig.5 The influence of melafen to the lag-phase of cellular answer of leucocytes. Kinetic curves of light scattering the cell suspension.

First - EAC cells, as a good model of cells with the full cellular transduction system. The active P2Y purinoreceptors are presented at the cellular plasmalemma surface at the 7-8 days of carcinoma growth [1]. Thus the ATP or ADP additions initiated the Ca^{2+} - signal transduction (Fig. 2). ATP is the first messenger that deals with the extracellular signal transductions pathways. ATP is released to the extracellular space. At least two subtypes of receptors for extracellular ATP are currently known: the G-protein–coupled P2Y receptors, which are methabotrophic receptors and the ATP-gated cation channels classified as P2X receptors. AEC cells gave a typical cellular response to a signal (ATP-addition) and sent the signal from the cell surface to inside and backward. At the EAK cells the methabotrophic purinoreceptors P2Y throughout the G-proteins activated PLC, then the I3P released Ca^{2+} from ER and retrograde signal (related to ER Ca^{2+}-store depletion) go to the cellular surface, and the large flow of Ca^{2+} introduced to the cell throughout the Ca^{2+}-release-activated Ca^{2+} channels (CRAC) [2].

As the result, there are the two facts of large increasing of intracellular Ca^{2+}- concentrations. The volume of cells changed, and because Ca^{2+}-dependent K^+ и Cl^- -channels, which regulated the cell volume. The compensators H_2O flows occurred to the cells interiors. Thus the light scattering of dilute suspension of EAC cells were changed too. We recorded of right angle light scattering of dilute suspension of EAC cells with Perkin–Elmer-44B spectrofluorometer at a wavelength of 510 nm. The control samples gave bimodal cellular response (Fig.3). Melafen inhibited the response development by the doze-dependent manner.

But melafen has a bidirectional effect to the EAC cells. We founded that at super low concentrations melafen (10^{-12}, 10^{-13} M) stimulated the signal transduc-

tion, increasing the Ca^{2+} -releasing from intracellular Ca^{2+}-store. But at the bigger concentrations melafen changed the vector of its action and begin to depress the overall cell response. At the case, when the melafen concentrations increased, the amplitudes of first and second extremes decreased. The second cell response - Ca^{2+}-entering through the plasma membrane was not activated by melafen, and it shown the bigger sensitivity to the melafen action – it was inhibited by the melafen at the smaller concentrations. Thus, melafen 10^{-7} M decreased by 50% the first extreme and by 70% - the second extreme. Melafen 10^{-4} M really eliminated the overall cell response in full; it inhibited the purine-dependent Ca^{2+}-transduction – both peaks. Hence, the carcinoma cells that characterized by uncontrolled cell division, can be depressed by such doses of melafen, which are harmless for erythrocytes that we obtain earlier. Thus melafen influence on two targets surfaces of cells simultaneously – on purinoreceptors PY2 and on CRAC, considerably reducing their activity in plants-growth stimulated doses. Really melafen changes the functions of surface receptors and intracellular signal transduction.

It will be interesting to test the melafen influence to the overall cellular answer of the normal cells that may be activated by ATP additions. Because that we recorded of right angle of light scattering of dilute suspension of dilute suspension of thymocytes and leucocytes. These cells have ranking among P2Y receptors have another types of purinoreceptors nonmethabotrophic channel formers P2X (leukocytes) [3] and its modification P2Z (thymocytes). The compositions of group of P2 receptors at thymocytes are showing both P2Z and P2X receptor activation characteristics are in depending on the stage of cellular growth [4]. The additions of APT to the thymocytes suspension caused the two-phase of change of cell volume (Fig.4).

Melafen influences on both phases. P2X and P2Z channel formers receptors are susceptible to influence from melafen under a wide range of concentrations. .

Additions of ATP to leucocytes suspension caused releasing of Ca^{2+} from intracellular stores through activating of metabotropic P2Y purine receptors (at the medium of measurement Ca^{2+} don't present). Thus we eliminated the possibility of introducing to the cell interior the extracellular Ca^{2+}. The melafen attendance shortens the time the phase lag up to cellular answer development. Analogously behave the cell EAC, which faster go out to the stable behavior in the presence of melafen. Impact on melafen to the channel-former P2X the leucocytes receptors are coming clear to up.

References

1. Zamai A.C., et. al.// Conference "Reception and intracellular signalization" Puschino 2005. p. 48-51 "The ATP influence to the tumor ascetic cells at different stages of cellular growth"
2. Pedersen SF, Pedersen S, Lambert IH, Hoffmann EK.//Biochim Biophys Acta. 1998 Sep 23;1374(1-2), p.94-106. "P2 receptor-mediated signal transduction in Ehrlich ascites tumor cells".

3. Di Virgilio, F. et al. // Blood 2001 97, p.587–600 “Nucleotide receptors: an emerging family of regulatory molecules in blood cells.”
4. Nagy PV, Fehér T, Morga S, Matkó J.// Immunol Lett. 2000 72 (1). p.23-30. “Apoptosis of murine thymocytes induced by extracellular ATP is dose- and cytosolic pH-dependent.”

EFFECT OF FULLERENE C_{60} ON ATPase ACTIVITY AND SUPERPRECIPITATION REACTION OF RABBIT SKELETAL MUSCLE ACTOMYOSIN

K. Andreichenko, K. Medynska, O. Shelyuk, N. Nurishchenko, S. Andreichenko, K. Bogutska, Yu. Prylutskyy

Taras Shevchenko National University of Kiev, ESC "Institute of Biology", Department of Biophysics, Vladimirskaya Str., 64, 01601 Kiev, Ukraine

Introduction. The application of nanostructures including fullerene C_{60} for biomedical purposes is one of the interesting aspects of nanoscience. Despite the large number of the studies on the interaction of fullerene C_{60} with biological objects *in vitro* and *in vivo* [1], almost no information on their impact on the functional properties of muscles. Only single investigations show changes in physiological and biochemical processes in the muscles under the influence of fullerene C_{60} and its derivatives. So, it was fount that fullerene derivative (monomalonic acid C_{60}; 10^{-5} M) inhibits the endothelium-dependent relaxation induced by acetylcholine but does not affect the agonist-induced contractile response of aortic smooth muscle of rabbit [2]. Fullerenol (polyhydroxylated derivative of fullerene C_{60}) inhibites the proliferative responses in a number of cells, including rat aortic and human coronary artery smooth muscle cells in a concentration dependent manner [3]. Fullerene-based nanocationite particles (porphyrin adducts of cyclohexyl fullerene C_{60}) to treat hypoxia-induced mitochondrial dysfunction in mammalian heart muscle [4]. Finally, fullerenol nanoparticles have been validated as potential candidates for the creation of artificial muscles because of their excellent proton conductivity, hydrophilicity and biocompatibility [5]. But the mechanisms of nanostructure’s action on muscle are still not clear.

ATPase reaction is the main driving force behind the process of muscle contraction as its chemical stage. The activity in the presence of mM concentrations of Mg^{2+} and enhanced by concentrations of Ca^{2+} of several mM is referred to as Mg^{2+},Ca^{2+}-ATPase. This activity is important considering the physiological conditions in muscle cells. The activity in the presence of EDTA (absence of divalent cations) and high concentrations of KCl is referred to as K^{+}-EDTA-ATPase [6]. However, the impact of fullerene C_{60} on the actomyosin ATPase activity, which is crucial to the contractile mechanism, is not established.

There is no doubt that the ATPase activity underlies the contractile processes of the actomyosin system, but it is noticed that not all the actomyosin ATPase activity is expressed as the contraction. The superprecipitation of actomyosin is generally accepted to be basically the phenomenon of skeletal muscle con-

traction *in vitro*. Superprecipitation reaction can be considered as a simplified model of muscle contraction.

Thus, the aim of this investigation was to measure the effect of fullerene C_{60} in different concentrations on ATPase and superprecipitation activity of rabbit skeletal muscle actomyosin.

Materials and methods. Actomyosin was prepared from rabbit skeletal muscle [7]. The animals used in this study were treated in accordance with the principles and guidelines of Tohoku University Council on Animal Care. The reaction mixture for Mg^{2+},Ca^{2+}-ATPase contained 0.2 mg/ml of actomyosin, 60 mM KCI, 0.1 mM ATP, 20 mM imidasole buffer (pH 7.5), 5 mM $MgC1_2$ and 0.1 mM $CaCl_2$, 1 mM EGTA; 0.2 mg/ml myosin, 1 mM ATP, 5 mM EDTA, 60 mM KCl, and 20 mM imidasole buffer (pH 7.5) for the K^+-EDTA-ATPase activity of actomyosin. Under these conditions ATPase activity of actomyosin was determined by measuring hydrolyzed inorganic phosphate (Pi). The reaction was started by the addition of ATP and stopped by the addition of an equal volume of cold 10% trichloroacetic acid. The amount of inorganic phosphate liberated during 5 min incubation was determined according to the Fiske and Subbarow method [8]. ATPase activity was expressed in nM $P_i \cdot min^{-1} \cdot mg^{-1}$ protein. ATPase activity of native actomyosin was taken over the control.

The superprecipitation activity was examined as described by Ebashi [9]. The superprecipitation was induced by the addition of 0.1 mM ATP in 0.2 mg/ml natural actomyosin, 1 mM $CaCl_2$, 1 mM $MgCl_2$, 50 mM KCl, 1 mM EGTA, and 20 mM Tris HCl at pH 7.5 and 25°C, and the change in the absorbance at 450 nm was followed. Registration of kinetic curves of superprecipitation of actomyosin was set out on SPECORD M40 spectrophotometer (Russia). Over 100% of the value was set superprecipitation of native protein. From obtained kinetic curves the value of superprecipitation was calculated by formula ($D_{max(450)}$ - D_0), where D_0 and $D_{max(450)}$ are the values of the initial and maximum optical density of actomyosin, respectively, during the superprecipitation reaction and $t_{1/2}$, - time which is needed for achievement of half of its value.

In the studied samples the changes of ATPase and superprecipitation activity of protein complex in the presence of fullerene C_{60} at concentrations ranging from 10^{-3} to 10^{-9} mg/ml were measured. A highly stable aqueous colloidal solution of unmodified fullerene C_{60} with a maximum concentration of 1.0 mg/ml was obtained by the method [10].

Statistical analysis of experimental results was done in the frames of the Student's t-test using Origin 8.0 software (OriginLab Corporation, USA).

Results and discussion. The ATPase activity of native actomyosin in the presence of magnesium and calcium (Mg^{2+},Ca^{2+}-ATPase activity or actin-activating ATPase) and chelator of Ca^{2+} ions - EDTA (K^+-EDTA-ATPase activity or actin-relaxing ATPase) was measured. The obtained results are presented in Fig. 1.

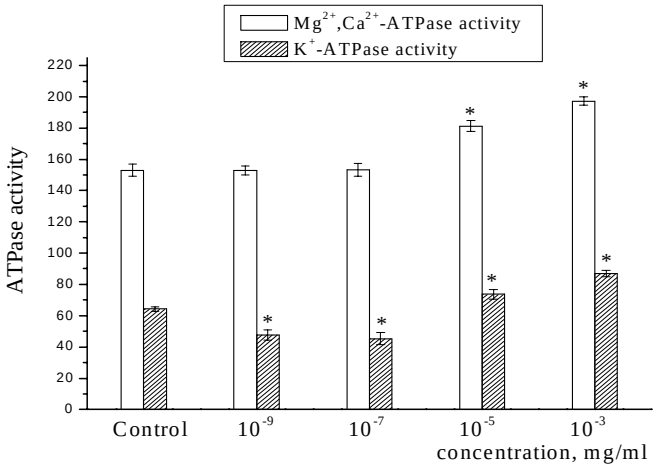

F

ig. 1. Mg^{2+},Ca^{2+}-ATPase and K^{+}-EDTA-ATPase activity of actomyosin under the fullerene C_{60} influence (M±m, n=9; *significant differences compared with a control at p<0,05).

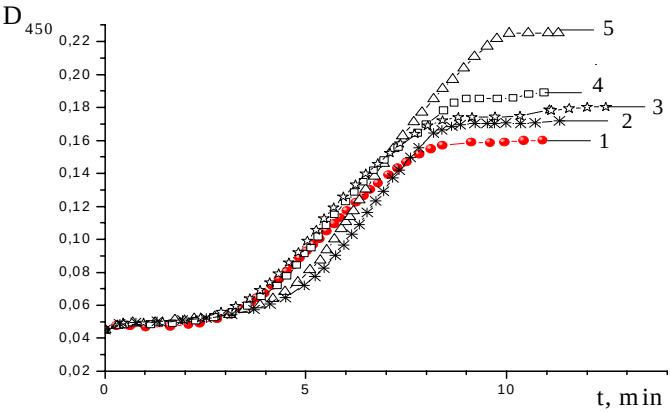

F

ig. 2. Typical kinetic curves of rabbit skeletal muscle actomyosin superprecipitation under the different concentrations of fullerene C_{60}: 1 – native actomyosin (control); 2 – 10^{-9}; 3 – 10^{-7}; 4 – 10^{-5} and 5 – 10^{-3} mg/ml.

Fullerene C_{60} in concentration 10^{-9} and 10^{-7} mg/ml does not affect the Mg^{2+},Ca^{2+}-ATPase activity of actomyosin, but inhibits K^{+}-EDTA-ATPase activity

on 29% and 26%, respectively. Fullerene C_{60} in concentration 10^{-5} mg/ml caused the increasing in Mg^{2+},Ca^{2+}-ATPase activity on 19% compared with control value. K^+-EDTA-ATPase activity of actomyosin also was elevated on 15% under above concentration of fullerene C_{60}. The influence of fullerene C_{60} in concentration 10^{-3} mg/ml on Mg^{2+},Ca^{2+}-ATPase and K^+-EDTA-ATPase activity was similar, namely it increased on 35%.

Fig. 2 shows the typical recording traces of the actomyosin superprecipitation under the fullerene C_{60} action.

The value of superprecipitation of actomyosin is increased for all concentrations of fullerene C_{60}. But only concentration 10^{-3} and 10^{-5} mg/ml provide significant differences compared with a control. The $t_{1/2}$ value is increased compare to control for all concentrations of fullerene C_{60}.

Conclusion. Thus, we conclude that fullerene C_{60} impacts on the function of actomyosin complex. It may be interesting approach to the further application of this nanosystem in the regulation of muscle contraction, especially for pathology condition. Additional experiments will be required to the explaining the mechanism of fullerene C_{60} action.

References

1. Medicinal Chemistry and Pharmacological Potential of Fullerenes and Carbon Nanotubes. Series: Carbon Materials: Chemistry and Physics. Cataldo F, Da Ros T (Eds.). Netherlands: Springer, 2008.
2. Satoh M, Matsuo K, Kiriya H, et al. Inhibitory effect of a fullerene derivative, monomalonic acid C_{60}, on nitric oxide-dependent relaxation of aortic smooth muscle. Gen Pharmacol 1997; 29: 345-351.
3. Lu LH, Lee YT, Chen HW, et al. The possible mechanisms of the antiproliferative effect of fullerenol, polyhydroxylated C_{60}, on vascular smooth muscle cells. Br J Pharmacol. 1998; 123: 1097-1102.
4. Amirshahi N, Alyautdin RN, Sarkar S, et al. Fullerene-based low toxic nanocationite particles (porphyrin adducts of cyclohexyl fullerene-C_{60}) to treat hypoxia-induced mitochondrial dysfunction in mammalian heart muscle. Arch Med Res 2008; 39: 549-559.
5. Rajagopalan M, Oh IK. Fullerenol-based electroactive artificial muscles utilizing biocompatible polyetherimide. ACS Nano 2011; 5: 2248-2256.
6. Muhlrad A., Peyser YM, Nili M, et al. Chemical decoupling of ATPase activation and force production from the contractile cycle in myosin by steric hindrance of level-arm movement Biophys. J. 2003; 84: 1047-1056.
7. Tartakovskiy AD. Biophysical and biochemical methods for studying muscle proteins. Leningrad: Nauka, 1978; 55-76 (in Russian).
8. Fiske C, Subbarow Y. The colorimetric determination of phosphorus. J. Biol. Chem. 1925; 66: 375-400.
9. Ebashi S. Calcium binding activity of vesicular relying factor. J. Biochem. 1961; 50: 236-244.
10. Scharff P, Risch K, Carta-Abelmann L, et al. Structure of C_{60} fullerene in water: spectroscopic data. Carbon 2004; 42: 1203-1206.

MECHANISMS OF MOTILITY LOSS BY SPERMATOZOA UNDER IONIZING IRRADIATION

S.V. Andreychenko, A.V. Klepko, N.E. Nurischenko

SE "National Research Centre for Radiation Medicine, NAMS of Ukraine", 53 Melnikova Str., 04050, Kyiv, Ukraine

According to the radiobiological law established by Bergonje and Tribando in the 20th century, ionizing radiation first of all damages physiologically active dividing cells, which are present in abundance in highly proliferative male germinal epithelium. Ionizing radiation produces highly reactive free radicals which cause lipid peroxidation and membrane damage. In contrast to other cells, spermatozoa do not possess an effective antioxidant system of lipid defense because of little catalase activity. On the other hand, it was shown that isolated rabbit spermatozoa have high radioresistance to gamma-irradiation, according to which the spermatozoa retained motility in the dose range 100-65000 rad [1]. After irradiation in the dose of 15000 rad spermatozoa were able to penetrate to egg cell and cause syngamy. Gamma-irradiation of frog spermatozoa did not influence their motility in the dose range up to 20000 rad. At higher doses gamma-irradiated sperm induced haploid and dihaploid parthenogetic embryo formation [2].

To elucidate the crucial elements of radiation damage in spermatozoa model experiments on isolated cultured spermatozoa of animals upon their irradiation by ionizing radiation in various doses are to be carried out. Then, on the basis of microscopic observations the insight of radiation pathogenesis development in spermatozoa might be gained, the special correlations between the stage of radiation injury and fertilizing ability of spermatozoa being established. In this connection the present research is intended to investigate the radiation effects on rat spermatozoa and to elucidate the mechanisms of radiation injury and recovery in these cells.

Materials and methods. Experiments were carried out on rats males of Wistar line in the age of 3-4 months and weight of 250-300g. Animals were decapitated under light narcosis with diethyl ether. Then extirpated epididymices were placed in phosphate buffer-saline (PBS). Epididymices in PBS were gamma-irradiated by Co^{60} on the experimental device "Investigator" (Russian Federation) with the dose rate 0,2 Gy/sec in the wide dose range up to 1900 Gy. Spermatozoid motility was assessed in a drop of PBS smeared on a glass slide at 37°C with the help of light microscope МБИ-6 (Russian Federation) at magnification x600. For this purpose 150 spermatozoa at random were selected. Quantitative ultramorphological (QUM) analysis was applied in evaluating the radiation damage development in rat spermatozoa. QUM analysis examines the organization and integrity of subcellular sperm organelles using both transmission electron microscopy (TEM) and scanning electron microscopy (SEM). With TEM and appropriate staining techniques, it is possible to view both cross-sections of the cell and two-dimensional images of ultrafine anatomical details. The SEM allows an overall view of sperm ultrastructure, especially of head and tail skeleton. Thus, the combined use of TEM

and SEM yields comprehensive results, supplying more details about pathological malformations in each subcellular organelle. Comparison of data for different radiation doses was made using analysis of variances, Anova, and unpaired Student's *t*-test with amendment of Bonferroni. All statistical tests were two sided and $p \leq 0,05$ was considered statistically significant [3].

Results and discussion. Rat spermatozoa belong to highly differentiated haploid sexual cells which are allocated for accomplishing unique physiological function dealing with a delivery of paternal genome to egg cell. Undoubtedly, there would be special conformity between anatomical make up and so complicated and multiple function of spermatozoon. Thus, spermatozoon movements are secured by tail oscillations, the energy for the said process being generated in mitochondria. The very mitochondria are set in the mitochondrial helix which surrounds the macrofibrils and axoneme.

Typically spermatozoon consists of 3 sections, i.e. head, midpiece and tail, respectively. Head contains nucleus with condensed chromatin and acrosome. Head is linked to midpiece by neck. In the neck a lateral centriole is visible, while the basal one disappeared giving rise to axoneme. Cross-section of midpiece reveals axoneme which is made up of 2 cenral microtubules surrounded by nine duplets of microtubules in addition. In the midpiece axoneme is surrounded with macrofibrils which are, in turn, encircled by mitochondrial helix. In the terminal part of the tail a set of macrofibrils disappears. Therefore axoneme retains around itself only a fibrous sheath covered by plasma membrane.

Gamma-irradiation of spermatozoa caused gradual loss of their motility in the nutrient solution in post-radiation period, the latter parameter showing obvious dose dependence (figure). Thus, in control (0 Gy) the sperm motility was equal to 95%. Then it started to drop with the dose increase. Therefore at 500 Gy the motility was equal to 62% of control mean value, at 1000 Gy – 23% and at 1900 Gy only 2%.

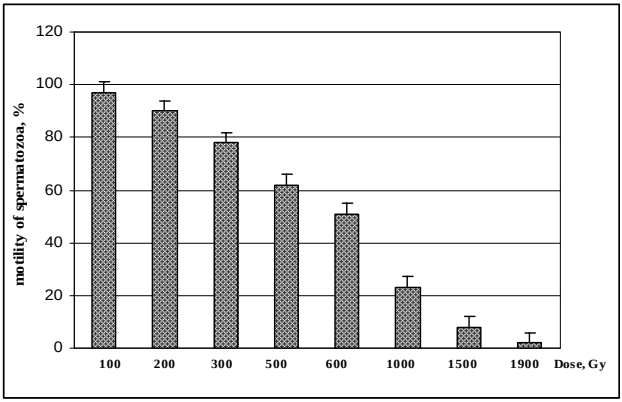

Radiation dose influence on spermatozoid motility

Scan electron microscopy showed the emerging of lipid droplets on spermatozoon's surface. Initially they appeared at relatively low doses on the tail and then encompassed the head at higher doses. Further dose elevation resulted in acceleration of lipid bodies' formation on the spermatozoon's surface. Moreover, at the dose of 40 Gy lipid droplets began to separate from spermatozoon. In the dose span 70-100 Gy the passages of spermatozoon free of plasma membrane were discovered.

Undressing of spermatozoon skeleton from plasma membrane exerted through initiating its vesiculation, whereby plasma membrane rolled down from spermatozoon. In consequence of this process a lot of irradiated spermatozoa proved partly or completely naked.

At sublethal doses the radiation lesions on spermatozoa started to emerge spontaneously in different sections in the form of necrotic plaques. Necrotic changes in spermatozoa were characterized by their wideness and deepness, the process comprehending the whole internal cytoskeleton of spermatozoon. As a result, the break-down of spermatozoon in the affected sites occurred, different spermatozoid fragments being released in the environment. Apart from this, at moderate doses (300 Gy) mitochondria swelled and became devoid of cristae. These changes indicated on the disturbances in electron transport and oxidative phosphorylation in mitochondria. Consequently, energy supply of spermatozoon at moderate doses was significantly suppressed. Furthermore, at sublethal doses spermatozoa were shown to lose partly their organelles, e.g. acrosomes and mitochondria.

Thus, direct radiation action on spermatozoa induces free radical formation and subsequent chain peroxidation of lipids. As a result, spermatozoid membrane becomes damaged and subject to rupturing. According to the biochemical investigations, animal and human spermatozoa are very vulnerable to radiation impact because of unsaturated fatty acids presence in great abundance in their contents. Admittedly, these compounds proved to be very sensitive to ionizing radiation due to double bonds as hot spots for radiation assault by hydroperoxide, electrons or hydroxyl radicals. In consequence lipid break-down through peroxidation chain reactions is launched resulting in further destruction and rupturing of internal and external membranes [4,5].

The detrimental effect of radiation on membranes causes the infringement of ion-transport across plasma membrane and electron transport in mitochondria. Consequently, electrogenic pumps slow down their activities, membrane potential diminishing. In such conditions ionic homeostasis in spermatozoon disturbs resulting in uncoupling between electron transport and phosphorylation. Therefore, electrons may easily find free oxygen molecules to form superoxide radicals, the latter being a progenitor for hydroperoxide and hydroxyl radicals.

Spontaneous raise of radical contents along with an abatement of antioxidant enzymic activities in irradiated spermatozoa triggers the membrane and cytoskeleton gradual destroying in spermatozoon. At the last stages of radiation damage development the breakdown of entire organelles may occur. In addition,

radiation may also affect DNA causing nucleotide damaging and accumulation of single and double strand breaks in DNA structure. However, in spermatozoon DNA exists in the nucleoprotamine complex as inactive component due to highly condensed state of chromatin and the absence of whatever DNA transcriptional activity. Therefore DNA damaging just for spermatozoon motility and functioning is of little importance.

References

1. Bedford J., Hunter R.H. The influence of X-irradiation of rabbit spermatozoa on fertilization and early cleavage. J. Reprod. Fert. 1968; 17:49-57
2. Kaufman M.H. Early mammalian development: parthenogenetic studies. Cambridge University Press 1983:111-197
3. Altman D.G. Practical statistics for medical research. Chapman and Hall 1991:32-294
4. Jensen T.K., Bonde J.P., Joffe M. The influence of occupational exposure on male reproductive function. Occupational Medicine-Oxford 2006; 56:544-553.
5. Fischbein A., Zabludovsky N., Eltes F., Grischenko V., Bartoov B. Ultramorphological sperm characteristics in the risk assessment of health effects after radiation exposure amoung salvage workers in Chernobyl. Env. Health Perspect 1997; 105:33-44

EFFECT OF LIPOPOLISACCHARIDE STRUCTURE ON THE FUNCTIONAL ACTIVITY OF HUMAN BLOOD PHAGOCYTES

O.Y. Antonova[1,2], M.M. Yurinskaya[1], M.B. Evgen'ev[3], M.G. Vinokurov[1,2]

[1]Institute of Cell Biophysics RAS, ul. Institutskaya, 3, Pushchino, Moscow oblast, 142290 Russia

[2]Pushchino State Institute of Natural Sciences, pr. Nauki, 3, Pushchino, Moscow oblast, 142290 Russia

[3]Engelhardt Institute of Molecular Biology RAS, ul. Vavilova 32, Moscow, 119991, Russia

Lipopolysaccharides (LPS) - components of a cellular membrane of Gram-negative bacteria - are highly potent activator of innate immunity cells, in particular monocytes and neutrophils. The interaction of LPS with blood phagocytes release a wide spectrum of proinflammatory cytokines among which the first secretes TNF-α (which stimulates release of other cytokines that extends the range of cells involved in the inflammatory process), and also produce reactive oxygen species (ROS). In recent years is shown, LPS play an important role not only in the development of sepsis, as well as a number of serious social diseases, such as cardiovascular diseases.

The full-size LPS (S-chemotype) consists of three areas: the hydrophobic lipid A, the core region**,** divided into inner and outer, also O-antigen. Depending on the length of polysaccharide and accordingly presence of the given in fields in the LPS molecule, they are classified as full-length LPS (S-chemotype) and core-deficient R-chemotype. It should be noted that at present the action of S-chemotypes of endotoxin on myeloid cells is sufficiently well studied, whereas

the effects of different forms of R-LPS are investigated relatively little, despite the fact that the majority of Gram-negative Enterobacteriaceae, along with S-LPS forms synthesize R-form of LPS [1]. In this regard, the aim of this study was to carry out a comparative study of the functional activity of blood phagocytes at interaction with various LPS chemotypes of enterobacteria *E. coli*.

Neutrophils were isolated from peripheral blood of healthy volunteers by differential centrifugation in a 2-layer gradient of Ficoll-verografin (1.119 g/ml and 1.077 g/ml). Monocytes were isolated by centrifugation of the mononuclear fraction in a concentration gradient of Percoll (1.064 g/ml). The viability of neutrophils and monocytes was monitored by flow cytometry with the use of propidium iodide. The viability of isolated cells was found to be 98–99%. Neutrophils ($2 \cdot 10^5$ cell/ml) and monocytes ($1 \cdot 10^5$ cell/ml) in HBSS in the presence of 2% blood plasma and 350 μM luminol were incubated with 20 ng/ml LPS for 25 minutes at 37°C. Samples were placed in a 1250 LKB luminometer (Sweden). Cells were stimulated by addition of 1 μM fMLP. Chemiluminescence (CL) was recorded for 10 minutes. TNF-α production by neutrophils was estimated by the cytotoxic effect of samples on target L-929 cells [2]. Experimental data were processed using the Sigma Plot software.

Effect of LPS chemotypes structure on the ROS - generating activity and apoptosis of neutrophils has been shown by us earlier [3], in the present work we carried out a comparative analysis of the respiratory burst and TNF-α production activation by blood phagocytes (neutrophils and monocytes) at interaction with various LPS chemotypes. The obtained results showed that all LPS chemotypes strongly enough activated cells, greatly increasing the value of CL. The most activating ability of LPS had a wild strain, i.e. S-form, which increases ROS production by neutrophils to 275% compared with the shortest Re-form (155 %). Our results showed that the decrease in the CL intensity by neutrophils in the series S> Ra> Rc> Rd> Re correlates with elongation of the polysaccharide length of *E. coli* endotoxin chemotypes studied. In monocytes, LPS chemotypes caused less significant changes in CL compared with neutrophils. Priming of these cells by Ra-LPS most effectively increased the CL (164 % in comparison with control cells). Interestingly, in the case of monocytes, the S-form (or full LPS) caused not the strongest activating effect and chemotypes, respectively, can be arranged in the following series: Ra> S> Rc> Rd ≥Re.

Investigation of the effect of different chemotypes of LPS showed that In the case of TNF-a production also is a tendency to reduce the effect with reduction the length of the polysaccharide chain of LPS chemotypes. Thus, the increase of TNF-α production by neutrophils varies from 39 pg/ml for the S-form up to 22 pg/ml for the Re-form. It should be noted that monocytes are not treated with LPS, characterized by very low production of TNF-α whereas after stimulation with different chemotypes of LPS (1 μg/ml) production of this cytokine is repeatedly enlarged. So monocyte stimulation by the S-form caused an increase in concentration of TNF-α up to 85 pg/ml. Ra- and Rc-forms showed quite similar values of TNF-α - about 73 pg/ml. The Re-form has the least inducing effect increasing the value of this cyto-

kine to 58 pg/ml while dependence between length polysaccharide parts of a molecule and its activating action accordingly remains. Thus, it is possible to conclude that Re-LPS, which has no core and O-antigen part, was less effective in the activation of the studied reactions of neutrophils and monocytes than the full-size LPS.

The physiological significance of the differences in the structure of the LPS chemotypes finds in recent years more and more acknowledgement. Kawai T. et al. have shown that the S-and R-form LPS use several different pathways to activate the cells. For example, S-LPS to interact with cells requires CD14 receptor and R-chemotypes have the ability to activate cells in the absence of this receptor [4]. Perhaps this is connected with this highest activating ability of the Ra-forms on ROS production by monocytes. The interaction of S-LPS with neutrophils an important role plays the presence in our experimental conditions of the plasma, lipopolysaccharide binding protein and solved form of CD14 receptor that compensates for the low expression of this receptor on the superficiality of neutrophils. Therefore, a significant activation of the respiratory burst and increased of TNF-α production by the neutrophils, invoked by S-form of LPS is observed.

The authors of [5] showed that the TLR4/MD-2 complex is able to discriminate between the S- and R-forms of LPS. Saccharides of the R-form include the saccharides of the inner and outer cores whose length may be determinative in the interaction with the receptors of target cells- neutrophils and monocytes.

References

1. Huber M., Kalis Ch., Keck S., Jiang Z., Georgel P., Du X., Shamel L., Sovath S., Mudd S., Beutler B., Galanos C., Freudenberg M.A. R-form LPS, the master key to the activation of TLR4/MD-2-positive cells. *Eur. J. Immunol.* 2006, vol. 36, pp. 701–711
2. Luckow V.A., Lee S.C., Barry G.F., Olins P.O. Efficient generation of infectious recombinant baculoviruses by site-specific transposon-mediated insertion of foreign genes into a baculovirus genome propagated in Escherichia coli**.** *J. Virol.* 1993. vol. 67, no 8. pp. 4566–4570.
3. Vinokurov M.G., Yurinskaya, M.M., Prokhorenko, I.R., and Grachev, S.V. Effect of various E. coli LPS chemotypes on apoptosis and activation of human neutrophils. *Byull. Eksp. Biol. Med.* 2006, vol. 147, no. 8, pp. 136–138.
4. Kawai T., Akira S. The roles of TLRs, RLRs and NLRs in pathogen recognition. *International Immunol*. 2009, vol. 21, no. 4, pp. 317–337.
5. Jiang Z., Georgel P., Du X., Shamel L, Sovath S, Mudd S, Huber M, Kalis C, Keck S, Galanos C, Freudenberg M, Beutler B. CD14 is required for MyD88-independent LPS signaling. *Nat. Immunol*. 2005, vol. 6, pp. 565-570.

STABILIZATION OF SKELETAL TROPOMYOSIN BY MUTATIONS IN THE CENTRAL PART OF ITS MOLECULE

N.V. Artemova[1], N.N. Sluchanko[1], A.M. Matyushenko[1,2], I.A. Nevzorov[1],and D.I. Levitsky [1,3]

[1] A.N. Bach Institute of Biochemistry, Russian Academy of Sciences, Moscow, Russia;

[2] Department of Biochemistry, School of Biology, Moscow State University, Moscow, Russia;

[3] A.N. Belozersky Institute of Physico-Chemical Biology, Moscow State University, Moscow, Russia

Recent studies have revealed two non-canonical residues in the central part of skeletal α-tropomyosin (α-Tm), Asp137 and Gly126, whose substitutions with canonical residues (mutations D137L and G126R) prevented characteristic trypsin cleavage of α-Tm at Arg133 and similarly affected the regulatory properties of α-Tm: at high Ca^{2+}, both these mutations resulted in almost 2-fold increase in AT-Pase activity of the regulated thin filaments composed of F-actin, α-Tm, troponin, and myosin S1 [1, 2]. Differential scanning calorimetry (DSC) was used to investigate the effect of G126R mutation on the thermal unfolding of α-Tm. It was shown that the central part of the wild type α-Tm unfolds at low temperature in a non-cooperative manner, whereas mutation G126R stabilizes this part of the α-Tm molecule and confers cooperativity to its thermal unfolding. Furthermore, the size of the flexible middle part of α-Tm (60–70 amino acid residues, i.e. about a quarter of the α-Tm molecule) was estimated from those DSC experiments [2].

In the present work, we continued these studies and applied DSC and circular dichroism (CD) to compare the effects of G126R and D137L mutations on the thermal unfolding of skeletal α-Tm. Firstly, we substituted the only Cys residue (Cys190) of α-Tm with an Ala residue, to avoid difficulties associated with necessity to reduce the SH-group of Cys190 before DSC experiments. Mutation C190A had no appreciable effect on the thermal unfolding of α-Tm. Like the wild type α-Tm with the thiols of Cys190 reduced, α-Tm with mutation C190A demonstrated three thermal transitions: low-cooperative transition with maximum at ~36°C, presumably corresponding to the thermal unfolding of the middle part of α-Tm, and two high-cooperative transitions with maxima at ~43°C and ~51°C, which in previous studies were assigned to the thermal unfolding of C-terminal and N-terminal parts of α-Tm, respectively [3]. In good agreement with previous results [2], mutation G126R strongly diminished the enthalpy of the low-cooperative unfolding in α-Tm C190A, significantly increased (by ~40%) the enthalpy of calorimetric domain corresponding to the thermal unfolding of the C-terminal part of α-Tm, and increased (by 2–3 °C) the thermal stability of both cooperative transitions. In contrast, mutation D137L had a dramatic effect on the thermal unfolding of the whole α-Tm molecule. In this case, no appreciable low-cooperative unfolding was observed at low temperature, and more than 60% of the molecule denatured as a cooperative transition with maximum at ~51°C. However, the most surprising effect was ob-

served with the triple α-Tm mutant (α-Tm C190A/G126R/D137L). This mutant protein demonstrated new high-temperature thermal transition at 63.5°C, which has never been observed in previous DSC or CD studies on α-Tm. We can conclude that mutation D137L, unlike G126R, not only stabilizes the central part of the α-Tm molecule, but also increases the thermal stability of the other parts, and concerted action of both these mutations is expressed in further significant stabilization of the α-Tm coiled-coil structure. Thus, the central part of natural skeletal α-Tm possesses two non-canonical residues associated with its internal flexibility and instability, and their replacement by canonical residues might gradually increase stability of the α-Tm coiled-coil.

This work was supported in part by RFBR (grant 12-04-00441) and by the Program "Molecular and Cell Biology" of Russian Academy of Sciences.

References

1. Sumida, J.P., Wu, E., and Lehrer, S.S. (2008) Conserved Asp-137 imparts flexibility to tropomyosin and affects function. *J. Biol. Chem.* **283**, 6728–6734.
2. Nevzorov, I.A., Nikolaeva, O.P., Kainov, Y.A., Redwood, C.S., and Levitsky, D.I. (2011) Conserved noncanonical residue Gly-126 confers instability to the middle part of the tropomyosin molecule" *J. Biol. Chem.* **286**, 15766–15772.
3. Kremneva, E., Boussouf, S., Nikolaeva, O., Maytum, R., Geeves, M.A., and Levitsky, D.I. (2004) Effects of two familial hypertrophic cardiomyopathy mutations in α-tropomyosin, Asp175Asn and Glu180Gly, on the thermal unfolding of actin-bound tropomyosin. *Biophys. J.* **87**, 3922–3933.

THE INFLUENCE OF RESISTANCE EXERCISE INTENSITY UPON THE REGULATORS OF MYOGENESIS IN HUMAN SKELETAL MUSCLE

A. Bachinin[1], D. Popov[1], T. Miller[1], I. Kravchenko[2], V. Furalyov[2]

1: SRC of RF – Institute for Biomedical Problems Russian Academy of Sciences, 76A Khoroshevskoye shosse, Moscow, 123007, Russia

2: A. N. Bach Institute of Biochemistry, Russian Academy of Sciences, 33, build. 2, Leninsky prospekt, Moscow, 119071, Russia

Choosing an optimal contractile activity protocol associated with resistance exercise for increasing of muscle mass is an important task for rehabilitation medicine and athletic events. The aim of the present study was to investigate the influence of resistance exercise intensity upon the regulators of myogenesis in human skeletal muscle.

Methods

Seven men adapted to strength training performed two resistance exercise sessions on separate days in a randomized order: high-intensity (HI, 8 x 12 knee extensions, 75% 1RM, 7 min recovery) and moderate-intensity resistance exercise (MI, 8x12 knee extensions, 50% 1RM, 7 min recovery). The duration of muscle activity during exercise in different sessions was equalized. The blood samples

were taken before, during and 15 min after exercise sessions for determination of lactate, glucose, cortisol (C), testosterone (T), growth hormone (GH), insulin (I) and insulin-like growth factor 1 (IGF-1) concentrations. The vastus lateralis muscle biopsies were collected before, 40 min, 5 and 22 h after the exercise session and analyzed by qPCR for mRNA expression of *IGF-1EA, IGF-1EC (MGF), Myostatin, MyoD, p21* and *MyHC-2x.*

Results

The peak lactate concentration during HI was 5.8(5.0-7.3) mM that was significantly higher ($p<0.05$) than during MI: 2.6(2.5-4.3) mM sessions. The concentrations of glucose during exercise and I, IGF-1 after exercise did not change and did not differ between sessions. The concentration of C after HI was higher ($p<0.05$) than after MI.

Myostatin mRNA abundance decreased ($p<0.05$) 22 h after HI: 0.1 (0.08-0.23)-fold relative to initial level, and did not change during recovery after MI session. Difference ($p=0.06$) of Myostatin mRNA abundance was found to be higher 5 h after HI exercise then after MI: 0.6(0.16-1.27)- and 1.3(0.28-6.6)-fold relative to initial level, respectively. The expression of IGF-IEA, IGF-IEC (MGF), MyoD p21 and MyHC-2x mRNA did not change during recovery and did not differ between exercise sessions as well.

Discussion

The current study demonstrated that in skeletal muscle of males adapted to strength training Myostatin mRNA expression during recovery was associated with intensity of resistance exercise.

The work is supported by the RFBR grant # 12-04-01668-a.

T-WAVE ALTERATIONS OF THE ELECTROCARDIOGRAM UNDER ISCHEMIC CONDITIONS IN THE CARDIAC MUSCLE: A MODEL STUDY

O.V. Baum[1], V.I. Voloshin[1], L.A. Popov[1], G.A. Muromtseva[2], and S.K. Prilutskaya[1]

[1] Institute of the Theoretical and Experimental Biophysics, Russian Academy of Sciences, Pushchino, Moscow Region, 142290, Russia;

[2] State Research Center of Prophylactic Medicine, Russian State Committee for Medical Technologies, Moscow, 101990 Russia

Introduction. One of the leading biomedical problems of today is coronary heart disease (CHD). The most important risk factor for sudden death in patients with CHD is myocardial ischemia. That is why this disease is a long-term priority of modern medicine. Therefore, it is important to develop methods of noninvasive diagnostics of ischemia, especially at the early stage of the disease, on the basis of new data on heart biophysics and physiology. Ischemia causes complex changes in electrophysiological properties of the cardiomyocytes, which proceed in several steps: changing the duration of phases of the transmembrane action potential (TAP); redistribution of the TAP durations on the surface of the

electrically active myocardium; local reduction of the resting potential and amplitude of the TAPs.

Perspective research methods in this area of knowledge are methods of mathematical and computer modeling [1], in particular, an analysis of the T-wave morphology in terms of different models, including some indexes of symmetry for its ascending and descending slopes [2]. In connection with the great scatter of opinions and hypotheses regarding the behavior of TAP parameters in development of ischemia, its modeling presents a complicated problem. An important aspect of solving the problem is development of the corresponding methodology.

Aim. The main objective of this study is to investigate with the help of computer models trends of alterations of the morphological characteristics of the T wave under changes of the TAP parameters in the ischemic area for the purpose of increasing the information content of algorithms for myocardial ischemia identification.

Methods. Several versions of the first approximation for "scenarios" of the TAP parameters changes into the ischemic zone under ischemia evolution as well as corresponding protocols of model experiments have been developed. Computer experiments were carried out using our system for 3D computer simulation of the heart electrical activity [3]. For our study, as a model for evaluation measurements of the T wave morphology in the simulation of myocardial ischemia by a local transformation of the TAP-curve form, we used a heart model some of whose parameters are reported in [1]. The initial ("normal") duration of TAPs on the outer and inner surfaces of the left ventricle were respectively 250 and 300 ms. The size of the modeled subendocardial lateral ischemic area (I) was about 10% of the total endocardium surface area in the left ventricle and consisted of 80 elements with the space model unit of 2 mm (Fig. 1).

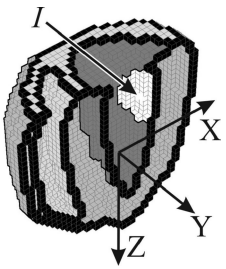

Fig. 1.

The following variants for dynamics of the TAP parameters have been separately considered: **A**. change in the duration of the plateau phase (*phase 2*) with a constant slope of the fast repolarization phase (*phase 3*); **B**. change in an amplitude of the plateau phase (at the same time, the total TAP duration is kept constant); **C**. shortening a duration of the phase 3 and changing its slope; **D**. decrease of the plateau duration with simultaneous changing the phase 3 steepness.

Temporal and amplitude parameters of the TAP varied by steps of 25 ms and 20 mV accordingly (see Fig. 2 as an example of the variant_1 for the TAP parameters dynamics, where 0,1,2,3,4,5 are experiment numbers).

Results and Discussion. Shown in Fig. 3 are a simulated initial ECG signal for lead I and alterations of its ST-T morphology under changing the transmural dispersion of the TAP duration in accordance with a protocol of the computer experiment.

For a medical evaluation of the ST-T interval changes the simulated ECGs were analyzed in terms of the Minnesota Code (MC) with the aid of the "Model_Uran" program, and for an initial quantitative estimation of the T wave symmetry the β_T parameter [2] was calculated as a ratio of the maximum values for the derivative on the left and right slopes of the T wave.

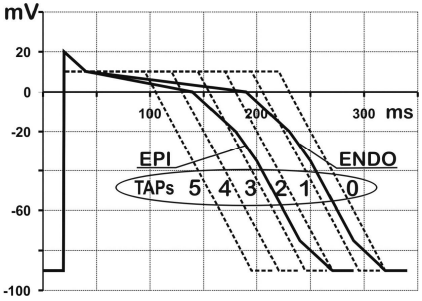

Fig. 2.

Just as for real ECGs in [2], some other parameters of the T-wave were also calculated in this work that would characterize its symmetry and/or additional properties of the repolarization process:

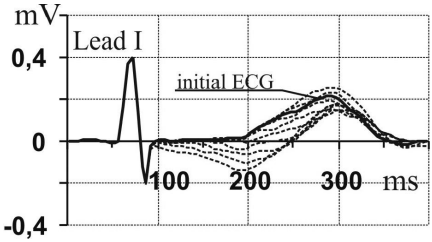

Fig. 3.

– difference between the left and right parts of the triangle area, formed tangent lines to the left and right slopes of the T wave, with an apex in crossing point between the lines and with a base in their crossing points with the time axis; the difference is weighted by sum of the area parts (Asim_1);
– weighted difference of the two parts of the T wave area at the left and right of T apex point in limits of the generalized T wave durations (Asim_2);
– some analogues of such statistical estimations as asymmetry and excess at formal consideration of the T wave as distribution of a conditional random value (Asim_3 and Exc);
– values and ratios of some intervals into the cardiocycle (JTa/JT, JTa/QT, TpTe, TpTe/JTa);
– displacement of the ST segment in time point of 80 ms from J point (ccST80);
– scalar interpretation of the ventricular gradient (G);
– angle of the integral vector for the T wave in the frontal plane;
– vector interpretation of the ventricular gradient **G** (QRS_T angle) and some others.

As an analysis of the results has shown (Fig. 4), some values of the different parameters obtained have appeared both expected according with theoretical conceptions and slightly paradoxical, that requires further investigations.

When the chosen anatomical position of the heart and localization of ischemia area, significant changes in the shape of the T wave were observed in the frontal leads (except Lead III), as well as in leads V3, V4, V5. The most sensi-

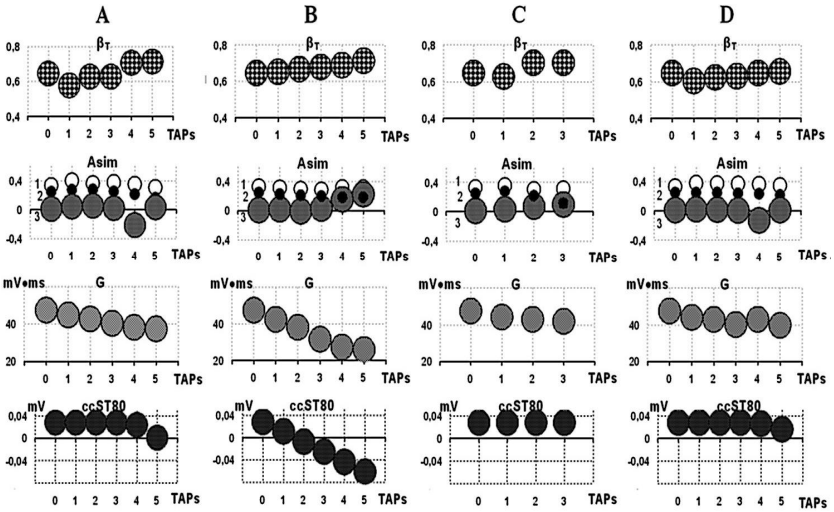

Fig. 4. Alterations of quantitative characteristics for the T waves simulated according to four versions (A,B,C,D) of dynamics for TAPs parameters (0,1,2,3,4,5 are experiment numbers plotted on the abscissa).

tive ECG parameters in this case are βT, G, and ssST80. Perspective parameters are also a ratio of average signal velocity on the left and right slopes of the T wave (VmL/VmR) and a ratio of time intervals between the T wave apex and points, where derivatives to the left and to the right of the apex are maximal (T1L/T1R). Using these parameters in a high-quality ECG registration can potentially help to detect such abnormalities, which are usually hidden from a physician under traditional ECG analysis in the time domain.

With regard to parameters such as “Asim”, it is necessary to formalize the concept of “T wave symmetry” and carry out a comparative study for quantitative measures of their evaluation and information content on samples “Norm” and “Ischemia” for real and simulated electrocardiosignals.

It should also be noted that the method of phase space (an amplitude of the signal and rate of its changing as a base for calculating the β_T [2]) is far from exhaustion. There are several points which require clarification and development of the method in the n-dimensional domain with using models of the heart electrical activity for a comprehensive assessment of the electrophysiological state of myocardium.

Conclusion. Obtained at this stage results are important for understanding the mechanisms of the ST-T interval genesis in ischemia and are of interest for the biophysically based development of algorithms to identify an electrophysiological state of the heart. Systemic comparative studies on the basis of modeling the ischemia of various localization, extensiveness, and degree of expression are necessary.

References

1. Baum O.V., Voloshin V.I., Popov L.A. Biophysical models of the heart electrical activity. – Biofizika. 2006 Nov-Dec; 51(6):1069-87.
2. Baum O.V., Chaikovsky I.A., Popov L.A., Voloshin V.I., Fainzilberg L.S., Budnik M.M. Electrocardiographic image of myocardial ischemia: real measurements and biophysical models. – Biofizika. 2010 Sep-Oct; 55(5):925-36.
3. Baum O.V., Voloshin V.I., Popov L.A. Realization of biophysical models for the cardiac electrical activity. – Biofizika. 2009 Jan-Feb; 54(1):97-113.

ROLE OF PHENOL ACIDS OF MICROBIAL ORIGIN IN THE DYSFUNCTION OF MITOCHONDRIA AND NEUTROPHILS IN THE SYSTEMIC INFLAMMATORY RESPONSE SYNDROME

N.V. Beloborodova[1], I.T. Bairamov[1], A.Yu. Olenin[2], V. Shubina[3], V.V. Teplova[3], N.I. Fedotcheva[3]*

[1]Research Institute of General Reanimatology, Russian Academy of Medical Sciences, Moscow, Russia,
[2]Lomonosov Moscow State University, Department of Chemistry, Moscow, Russia,
[3]Institute of Theoretical and Experimental Biophysics, Russian Academy of Sciences, Moscow region, Pushchino, Russia;
nfedotcheva@mail.ru

The systemic inflammatory response syndrome (SIRS) is the most frequent complication in critical states that develop as a result of severe diseases, traumata, and sepsis. The development of SIRS is a complex process, which is accompanied by hematological, hemodynamic, and metabolic disorders [1-3]. According to these disorders, two stages of SIRS are recognized: the initial proinflammatory stage, which involves the activation of neutrophils, tissue macrophages, an increase in the production of cytokines and reactive oxygen species (ROS), and the later stage, which is characterized by a decrease in the level of cytokines and neutrophils, the appearance of the signs of polyorganic insufficiency and persistent tissue hypoxia. The mechanisms of the development of these conditions remain still obscure. It was assumed that the level of oxidative stress is crucial in the genesis and outcome of SIRS [4]. Along with neutrophils, mitochondria, the main producers of ROS in tissues, play a very important role in the production of ROS in tissues.

It was shown that, in critical states, such as pneumonia associated with artificial lung ventilation and sepsis, a decrease in the amount of phenylacetic and phenylpropionic acids and a multiple increase in the level of hydroxyphenylacetic, phenyllactic, and hydroxyphenyllactic acids relative to the profile of these metabolites in healthy people occur [5]. In this work, we studied the role of low-molecular-weight phenolic acids of microbial origin in the dysfunction of mitochondria and neutrophils. For this purpose their effect on the production of ROS in mitochondria and neutrophils was investigated.

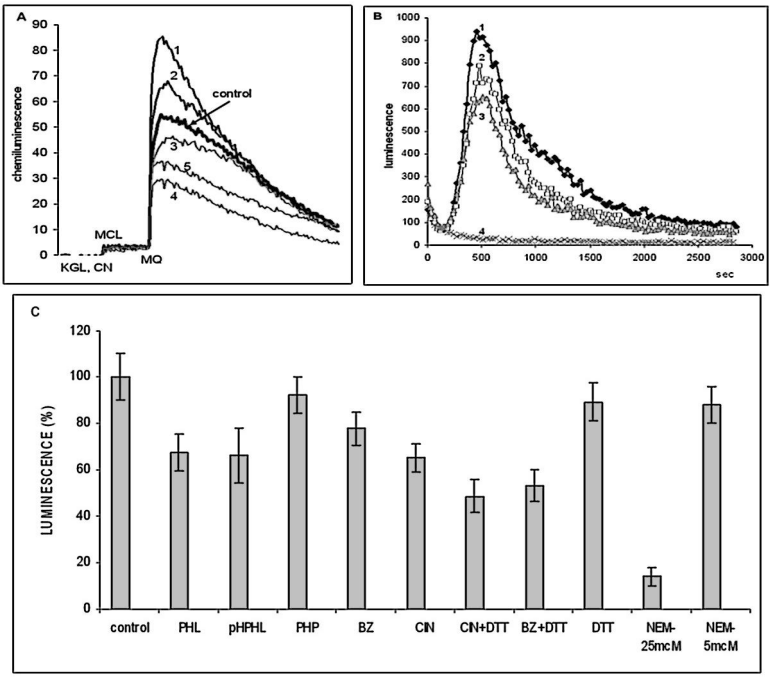

Effect of phenolic acids on ROS production in mitochondria and neutrophols. A-chemiluminescence of (MCLA) in mitochondria in the presence of the respiration inhibitor cyanide (CN) и redox-cycler menadione (MQ), 1 - phenylpropionate (PHP), 2 - phenylacetate (PHA), 3 - p-hydroxyphenylpropionate (pHPHP), 4 - phenyllactate (PHL), 5 - p-hydroxyphenyllactate (pHPHL), 100 μM; B – chemiluminescence of luminol in PMA-activated neutrophils, 1 - control, 2- benzoic acid (BZ), 3 - cinnamic acid (CIN), 100 μM, 4 - NEM, 25 μM; C - effect of phenolic acids and thiols reagents (DTT, 1 mM and NEM, 5 и 25 μM) on ROS production in neutrophils.

It was found that phenylpropionic and phenylacetic acids, as well as cinnamic and benzoic acids, which are the products of anaerobic metabolism of aromatic compounds, stimulated the superoxide anion and hydrogen peroxide production in liver mitochondria. In contrast, they inhibited the production of ROS by activated neutrophils. Dithiotreitol removed the effect of cinnamic and benzoic acids in mitochondria, but not in neutrophils. The effect similar to the effect of phenolic acids was produced by the SH-reagent N-ethylmaleimide (NEM), which activated the superoxide formation in mitochondria and inhibited it in neutrophils.

The production of these low-molecular-weight phenolic acids by the members of the main groups of human anaerobic flora has been studied by gas chromatography–mass spectrometry (GC–MS). It was shown that, along with lactate, bifidobacteria and lactobacilli produced in vitro considerable amounts of phenyl-

lactic and *p*-hydroxyphenyllactic acids (64.9 and 35.4 μg/ml, respectively). *Clostridia*, whatever the species, produced phenyllactic acid, and *C. sporogenes*, as distinct from *C. perfringens*, produced great quantities of phenylpropionic and *p*-hydroxyphenylpropionic acids (182.7 and 129.5 μg/ml, respectively). *Eubacterium lentum* produced phenyllactic acid at a high concentration (137.2 μg/ml). It was demonstrated for the first time that the concentrations of these metabolites excreted by bacteria, in particular enterobacteria (*Klebsiella pneumonia, Escherichia coli*, and *Staphylococci*), considerably vary depending on the form of their growth: as plankton or biofilms.

When affecting targets in the organism, microbial metabolites can enhance the negative effect of the inflammatory syndrome. Other phenylcarboxylic acids, in particular phenyllactate and hydroxyphenyllactate, which decrease ROS production in both mitochondria and neutrophils, can have the protecting effect on organs and tissues. The increase in phenyllactate and hydroxyphenyllactate concentrations correlates well with an increase in the lactate level, which makes possible their application as biomarkers of the polyorganic insufficiency in the progress of SIRS. The dysfunction of mitochondria and polyorganic insufficiency are reversible processes since SIRS is not accompanied by the necrosis of cells and tissues. Owing to this, the mitochondrial functions are completely restored in the case of favorable course. Recent trends are towards the use of mitochondrial therapy aimed at providing cells and tissues with particular substrates, cofactors, and antioxidants. In some cases, the application of antioxidants in induced sepsis led to the enhancement of oxidative phosphorylation and a decrease in the ROS formation in mitochondria as well as to a partial restoration of hemodynamic parameters and functions of the organism [6,7]. In addition, antioxidants, in particular N-acetylcysteine, were effective in decreasing ROS production in endothelial and epithelial cells [8]. However, antioxidants are more effective when applied prior to the appearance of the signs of polyorganic insufficiency since at later stages of SIRS development antioxidants become almost ineffective. These data enable one to consider mitochondria as a target for the correction of polyorganic insufficiency, especially if specific stages of SIRS development are taken into account.

This work was supported by the Ministry of Education and Science (GK no. 16.512.11.2227).

References

1. Sriskandan S., Altmann D.M. The immunology of sepsis. J. Pathol. 2008. 214(2): 211-23.
2. Bhatia M, Moochhala S. Role of inflammatory mediators in the pathophysiology of acute respiratory distress syndrome. J Patholl 2004, 202(2):145-56.
3. Fink M.P. Bench-to-bedside review: Cytopathic hypoxia. Critical Care. 2002, 6:491-499.
4. Rudiger A, Stotz M, Singer M. Cellular processes in sepsis. Swiss Med Wkly. 2008, 138(43-44):629-34.
5. Белобородова Н.В., Архипова А.С., Белобородов Д.М., Бойко Н.Б., Мелько А.И.,

Оленин А.Ю. Хроматомасс-спектрометрическое определение низкомолекулярных ароматических соединений микробного происхождения в сыворотке крови больных сепсисом // Клиническая лабораторная диагностика. 2006. Т. 2. С. 3–6.
6. Víctor VM, Espulgues JV, Hernández-Mijares A, Rocha M. Oxidative stress and mitochondrial dysfunction in sepsis: a potential therapy with mitochondria-targeted antioxidants. Infect Disord Drug Targets. 2009, 9(4):376-89.
7. Lowes DA, Galley HF. Mitochondrial protection by the thioredoxin-2 and glutathione systems in an in vitro endothelial model of sepsis. Biochem J. 2011 May 15;436(1):123-32.
8. Lowes DA, Almawash AM, Webster NR, Reid VL, Galley HF. Melatonin and structurally similar compounds have differing effects on inflammation and mitochondrial function in endothelial cells under conditions mimicking sepsis. Br J Anaesth.2011, 107(2):193-201.

THE MITOCHONDRIAL PALMITATE/Ca^{2+}-INDUCED PORE AS A NONSPECIFIC SYSTEM OF Ca^{2+} EFFLUX

K.N. Belosludtsev, A.S. Trudovishnikov, N.V. Belosludtseva, G.D. Mironova

Institute of Theoretical and Experimental Biophysics RAS, Institutskaya, 3, Pushchino, 142290, Russia;

Pushchino State Natural Science Institute, Prospekt Nauki, 3, Pushchino, 142290, Russia

Mitochondrial Ca^{2+} uptake and release play a fundamental role in the control of different physiological processes, such as cytoplasmic Ca^{2+} signalling, ATP production and hormone metabolism, while dysregulation of mitochondrial Ca^{2+} handling triggers the cascade of events that lead to cell death. The balance between Ca^{2+} influx and efflux across mitochondrial inner membrane establishes mitochondrial Ca^{2+} homeostasis. The basic mechanisms of mitochondrial Ca^{2+} homeostasis have been firmly established for decades, but the molecular identities of the channels and transporters responsible for Ca^{2+} uptake and release remain unclear [1]. It is well-known, that the major player responsible for mitochondrial Ca^{2+} uptake is electrophoretic ruthenium red (RR)-sensitive Ca^{2+} uniporter. Its structure was identified very recently [2]. In addition, several other pathways are considered to exist for mitochondrial Ca^{2+} influx. They are rapid mode (RaM) of mitochondrial Ca^{2+} transport, mitochondrial ryanodine receptor (mRyR), uncoupling proteins 2 and 3, and Letm1 mitochondrial Ca^{2+}/H^{+} antiporter [1-3].

The molecular structures of the transporters responsible for Ca^{2+} extrusion from mitochondria are more obscure. A Na+-dependent (mitochondria of excitable tissue (brain and heart)) and a Na+-independent (mitochondria of non-excitable tissue (liver and kidney)) mechanism of Ca^{2+} efflux are found in mitochondria. But if the molecular structure of transporter responsible for the Na^{+}/Ca^{2+} antiport was identified very recently [4] then a structure responsible for the Na^{+}-independent mechanism does not be still remain. Today it is considered

that the Na^+-independent mechanism of mitochondrial Ca^{2+} efflux may mediate a mysterious H^+/Ca^{2+} exchanger and cyclosporine A (CsA)-sensitive mitochondrial permeability transition pore (MPTP) whose transient and reversible opening could be an energetically favorable way to release mitochondrial Ca^{2+} in a Na^+-independent manner [1]. However, detecting of such state of CsA-sensitive pore is very difficult.

In this work we supposed that the system responsible for mitochondrial Ca^{2+} release can be the lipid pore induced by palmitic acid and Ca^{2+}. The opening of this pore does not inhibited by CsA. Mitochondrial lipid palmitate/Ca^{2+}-induced pore opens temporarily and after the pore closure the membrane integrity and mitochondrial membrane potential will be restored [5,6]. The mechanism of palmitate/Ca^{2+}-induced pore opening may be explained in view of our recent data that binding of Ca^{2+} to palmitic acid leads to its segregation into distinct solid membrane domains. This is in good agreement with the theory of lipid pore formation upon chemotropic phase transition [7,8]. Earlier we found that the lipid palmitate/Ca^{2+}-induced pore can participate in mitochondrial Ca^{2+} recyclization and the pore formation can result from an activation of mitochondrial Ca^{2+}-dependent phospholipase A_2 [9].

We suppose that the release of Ca^{2+} from mitochondria after the ion accumulation in organelles is mediated by next mechanism. Intramitochondrial Ca^{2+} activates phospholipase A_2, levels of free fatty acids (including palmitic acid) is elevated, and the formation of lipid palmitate/Ca^{2+}-induced pores happens. The opening of this pore leads to the release of mitochondrial Ca^{2+} ions. If such mechanism is feasible then the release of Ca2 + from mitochondria must be inhibited by phospholipase A_2 inhibitors and increased by the addition of palmitic acid. To prove this hypothesis, next experiments were carried out. An typical experimental protocol of the mitochondrial Ca^{2+} efflux is to load liver mitochondria with a single Ca^{2+} pulse and then selectively blocking with Ruthenium Red ((RR) inhibitor of Ca^{2+} uniporter) (fig. 1A). All the experiments were carried out in the presence of 1 μM CsA to prevent the formation of MPT pore.

Fig. 1 shows that when Ca^{2+} was added to energized mitochondria, mitochondrial Ca^{2+} uptake was rapid and a steady state representing the balance between Ca^{2+} uptake and efflux rates was achieved approximately 3-4 min after the pulse. The unidirectional Ca^{2+} efflux rate was then measured after application of RR (fig. 1, trace 1). The mitochondrial Ca^{2+}-dependent phospholipase A_2 inhibitor 14 μM $AACOCF_3$ suppressed the RR-sensitive Ca^{2+} release from mitochondria (Fig. 1A). At the same time inhibitors of the Ca^{2+}-independent PLA_2 (BEL) were ineffective.

It should be noted that in a Na^+-free medium $AACOCF_3$ blocked the RR-dependent Ca^{2+} release from brain mitochondria indicating the similarity of mechanisms of Ca^{2+} release from mitochondria isolated from excitable and non-excitable tissues (data not presented).

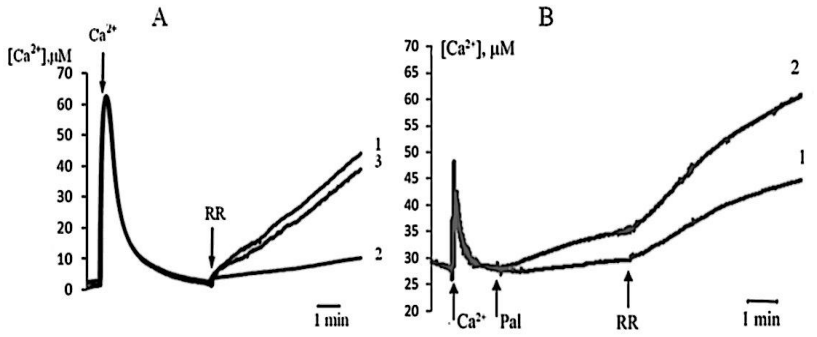

Fig. 1. The effect of phospholipase A_2 inhibitors (A) and palmitic acid (B) on RR-sensitive Ca^{2+} efflux from liver mitochondria.

Addition: 100 μM Ca^{2+}, 1 μM RR; A) 1 – control, 2 – 15 μM $AACOCF_3$, 3 – 10 μM BEL; B) 1 – control; 2 – 15 μM Pal.

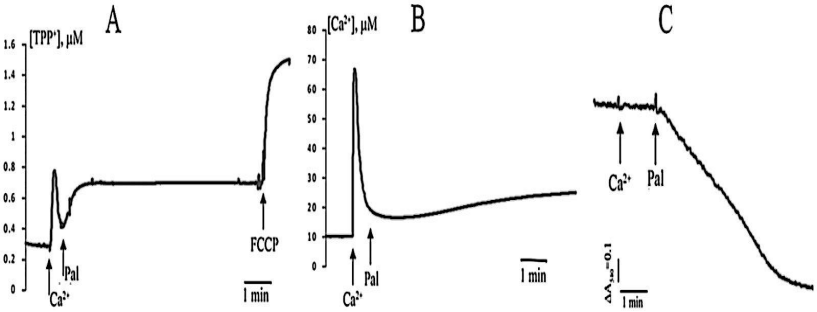

Fig. 2. The changes in Δψ (A), $[Ca^{2+}]$ (B) and CsA-insensitive swelling of mitochondria (C) induced by 70 μM Ca^{2+} and 15 μM Pal.

The addition of palmitic acid after mitochondrial Ca^{2+} uptake resulted in little efflux of Ca^{2+} ions from mitochondria even without the addition RR (fig. 1B). Under these conditions, a Δψ slightly decreased and a large-amplitude mitochondrial swelling was observed (fig. 2). It is suggested that under these conditions the mitochondrial CsA-insensitive lipid pore induced by palmitic acid and Ca^{2+} opens. After the addition of RR Ca^{2+} was rapidly released from mitochondria. The rate of mitochondrial palmitate-induced RR-sensitive Ca^{2+} efflux was higher than in case of mitochondrial RR-sensitive Ca^{2+} release in the absence of palmitic acid (fig. 1B).

Thus we can assume two explanations of our results. 1) RR-sensitive Ca^{2+} release from mitochondria is mediated by the opening of lipid palmitate/Ca^{2+}-induced pore. In view of this mechanism one can explain the effects of Ca^{2+}-dependent phospholipase A2 inhibitors. Inhibitors of Ca^{2+}-dependent phospholi-

pase A_2, which prevent the Ca^{2+}-induced accumulation of free fatty acids (including palmitic acid) in the mitochondrial membrane, suppress the formation of palmitate/Ca^{2+}-induced pores in mitochondria and Ca^{2+} release via these pore from organelles. 2) palmitic acid (exogenous or endogenous nature) may activate H^+/Ca^{2+} exchanger which results in an increased release of Ca^{2+} from mitochondria. However, the molecular structure responsible for H^+/Ca^{2+} exchange does not be still identified. Moreover, the activation of H^+/Ca^{2+} antiporter cannot explains the mitochondrial swelling in the presence of palmitic acid and Ca^{2+}. Therefore in this case one could tell about a sum of processes induced by palmitic acid (the activation of H^+/Ca^{2+} antiporter, the opening of lipid pore). As a result it is very difficult to distinguish what structure is responsible for the Ca^{2+} efflux from mitochondria.

In our biased opinion, the simplest explanation is that the mitochondrial lipid pore induced by palmitic acid and Ca^{2+} can participate in mitochondrial Ca^{2+} cycle as non-specific system of Ca^{2+} efflux from mitochondria. Based on the facts that this pore is capable to spontaneously close and after its closure a functional integrity of mitochondria will be restored, mitochondrial lipid palmitate/Ca^{2+}-induce pore could be considered as another potential player in the mechanism of mitochondrial Ca^{2+} homeostasis.

This work was supported by grants from RFBR (10-04-00920-a, 12-04-00430-a), DPDST (4.3010.2011) and President of Russian Federation for young PhD (МК-145.2012.4).

References

1. Gunter T. and Sheu S. (2009) Biochem. Biophys. Acta, 1787, 1291-1308.
2. Baughman T. et al. (2011) Nature, 476, 341-345.
3. Pan S. et al. (2011) Sci. China Life Sci., 54, 763-769.
4. Palty R. et al. (2010) Proc. Natl. Acad. Sci. USA, 107, 436-441.
5. Mironova G.D. et al. (2004) J. Bioener. Biomembr., 36, 171-178.
6. Sultan A., and Sokolove P. (2001) Arch. Biochem. Biophys., 386, 31-51.
7. Agafonov A. et al. (2007) J Membr. Biol., 21, 57-68.
8. Антонов В.Ф., Шевченко Е.В. (1995) Вестн. РАМН, 10, 48-55
9. Mironova G. et al., (2007) J. Bioener. Biomembr., 39, 167-174.

STUDY OF CYTOTOXICITY OF FULLERENE C_{60} DERIVATIVES

A.G. Bobylev [1], A.D. Okuneva [1,2], L.G. Bobyleva [1], I.S. Fadeeva [1], R.S. Fadeev [1], Z.A. Podlubnaya [1,2]

[1]Institute of Theoretical and Experimental Biophysics, Russian Academy of Sciences, ul. Institutskaya 3, Pushchino, Moskow Region, 142290 Russia; [2]Pushchino State University, pr. Nauki 3, Pushchino, Moscow Region, 142290 Russia

Currently, the fullerenes are considered as potential drugs due to such unique properties as the inhibition of HIV-1 protease, photomodification of DNA, neuroprotection, high antioxidant activity and others [1-5]. The first experiments

with fullerenes were directed to the study of their toxic properties. The effect of colloidal solutions of C_{60} fullerenes on the growth of 22 different bacterial lines was studied. However, in this study the negative effect of fullerene on the growth of bacteria was not observed. The same results were obtained in the study on toxicity of fullerenes in human cell cultures of monocytes, leukocytes and macrophages [6]. Other authors also confirm the absence of toxic properties of fullerenes [1]. On the contrary there are evidences of their toxicity [7-11].

Earlier we revealed the ability of some fullerene C_{60} derivatives to destroy amyloid fibrils of muscle X-protein and brain Aβ(1-42)-peptides *in vitro* [12-16]. Amyloid fibrils of Aβ(1-42)-peptide participate in the pathogenesis of Alzheimer's disease. Our experiments with muscle actin filaments showed that only sodium salt of polycarboxylic derivative of fullerene C_{60} was able to destroy these filaments [17]. We carried out also the comparative study on the cytotoxicity of water-soluble derivatives of C_{60} fullerene in cell culture of human larynx carcinoma HEp-2.

It was showed that sodium salt of polycarboxylic derivative of fullerene C_{60} in the concentration range 0.016–2 mg/ml had a pronounced toxic effect on HEp-2 cells, which excludes its further use on biological objects.

We showed that complexes of C_{60} fullerene with polyvinylpyrrolidone (m.w. polyvinylpyrrolidone 10000 and 25000) did not produce toxic effect on HEp-2 cells. In this cell culture 100% survival was observed after in the presence of the complexes C_{60} fullerene with polyvinylpyrrolidone and polyvinylpyrrolidone polymer (as a control) in the concentration range of 0.016–2 mg/ml. C_{60}-alanine was also non-toxic in the same range of concentration.

We investigated the toxicity of C_{60}-NO_2-proline. This C_{60} derivative in the concentration range of 0.001-0.2 mg/ml did not have a toxic effect on the HEp-2 cells culture.

We were unable to investigate the cytotoxicity of C_{60}-$(NO_2)_2$-proline and C_{60}-NO_2-proline-NO_2, due to their ability to aggregate with each other rapidly and irreversibly and to loss of the solubility. The absence of toxicity of these water-soluble C_{60} derivatives opens perspectives for the development on their basis effective and non-toxic drugs.

This work was supported by Program of Presidium RAS "Fundamental sciences - for medicine", 2012 and by grants RFBR № № 09-04-01161, 10-04-00141 and also by the Federal Agency for Science and Innovations within the Program "Research and scientific-pedagogic personnel of innovative Russia" (State contract nos. 02.740.11.0710).

References

1. Jensen A.W., Wilson S.R., Schuster D.I. // Bioorg. Med. Chem. 1996. V. 4. P. 767-779.
2. Da Ros T., Prato M. // Chem. Commun. 1999. P.663-669.
3. Wilson S.R., Kadish K., Ruoff R. // Wiley, New York. 2000. P. 437–465.
4. Dugan L.L., Gabrielsen J.K., Yu S.P., Lin T.S., Choi D.W. // Neurobiology of Disease. 1996. V. 3. P. 129-135.

5. Chiang L.Y., Lu F.-J., Lin J.-T. // J. Chem. Soc. Chem. Commun. 1995. V.12. P. 1283-1284.
6. Chiron J., Lamande J., Moussa F., Trivin F., Ceolin R. // Ann. Pharm. Fr. 2000. V. 58. P. 170-175.
7. Oberdörster E. // Environmental Health Perspectives. 2004. V. 112. P. 1058-1062.
8. Sayes C.M., Liang F., Hudson J.L., Mendez J., Guo W., Beach J.M., Moore V.C., Doyle C.D., West J.L., Billups W.E., Ausman K.D., Colvin V.L. // Toxicology Letters. 2005. V. 161. P. 135–142.
9. Sayes C.M., Gobin A.M., Ausman K.D., Mendez J., West J.L., Colvin V.L. // Biomaterials. 2005. V. 26. P. 7587-7595.
10. Lyon D.Y., Adams L.K., Falkner J.C., Alvarez P.J.J. // Environ. Sci. Technol. 2006. V. 40. P. 4360-4366.
11. Fortner J.D., Lyon D.Y., Sayes C.M., Boyd A.M. // Environ. Sci. Technol. 2005. V. 39. P. 4307-4316.
12. Marsagishvili L.G., Bobylev A.G., Shpagina M.D., Troshin P.A., Podlubnaya Z.A. // Biofizika. 2009. V. 54(2). P. 202-205.
13. Bobylev A.G., Marsagishvili L.G., Shpagina M.D., Подлубная З.А. // Tehnologii zivyh sistem. 2009, V. 6(7). P. 46-53.
14. Bobylev A.G., Marsagishvili L.G., Shpagina M.D., Romanova V.S., Kotelnikova R.A., Podlubnaya Z.A. // Biofizika. 2010. V. 55(3). P. 394-399.
15. Bobylev A.G., Marsagishvili L.G., Podlubnaya Z.A. // Biofizika. 2010. V. 55(5). P. 780-784.
16. Bobylev A.G., Kornev A.B., Bobyleva L.G., Shpagina M.D., Fadeeva I.S., Fadeev R.S., Deryabin D.G., Balzarini J., Troshin P.A., Podlubnaya Z.A. // Organic & Biomolecular Chemistry. 2011. V.9. P. 5714-5719.
17. Bobylev A.G., Shpagina M.D., Bobyleva L.G., Okuneva A.D., Piotrovsky L.B., Podlubnaya Z.A. // Biofizika. 2012. (in press).

ROLE OF EXTRACELLULAR AND INTRACELLULAR Ca^{2+} IN CONTRACTILE RESPONSES MEDIATED BY M3-RECEPTORS IN CHICK AMNION

O.V. Boiko

Kol'tsov Institute of Developmental Biology, Russian Academy of Sciences, Vavilov St., 26, Moscow, 119334, Russia

Carbachol causes dose-dependent M3 receptor-mediated contractions in non-innervated chick amnion. Isometric contractions of the isolated 11-14-day amnion, induced by a single submaximal concentration of carbachol (50 μM), were recorded. The reaction consisted of a sustained tonic contraction with superimposed rhythmic activity. Nifedipine (0.1 μM), a blocker of voltage-dependent L-type Ca^{2+} channels, completely abolished both spontaneous and carbachol-induced rhythmic contractions of the chick amnion. The tonic response to carbachol was reduced up to 60% after 10 minutes exposure to 0.1 μM nifedipine, and up to 30% after the action of 1 μM nifedipine, compared with respective controls. Thus, rhythmic amniotic contractions are largely activated by Ca^{2+}, entering through the voltage-dependent L-type calcium

channels. Nifedipine-insensitive component of the tonic reaction may be provided by calcium from intracellular sources. Incubation with thapsigargin (2 μM, 20 min), an inhibitor of cytoplasmic Ca^{2+}-ATPase, which depletes Ca^{2+} stores, reduced the tonic response to carbachol up to 35-40%. Consequently, tonic contractions of the amnion depend on intracellular calcium release. Influx of calcium via L-type channels is often accompanied by the release of stored calcium through the ryanodine receptors. Ryanodine (1 μM), an agonist of ryanodine receptors at this concentration, caused an increase in the amplitude of the contractile response to carbachol by activation of stored Ca^{2+} release. Ryanodine at higher concentrations (5-20 μM) dose-dependently inhibited the tonic response to carbachol, as well as the amplitude of contractions. Incubation with ryanodine (10 μM, 5 min) reduced the tonic response to carbachol 3-fold compared to control. In the presence of ryanodine (10 μM), nifedipine (0.05 microM) completely blocked the reaction to carbachol in amnion.

THE CHANGES OF DIAPHRAGM AND GASTROCNEMIUS MUSCLE IN RATS AFTER AEROBIC TREADMILL TRAINING

A.A. Borzykh[1], G.S. Boleeva[1,2], A.A. Andreev-Andrievskii1[1,2], O.S. Tarasova[1,2], A.P. Sharova[1], O.L. Vinogradova[1]

[1]SRC RF - Institute for Biomedical Problems RAS, Khoroshevskoe shosse 76A, Moscow, 123007, Russia

[2]Biological Department, Lomonosov Moscow State University

Respiratory muscles are rhythmically active during whole life of the organism. Due to such special function respiratory muscles differ from locomotory muscles by their structure and metabolic characteristics. Therefore, mechanisms of adaptation to exercise training may be also different in these muscles. Importantly, the effects of exercise on muscle tissue are critically dependent on the training protocol. Therefore, the aim of this work was to compare the effects of different treadmill training protocols on myosin composition, fiber cross-section area and activity of Krebs cycle enzymes in medial head of gastrocnemius muscle (GM) and costal part of diaphragm (DIA).

Male Wistar rats were treadmill trained 6 days/wk during for 8 wks. We used two exercise protocols, which differed in duration of training session and total performed work. In the first exercise training protocol (ET1) the rats were running 60 min/day at a speed of 25 m/min. In the second training protocol (ET2) running speed was 18 m/min but the duration of training session was increased from 60 min to 85.5 min/day, consequently, the total work was increased by 15%. Control rats were walking on the treadmill at 10 m/min twice weekly to maintain running skill.

During the running sessions lactate concentration was measured electrochemically in blood microsamples taken from the tail tip. At the beginning and the end of ET1 protocol the changes of systemic aerobic performance were evaluated by estimating maximal oxygen consumption (VO_{2max}) and blood lactate accumulation (lactate threshold) in the test with increasing load. Oxygen consumption was

determined using metabolic treadmill and open circuit calorimeter (Columbus Industries, USA). In ET2 only lactate threshold was determined, because its change after ET1 was more prominent than the change of VO_{2max}.

After completion of the training protocols expression of MHC isoforms, cross-section area and succinate dehydrogenase activity (SDH) were studied in individual fibers by immunohistochemistry. Citrate synthase (CS) activity was measured in whole muscle homogenates spectrophotometrically.

During the training sessions blood lactate concentration did not exceed 2.5 mmol/L confirming mainly aerobic energy supply of working muscles. Both training protocols increased aerobic performance of the rats. After ET1 protocol VO_{2max} in trained rats was 15% higher compared to controls. Rightward shifts of the running speed – lactate concentration relationships were observed after both ET1 and ET2 protocols.

In sedentary rats CS activity in DIA was 1.8 times higher compared to GM, whereas CSA of both fast and slow fibers in DIA was less than in GM. Relative contributions and cross-section areas of either slow or fast fibers in both muscles were not changed after ET1. On the other hand in red part of GM a significant increase of SDH activity was observed in both types of muscle fibers, whereas no increase of SDH activity was observed in DIA.

After ET2 protocol CS activity increased in GM, but not in DIA. However, ET2 resulted in prominent changes of DIA: an increase of relative contributions of slow and hybrid fibers as well as decrease of slow and fast fiber CSA. In contrast to DIA, the composition and fiber CSA were not changed in GM.

Our results show that the adaptation to aerobic exercise training is different in GM and DIA. Activity of Krebs cycle enzymes increases in GM after both training protocols. Since even in sedentary animals DIA is characterized by a high oxidative potential, exercise-induced changes of this muscle are observed only after training with a longer duration protocol (ET2) and carried out by the different mechanisms, which should improve DIA aerobic performance. A smaller fiber cross-section area is favorable for the supply of working DIA by oxygen and substrates of aerobic metabolism. A higher fraction of slow muscle fibers must increase DIA endurance during long-lasting exercise. The difference of adaptation mechanisms between DIA and GM is explained by their different functional roles in the organism.

Supported by the RFBR (grant 09-04-01701-a).

MICROPROCESSOR SYSTEM FOR EARLY DIAGNOSTIC OF THE PATHOLOGICAL CHANGES IN HUMAN'S VISUAL SYSTEM "AMELIA-2"

L.S. Bulat

Institute for information transmitting problems (Kharkevich Institute), Bolshoy Karetny per. 19, Moscow, 127994, Russia

The Institute for information transmitting problems in face of designers: Constantine Goluptsov, Vladimir Trunov and Lev Bulat made a new touch-screen

controlled medical device. This device was designed for use in ophthalmologic clinics, cabinets. Its simple construction can give the possibility to a user to work with it even at home. The main goal of this device is the detection of human's eyes pathologies on early stages.

The device allows to measure the critical flicker fusion frequency (CFFF) with red, green, or dark-blue stimulus, threshold of eye electric sensitivity, electric labiality of the optic nerve, and to record retina biopotentials in response to light stimulus. The information is processed to make up individual therapeutic regimens of light-stimulation using the same device. This treatment provides lowering of intraocular pressure in patients with glaucoma, visual fatigue relief, and reduces the risk and/or severity of myopia in children and adults. The device was tested on more than 150 patients with various visual disorders, such as partial optic nerve atrophy, accommodation spasm, visual exhaustion, etc.

Amelia-2 device is supplied with light-emitting diode matrixes inserted into standard trial frames providing registration of critical flicker fusion frequency measurements at various points of visual field. All these diagnostic and therapeutic options are combined in a single device.

The device is protected by patents of the Russian Federation.

The device was awarded on Russian and foreign exhibitions in Moscow, Sevastopol, Nierenberg and Al-Kuwait.

Technical characteristics

Frequency of light stimulus flashings	20 − 60 Hz
Stimulus duration	10 ± 1% mS
Error of digital scale readings	± 0.5 Hz
Light color	red, green, blue
Current amplitude at electro stimulation	from 70 μA to 300 μA
Electric impulse duration	from 10 ms to 100 ms
Stand-alone power supply and network adapter	9 V
Power	3 ± 0.3 W
Weight	1.5 kg

EFFECT OF ALLOPLASTY WITH NEWBORN MUSCLE TISSUE AND He-Ne LASER ON REGENERATION OF SKELETAL MUSCLES IN AGED RATS

N.V. Bulyakova, V.S. Azarova

Establishment of the Russian Academy of Sciences, A.N. Severtzov Institute of Ecology & Evolution RAN, Leninskii prosp.,33, Moscow, 119071, Russia

Biologists and clinicians are developing various methods for improving the regeneration of traumatized skeletal muscles. One way of doing this is cell therapy: introducing initially cultured stem cells or myoblasts into injured muscles. Myoblasts isolated from the muscle tissue of embryo, newborn, or adult animal can

take part in the regeneration of skeletal muscles. But one of the disadvantages of cell transplant method is that most donor cells fail to survive.

Instead of cells being obtained by culturing, a positive effect was also observed after implantation of fresh minced muscle tissue cut out during operation (the tissue therapy method). As a result, an additional quantity of muscle cell-satellites, myoblasts is implanted. It has been shown that during regeneration, quiescence satellite cells lying beneath the basement membrane of muscle fragments transform into myoblasts, divide, fuse, and form new muscle fibers. Effect was shown in experiments on laboritary animals.

Numerous investigators have demonstrated that with advancing age, skeletal muscle regenerative capacity impaires resulted in satellite cells senescence, decrease the absolute number(to 2.4%) and doubling potential of satellite cells, increased satellite cell susceptibility to apoptosis, and changing factors within the local environment. In the skeletal muscles of the hind legs of newborn rats, the everage number of satellite cells equals 30%. Muscle tissue is capable of active growth and regeneration.

The aim of this research was to determine the efficiency of alloplasty with minced muscle tissue from gastrocnemius muscles of newborn rats as a tissue therapy method for traumatized gastrocnemius muscles in aged rats. Implantation of genetically foreign tissues is possible when using immunodepressants. According to the literature data, laser action under specific conditions and doses can weak the transplantational immunity, at least during early stages of alloplasty.

This study was performed on rats aged 18 months. Both gastrocnemius muscles were cut across. Then in 3-4 newborn rats, the both gastrocnemius muscles were excised, minced in a sterile Petri dish with scissors, and implanted in the transverse dissection area of gastrocnemius muscles in aged rats. The newborn rats were 1.5-3 days old. All operations on rats were conducted under nembutal anesthesia. Muscle regenerates were tested 14 days after alloplasty, when it is possible to evaluate the regenerative capacity of allogeneic muscle tissue.

In control, alloplasty the area of muscle trauma was carried out without initial laser radiation. In experiment, in order to reduce the transplantational immunity, the both hind legs of rat-recipient were subjected to the action of laser radiation before the operation. Conditions of action of the He-Ne laser: wavelength, 0.63μm, laser beam was defocused with lens, diameter of the radiation field, 2-2.5 cm, power density, of 2.5-3 mW/cm^2 , 10 exposures for 5 minutes during 14 days, a total dose of 7.5-9.0 J/ cm^2 on earch legs.

In control animals, after 14 days, alloplant exert an aggressive effect on the state of muscle tissue in traumatized muscles of recipient. In the majority of gastrocnemius muscle regenerates, the proximal stumps decreased. The most of muscle fibers were in a state of ischemia and dark stained, were lost or divided into fragments. In the distal stumps, muscle fibers were partially exposed connective tissue replacement. The proximal and distal muscle stamps shortend for the destruction in traumatized muscle tissue and deficient longitudinal stretch. The morphology structure in both stumps was changed. Muscle fibers have a

wavy shape, expanding septum, perimizy as swollen cords with a homogeneous ground substance. There were large hyperemic blood vessels. In most places along the edges of the stumps, there were thinning and death of muscle fibers over a rather long distance, an increase in the space between them, and increasing leukocyte infiltration. Simultaneously, at the ends of stumps, minor amounts of injured muscle fibers with different degrees of regenerative activity were noted. Muscle fibers did not penetrated deep into the defect. In area of implant, the formation of granulate tissue and regeneration of allogenic muscle tissue were observed. There were fragments consisted of viable narrow newborn myofibers preservating under ishemia. Under sarcolemma of myofibers in which destructive products were resorbed by macrophages, satellite-cells and myoblasts appeared. Active leukocyte infiltration was observed. In area of implantation, the formation of adipouse tissue between allogenic muscle fibers was noted in 87% of cases, and the apearence of the cartilage nodules – in 37% of cases.

In muscle tissue of experiment animals, the destructive changes in muscle fibers and disturbance of normal morphological structure in stumps were also observed. However, effect of He-Ne laser radiation before allotransplantation exerted preservation of larger quantity of muscle tissue and size of the proximal stump as a whole. At the ends of stumps, more regenerative activity of injured muscle fibers was found. Muscle fibers grew into the defect. The regeneration of muscle fibers was observed in septums. In area of trauma, the formation of granulate tissue took place. The leukocyte infiltration was moderate. Allogenic muscle tissue regenerated more activly. The more amount of viable allogenic muscle tissue was retained. At the same time in area of trauma, the formation of adipose tissue in 37% regenerates and the apearance of cartilage nodules in 75% cases were observed.

Thus, in spite of capacity of newborn rat muscle tissue for intensive growth and regeneration, and presence of numerous satellite cells and myoblasts the alloplasty with newborn muscle tissue as a tissue therapy method for traumatized skeletal muscles in aged rats was not effective. On the one hand, the failure regeneration of implanted muscle tissue of newborn into aged animals may be function of the environment for regeneration provided by the aged host. On the other hand, it has been shown that the connective tissue of skeletal muscles (in newborn or when regenerating) contains noncommitted pleuripotent mesenchymal resident stem cells. They are capable of giving up to cells with different phenotypes including fibroblasts, chondrocytes, osteoblasts, and adipocytes. The quantity of connective and muscle tissue in newborn rats was equal to 50/50.

In our experiments, muscle satellite cells and myoblasts present in the newborn muscle tissue fragments were introduced into the trauma region together with connective tissue and other cell elements of surrounding tissues. The similar effect was observed when implanting of newborn muscle tissue into traumatized muscles of adult rats. Under alloplasty of the muscle trauma area with minced muscle tissue of rats of the same age, the described above phenomenon did not observed.

INTERLEUKIN-6 -174 G>C POLYMORPHISM AND RISK OF EARLY ATHEROSCLEROSIS: THE CARDIOVASCULAR RISK IN YOUNG FINNS STUDY

N. Chumaeva[1,2], M. Hintsanen[1,3], T. Lehtimäki[4], O.T. Raitakari[5,6], L. Keltikangas-Järvinen[1]

[1]Institute of Behavioural Sciences, University of Helsinki, P.O. Box 9, 00014 Helsinki, Finland;
[2]Institute of Cell Biophysics RAS, Institutional Street 3, Pushchino, Moscow region 142290, Russia;
[3]Helsinki Collegium for Advanced Studies, University of Helsinki, Helsinki, Finland;
[4]Laboratory of Atherosclerosis Genetics, Department of Clinical Chemistry, Centre for Laboratory Medicine, Tampere University Hospital, Finland;
[5]Department of Medicine, University of Turku and Turku University Hospital, P.O. Box 52, 20521 Turku, Finland;
[6]Department of Clinical Physiology, University of Turku, P.O. Box 52, 20521 Turku, Finland

Introduction. Atherosclerosis is considered as a state of chronic low-grade inflammation within the arterial wall [1]. Chronic stress accompanies the atherosclerosis related diseases, and the proinflammatory cytokine interleukin-6 (IL-6) is suggested as a link between chronic stress and cardiovascular diseases [2]. Interleukin-6 plasma levels are regulated by the G174C polymorphism of IL-6 gene [3]. The C allele and the CC genotype of IL-6 -174 polymorphism have been related to lower IL-6 plasma levels whereas the G allele and especially the GG genotype – with increased IL-6 plasma level [3]. High levels of IL-6 production are associated with atherosclerosis extent [4] and, on the other hand, with higher stress level [5]; while low levels of IL-6 in plasma are related to better stress coping [5]. This suggests that the G allele may be responsible on stress-related disease risk. Chronic stress state (vital exhaustion (VE)) has been recognized in post-myocardial infarction patients [6]; and high VE level is associated with a 2-fold higher risk of heart failure [7]. Exhaustion has been found to be associated with IL-6 reflected inflammatory activity [8]. In the present study, the associations of the -174G>C IL-6 polymorphism with chronic stress and with preclinical atherosclerosis, assessed by carotid intima-media thickness (IMT), were examined in 1673 women and men aged 24-39 years participated in the Cardiovascular Risk in Young Finns study. The CC, CG and GG IL-6 gene variations were tested separately, and also the CG and GG individuals were grouped together into the joined CG+GG group because the G allele has been found to show a dominant mode in their respective genes [3].

Methods and participants. The subjects are 798 women and 695 men participating in the Cardiovascular Risk in Young Finns study. This study is one of the largest epidemiological population-based studies, which has been monitor-

ing the development of risk factors for coronary heart disease a total of 3596 participants since 1980 [9]. ***Ultrasound imaging:*** Ultrasound studies of the carotid arteries were performed using Sequoia 512 ultrasound mainframes (Acuson, Mountain View, CA, USA) with 13.0 MHz linear array transducer, as previously described [10]. Carotid IMT was measured on the posterior (far) wall of the left carotid artery. At least four measurements were taken approximately 10 mm proximal to the bifurcation to derive mean carotid IMT. The between-visit coefficient of variation of IMT measurements was 6.4% and the intra-observer CV was 3.4% [10]. ***IL-6 -174 G>C genotyping:*** Genomic DNA was extracted from whole blood using a commercially available kit (Qiagen Inc., Hilden, Germany). IL-6-174 G>C genotyping (rs1800795) was performed by employing the 5'-nuclease assay and fluorogenic allele-specific TaqMan probes and primers [11]. PCR was performed in 384-well plates in a total volume of 5μl, using ABI Prism 7900HT Sequence Detection System (Applied Biosystems, Foster City, CA, USA) with the following conditions: 2 min at 52 ºC, 10 min at 95 ºC followed by 40 cycles of 95 ºC for 15 sec and 60 ºC for 1 min. PCR reactions for the rs1800795 contained genomic DNA, 1×Universal PCR Master Mix, 900nM of each primer and 200nM of each TaqMan probe. The gDNA and master mix were pipetted on 384-plates by an automated TECAN Freedom EVO-100 robot (Tecan Schweiz AG, Männedorf, Switzerland). For quality analysis random duplicates, empty controls (water) and known control samples were run in parallel with unknown DNA samples. ***Clinical Characteristics:*** The effects of serum LDL- and HDL-cholesterol levels, triglycerides, plasma insulin level, systolic and diastolic blood pressure were studied. For the determination of serum lipoprotein levels, venous blood samples were drawn after an overnight fast. All measurements of lipid levels were performed in duplicate in the same laboratory. LDL-cholesterol concentration was calculated by the Friedewald formula [12]. Standardized enzymatic methods were used for measuring levels of triglycerides and HDL-cholesterol [13]. Serum insulin was measured by microparticle enzyme immunoassay kit (Abbott Laboratories, Diagnostic Division, Dainabot, Japan). Blood pressure was measured with a random-zero sphygmomanometer. Average of three measurements was used in the analysis. ***Chronic stress assessment:*** Chronic stress was assessed using the Maastricht Questionnaire (MQ) [14]. Increased levels of serum IL-6 concentrations have been related with high MQ scores which indicate high level of VE [15].

Results and discussion. The association between IL-6 -174 G>C polymorphism and VE was found for the whole sample. Individuals having the G allele demonstrated higher VE, than individuals with the CC genotype. The association between higher chronic stress level and greater IMT was found in men with the CG+GG genotype in the presence of cardiovascular risk factors. The results imply that in men with the G allele chronic stress predicts higher risk of subclinical atherosclerosis in the presence of cardiovascular risk factors. In line with our findings, the genetic effect of IL6 -174 G>C polymorphism on cardiovascular risk factors and markers of atherosclerosis was found only in men [16;17]. In our pre-

vious studies, the interactions between chronic stress and cardiac autonomic reactivity on IMT [18] and between VE and arterial elasticity on IMT have also been found in men [19]. Most of the cardiovascular risk factors increasing the risk of atherosclerosis are more harmful for men than for women [20]. Men have been shown to be more influenced by stress and having less stress coping potential [21]. The mechanism explaining the relations between IL-6 gene polymorphism and chronic stress suggests the IL-6 induced activation of the hypothalamic-pituitary-adrenocortical-axis and increasing of catecholaminergic neurotransmission in the brain [22]. The IL-6 affects metabolic, endothelial and coagulant events, contributing to atherosclerosis development [23].

Conclusions. The associations between VE and IL-6 -174 G>C polymorphism found in our study suggest that individuals having the GG genotype are more stressed, thereby providing evidence that chronic stress has genetic and inflammatory basis. As a novel finding, we showed that the G allele individuals may have more adverse cardiovascular consequences of exhaustion than those with the C genotype. The G allele may be responsible for higher stress related risk of early atherosclerosis in men, especially in the presence of cardiovascular risk factors. As a practical implication, our findings enhance understanding on individual differences in stress-reactivity and mechanisms of atherogenesis. A higher risk of cardiovascular diseases associated with chronic stress may be of importance in the planning of future preventive programs. Stress reduction strategies and early intervention programs aimed at reducing symptoms of exhaustion may enhance cardiovascular health in the long run, especially in genetically susceptible individuals.

This study was supported by the Wihuri Research Foundation (N.C.); Emil Aaltonen Foundation, Ella & Georg Ehrnrooth Foundation, Finnish Foundation for Cardiovascular Research and Research Funds of the University of Helsinki (M.H.).

References

1. Ross R. Atherosclerosis: an inflammatory disease. *N Engl J Med* 1999:340:115-126.
2. Yudkin JS., et al. Inflammation, obesity, stress and coronary heart disease: is IL-6 the link? *Atherosclerosis* 2000:148:209-214.
3. Fishman D., et al. The effect of novel polymorphisms in the interleukin-6 (IL-6) gene on IL-6 transcription and plasma IL-6 levels, and an association with systemic-onset juvenile chronic arthritis. *J Clin Investigation* 1998:102:1369-1376.
4. Kablak-Ziembicka A., et al. Relationship between carotid intima-media thickness, cytokines, atherosclerosis extent and a two-year cardiovascular risk in patients with arteriosclerosis. *Kardiol Pol* 2011:69:1024-1031.
5. Sjögren E., et al. Interleukin-6 levels in relation to psychosocial factors: Studies on serum, saliva, and in vitro production by blood mononuclear cells. *Brain Behavior Immunity* 2006:20:270-278.
6. Appels A. Exhaustion and coronary heart disease: the history of a scientific quest. *Patien Educ Couns* 2004:55:223-229.

7. Rod NH, Andersen I, Prescott E. Psychosocial risk factors and heart failure hospitalization: a prospective cohort study. Am J Epidemiol 2011:174:672-680.
8. Yanszky I., et al. Self-rated health and vital exhaustion, but not depression, is related to inflammation in women with coronary heart disease. *Brain Behav Immunity* 2005:19:555-563.
9. Raitakari OT., et al. Cohort profile: The Cardiovascular Risk in Young Finns study. *Int J Epidemiol* 2008:37:1220-1226.
10. Juonala M. Cardiovascular risk factors and their associations with markers of subclinical atherosclerosis in young adults. The Cardiovascular Risk in Young Finns Study. Annales Universitatis Turkuensis, D645;2005.
11. Livak KJ. Allelic discrimination using fluorogenic probes and the 5' nuclease assay. *Genetic Analysis: Biomolecular Engineering* 1999:14:143-149.
12. Friedewald WT, Levy RI, Fredrickson DS. Estimation of the concentration of low-density lipoprotein cholesterol in plasma, without use of the preparative ultracentrifuge. Clin Chem 1972:18:499-502.
13. Porkka KV., et al. Trends in serum lipid levels during 1980-1992 in children and young adults. The Cardiovascular Risk in Young Finns Study. *Am J Epidemiol* 1997:146:64-77.
14. Appels A, Höppener P, Mulder P. A questionnaire to asses premonitory symptoms of myocardial infarction. *Int J Cardiol* 1987:17:15-24.
15. Meyer T., et al. Elevated serum levels of interleukin-10 and tumor necrosis factor are both associated with vital exhaustion in patients with cardiovascular risk factors. *Psychosomatics* 2010:51:248-256.
16. Hulkkonen J., et al. Polymorphism in the IL6 promoter region is associated with the risk factors and markers of subclinical atherosclerosis in men: The Cardiovascular Risk in Young Finns Study. *Atherosclerosis* 2009:203:454-458.
17. Riikola A., et al. Interleukin-6 promoter polymorphism and cardiovascular risk factors: the Health 2000 Survey. *Atherosclerosis* 2009:207:466-470.
18. Chumaeva N., et al. Interactive effect of long-term mental stress and cardiac stress reactivity on carotid intima-media thickness: The Cardiovascular Risk in Young Finns study. *Stress* 2009:12:283-293.
19. Chumaeva N., et al. Sex differences in the combined effect of chronic stress with impaired vascular endothelium functioning and the development of early atherosclerosis. *BMC Cardiovasc Disorders* 2010:10:34.
20. Roeters van Lennep JE, Westerveld HT, Erkelens DW, van der Wall EE. Risk factors for coronary heart disease: Implications of gender. *Cardiovasc Res* 2002:53:538-549.
21. van Snick J. Interleukin-6: an overview. *Annu Rev Immunol* 1990:8:253-278.
22. Weidner G. Why do men get more heart disease than women? An international perspective. *J Am Coll Health* 2000:48:291-294.
23. Loppnow H, Werdan K, Buerke M. Vascular cells contribute to atherosclerosis by cytokine- and innate-immunity-related inflammatory mechanisms. *Innate Immun* 2008:14:63-87.

THE SARCOLEMMA OF MYOMETRIUM IS POSSIBLE TARGET OF NITRIC OXIDE ACTIVITY IN UTERA

Iu.V. Danylovych, PhD; G.V. Danylovych, PhD

Palladin Institute of Biochemistry, National Academy of Science of Ukraine, Kyiv-30, Leontovycha str., 9, 01601, danylovych@biochem.kiev.ua

Nitric oxide-mediated relaxation of myometrium, unlike vascular or gastrointestinal smooth muscle, is independent of elevation of cyclic guanosine 5 – monophosphate. We propose that impotant target of NO action in myometrium is direct influence on Ca^{2+}-transport into sarcolemma.

Investigations were conducted on a models of intact myocytes from uterus of rats using fluorescent Ca^{2+} probe FURA-2AM and pig myometrium sarcolemma vesicules using $^{45}Ca^{2+}$. As NO-donors was used sodium nitrite and nitroprusside.

The thapsigargin- and K^+-induced ways of the entrance of Ca^{2+} into the myocytes are identified. The entry of a cation, activated by high-potassium depolarization is sensitive to cadmium and nifedipine and thapsigargin-dependent – to low concentrations of lanthanum. K^+-induced entrance are potentiated by sodium nitroprusside and nitrite; thapsigargin-induced entrance are depressed by sodium nitroprusside and potentiated by sodium nitrite. The influence of sodium nitrite (10^{-9}-10^{-5} M) on Ca^{2+} input into plasmalemma vesicles was investigated too. It was established that sodium nitrite increased Ca^{2+}-permeability of plasmalemma.

Thus the direction of the action of NO-donors on the passive entrance of Ca^{2+} into myocytes depends on the specific way of its entry the cells (Ca^{2+} transduction specific).

The growth sarcolemma permeability for calcium ions is result of polarization changes of plasma membrane myocytes. Possibility of the use of flow cytometry analysis for investigation mitochondria and plasma membrane polarization in myometrium cell suspension using potential-sensitive probe $DiOC_6(3)$ has been demonstrated. Decrease in fluorescence response in adding agents that depolarize plasma membrane (ouabain) or mitochondria (sodium azide), and the increase of fluorescence in the presence hyperpolarizating factors, including K^+-ionophore valinomycin and calcium ions has been shown.

In further experiments revealed that in myocytes with mitochondrial depolarization nitroprusside and sodium nitrite causes pronounced sarcolemma polarization in the presence of physiological concentrations of Ca^{2+}. For low concentrations of cations or in environments that contain EGTA effect was significantly lower or not observed. Intensity of polarization depended also on the concentration of the used compounds. In the presence of nitrendypine as inhibitor voltage-operated calcium channels the polarization effect of NO was not expressed. The use of blockers of K^+ channels, as tetraetylammonium and 4-aminopyridine, leaded depolarization

of sarcolemma, against a growth of membrane potential for the actions of nitroprusside and sodium nitrite is almost not observed.

From our findings we can suggest that nitric oxide or its derivatives result in Ca^{2+}-dependent polarization of myometrial cells sarcolemma, which is caused by activation of K^+-permeability of the membrane. This phenomenon may underlie the decrease in excitability sarcolemma that occurs during pregnancy.

SMOOTH MUSCLE FROM MUSSEL *CRENOMUTYLUS GRAYANUS* DOES NOT CONTAIN CALDESMON

A.V. Dobrzhanskaya, I.G. Vyatchin, S.S. Lazarev, O.S. Matusovsky, N.S. Shelud'ko

Zhirmunsky Institute of Marine Biology, Far Eastern Branch of the Russian Academy of Sciences, Palchevsky str. 17, Vladivostok, 690059 Russia

Vertebrate smooth muscle thin filaments made up of actin, tropomyosin, caldesmon, calponin and calmodulin as a Ca^{2+}-binding protein. Caldesmon together with calmodulin plays the role of troponin in these muscles. It has been suggested that the caldesmon type regulation also exist in molluscan smooth "catch" muscles (Bennett and Marston, 1990).

Previously we showed by SDS-PAGE that Ca^{2+}-regulated thin filaments isolated from smooth muscle of Crenomytilus grayanus contain, as a main protein, actin, tropomyosin and 40 kDa calponin-like protein, but not caldesmon (Dobrzhanskaya et al, 2010). In the current work we attempted find a caldesmon not only in mussel thin filaments but in the homogenate, heat-extract and fractions of heat-stable proteins from whole mussel smooth muscle. We did not reveal any polypeptide having the same electrophoretic mobility as the h-caldesmon. Furthermore, no one of the water-soluble heat-stable protein fractions inhibit of actomyosin MgATPase activity in tropomyosin-dependent manner. Also the immunoblotting analysis showed the absence of caldesmon in isolated thin filaments, in the homogenate and heat-stable extract from whole muscle.

As mention above, we showed that *Crenomytilus* smooth muscle thin filaments contain a calponin-like protein 40 kDa (Dobrzhanskaya et al, 2010). In the current work by immunoblotting analysis we confirmed the presence of calponin-like protein in isolated mussel thin filaments. By co-sedimentation assay we showed that the calponin-like protein interacts with F-actin in tropomyosin-independent manner. The selective removal of calponin-like protein from thin filaments does not affect on degree of Ca^{2+}-regulation of isolated mussel thin filaments.

Thus, we revealed that isolated thin filaments of *Crenomytilus grayanus* does not contain caldesmon but contain calponin-like protein, which is not involved in the Ca^{2+}-regulation of thin filaments.

The work was supported by grant № 12-III-B-06-074 from Far Eastern Branch of the Russian Academy of Science and in part from Russian Foundation for Basic Research (grants 10-04-00550 and 11-04-98501).

TOPOLOGY AND POLARITY OF CILIARY EPITHELIUM IN *XENOPUS LAEVIS* EMBRYONIC ECTODERM AS RELATED TO MECHANICAL STRESSES

A.Yu. Evstifeeva

Moscow State University, Moscow, 119992, Russia
E-mail: alyona-evst@yandex.ru

Studies of epithelial pathologies are mostly focused on exploring the molecular basis of different diseases on the single cells level. In these studies the holistic properties of epithelia, including their topology, are as a rule missed. Meanwhile, as shown in *Rana temporaria* embryos, topological reconstructions that is the changes in the relative amounts and mutual arrangement of different cell types can by connected with the basic pathological events (Savostianov, 2005). Therefore it looks timely to explore the factors affecting epithelial topology.

Mechanical stresses might be one of these factors. This idea is supported by mechanodependent differentiation of stem cells (Engler et al., 2006) as well as the results of cell mosaics modeling under different mechanical parameters of cell layers (Farhadifar et al., 2007). However experimental data demonstrating the effects of mechanical stresses upon epithelial topology are almost lacking. Our study is aiming to fill this gap.

We have studied the role of stretching and relaxation of embryonic samples upon the density, the arrangement into parallel rows and the polarity (estimated by directionality of the fluid flow) of ciliary cells (CC) in *Xenopus laevis* embryos.

Double explants (sandwiches) from the ventral and dorsal areas (VS and DS correspondingly) of the early gastrula embryos, as well as the sandwiches from latero-ventral ectoderm together with underlain mesoderm have been prepared. The sandwiches were attached by glass needles to the agarose substrate, stretched within an hour to 100-230% of the initial length and incubated about a day in MMR solution up to stage 28 by Nieuwkoop & Faber (1956). Control sandwiches and sandwiches from stage 13 were incubated without stretching. Relaxation of mechanical stretching was performed by inserting within a neural plate a wedge containing same stage ventral embryonic tissue from another embryo. Operated embryos were incubated for the same time period.

After the end of incubation the maps of fluid flows generated by CC were composed and CC densities (CC amounts to the given samples squares ratios) were measured. With the use of the original program a degree of CC involvement into parallel rows and the rows' orientation according to anteroposterior (AP) body axis were determined.

As shown by measurements, the relaxation of mechanical stresses at the early neurula stage and 1 h long stretching at the early gastrula stage do not affect significantly CC density, their involvement into rows and a polarity. On the other hand, CC density and their involvement into rows in non-

stretched DS is significantly greater than the same indices in non-stretched VS, while in the stretched DS and VS these differences disappear. One may conclude therefore that mechanical stretching affects CC topology in the dorsal and ventral tissue sandwiches in the opposite way. Also, the differences in fluid flows directionality between DS and VS have been observed. In most of DS they were strictly ordered in relation to AP axis, while in VS only a regional, rather than holistic order took place. CC density in 13 stage sandwiches was significantly higher than in VS, although the ectoderm of the both kinds of samples had the same prospective significance. The observed CC density differences can be connected with a more smooth (more tensed) 13 stage sandwiches surface as compared with that of VS. In the intact embryos CC rows tend to orient perpendicularly to AP, while in explants their orientation is much more disordered.

We are planning to study more prolonged and fluctuating mechanical regimes upon CC arrangement and dynamics.

References

1. Savostianov, G.A. (2005). Foundations of Structural Histology. Spatial Organization of Epithelia, 375 P., Nauka, St Petersburg.
2. Engler A.J. at al. (2006). Matrix Elasticity Directs Stem Cell Lineage Specification. *Cell* 126, 677–689
3. Farhadifar R.et al. (2007). The Influence of Cell Mechanics, Cell-Cell Interactions, and Proliferation on Epithelial Packing. *Current Biology* 17, 2095–2104
4. Nieuwkoop P. & Faber R. (1956). Normal table of *Xenopus laevis* (Daudin), pp. 243, North Holland Publ. Co., Amsterdam.

INCREASING OF TUMOR CELLS RESISTANCE TO ANTI-CANCER RECOMBINANT PROTEIN IZTRAIL IN DENSE CONFLUENT CULTURES

R.S. Fadeev, A.V. Chekanov, N.V. Dolgikh, V.S. Akatov

Pushchino State Institute of Natural Sciences, pr. Nauki, 3, Pushchino, 142290, Russia;

Institute of Theoretical and Experimental Biophysics, Institutskaya st., 3, Pushchino, 142290, Russia

Background. One of the main and most urgent goals of oncology is to develop a novel anticancer therapeutic agent that selectively kills tumor cells, without damaging normal cells. Over the last decade, there has been great interest focusing on the usage of cytokine TRAIL as an attractive candidate for anticancer therapy. TRAIL (TNF alpha Related Apoptosis Inducing Ligand) is a transmembrane protein that is expressed on the surface of immune system cells, such as natural killer cells and dendritic cells. TRAIL selectively induces apoptosis in cancer cells through engagement of death receptors (DR4 and DR5). It is considered that normal cells escape TRAIL-induced apoptosis because of the inhibition of some stage of intracellular signaling pathways of TRAIL-induced apoptosis. The resistance is induced also by the high expres-

sion of three decoy receptors (DcR1, DcR2 and osteoprotegerin) that bind ligand TRAIL but cannot trigger apoptotic signal. However in vitro studies have shown that some tumor cells are resistant to TRAIL-induced apoptosis. Therefore, the administration of recombinant proteins TRAIL alone cannot be a highly effective strategy for the treatment of TRAIL-resistant tumors. Currently an active search for substances that enhance the sensitivity of tumor cells to TRAIL-induced apoptosis is being conducted. On the other hand, it is known that cancer cells can acquire resistance to chemotherapeutic drugs, oxidative stress in high density culture. This phenomenon is termed as a multicell resistance, cell adhesion-dependent resistance or density dependent resistance of tumor cells. The mechanisms of the resistance development are currently unclear. It is supposed, that this phenomenon is associated with activation of intracellular survival signaling cascades, through the formation of intercellular contacts involving calcium-binding intercellular adhesion molecules, due to reducing cell proliferation or to the increased activity of the multidrug resistance proteins (MRP, Pgp) in dense cultures. However it is unclear whether such resistance is appeared in TRAIL-induced apoptosis. Thus, the aim of this work is to determine whether the tumor cells will be resistant against TRAIL in dense confluent cultures.

Materials and Methods. Recombinant human protein izTRAIL was produced in a bacterial expression system by the method developed in our laboratory (ITEB RAS). Protein izTRAIL initiates apoptosis in a broad range of cancer cell lines of different origin at a concentration range from 1 to 10 ng/ml. In contrast, izTRAIL is nontoxic to normal cells at concentrations higher than 10 mkg/ml. The work was carried out using cell lines of human larynx carcinoma HEp-2, human lung carcinoma A 549, human epithelial carcinoma A 431, human ovarian carcinoma OVCAR-3 and others. Cytotoxic effect of izTRAIL on cancer cells was assessed by crystal violet assay. The amount of dye taken up was measured with plate reader (Tecan). Cell cycle distribution of cells in cultures was analyzed by flow cytometry PARTEC III. The percentage of live, apoptotic, mitotic cells were determined using a fluorescence microscope Leica DM6000 and a double vital staining of cells with nuclear dyes Hoechst 33342 and ethidium bromide.

Results. It was observed that resistance to izTRAIL of all tumor cell lines used was considerably increased in dense confluent cultures. In particular, the human epidermal carcinoma cells (cell line A 431), became completely insensitive to izTRAIL-induced apoptosis in dense confluent cultures. It was found that increasing of tumor cells resistance can be initiated in confluent cultures without changes in the proliferative characteristics of cell populations. This indicates that the increase in tumor cell resistance in dense populations is not related to their proliferative status. It was shown that the dissociation of calcium-dependent cell-cell contacts with EGTA did not suppress tumor cell resistance to protein izTRAIL in dense confluent cultures. This means that the increased resistance of tumor cells in confluent cultures can be implemented without the involvement of cell-cell contacts.

Conclusions. The sensitivity of tumor cells of different origins to TRAIL apoptosis is dramatically decreased in high density confluent cultures. A similar increase in resistance of tumor cells to TRAIL induced apoptosis may occur in vivo, and therefore, this phenomenon should be considered in the development of methods of anticancer therapy using recombinant TRAIL proteins. Particularly the methods of overcoming of such resistance must be developed, which include application of selective targeted drugs in nontoxic concentrations. To increase the effectiveness of such developments, it is essential to understand the mechanisms underlying TRAIL resistance of the tumor cells in dense confluent cultures.

This work was supported by the Ministry of Education and Science of Russian Federation, contracts №16.512.11.2261; № 02.740.11.0710; and Analytical departmental target program №4.3887.2011 and was made using devices of the Regional Center for Collective Use at the Institute of Theoretical and Experimental Biophysics RAS.

USE OF MUSCLE PROTEOMICS IN ECOTOXICOLOGY

M.A. Fedorova, N.V. Kuleva, R. Hoffmann

Institute of Bioanalytical Chemistry, Center for Biotechnology and Biomedicine, Faculty of Chemistry and Mineralogy, Leipzig University, Deutscher Platz 5, 04103, Leipzig, Germany,
Department of Biochemistry, Faculty of Biology and Soil Science, St. Petersburg State University, Universitetskaya nab.7/9, St.Petersburg,197034,Russia.

Environmental factors acting on living organisms are able to change gene expression in their tissues. These changes can be monitored with s set of new technologies provided by proteomics which detect the effects on the level and status of individual proteins within proteomes and subproteomes in a wide range of biological contexts (1). This approach has obvious applications to environmental (or ecological) toxicology, as it has the potential to identify previously unknown protein biomarkers and to gain insights into the underlying toxic mechanisms. Since the proteome is highly dynamic it holds out the promise of detecting subtle changes in sentinel species as they adapt to altered environmental conditions. A key goal of ecotoxicology is the ability to predict likely environmental effects of new and emerging substances and technologies, and proteomics could be ideal approach to aid risk assessment.

Muscle proteomics and ecotoxicology could communicate in the field of redox proteomics. Many environmental pollutants and natural physical events such as different types of radiation produce so-called “reactive oxygen species”(ROS) including molecular oxygen, superoxide radical, singlet oxygen, hydrogen peroxide, nitric oxide and others. Most biological systems produce such ROS as an inherent part of their biochemistry. ROS can cause serious toxicity because they are capable of interacting rapidly and efficiently with different biomolecular targets. Because most or-

ganisms are exposed to ROS either as result of external or internal chemical and physical events, cells have evolved very elaborate defence mechanisms to protect their own key components from oxidative damage. Oxidative stress (OS) refers to a status, when the cellular antioxidant defence is overwhelmed my oxidative species. Oxygen-mediated toxicity and cell response to it are of increasing interest in ecotoxicology.

In our work made on muscle subproteome (2) acute OS was induced by X-ray irradiation of rats using a dose of 5 Gy. By gel-based proteomics we could identify up- and down-regulated proteins in high ionic strength muscle extracts. In our study 35 from 440 protein spots detected by two-dimensional gel electrophoresis changed the intensity after irradiation. Among these, eleven proteins were up-regulated (e.g.myosin regulatory chain 2 and slow skeletal troponin T) and nine proteins were down regulated (e.g. skeletal alpha-actinin3, glycogen-phosphorylase, pyruvate kinase, and fast skeletal troponin T). Similar proteome changes were observed during aging, which is also accompanied by OS and functional lesions in muscle tissue (3).

OS usually results in reversible and irreversible modifications in proteins and redox proteomics offers tools to identify them. In another study on the muscle proteome (4) we fractionated the high salt extract of muscle proteins by electrophoresis in two dimensions by applying first non-reductive and then reductive conditions in SDS-PAGE. This diagonal redox electrophoresis has revealed significant alterations of intra- and intermolecular disulfide bridges for several muscle proteins: actin, creatine kinase and different isoforms of myosin light chains. Though the levels of these reversible modifications were increased by OS, the same proteins were also subjected to irreversible oxidation (carbonylation).

Carbonylation is a biomarker of OS in different biological systems and can be detected by Western blotting (2). In our OS model based on the muscle subproteome, at least 36 proteins were carbonylated. Functionally most affected proteins were involved either in regulation of muscle contraction (light chains of myosin, tropomyosin, actin, aggregates of actin ,C-protein, troponins I and T (fast and slow) or are part of carbohydrate metabolism. It was interesting to see that different proteins were modified by different kinetics, indicating a complex regulation pattern that depends not only on the ROS level but also on ROS scavenging, protein degradation and synthesis.

Carbonylation is an irreversible oxidative modification that cannot be repaired by cellular enzymes. Proteins oxidized under mild OS can be degraded directly by the 20S proteasome without ubiquitination, whereas modestly oxidized proteins are degraded rapidly by proteases. Strong OS produces highly carbonylated proteins that cannot be degraded and tend to aggregate.

Such aggregates were also observed in our work devoted to effects of OS on actin filaments from foot of mussel Mytilus edulis exposed in vivo to copper ions (5). Using immunblotting techniques we found that copper ions induced carbonylation in foot actin accompanied by cross-linked oligomers and truncated monomers. The carbonylated structures of actin and the corre-

sponding changes in its functional properties may be biomarkers for environmental monitoring.

In conclusion, proteomics can serve as a route for identification of toxicity targets in ecological toxicology. Muscle proteome being very heterogeneous in composition, highly plastic and sensitive to environmental changes is a good model for ecotoxicological studies.

References

1. Dowling V.A., Sheehan D. Proteomics as a route to identification of toxicity targets in environmental toxicology.2006.Proteomics,6, 5597-5804.
2. Fedorova M., Kuleva N., Hoffmann R. Identification, quantification and functional aspects of skeletal muscle protein-carbonylation in vivo during acute oxidative stress.2010. J. Proteome Research , 9,2516-2526.
3. Ohlendieck K. Skeletal muscle proteomics: current approaches, technical challeges and emerging techniques.2011, Skeletal Muscle 1:6.
4. Fedorova M., Kuleva N., Hoffmann R. Reversible and irreversible modifications of skeletal muscle protein in a rat model of acute oxidative stress.2009.Biochim.Biophys.Acta, 1792,1185-1193.
5. Vikhoreva N.,Vikhorev P.,FedorovaM.,Hoffmann R.Mansson A.Kuleva N. The in vitro motility assay parameters of actin filaments from Mytilus edulis exposed *in vivo* to copper ions.2009.Arch.Biochem.Biophys.,491,32-38.

DIFFERENTIAL CONTRIBUTIONS OF GOLGI TO MICROTUBULE ORGANIZATION IN AFFINED CELLS

A.I. Fokin [1], I.B. Brodsky [1], E.S. Nadezhdina [1,2], A.V. Burakov [1]

[1] *A. N. Belozersky Institute of Physico-Chemical Biology, Moscow State University*

[2] *Institute of Protein Research, Russian Academy of Science*

Microtubules in mammalian culture cells are usually arranged in a fan-like fashion. This radial array is organized by centrosomes and the Golgi, but their contributions differ in various cells. We studied microtubule organization in two affined epithelia-like cultures — Vero and BS-C-1 — both of which originated from green monkey kidney. We observed that centrosome activity was constant in these cells, although Golgi microtubule-organizing activity was greater in BS-C-1 than in Vero cells. In BS-C-1, the Golgi was more frequently a single or second microtubule-organizing center, harboring more extensively nucleated microtubules in the regrowth assay than Vero cells. Disruption of the Golgi with brefeldin A affected microtubule organization to a greater extent in BS-C-1 than in Vero cells. Centrosome-lacking cytoplasts in Vero cells had sparse and chaotic microtubules, whereas those in BS-C-1 cells assumed a radial microtubule array.

We concluded that even closely related cells can implement disparate pathways of microtubule organization, receiving different contributions from centrosome and Golgi activities. Likely, the capacity of Golgi to organize microtubules is regulated during cellular differentiation or progression in culture.

MIGRATORY ACTIVITY OF TRANSFORMED EPITHELIAL CELLS: THE ROLE OF E-CADHERIN

N.A. Gloushankova, I.Y. Zhitnyak, D.V. Ayollo, S.N. Rubtsova

Institute of Carcinogenesis, N.N. Blokhin Cancer Research Center of the Russian Academy of Medical Sciences, Kashirskoe shosse 24, Moscow, 115478, Russia

The destruction of stable cell–cell adhesion and the acquisition of motile behavior are essential for neoplastic evolution of tumor cells of epithelial origin. It is well known that some human tumors (ductal breast carcinomas, colorectal carcinomas, and melanomas) retain E-cadherin expression. Earlier we established that in IAR-6-1 and IAR1170 epithelial cells neoplastic transformation led to the dramatic rearrangement of AJs: the E-cadherin-based continuous adhesion belt was replaced by radial strands oriented perpendicularly to the cell-cell boundaries.

Using the distance map method, we analyzed the dynamics of AJs in IAR-6-1 cells stably expressing GFP-E-cadherin. In transformed IAR cells, AJs were dynamic and unstable.

The mean rate of movement of radial AJs in IAR-6-1 cells was 189 ± 21 nm/min. At the site of the cell-cell contact, GFP-E-cadherin initially aggregated into dot-like clusters. The majority of GFP-E-cadherin clusters grew and transformed into radial strands. Newly formed AJs were able to rearrange and relocate in the contact zone. The formation of radial AJs depends on myosin II-mediated contractility. In transformed cells, AJs were associated with straight actin bundles. Along with F-actin actin-binding proteins vinculin, zyxin and α-actinin were also recruited to cell-cell contacts.

Live-cell imaging of sparse cultures revealed significant differences in motile behavior of transformed IAR-6-1, IAR1170 and IAR1162 epithelial cells that did not express E-cadherin. We analyzed the movements of individual and contacting cells. Transformed IAR1162 cells could migrate over the substrate individually or form islands. IAR1162 cells in these islands easily broke cell–cell contacts, moving relative to each other and leaving the islands. We did not observe directed movements of groups of contacting IAR1162 cells. IAR1170 and IAR-6-1 transformed epithelial cells often formed islands. IAR1170 and IAR-6-1 cells often migrated in groups of cells (collective migration). In comparison with individual cells, the movement of cell groups was more directional. Cell–cell contacts in the islands were unstable. Transformed IAR1170 and IAR-6-1 cells could break contacts and migrate individually forming new contacts with neighboring cells. The expression of exogenous E-cadherin changed motile behavior of transformed IAR1162 epithelial cells, which lost endogenous E-cadherin. We revealed collective migration of 1162D3-EK2 epitheliocytes.

We also studied the migratory activity of transformed IAR cells in Bio-Coat migration chambers containing polycarbonate membrane inserts with 8-μm pores. The highest migratory activity was characteristic of transformed IAR-6-1 and IAR1170 epithelial cells, which expressed E-

cadherin. The migratory activity of IAR1162 cells, which lost E-cadherin as a result of transformation, was significantly lower. The cells of 1162D3-EM5, 1162D3-EK2, and 1162D3-EJ7 clones with high level of exogenous E-cadherin expression could migrate through polycarbonate membrane with 8-μm pores more easily than the cells of 1162D3 clone. The studies performed demonstrate the role of E-cadherin in collective cell movement that represents an efficient migration strategy of transformed epithelial cells. Plasticity of E-cadherin-based AJs is very important for carcinoma cell dissemination.

MIGRATION OF HUMAN ADIPOSE TISSUE-DERIVED MESENCHYMAL STEM CELLS (HASC) UNDER INFLAMMATORY CONDITIONS

O.A. Grigorieva, I.V.Korovina, V.Y. Sysoeva

Faculty of basic medicine, Lomonosov Moscow State University, Lomonosovsky pr., 31-5, 119192, Moscow, Russia

Adult perivascular mesenchymal cells play crucial role in tissue regeneration. Many authors referred to their ability to migrate to damaged area under influence of certain stimulus, some of them have been identified (SDF-1, PDGFBB), but still the mechanism of hASC homing remains unknown. In case of tissue damage inflammation triggers the first stage of regeneration and stimulates various cell types to proliferate and migrate into damaged area. Mesenchymal cells seem to transfer signals from immune cells to resident tissue stem cells. For example, in case of skin wounding infiltrating macrophages act through soluble factor and stimulate fibroblasts which appear to be mesenchymal cells of skin. Fibroblasts through secretion of KGF stimulate keratinocytes to proliferate and migrate into damaged area. So inflammation seems to be crucial for mesenchymal cells activation during tissue regeneration. To modulate inflammatory conditions in vitro we used contactless co-cultivation of hASC and macrophages derived from THP-1 cell line. Expression profile of chemokines, interleukines and receptors genes in hASC was analyzed with RTArrays assays (SABiosciences). This analysis revealed up to 100-fold increase in expression of pro-inflammatory interleukines (IL1, IL6, IL8) and chemokines, which take part in inflammatory and mesenchymal cells migration (CCL1, CCL2, CCL5, CXCL3, CXCL9, etc.). Revealed expression of these chemokines receptors in hASC under inflammatory conditions suggests their possible paracrine affection and role in mesenchymal cells migration. Anyhow migration rate of hASCs measured in scratch-assay increased more when twice under modulated inflammatory conditions. Directional migration of these cells measured with xCELLigence system (Roche) toward activated macrophages appeared to increase on case of migration through fibronectin-coated membrane, but not in case of collagene I-coated membrane. It has been shown that fibronectin can stimulate mesenchymal cells migration through PDGFRβ signaling activation. We revealed increased PDGFRβ expression and protein level (using RT-PCR and immunocytochemical technic) under inflammatory conditions in our system.

Although phosphorilated Akt, one of cell signal mediators, participating in actin reorganization and following cells migration, appeared to decrease in presence of macrophages, we revealed increase of phospho-Akt when cells were seeded on fibronectin-coated plastic even when exposed to inflammatory conditions. All received data suggest important role of fibronectin in mesenchymal cells migration under inflammatory conditions.

MOLECULAR DYNAMICS STUDY OF THE MYOSIN II MOTOR DOMAIN CONFORMATIONAL MOBILITY: INSIGHT INTO AN EFFECT OF THE CYSTEINE RESIDUES OXIDATION

D.S. Kanibolotsky

Educational and Scientific Centre "Institute of Biology", Taras Shevchenko National University of Kyiv, 2 Academician Glushkov prosp., corpus 12, Kyiv, 03022, Ukraine

Proteins oxidation by reactive oxygen species (ROS) is caused by a large number of muscle pathologies, such as alcoholic myopathy, muscle injuries and several forms of muscular dystrophy, including that realized due to aging [1]. Besides the ROS participation in the regulation of inflammatory response, the high pathogenic activity of the ROS can cause damage the muscle fibers and muscle proteins. In particular, the proteins cysteine residues can be oxidized by the ROS up to cysteic acid (Cya) [2]. It was shown that the ROS oxidation of the myosin sulfhydryl groups decreases myosin ATPase activity and enhances the myosin-actin interaction [1]. However, the detailed mechanism of the effect of the cysteine residues oxidation on the myosin ATPase activity and the myosin contractility is not fully clarified. Therefore, the aim of the present study is to assess the effect of oxidation of cysteine residues on the conformational mobility of the myosin motor domain form the mammalian skeletal muscle.

3D model of rabbit skeletal muscle myosin II motor domain (amino acid residues Met1-Leu785) in a post-rigor conformation has been built using the Swiss-Model server [3] http://swissmodel.expasy.org/. Protein Data Bank structure 2mys of chicken myosin II head has been used as a template, because the chicken myosin II is more similar to rabbit skeletal muscle myosin II among all the crystallized proteins (93% similarity and 87% identity according the BLAST algorithm). MgATP has been inserted into the catalytic site of the model. Molecular dynamics (MD) simulation of the native myosin II motor domain in 10 ns time scale have been performed using Gromacs 4.0.7 package [4] and Gromos 53a6 force field [5]. Solvent accessible surface areas of the cysteine residues sulfhydryl groups have been calculated for the MD trajectory. It has been determined, that the SH groups of all 10 cysteine residues (38, 123, 402, 403, 479, 522, 540, 676, 699 and 709) manifest more than zero accessible surface areas, consequently all of them can oxidize. All cysteine residues have been changed to Cya, 53a6 force field has been modified for Cya residues support, and new 10 ns MD trajectory of the oxidized protein has been calculated. Root-mean-square fluctuations (RMSF) of C_α atoms have been calculated for

steady part of both trajectories (3850-10000 ps). The same protein fragments reveal maximal flexibility of C_α atoms (RMSF > 0.18 nm) in native and oxidized motor domain: N-terminus (Met1-Ala8), SH3 subdomain (Lys36-Phe78), loop 1 (Ala200-Leu218), loop 4 (Met364-Val362), cardiomyopathy loop (Cys402-Asn418), relay loop (Gly507-Phe515), loop Leu559-Asn563, loop 3 (Lys567-His578), loop 2 (Leu622-Val651), loops Tyr726-Ser742 and Asn751-Glu758 in converter domain (Ser715-Lys770) and C-terminal residue (Leu785). The following amino acid residues are more flexible in native protein than in oxidized one (RMSF(native) – RMSF(oxidized) > 0.04 nm): Ser3-Ile9, Gly11 (N-terminus), Asn57, Leu65 (tips of the SH3 subdomain beta-hairpins), Asn136 (loop Pro128-Asn136 after second β-strand (Phe122-Asn127) of central seven-stranded β-sheet), Glu138 (helix Pro137-Ala142), Lys206, Lys207, Glu209-Lys213, Gln215 (loop 1), Thr307-Pro309, Phe314, Val322-Ser324 (loop Leu304-Asp326), Asn336, Asp339 (helix Asp327-Leu341), Arg371-Gln374 (loop 4), Arg405-Thr414 (cardiomyopathy loop), Phe512-Phe515 (relay loop), Gly516-Ala520 (helix Gly516-Glu527 after the relay loop), Ala629-Ser647 (loop 2), Tyr719-Ile728, Glu747, Lys748, Gly772 (converter domain). The following amino acid residues are more mobile in the oxidized myosin II motor domain (RMSF(native) – RMSF(oxidized) < –0.04 nm): Gln149, Glu150 (loop Tyr143-Ile155), Arg170 (loop Arg170-Asp171 between helix Phe156-Asp169 and fourth beta-strand Asn172-Thr178 of central beta-sheet), Glu509 (relay loop), Pro529 (loop Lys528-Gly531 between helices Gly516-Glu527 and HR), Asn563 (loop Leu559-Asn563), Thr626-Gly628 (loop 2), Gly737-Ile740, Asp754, Asp756-Glu758 (loops on the converter domain).

Energies of interaction, hydrogen bonds and distances between cysteine and neighboring amino acid residues have been monitored to elucidate mechanism of influence of the sulfhydryl groups oxidation on the myosin II motor domain flexibility. Cys38 is situated in the first β-strand of five-stranded β-barrel of the SH3 subdomain. SH group of Cys38 forms hydrogen bond with carbonyl oxygen of Phe78. Replacement of the thiol by sulphonic acid causes repulsion of the Cya38 side chain from oxygen atoms of Phe78 and Phe39 and attraction to NH group of Phe39. These interactions of oxidized Cys38 lead to reorientation of the residue and to a weakening of H-bond between carbonyl oxygen of Cya38 and NH group of Gly50.

Residues Cys402 and Cys403 are part of the cardiomyopathy loop. Sulfhydryl group of Cys402 from time to time forms H-bonds with carbonyl oxigens of Ala375 (in loop 4) and Leu398 (in α-helix Ser394-Leu401). Negatively charged sulfo group of Cya402, on the contrary, repulses oxygen atoms of Ala375 and Leu398. Bulk sulfo group of Cya402 clashes against C_δ atom of Pro377 and $CH_{\varepsilon 1}$ group of Phe366. These repulsions cause increasing of distances from Cya402 C_α atom to C_α atoms of Phe366, Ala375 and Pro377. On the other hand, sulfo group of Cya403 is repulsed from SO_3^- and carbonyl groups of Cya402 and pushes on the side chain of Gln374. Therefore distance between loop 4 and cardiomyopathy loop is increasing and conformational

space of these loops is shrinking after residues 402 and 403 oxidization. Because loop 4 and cardiomyopathy loop participate in actin binding, conformational change of the loops can influence actin-myosin interaction and muscle contraction.

Cys479 is placed in the N-terminus of the relay helix (Leu475-Glu506) after the switch 2 (Ile464-Ser474). Carbonyl oxygen of Leu475 is H-bound as with main chain amide as with sulfhydryl group of Cys479. Modification of Cys479 to cysteic acid induces repulsion of the sulfo group from carbonyl group of Leu475, which leads to reorientation of the Cya479 side chain, as well as of the main chain. Change of the Cys/Cya479 conformation causes rupture of H-bond between Cya479 NH group and Leu475 carbonyl, partial melting of relay helix N-terminus and reorientation of switch 2. Since switch 2 takes place in fixation of ATP molecule, and relay helix – in myosin power stroke, so Cys479 oxidation can impact on the both processes.

Cys522 and Cys540 are situated after relay loop in the Gly516-Glu527 helix and HR helix (Ile532-Cys540), respectively. Replacement of Cys522 SH moiety by SO_3^- provokes electrostatic repulsion from Glu485 carboxyl (in the relay helix) and steric conflict with C_δ atom of Ile526. This causes residue 522 reorientation, increasing of distance between C_α atoms of residues 485 and 522, breaking of H-bond between Cya522 carbonyl and Ile526 amide and partial untwisting of Gly516-Glu527 helix. Sulfo group of Cya540 is repulsed from carbonyl of Leu536 and clashes against side chain of Asn599 in Trp595-Lys600 helix. The Trp595-Lys600 helix contacts with N-terminus of the relay helix, with strut (Asp601-Asn604) and with N-terminus of HW helix (Ser652-Arg667). Relay loop, relay, HR and HW helices and strut participate in signal transduction from local conformational changes in ATP binding site, caused by nucleotide hydrolysis and its products release, to the global conformational transitions of the myosin head [6]. That is why oxidation of the Cys522 and Cys540 residues can modify coupling between ATPase activity and myofibrillar contractility.

Cys676 is included in the third β-strand (His670-Leu677) of central seven-stranded β-sheet. Adjacent, the fourth β-strand (Asn172-Thr178) is linked to P loop (Gly179-Lys185), which is important for ATP binding and release of products of its hydrolysis (orthophosphate residue and ADP). Sulfhydryl group of Cys676 sporadically forms H-bond with oxygen atom of Gly184, while NH group of the Cys676 is donor of H-bond for Thr178 oxygen. Sulfo group of Cya676 electrostatically repulses Gly184 oxygen, conflict with side chains of Ile177 and Asn188 and attracts amide hydrogen of Gly184. As a result, distances between Sγ atom of Cya676, on the one hand, and O atom of Gly184, $C_{\gamma 2}$ atom of Ile177, N_δ of Asn188, on the other hand, as well as between C_α atoms of Cya676 and Ile177, increase, while the distance between S_γ of Cya676 and N atom of Gly184, on the contrary, decreases in the oxidized myosin II. Reorientation of the Cya676 side chain leads to reorientation of the main chain and to weakening of H-bond between Thr178 carbonyl and Cya676 amido group.

Residue Cys699 is located in the C-terminus of SH2 α-helix (His690-Cys699) in close proximity to the SH1 α-helix (Leu703-Arg710), which in turn connects the converter domain with the rest of the motor domain. In the native protein, sulfhydryl group of the Cys699 sporadically donates H-bond to carbonyl oxygen of Phe467 (in the switch 2), main chain oxygen of the Cys699 serves as an H-bond acceptor for η hydroxyl group of Tyr584 (on the tip of the "wedge" β-hairpin, Phe579-Tyr590), while NH group of Cys699 is donor of H-bond for carbonyl oxygen of Hys695. Oxidation of Cys699 provokes formation of direct contacts between Cya699 and His695 side chains, repulsion of the sulfo group from oxygen atom of Phe467, formation of new H-bond between Tyr584 hydroxyl and Cya699 sulfo group, breaking of H-bond between Tyr584 hydroxyl and Cya699 carbonyl and weakening of the bond between His695 carbonyl and NH group of Cya699.

Influence of oxidation of Cys123 and Cys709 on myosin II head conformation has not been revealed in the present study.

References

[1] Prochniewicz E., Spakowicz D., Thomas D.D. Biochemistry. 2008, 47 (45), P. 11811-11817.

[2] Nachmias V.T. et al. Biochim. Biophys. Acta. 1982, 700 (2), P. 198-205.

[3] Bordoli L. et al. Nature Protocols. 2009, 4, P. 1-13.

[4] Hess B. et al. J. Chem. Theory Comput. 2008, 4 (3), P. 435-447.

[5] Oostenbrink C. et al. J. Comput. Chem. 2004, 25 (13), P. 1656-1676.

[6] Ovchinnikov V., Trouta B.L., Karplus M. J. Mol. Biol. 2010, 395 (4), P. 815-833.

CHAPERONIN HSP60 AS IMPORTANT REGULATORY MOLECULE AT HEART FAILURE PROGRESSION

L. Kapustian, V. Bobyk, O. Rozhko, I. Kroupskaya, D. Ryabenko*, L. Sidorik

Institute of Molecular Biology and Genetics NAS of Ukraine,150 Zabolotnogo street,03680, Kyiv, Ukraine

**Strazhesko Institute of Cardiology MAS of Ukraine, Kyiv, UKRAINE*

The study of the mechanisms of anti-stress response is quite important for evaluation of heart failure origin and progression and for development of new effective therapeutic tools based on the apoptotic signaling blockage. Specialized family of anti-stress proteins including molecular chaperons, their co-chaperons, and target proteins plays a critical role in pro- and anti-apoptotic signaling.

Hsp60, the main mitochondrial chaperone, is of special interest since recent data evidence the location of 10-30% of this protein in cytoplasm of cardiomyocytes. Recently it has been shown on the cultured neonatal cardiomyocytes that molecular chaperone Hsp60 is capable to form complexes with proapoptotic proteins Bax and Bak, not allowing them to precipitate the apoptosis. The decrease in Hsp60 level in cardiomyocytes resulted in translocation of Bax protein to mitochondria and launch of apoptosis.

On the other hand, the important role of Akt and p70S6K kinases in apoptosis regulation has been observed recently. Akt is a serine-threonine kinase involved in multiple cellular processes. In the heart, Akt activation has been demonstrated to increase cell size and decrease apoptosis. Heart-specific isoform Akt1 activation is thought to be beneficial for the failing heart.

p70S6 kinase is one of the crucial protein required for cell growth and G1 cell cycle progression. p70S6 kinase phosphorylates the S6 protein of the 40S ribosomal subunit and is involved in translational control. Recently the pro-apoptotic molecule BAD was identified as one of the main p70S6K and Akt1 targets phosphorylated on the Ser^{112}- and Ser^{136}-residues by both kinases.

We investigated possible changes of expression and activity of p70S6K1 and Akt1 kinases in myocardium at heart failure progression using experimental mouse models of inducible myocarditis and DCM-like pathology developed in our laboratory. We observed significant changes in the level of p70S6K1 expression and have not found the changes of Akt1 expression level in diseased myocardia. At the same time we observed changes in its activity at the final stage of the disease progression compared with normal myocardium.

Many signal transduction cascades which control cell cycle, homeostasis and apoptosis are dependent on the assistance by molecular chaperones. Thereby the molecular chaperons can maintain of their target proteins in active or inactive conformations. Based on bioinformatic prediction of possible functional complexes formation between molecular chaperone Hsp60 and Akt1 kinase from one side, and between Hsp60 and Akt1 from other side - we have detected this interactions for the first time by co-immunoprecipitation method in normal and pathological myocardia.

We supposed that Hsp60 could form *in vivo* functional complexes with p70S6K and Akt1 that play a crucial role in regulation of stress-induced apoptotic signal pathways in cardiomyocytes. The mechanism of such complexes formation should be elucidated. We presume that Hsp60 is a general connecting-link in the regulation of cardiomyocytes apoptotic signalling at heart failure progression.

ENDOTHELIAL MONOLAYER PERMEABILITY FOR MACROMOLECULES IS ASSOCIATED WITH THE HIGH MOLECULAR WEIGHT MYOSIN LIGHT CHAIN KINASE ACTIVITY

O.A. Kazakova, M.V. Samsonov, A.Y. Khapchaev, E.L. Vilitkevich, A.V. Nikashin, M.V. Sidorova, Zh.D. Bespalova, V.P. Shirinsky

Institute of Experimental Cardiology, Russian Cardiology Research and Production Center, Moscow, 121552, Russia

It is widely accepted that stress-induced acto-myosin activity evokes endothelial cell contraction and results in disintegration of intercellular contacts, increased endothelial permeability, and tissue edema. High molecular weight myosin light chain kinase (MLCK210) is a specialized calcium/calmodulin

(Ca^{2+}/CaM)-dependent protein kinase that phosphorylates and activates myosin in endothelial cells. Indeed, pharmacological or genetic inactivation of MLCK210 in endothelium allows protect the barrier function of endothelial monolayer. These data support the key role of MLCK210 in endothelial permeability. However, some experimental data concerning the mechanisms of MLCK210 activation in endothelial cells are not in concert with the general paradigm of MLCK activation. It is well known that MLCK affinity to CaM stays in nanomolar range suggesting that this enzyme is rapidly activated following an increase in free intracellular calcium concentration ($[Ca^{2+}]_i$). This is exactly what happens in smooth muscle: an increase in $[Ca^{2+}]_i$ evokes rapid activation of smooth muscle MLCK isoform and phosphorylation of myosin regulatory light chains (RLC). In endothelial cells, in contrast to smooth muscle, an increase in $[Ca^{2+}]_i$ is insufficient to instantly activate MLCK210 indicating that some additional mechanisms of MLCK210 inhibition are present in these cells. In order to get insight into these mechanisms, we investigated the time-course of MLCK210 activation in endothelial cells and its relation to endothelial monolayer hyperpermeability.

Using two structurally distinct inhibitors of MLCK (either ML-7 which competes for ATP binding, or a specific cell-permeable peptide inhibitor of MLCK PIK1 (Nα-methyl-Arg-Lys-Lys-Tyr-Lys-Tyr-Arg-Arg-Lys) and Rho-kinase inhibitor Y27632, we analyzed the dynamics of myosin RLC phosphorylation in EA.hy926 endothelial cells following stimulation with alpha-thrombin – a potent natural edemagenic agent that readily induces endothelial barrier dysfunction. In the presence of Y27632 the peak of RLC monophosphorylation was observed 20 min following thrombin addition. In contrast, in the presence of MLCK inhibitors, myosin RLC were rapidly phosphorylated within the first 5 min following cell stimulation with thrombin. These data indicate that while both Rho-kinase and MLCK210 contribute to myosin RLC monophosphorylation, the activation of these enzymes is temporarily distinct.

Analysis of FITC-albumin diffusion through EA.hy926 monolayer stimulated with thrombin revealed sharp increase in permeability of the monolayer to FITC-albumin 30 min after thrombin addition. The increase in FITC-albumin passage through the monolayer correlated with the peak of MLCK210 activity and the restoration of the monolayer barrier coincided with the return of P-MLC to the initial levels. MLCK210 inhibitors abolished thrombin-induced FITC-albumin hyperpermeability of endothelium.

Altogether, our results indicate that the permeability of endothelial cell monolayer to macromolecules is associated with the activity of MLCK210. Considering the fact that thrombin addition results in fast increase of $[Ca^{2+}]_i$ in endothelial cells, our findings of the delayed activation of endothelial MLCK support the hypothesis that MLCK210 in endothelial cells is the subject for unconventional regulation through the additional inhibitory mechanisms that prevent immediate enzyme activation after the impact of Ca^{2+}-mobilizing edemagenic factors.

Supported by RFBR grant 11-04-01343-a to VPS

TROPOMYOSIN AS A REGULATOR OF ACTIN DYNAMICS

Sofia Yu. Khaitlina[1], Horst Hinssen[2]

[1]Institute of Cytology, Russian Academy of Sciences, Tykhoretski Av. 4, 194064 Sankt-Petersburg, Russia,
[2]Biochemical Cell Biology Group, University of Bielefeld, Germany

Tropomyosin has been primarily regarded as a muscle protein that regulates the interaction of actin-containing thin filaments with myosin-containing thick filaments to allow contraction (Perry, 2001). However, multiple tropomyosin isoforms are also expressed in nonmuscle cells where tropomyosin participates in a number of cytoskeleton-mediated cellular processes (Gunning et al., 2008). Moreover, recent studies in a variety of systems have shown that the diversity of actin cytoskeleton functions is paralleled by a diversity of tropomyosin isoforms, i.e. many functions of the actin cytoskeleton are related to spatial segregation of tropomyosin isoforms (Gunning et al. 2008; Wang, Coluccio, 2010; Lees et al., 2011). To reveal the mechanisms underlying these relations it is important to understand how tropomyosin interacts both with actin and actin-binding proteins that are involved in the regulation of actin dynamics.

Tropomyosin has been found in virtually all life forms except bacteria and plants (Lees et al., 2011). In mammals, there are four genes that code for tropomyosin: α, β, γ, and δ, also referred to as *TPM1*, *TPM2*, *TPM3*, and *TPM4*, respectively. Alternative splicing of these four genes, the use of multiple promoters, and the choice of polyadenylation site lead to expression of at least 22 different tropomyosins in humans. Altogether, there are over 40 mammalian tropomyosin isoforms, 18 of which are expressed in nonmuscle cells (Gunning et al., 2008). Tropomyosin is a two-chained □-helical coiled coil (often referred to as a"dimer") that associates end-to-end to form continuous strands along both sides of the actin filament, such that one molecule spans the length of seven or six actin monomers. This binding requires regions of local instability or disorder that allow the coiled coil to bend and conform to the actin filament helix. The flexibility derives from bends and local unfolding at regions with a destabilized coiled-coil interface, as well as from the dynamic end-to-end complex (Hitchcock-DeGregori, 2010). Both stiffening the actin filament and flexibility/instability of the binding are important for regulation by tropomyosin of actin dynamics.

Tropomyosin does not bind globular actin; tropomyosin molecules attach to actin filament conjointly rather than separately, in a way indicating very high cooperativity. Cooperative binding strengthens tropomyosin's affinity for actin that is quite weak when single tropomyosin molecules bind to actin individually (Tobacman, 2008). This implies that the effect of tropomyosin on actin polymerization, if any, is rather complicated. Studies addressing this issue did not yield consistent results. Experiments *in vitro* showed that tropomyosin accelerated (Pragay, Gergely, 1968) or inhibited (Lal and Korn, 1986) spontaneous polymerization of ATP-actin, and altered the monomer

association and dissociation rates at both ends of the filament (Lal and Korn, 1986). Another study reported that tropomyosin prevented filament fragmentation but had no major effect on association or dissociation of monomers from filaments ((Hitchcock-DeGregory et al., 1988). These discrepancies can be rationalized in terms of the rate of binding of tropomyosin to actin filaments. Actin polymerization is not retarded by tropomyosin if it is faster than binding of tropomyosin to actin filaments; but the rate of polymerization decreases if it is slower than binding of tropomyosin at the ends of actin filaments. It was assumed that actin-bound tropomyosin molecules which extend beyond the ends of actin filaments retard association of actin monomers with filament ends (Wegner, Ruhnau, 1988).

Further studies showed, however, that the effect of tropomyosin on actin polymerization is not simply mechanical. Tropomyosin stopped disassembly from the pointed end of actin filament, without capping the filament end to elongation (Broschat, 1990). Also at the barbed filament end, tropomyosin-induced conformational changes manifested themselves by the altered mode of binding of cytochalasin (Suzuki, Mihashi, 1991) and by a higher resistance of stress fibers to cytochalasin and latrunculin in the tropomyosin overexpressed cells (Creed et al., 2008). Moreover, tropomyosin restored polymerization of non-polymerizable yeast actin mutant in which the hydrophobic cross-strand contacts were impaired (Wen et al., 2000), and inhibited an enhanced dynamics of proteolytically modified actin in a cooperative manner (Khaitlina, Strzelecka-Golaszewska, 2003). Thus stabilization by tropomyosin of actin filament involves conformational changes within the filament that seem to modify the monomer-monomer contacts along the filament.

Lateral localization of tropomyosin along actin filaments obviously raises the question of interaction between tropomyosin and other actin-binding proteins. Tropomyosin was shown to slow down depolymerization of actin with DNase I (Hitchcock-DeGregory et al., 1976) and to protect actin filaments from disassembly with ADF/cofilin (Ono, Ono, 2002; Mazur et al., 2010). Moreover, purified ADF/cofilin did not interact with the native actin filaments unless tropomyosin was removed. Tropomyosin and ADF/cofilin were localized by fluorescence staining to different places in muscle, indicating that their mutual exclusivity is also exhibited *in vivo* (Ono, Ono, 2002). Similarly exclusive with tropomyosin seems to be Arp2/3 complex that binds to the side of an existing actin filament nucleating a new filament to form a branch. The presence of tropomyosin on an existing filament inhibits the action of Arp2/3 complex (Blanchoin et al., 2001). This would well correlate with the fast branched actin polymerization at the cell leading edge if the absence of tropomyosin in lamellipodia would not be controversial (Des-Marais et al., 2002; Hillberg et al., 2006). In the early works, a partial protection of F-actin against fragmentation by gelsolin was also shown by flow birefringence measurements and electron microscopy (Fattoum et al., 1983; Ishikawa et al., 1989; Dabrowska et al., 1996). However, this effect appears to be more complicated because interaction between gelsolin and tropomy-

osin was postulated from the results of affinity chromatography of gelsolin on immobilized tropomyosin (Koepf, Burtnick, 1992; Reid et al., 1993) and from the effect of gelsolin on tropomyosin aggregation (Maciver et al., 2000). A special work was therefore designed to reveal the effects of tropomyosin on gelsolin functional properties including severing by gelsolin of tropomyosin-decorated filament.

The results of limited proteolysis showed that tropomyosin clearly inhibited cleavage of Ca-activated gelsolin with thermolysin and accelerated cleavage with trypsin which confirmed gelsolin/tropomyosin complex formation in the presence of Ca^{2+}. Interaction with tropomyosin did not prevent formation of the 2:1 G-actin/gelsolin complexes, tropomyosin did not diminish affinity of G-actin to gelsolin and did not affect nucleating activity of gelsolin in actin polymerization. To evaluate the effect of tropomyosin on the severing activity of gelsolin we determined viscosity and the relative number concentrations of the filaments in the solutions of F-actin fragmented with gelsolin alone or with gelsolin/ tropomyosin complexes. Comparison of skeletal and smooth muscle actins, skeletal and smooth muscle tropomyosins, and □- and □-tropomyosin homodimers showed that interaction of gelsolin with tropomyosin resulted in 40-60% less efficient fragmentation of F-actin than that by gelsolin alone. Thus, being bound to gelsolin tropomyosin does not seem to interfere with capability of gelsolin to nucleate actin polymerization but inhibits severing activity of gelsolin toward actin filaments. In contrast, efficiency of fragmentation by gelsolin was similar for F-actin alone and F-actin decorated with tropomyosin. Thus, being bound to actin filaments tropomyosin did not prevent severing of the filaments by gelsolin. These results suggest that tropomyosin is involved in regulation of actin dynamics not via protection of the filaments against severing by gelsolin but rather by binding gelsolin in solution to promote formation of new actin filaments.

PHOSPHORYLATION OF N-TERMINAL ACTIN-BINDING DOMAIN OF THE MYOSIN LIGHT CHAIN KINASE IN CELLS AND *IN VITRO*

A.Yu. Khapchaev, V.P. Shirinsky

Institute of Experimental Cardiology, Russian Cardiology Research and Production Center, Moscow, 121552, Russia

Myosin light chain kinase (MLCK) is a highly specialized calcium/calmodulin (Ca^{2+}/CaM)-dependent protein kinase that phosphorylates and activates smooth muscle and non-muscle myosin II to drive actomyosin motile events. High affinity actin-binding site of MLCK consists of a set of DFRXXL motifs equally spaced in the primary structure of the protein. 210 kDa MLCK has five such motifs in the middle of the molecule while 108-130 kDa MLCK possesses motifs three to five at its N-terminal end. Sequence analysis identifies several putative phosphorylation sites in a vicinity of DFRXXL motifs. Additionally, our previous in vitro studies demonstrated that phosphorylation of recombinant N-terminal domain of 108-130 kDa MLCK encompassing 75 N-terminal amino acids (N75) by MAP kinase at

Thr43 significantly reduces N75 affinity to F-actin. These results suggest that phosphorylation adjacent to DRFXXL motifs may regulate MLCK association with actin cytoskeleton. However, to the best of our knowledge, there are no reports concerning the phosphorylation of actin-binding domain of MLCK in cells.

In order to investigate the putative phosphorylation of the N-terminal domain of MLCK in cells, HEK293-T cells were transfected with the genetic construct encoding N75 and grown in the presence of $NaH_2{}^{32}PO_4$. Exogenous N75 and endogenous MLCK were precipitated using monoclonal anti-MLCK antibody (K36, Sigma). We observed ^{32}P label incorporation in both N75 and MLCK. Remarkably, the extent of radioactive phosphate incorporation in both proteins was significantly reduced in the presence of CaM inhibitor W7 suggesting a role for CaM-dependent kinases and possibly CaM binding to N75. Indeed, CaM-dependent kinase II (CaMKII) readily phosphorylated purified N75 in vitro. Moreover, N75 could be phosphorylated in vitro by catalytic subunit of cyclic-AMP-dependent protein kinase (PKA), p21-activated protein kinase 2 (PAK2), mitogen-activated protein kinases (MAPK) $p42/44^{erk}$ and p38, and protein kinase C alpha (PKCa).

Based on the functional consequences of N75 phosphorylation by MAPK in vitro, it is tempting to suggest that phosphorylation within actin-binding domain of MLCK by abovementioned protein kinases may also decrease its affinity to actin and lead to dissociation of MLCK from actin filaments. While in smooth muscle this might be of minor significance due to very high myosin concentration, in non-muscle cells where myosin concentration is relatively low the separation of MLCK from microfilaments may substantially reduce the efficiency of myosin II recruitment to actin accomplished by MLCK and, therefore, negatively affect local force generation.

Altogether, our findings indicate that N-terminal domain of MLCK could be phosphorylated in non-muscle cells and in vitro, in particular, in a CaM-dependent way and suggest that this phosphorylation may regulate actomyosin assembly and activity in non-muscle cells.

Supported by RFBR grant 11-04-01343 to VPS.

PROGRESS IN DEVELOPMENT OF THE NOVEL ANTIEDEMIC DRUGS BASED ON PEPTIDE INHIBITORS OF THE MYOSIN LIGHT CHAIN KINASE

A.Yu. Khapchaev, M.V. Sidorova, O.A. Kazakova, M.V. Samsonov, E.L. Vilitkevich, V.N. Bushuev, A.A. Abramov, V.L. Lakomkin, V.I. Kapelko, Zh.D. Bespalova, V.P. Shirinsky

Institute of Experimental Cardiology, Russian Cardiology Research and Production Center, Moscow, 121552, Russia

Acute lung and brain edema is the serious medical condition associated with 40-60% in-hospital mortality in spite of intensive medical interventions. This situation is due in part to the lack of effective antiedemic drugs available on the market. In order to meet the need for such medicines we ini-

tiated the search for the substances with antiedemic activity among the inhibitors of the myosin light chain kinase (MLCK) – a key regulator of vascular endothelium paracellular permeability. The rationale to choose MLCK as molecular target for preventing tissue edema comes from the demonstration that MLCK activity is involved in reduction of endothelial monolayer integrity following the impact of various stress-factors such as thrombin, histamine, reactive oxygen species, bacterial endotoxins, excessive mechanical deformation, etc. Small molecule organic inhibitors of endothelial MLCK such as ML-7, ML-9 and other prevent the loss of endothelial barrier function, however, the majority of these substances has pharmacologically unprivileged chemistry and is not suitable for drug development due to unwanted side effects. Peptide inhibitors of MLCK are not of xenobiotic origin and demonstrate better selectivity towards MLCK due to a different mechanism of recognition. While small organic MLCK inhibitors compete with endogenous ATP in an ATP-binding pocket of the enzyme and may theoretically bind multiple other nucleotide-binding proteins, peptide inhibitors compete with the myosin light chains and utilize a highly specific substrate recognition process unique for MLCK.

In general peptides are not cell-permeable molecules but peptide inhibitors of MLCK are an exception to this rule. Both Peptide 18 (also called PIK or Peptide Inhibitor of Kinase) designed by Lukas et al. (1999) as modified autoinhibitory sequence of MLCK and peptide MLC_{11-19} designed by Pearson et al. (1986) that represents part of the 20 kDa myosin light chain sequence can enter live cells by a yet unknown mechanism. The cell permeating activity of these peptide molecules is attributed to the presence of positively charged amino acid clusters in their structure (PIK=**RKK**YKY**RRK**; MLC_{11-19}=**KKR**AARATS) which renders them similar to the transduction peptide TAT of a corresponding HIV-1 protein (Schwarze et al., 1999).

Another weak side of many peptides as potential drugs is their low stability in biological milieu such as blood or gut juice due to rapid degradation by extracellular peptidases. Thus, the major challenge in developing antiedemic drugs based on peptide inhibitors of MLCK is to make them stable to proteolytic degradation without loss of inhibitor and cell-permeating activity. We first approached this problem by designing a peptidase-resistant D-amino acid version of PIK (D-PIK) and were able to demonstrate that D-PIK prevents thrombin-induced endothelial hyperpermeability in vitro and endotoxin-induced or oleic acid-induced acute lung edema in rats (Marchenko et al., 2009). However, D-PIK as well as its L-PIK-like version retroenantio-PIK turned out to be weak MLCK inhibitors. In addition, the synthesis of peptide from D-amino acids is significantly more expensive than the synthesis of L-amino acid based peptide making the future D-PIK drug less affordable to patients. Therefore, our next step was to introduce targeted protective modifications in the structure of L-PIK that would increase its stability in blood without loss of inhibitory and cell-permeating activities.

Since we expect intravenous administration of antiedemic peptides to

the patients in an intensive care unit we specifically focused our efforts on increasing stability of modified PIK peptides in human blood plasma. We used ^{1}H-NMR analysis to assess the time course of L-PIK degradation in blood plasma and identified the sites primarily attacked by peptidases. We observed that degradation starts from N-terminus and designed several protective modifications of Arg1. The best modification contained methyl group attached to N^{α} of Arg1 [N^{α}MetArg^1]-L-PIK. Resultant peptide designed PIK1 had MLCK inhibitory activity similar to that of L-PIK but 2.5-fold longer half-life in blood plasma than L-PIK. PIK1 was as potent as L-PIK in preventing thrombin-induced hyperpermeability in vitro and protected rats from lipopolysaccharide (LPS)-induced lung edema. NMR analysis of PIK1 demonstrated that its degradation no longer started at the N-terminus but rather occurred at a slower rate from the C-terminal end. To block this process we introduced the set of site specific modifications in PIK1 and obtained PIK2, 3, 4 and 5 peptides. PIK2 and PIK5 peptides were stable in blood plasma for more than 7 hours. Other peptides were less stable than PIK2 and PIK5 but exceeded the stability of PIK1. Based on MLCK inhibition potency synthesized peptides were rated in the following way: PIK2>L-PIK=PIK1, PIK3, PIK4, PIK5> D-PIK>retroenantio-PIK. PIK2 appeared to be more potent MLCK inhibitor than L-PIK/PIK1 and was able to protect endothelial monolayer barrier against thrombin challenge in vitro at lower concentrations than PIK1. In agreement with these results, PIK2 attenuated LPS-induced lung edema in rats and demonstrated tendency for increased animal survival when administered at lower dose than PIK1.

Altogether, these results indicate that we produced an optimized L-PIK-based version of MLCK inhibitor that prevails over known L-PIK analogs in an antiedemic potency. This molecule is our leading compound in the development of the novel antiedemic drugs to fight acute lung and brain edema.

Supported by the Federal Contract 16.512.12.2003 with the Ministry of Education and Science of Russia and RFBR grant 11-04-01343-a

CHANGES OF THE SKELETAL MUSCLE CONTRACTION PARAMETERS DURING ACUTE ISCHEMIA

O.M. Khoma[1], O.V. Dolgopolov[2], D.M. Nozdrenko[1], M.S. Miroshnichenko[1]

[1]Taras Shevchenko Kyiv National University, Department of Biophysics, Volodimirska Str., 64, 01033, Kyiv, Ukraine;

[2]Institute of Traumatology and Orthopedics of Medical Sciences of Ukraine, Vorovskogo Str., 01601 Kyiv, Ukraine.

Clinical features of compartment syndrome are difficult to study and they are not systematized due to complex parallel processes in the genesis of severe skeletal trauma. Criteria for classification of the severity and stage of the syndrome depending on the processes of compensation/decompensation of the regional blood flow are also not defined. Published data on interstitial

pressure in fractures are rare. This most important criterion, which allows adequate assessment of regional blood disorder, has not yet been sufficiently implemented in clinical practice. Of fundamental importance, there is lack of clinical-anatomical and experimental studies aimed at developing an algorithm for the diagnosis and choice of treatment in patients with closed fractures. Therefore, research in this area is very important as it has both theoretical and practical relevance.

Experiments were performed on adult rats weighing 200-300 g. The duration of the experiment was 8 hours, while the acute ischemia lasted 5 hours. Blood pressure was measured using cannula inserted into the transverse colli artery. A set of tensoresistors was used as pressure sensor.

Muscle ischaemisation was performed through an incision of the skin (length 1.5-2.5 cm) of the inner sagittal-cranial thigh, fixed with an automatic wound extender. The femoral artery was ligated, which led to the cessation of regional blood flow and development of tissue ischemia 5 hours after surgery. After five days, the degree of ischemia in the operated extremity was sufficient to perform the main part of the experiment.

Standard techniques included preparation and cannulation (for drug infusion and blood pressure measurements), tracheotomy, and laminectomy of the lumbar spinal cord. Muscle was carefully freed from surrounding tissue, while its vascularisation remained intact. Muscle tendons were cut and attached to steel hooks of the mechanostimulator. To apply modulated stimulation of efferents in the L7-S segments, the ventral roots were cut immediately at their exit from the spinal cord. To record strength of contraction of skeletal muscle fiber bundles custom-made tensometer (Department of Biophysics, Taras Shevchenko Kyiv National University) was used.

The results show that incomplete vascular ischemia is accompanied by significant changes in the structure of muscle fibers. As a result, the possibility of adequate realization of motoneuron activity innervating the muscle was decreased. This was primarily seen as muscle inability to maintain a steady level of the force response. It was also found that incomplete vascular ischemia caused significant changes during the pre-tetanus stages of contraction. Reduction of the rate of force production made it impossible to produce controlled muscle movements, which could lead to a complete loss of control over the damaged extremity (Fig. 1).

The period of linear decline in the frequency of stimulation (Δt_1), which on the graph of force changes coincides with the F1 segment and reflects the transition to the new muscle stationary level of contraction, in this case shows the rate of change of force response. As shown in Fig. 1, the rate of change of force in this segment decreases linearly with time of ischemia and correlates with the total force response.

Pre-tetanus stimulation (Δt_3) which causes single muscle contractions shows a linear decrease of the force response at all time intervals studied. With increase of the frequency of stimulation to a new steady level (interval Δt_4) after the pre-tetanus plateau is passed (Δt_3) the rate of change of force

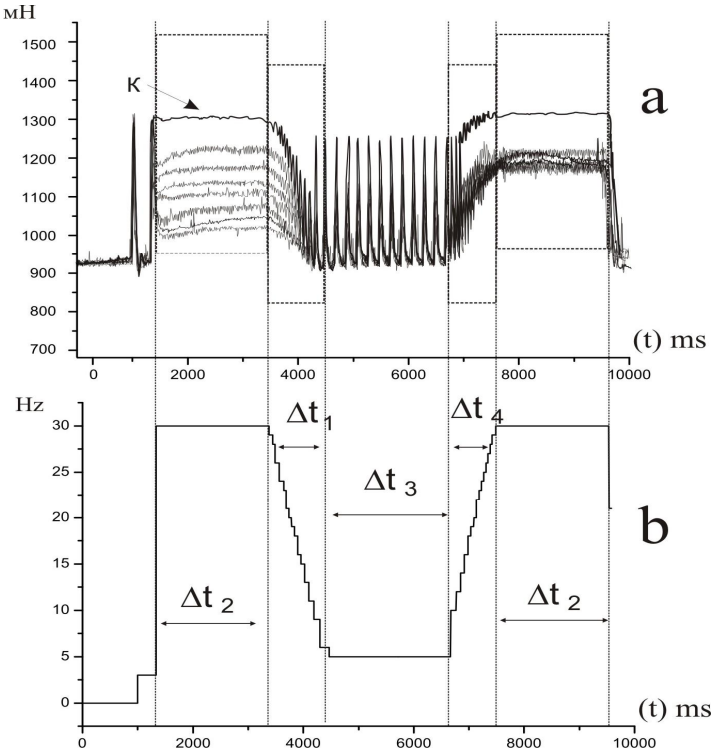

Traces of force generation in ischemic m. gastrocnemius during modulated stimulation. (A) - traces of change of muscle force response. (B) - frequency patterns of the applied electrical stimulation. Δt_1 - Δt_4 time intervals of stimulation. K- control, traces of force generation in nonischemic *m. gastrocnemius*

does not change at all time intervals and is approximately 80% of control. Thus, ischemic muscle transits to a new stationary level of contraction with about 20-30% loss in the maximal force.

Thus, this property of ischemic muscle contraction can to some extent compensate the reduction in the force of ischemic muscle response and reduce the loss in muscle performance moving muscle to a new steady level of only 20-30% lower than the physiological norm. This may be a compensatory protective mechanism of the damaged muscle.

During acute ischemia there are also significant changes during pretetanic contraction. Reduction in the rate of force generation makes controlled movements impossible that can lead to a complete loss of control over the damaged limb. In any case, it is evident that five hour ischemia causes irreversible pathological changes both at the level of individual muscle fibers and at the level of nerve-muscle transmission. In this case, execution of central

nervous commands will be accompanied by uncontrollable motor responses with incorrect positioning of the joints and tremor of the ischemic muscle.

The compensatory component of the regulation of muscle contraction that involves reduction in the overall muscle performance to maintain control of muscle contraction allows the muscle to adequately respond to motor commands. However, elevated fatigue processes in the ischemic muscle limit duration of these compensatory mechanisms as a result of almost complete suppression of the force response.

FLUORESCENT NANOSCOPE

Andrey A. Klimov [1], Dmitry A. Klimov [2]

[1] ITEB RAS, 142290 Pushchino, Moscow Region, Institutskaya street 3, Russia;

[2] President, Stereonic International Inc. dk@stereonic.com

Late 90's have met with increasing interest to nano-bio systems in basic and applied research, but researchers were limited in their ability to visualize biological structures and processes in native (liquid) environment on nanometer scale. Over the centuries, optical microscopy based on use of lenses has been limited in resolution to approximately 200 nm due to physical properties of light registering methods. It was believed that this is a limit that can not be overcome. Recent boom in development of sub diffraction techniques (NSOM, STED, RESOLFT, PALM, FPALM, STORM, dSTORM, GSDIM etc.) showed that not only the limit can be overcome, but also that there is a number of different strategies to doing so.

We discuss the concepts of a nanometer-scale-resolution fluorescence microscopy that can be used in a number of different areas of research, diagnostics, quality assurance etc. These technologies are based on photoactivation-excitation-registration-bleaching principle that can be applied for a wide range of fluorescent dyes including caged fluorescein- and rhodamine- based dyes and photoactivatable, photoconvertible and photoswitchable proteins.

Our team develops a sub diffraction technique based on photoactivation-excitation-registration-bleaching cycle (first publication: patent RU2305270 priority date May 18, 2005 and subsequent PCT publication PCT/RU2006/000231 and US patents 7,803,634 and 8,110,405 [1], 5 days before a provisional application 60/683,337 for similar technology was filed by our first competitors Eric Betzig et. al. to US Patent Office and long before other applications for similar technologies were filed by several other teams to Patent Offices in different countries or were sent as articles to different journals). It was shown that this approach allows obtain resolution up to 2 nm, i.e. 100 times higher than in a conventional microscope. Key articles were acknowledged as breakthroughs of the year by Science Magazine in 2006 [2] and by Nature Methods in 2008 [3]: several teams started development of similar techniques such as PALM [2], STORM [4] and GSDIM, licensed their technologies to major microscope manufacturers (Carl Zeiss,

Leica Microsystems and Nikon), which lead to deployment of first commercial microscopes with resolution around 20 nm in 2009.

The idea behind a plurality of localization microscopy technologies ("Fluorescent Nanoscopy", PALM, FPALM, STORM, dSTORM, GSDIM are the most well known acronyms for these techniques) is to overcome the limits of optical microscopes by sparsely photoactivating fluorescent molecules which are densely covering objects structures surfaces and invisible before activation. Only a small percentage of labels in the specimen is activated on each step (i.e. converted from non-fluorescent state to fluorescent state). This way, activated molecules that are located far from each other are visible as separate spots, covering tens of pixels on CCD or EMCCD or ICCD. The positions of activated molecules can be identified by localization of centers of these spots with sub pixels accuracy. Localization precision depends on the signal level (i.e. amount of photons captured by the camera) and the signal-to-noise ratio (i.e. background fluorescence of the specimen, its immobility when thousands of frames are captured, sensitivity, internal noise and other properties of the camera). After that the dye fades away due to photobleaching or temporal deactivation, a new portion of molecules is activated and new frame is captured. This process (activation, image capturing and photobleaching) is consecutively repeated until an adequate amount of frames (typically, above 1000) is captured, each of the frames providing information about separate molecules, which is enough to assemble the high-content image by reconstruction of positions of centers of collected spots.

Due to the time-lapse nature of these methods (i.e. long exposition time – typically ~10 minutes) high resolution imaging is easily possible for non-moving macromolecular structures such as, cytoskeleton, microtubules, focal adhesion complexes, nuclei, mitochondria, reticulum etc, rigidly bound one with another and with glass slide. It is possible to use information about movement of special bleach-resistant fluorescent labels, attached to macromolecules for calculation of coordinates of activated fluorescent molecules in internal coordinates of slow-moving macromolecular structures.

Single-particle-tracking PALM (sptPALM) [5] was shown to allow consecutive tracing hundreds of molecules within a diffraction-limited spot, which was previously considered impossible. This approach allows visualize movement of subcellular structures or at least to measure timing and quantify movement of biological substances within the cell – identify signaling pathways, response to external influences, transportation of proteins, not to mention larger structures such as liposomes, mitochondria etc. Morphological changes in endoplasmic reticulum is one of those processes that has been already visualized with molecular-level precision in native environment.

Fluorescent nanoscopy may be used for different investigations in different areas of science, one of them being Biophysics, fundamental issues in life sciences, that can be questioned and examined through visualization of molecular transportation system with its "railroads" and "carriers". Methods using single molecule tracking and single particles tracking in living systems are used for tens

of years, but only in few latest articles (e.g. [5]) authors combined photoactivated localization microscopy (PALM) with live-cell single-particle tracking to create a new method termed sptPALM. They created spatially resolved maps of single-molecule motions by imaging the membrane proteins Gag and VSVG, and obtained several orders of magnitude more trajectories per cell than traditional single-particle tracking allows. By probing distinct subsets of molecules, sptPALM can provide insight into the origins of spatial and temporal heterogeneities in membranes. In [9] slide 46 shows that actin molecules labeled by photoactivatable GFP are moving toward center of cell alongside of actin filament. By our opinion, the best explanation for this their superresolution observation is next: actin filaments are polymerizing at the end close to surface of cell and depolimerize close to nuclei of cell. In [10, 11] it was shown that using photoactivated localization microscopy, movement of individual actin molecules and actin filaments within living dendritic spines can be measured.

We expect appearance of many new combinations of old methods with different variants of new fluorescent nanoscopy, using which it should become possible to visualize with resolution better than 20 nm not only structures of objects, but some unknown processes, which may be detected by Fluorescent Nanoscopy, such as movement of different parts of object, photochemical conversion, synthesis of genetically modified molecules, containing fluorescent proteins, chemiluminescence's, detection of antigens etc.

Experimental method

We have made a Fluorescent Nanoscope according to scheme described in [1], using inverted microscope, laser 473 nm, 500 mW, objectives 10x and 20x for visual search of object on quartz glass slide. Objective 100x, A=1.23 for collecting light of fluorescing molecules. Just after objective the light that was collected by objective is sent to Semrock filter LP02-473RS-25, having density more than D=6 at 473nm and transmitting over 95% light at wavelength more than 480 nm. In addition to Semrock filter we can use Chroma filter 520/40. We can also use laser 532 nm 100 mW, Semrock filter LP03-532RS_Spectrum, having density more than D=6 at 532nm and transmitting over 95% light at wavelength more than 540 nm. Images of object can be captured as single frames or as a video with resolution up to 128*128 at 14 bit by EMCCD video camera Andor iXon DV-860 which is able to register fluorescence of single molecules when EMCCD is cooled down to -40C to -80C. Data received from the camera is stored in and processed by a computer, which is also used to control the camera and to switch laser and UV light so that UV light illuminates the object only between frame captures, but not during any of them. For illumination and activation of molecules of caged dye Invitrogen C20050 we have made a set of illuminators-condensers, some of them being able to send laser light through object under angle from 80˚ to 90˚ to optical axe of microscope so, that this light beam is not collected by ours objectives. Others self-made condensers can illuminate object under on angle of full internal reflection of laser light on the border between quartz slide, having reflection coefficient n=1.48 and object in water, having reflec-

tion coefficient n=1.34. We selected quartz slides for 2 reasons: first of all quartz has a very low level of Raman scattering of laser light, and second – it is able to transmit UV light of UV LEDs, used for activation of caged dyes molecules. All non-quartz optical glasses that we have tested in our experiments produced an extremely high level of background signal inside the glass with wavelengths of the background light being approximately 20-60 nm longer, than wavelength of excitation laser beam (i.e. wavelength similar to that of the fluorescent molecules) which means that these non-quartz materials can not be used in fluorescent nanoscopy in any part of device, where these glasses may be illuminated by direct laser beam. But lenses of objective may be made from usual glass, if the object is illuminated as we described earlier and if exciting laser beam is not sent to object trough objective, as it usually done in fluorescent microscopy. Our scheme of illumination allows use of relatively cheap objectives instead of extremely expensive quartz objectives.

Now we are conducting experiments with different setups to find best protocols for Fluorescent Nanoscopy.

Our current development efforts are aimed at solving numerous problems which will allow assembly of a high-resolution, low-noise device for 3D color nanoscale resolution imaging of thick samples in liquid (native) environment [7].

The concept itself has been shown to allow achievement of 2 nm precision of localization of fluorescent molecules using TIRF microscopy, i.e. only for object structures on a distance up to 150 nm from the border between glass and object. Improvement of resolution for thick samples faces a number of problems related to physical properties of interaction of light with all molecules in object, not only with fluorescent molecules. Internal fluorescence of object structures can affect accuracy of activated molecules coordinates' determination, but it may be effectively suppressed by prolonged illumination of the object by light with wavelength not affecting dye molecules, which must not absorb such light in non-activated state.

One of the most significant problems for visualization of single molecules fluorescence in thick objects is portion of light produced by Raman scattering of excitation light in object structures and in water. Raman scattered light has wavelength tens nm longer, than wavelength of light exciting fluorescence. Spectral characteristics of Raman scattering are similar to those of most of the fluorescent dyes, so it is impossible to filter fluorescence of probes from the background using just light filters or other passive optical components. The scattered light is able to pass through optical filters, which are supposed to pass only light of activated fluorescing molecules and to stop excitation light. Intensity of Raman scattered light is increasing with objects' thickness and at some thickness of objects fluorescence, produced by activated fluorescing molecules, becomes less than light produced by Raman scattering. At some point determination of coordinates of activated fluorescing molecules becomes impossible. It is well known that Raman scattering can not be eliminated, but it lasts only as long as the object is being illumi-

nated. It is also known that typical time for Raman scattering is around 1ns, whereas typical half-lifetime of excited state of most of fluorescent dyes is above 3ns. So, the only way to make internal background light insignificant for determination of coordinates of activated fluorescing single molecules in thick object is to use time-resolved approach, in which during the time of capturing of one frame the object is illuminated by thousands of light pulses with duration around 1 ns. For the time while internal fluorescence of object is strong, fluorescent light and light of Raman scattering must not be registered by camera, but few ns after end of light impulse the camera must be able to start registration of fluorescence of specially designed activated molecules, with typical half-lifetimes of their excited states being few times longer, than those for any types of background fluorescing structures.

3-rd (axial) coordinate of fluorescing molecule may be determined by using 2 cameras (or 2 parts of matrix of one camera) for which focal planes are slightly different. In this case light distribution in spots produced by the same molecule in 2 images will be dependent from distance of fluorescent molecule from each focal plane. This difference may be calibrated as axial coordinate as it was proposed in [1] and validated in [8].

Different structures of object may be covered by different dyes and thus produce fluorescent light in different wavelengths. It is possible to separate their fluorescence, register fluorescence of different molecules on different cameras and get pseudo-colored image with distribution of different structures in object, such as proteins, lipids, nucleic acids etc.

Next steps of development may lead to major reduction of device cost, since expensive EMCCD and sCMOS cameras with their unchallenged characteristics become less important for the improved schemes. Background fluorescence which typically consists of internal fluorescence of the specimen itself, fluorescence of slides and cover slips and chemical substances used for fixation of the specimen can be reduced by changes in the detection protocol, illumination system and selection of appropriate chemicals for imaging. We see the earlier mentioned time-resolved approach as the most promising for fluorescent nanoscopy, and we currently validate different options for its implementations. After our investigation of existing ICCD cameras, often used for time resolved microscopy, we found, that they have amplitude-spatial characteristics not good enough for fluorescent nanoscopy. We found a way to improve their amplitude-spatial characteristics and we hope to find a way to construct such cameras for fluorescent nanoscopy of thick objects. We also check other ways for time-resolved nanoscopy based on use of different fast optical shutters and existing EMCCD, ICCD and other cameras.

We wrote a program on Visual Basic 6.0 GetC.exe which is used for calculation of coordinates of fluorescent molecules in visible part of object. Our software can adjust calculated coordinates in accordance with slight movement of object that takes place over the time of capturing of thousands frames.

Images of captured video contain not only spots, produced by fluorescing molecules, but background image produced by fluorescence and Raman

scattered light in object structures, glasses, media etc. For calculation of centers of spots background fluorescence must be subtracted from each pixcel in each frame. Direct subtraction of background images from images in each frame is not satisfactory, because brightness of frames differ because of object photobleaching and intensity of laser beam light fluctuate in time. Next macros for program ImageJ [6] helps make average of all frames in video and subtract its normalysed values from each frame.

```
stack1 = getImageID; w = getWidth(); h = getHeight(); n=nSlices;
newImage("Plots", "32-bit", w, h, 1); stack2 = getImageID;  setPaste-
Mode("Add");
selectImage(stack1);   run("Select All");  {for(i=1; i<n+1; i++) {show-
Progress(i, nSlices);
selectImage(stack1); setSlice(i); run("Subtract...", "value="+1000);
run("Copy");
// You must set your own value in this line to subtract threshold from each
frame.
selectImage(stack2); run("Paste"); }}
selectImage(stack2);  run("Divide...", "value="+n);   setPaste-
Mode("Subtract");
  for(i=1; i<n+1; i++) { showProgress(i, nSlices);  {selectImage("Plots");
run("Select All");
 getRawStatistics(nPixels, mean, imin, imax); meanP=mean;
selectImage(stack1);   setSlice(i);  getRawStatistics(nPixels, mean, imin,
imax); meanS=mean;
scale =meanS/meanP;  selectImage("Plots");  run("Multiply...",
"value="+scale); run("Copy");
selectImage(stack1); setSlice(i);   run("Paste");
getRawStatistics(nPixels, mean, imin, imax); run("Subtract...",
"value="+imin); }}
```

After completion of this macros work we receive a stack with previous name, which contain images of differences between values of pixels in each frame and normalized for this frame average of all frames. Using command Analyze/Histogram for all stack we can find the best minimum and maximum values for all pixels, then we use command Process/Math/Min to set best minimum value for stack and command Process/Math/Max to set maximum value for all stack to avoid cropping pixels values when file is converted to 8 bit by command Image/Type/8-bit. Then we save stack as file with extension AVI, which may be used for centers spots calculation in our program GetC.exe.

Next Macros is used to get Sum of all differential frames or for some part of stack. To make new stack from part of initial stack we use commands: Image/Duplicate.

```
stack1 = getImageID; w = getWidth(); h = getHeight(); n=nSlices;
 newImage("Plots", "32-bit", w, h, 1); stack2 = getImageID; setPaste-
Mode("Add");
selectImage(stack1); run("Select All");  for(i=1; i<nSlices+1; i++) {
```

showProgress(i, nSlices);
selectImage(stack1); setSlice(i); run("Copy"); selectImage(stack2); run("Paste");}

If Sum of all differential frames looks unstructured as for all frames, so for any part of stack, noisy, the most probable our object was not changing its position while all frames were captured in video. Only then saved AVI file may be used for centers spots calculation without additional work for determination shift of object for the time while video was captured. But if we see some structures in Plot, object changed its position and for future centers of spots calculations, we use another macros, which makes summation and averaging of smaller parts of stack frames:

stack1 = getImageID; w = getWidth(); h = getHeight(); n=nSlices;
newImage("Plots", "32-bit", w, h, n-10); stack2 = getImageID; setPasteMode("Add");
selectImage(stack1); run("Select All"); for(i=1; i<n-9; i++) {showProgress(i, nSlices);
for (y=1; y<11; y++) {selectImage(stack1); setSlice(i+y); run("Copy");
selectImage(stack2); setSlice(i); run("Paste");}
selectImage(stack2); setSlice(i); run("Divide...", "value="+10);}

Then we use commands Image/Duplicate for initial stack for numbers of frames from 1 to n-10 to make the same number of frames as in duplicated stack, so in stack where each frame is an Average of 10 frames.

To subtract Average of 10 frames from previous frame we use command Process/Image Calculator…/. In open windows we put name of duplicated stack in first line with name “Image1”, in line “Image2” we put name of stack where each frame is an average of 10 frames, “Operation”=Subtract, mark in box “Create new window”. When we press OK we get new stack, where each frame represent difference of pixel values in any Duplicated stack and the same pixel in stack with averaged next 10 frames. Subtraction of averaged frames diminishes noise in comparison with subtraction of next frame of initial stack from previous, but decreases a total number of frames which will be used for centers spots calculation. We convert received differential stack to 8 bit format and save it as AVI file for centers spots calculation with adjustment of coordinates for shift of object. If evaluated by presented macroses shift is too big, we can use a command SearchShift in our program GetC.exe, which calculates shift of chosen part of image for all frames and uses this values for correction of calculated centers of spots coordinates.

References

1. Klimov A. A. et. al. Patent “Fluorescent Nanoscopy Method”, №RU2305270, PCT/RU2006/000231, WO2006123967, US7803634, US8110405 priority date: May 18, 2005
2. Betzig E. et al. // Science–2006– V.313(5793); P.1642-5.
3. Editorial, Method of the Year 2008//Nature Methods–2009– V. 6, 1
http://sciencestage.com/v/9799/nature-methods:-method-of-the-year-2008.html
4. Rust M.J. et al. // Nat Methods–2006– V.3(10); P.793-5

5. Suliana Manley et al. // Nature Methods–2008– V.5; P.155 – 157
6. http://imagej.nih.gov/ij
7. Klimov A.A., Klimov D.A.// Biophysics–2009–V.54(5); P.661–666
8. Juette M.F. et al. // Nat Methods–2008– V.5(6); P.527-9
9. http://media.hhmi.org/ibio/lippincott-schwartz/lippincott-schwartz_powerpoint_pt3.pdf
10. Frost N.A., Shroff H., Kong H., Betzig E., // Blanpied Neuron–201009–V.67; P.86-99
11. Tatavarty V, Kim E-J, Rodionov V, Yu J // PLoS ONE–2009– V. 4(11): e7724.
12. http://www.plosone.org/article/info:doi%2F10.1371%2Fjournal.pone.0007724

TEMPERATURE DEPENDENCE OF FORCE-VELOCITY RELATION OF FAST AND SLOW SKELETAL MUSCLE.

P.V. Kochubey, S.Y. Bershitsky

Institute of Immunology and Physiology, Ural Branch of the Russian Academy of Sciences, Yekaterinburg, 620041, Russia

There are many works concerning influence of temperature on shortening velocity of skeletal muscle. However data obtained with different methods vary greatly [0, 0, 0]. Here we present the results of studying temperature dependence of shortening of slow and fast skeletal rabbit muscles obtained with a technique of Joule temperature jump (T-jump) in single permeabilized muscle fibers as described earlier [0]. Fast fibers were taken from *psoas* muscle (100% type 2X fast myosin) and slow ones from *soleus* muscle (100% type 1 slow myosin). Single fibers were permeabilized with a 50% glycerol in storage solution, and activated at 1-2°C by Ca^{2+} contained solution (pCa=5). To measure force at certain temperature and shortening velocity we used the following protocol (Fig. 1). Activated fiber was transferred to air trough where temperature was ~5°C and in series heated up by T-jump to final temperature of 10°C, 15°C, 20°C, 25°C, 30°C, 35°C.

We found that tension in the fast and slow fibers linearly and equally depend on temperature: P = 0.12T, where P is tension normalized for its value at 5°C tension (30±10 kPa) and T is temperature in °C, temperature coefficients, Q_{10}, were 1,65 for fast fibers and 1,57 for slow ones. Maximal velocity of shortening of the fast fibers rose with temperature exponentially. Activation energy, E_a, and Q_{10} of maximal shortening velocity obtained from Arrhenius plot (Fig. 2) were 52.6 kJ/mol and 1.83, respectively. Surprisingly no temperature dependence of maximal shortening velocity was found in slow fibers (V_{max} was 4.31 m,l./s{4.28; 5.77}at 15°C, and 3.45 m.l./s{2.93; 4.96}at 35°C). The optimal velocity (V_{opt} - is the velocity at which power is maximal [0]) as the maximum velocity has no temperature dependence for slow fibers and temperature dependence for fast fibers has an exponential nature with E_a= 63.69 52.6 kJ/mol, Q_{10}=2.26. Maximal power of the fast and slow fibers has linear dependence on temperature and is described by equations: M = 4.1T - 41.47 (R^2=0.98), Q_{10}=3.064 for fast and M = 1.23T + 0.22 (R^2=0.98), Q_{10}=1.52 for slow fibers, where M is power kW/m^3 and T is a temperature °C.

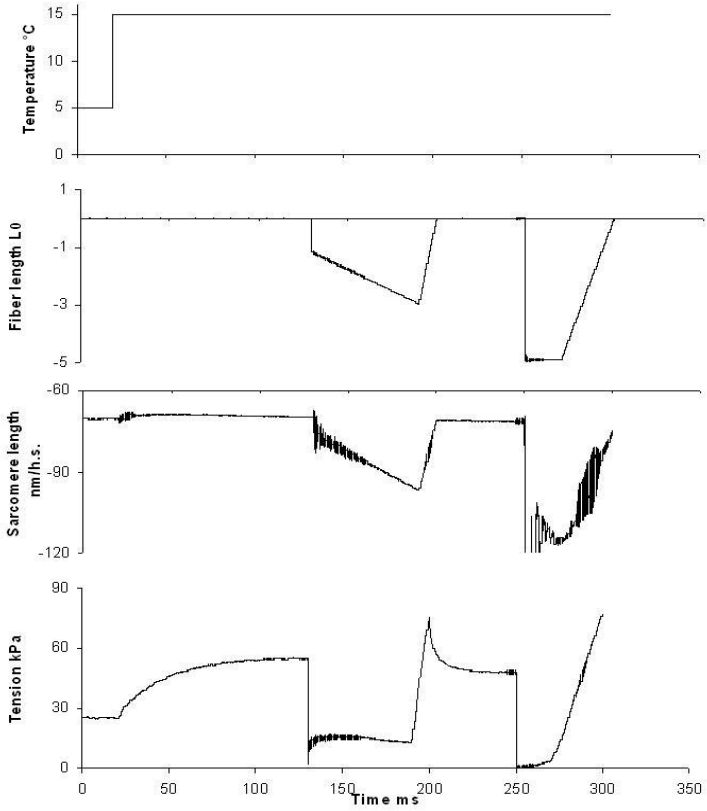

Fig. 1. Example of experimental record in slow muscle fiber. Traces from top to bottom are: temperature (°C), changes in total fiber length (in initial length of fiber (L_0)), changes in sarcomere length in a central segment of the fiber (in nanometres per half-sarcomere, nm/h.s.), and tension (kPa). Fiber dimentions: length 3 mm, cross-section area 6010 μm^2, sarcomere length 2.5 µm.

Our results differ from earlier works [0, 0]. We have not found the difference in temperature dependence of slow and fast fibers that agrees with result of other works [0, 0]. However in our work this dependence was linear. . We also have not revealed difference in maximal and optimal velocities of the slow fibers probably due to a high dispersion in the data. Such high dispersion was described earlier [0, 0]. Our data on temperature dependence of V_{max} and V_{opt} of the fast fibers are similar to those obtained in the *in vitro* motility assay on the fast rabbit myosin [0], but differ from the data obtained on intact fast rat fibers [0]. Maximal power has a linear dependence on temperature for both fast and slow fibers.

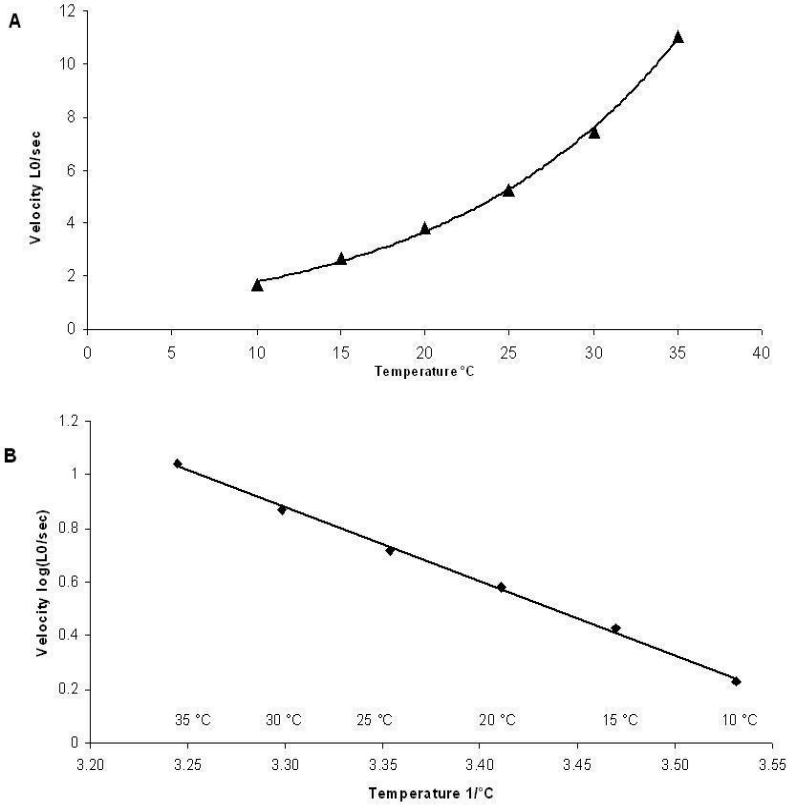

Fig. 2. Effect of temperature on maximum velocity of fast skeletal muscle contraction. A: increase of V_{max} of fast skeletal rabbit muscle. B: the same data presented in an Arrhenius plot.

This work was supported by RFBR and Presidium of RAS.

References

1. J. Gulati, Force-velocity characteristics for calcium-activated mammalian slow-twitch and fast-twitch skeletal fibers from the guinea pig, Proc Natl Acad Sci U S A 73 (1976) 4693-4697.
2. K.W. Ranatunga, Temperature dependence of mechanical power output in mammalian (rat) skeletal muscle, Exp Physiol 83 (1998) 371-376.
3. R. Rossi, M. Maffei, R. Bottinelli, M. Canepari, Temperature dependence of speed of actin filaments propelled by slow and fast skeletal myosin isoforms, J Appl Physiol 99 (2005) 2239-2245.
4. S.Y. Bershitsky, A.K. Tsaturyan, The elementary force generation process probed by temperature and length perturbations in muscle fibres from the rabbit, J Physiol 540 (2002) 971-988.

5. D.R. Claflin, J.A. Faulkner, The force-velocity relationship at high shortening velocities in the soleus muscle of the rat, J Physiol 411 (1989) 627-637.
6. G. Salviati, R. Betto, D. Danieli Betto, Polymorphism of myofibrillar proteins of rabbit skeletal-muscle fibres. An electrophoretic study of single fibres, Biochem J 207 (1982) 261-272.

CARDIAC MYOSIN ISOFORMS AND DIFFERENT CONTENT OF TROPOMYOSIN CHAINS MODULATE THE ACTIN-MYOSIN INTERACTION

G.V. Kopylova, D.V. Shchepkin, L.V. Nikitina

Institute of Immunology and Physiology, Ural Branch of the Russian Academy of Sciences, Ekaterinburg, 620041, Russia

Interaction of myosin with actin in striated muscle is controlled by Ca^{2+} via thin filament associated proteins: troponin and tropomyosin. In cardiac muscle there is a whole pattern of myosin and tropomyosin isoforms.

Tropomyosin is one of regulatory proteins of the thin filament of striated muscle. Expression of tropomyosin isoforms in the heart depends upon species and age of the animal (1). α-Tropomyosin prevails in adult murine, rabbit and human hearts. β-Tropomyosin is mainly expressed during fetal development in murine hearts. Changes in the expression of these isoforms are also associated with cardiac pathologies (2).

In myocardium of mammals not only tropomyosin isoform ratio but also that of myosin heavy chains (MHC) changes during ontogenesis. In myocardium of mammals there are two isoforms of heavy chains: α and β (3). In ventricle together with ventricular isoform of light chains they form two main isomyosins: V1 and V3, homodimers consisting of α- and β-heavy chains, respectively (3). In atria α- and β-heavy chains together with atrial light chains form A1 (αα) and A2 (ββ) isomyosins (4).

It is known that isoforms of cardiac myosin, both ventricular and atrial, affect mechanical characteristics of acto-myosin complex. In particular, it was shown that sliding velocity of both F-actin (5) and the thin filament (6) in the in vitro motility assay depends on the ratio of isomyosins. Force developed by cross-bridges of cardiac isomyosins is also different (7).

On the other hand, tropomyosin participates in control of actin-myosin interaction. According to published data tropomyosin directly affects mechanical characteristics of acto-myosin complex (8) and this influence depends on the ratio of tropomyosin isoforms (9).

The aim of this work is to investigate the regulatory effect of tropomyosin on actin-myosin interaction. For this we studied the dependence of the sliding velocity of actin and actin-tropomyosin filaments in the in vitro motility assay on myosin and tropomyosin isoforms.

The results of the experiments showed that the addition of tropomyosins with different content of α- and β-chains to the actin filament has varied effects on the sliding velocity of actin-tropomyosin filaments (Fig. 1,2). In the other words the regulatory effect of tropomyosin depends on the proportion of its α- and β-chains.

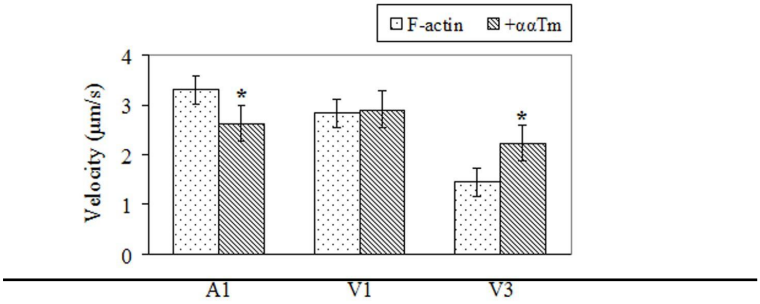

Fig. 1. The sliding velocity of actin and actin-Tm filaments consisting of cardiac rabbit ααTm over cardiac myosin isoforms in the *in vitro* motility assay. The columns and error bars are mean ± S.D. Asterisks indicate significant difference, $p < 0.05$.

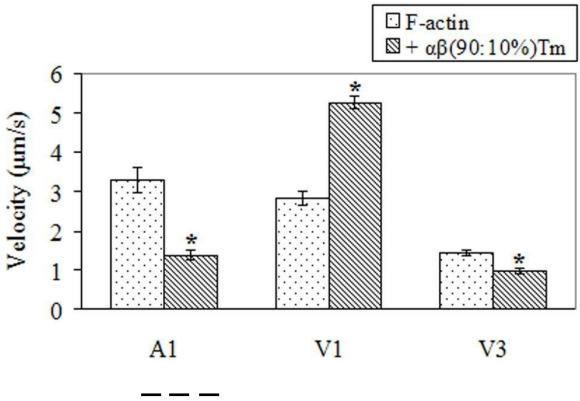

Fig. 2. The sliding velocity of actin and actin-Tm filaments containing cardiac bovine αβ (90 : 10 %) Tm over cardiac myosin isoforms in the *in vitro* motility assay. The columns and error bars are mean ± S.D. Asterisks indicate significant difference, $p < 0.05$.

Noteworthy that the addition of tropomyosins with increased content of β-chains, as typical for cardiac pathologies, reduced the velocity of actin-Tm filaments over all types of cardiac isomyosin both atrial and ventrical (Fig. 3). In turn different isoforms of myosin also affect the velocity of actin-tropomyosin filaments containing the same tropomyosins. This means that the interaction of myosin with F-actin is influenced by both myosin and tropomyosin isoforms. Exact mechanism of this influence is unknown but it can be explained for the reason of following data.

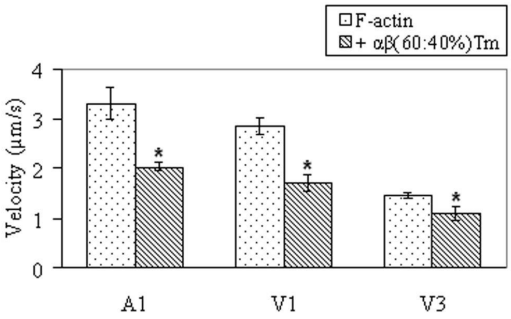

Fig. 3. The sliding velocity of actin and actin-Tm filaments consisting of αβ (60 : 40 %) Tm from *psoas* rabbit muscle over cardiac myosin isoforms in the *in vitro* motility assay. The columns and error bars are mean ± S.D. Asterisks indicate significant difference, $p < 0.05$.

Tropomyosin on actin filament participates in control of actin-to-myosin interaction and according to published data directly affects mechanical characteristics of acto-myosin complex (8). Using the in vitro motility assay it was shown that skeletal tropomyosin added to actin filaments increased force of skeletal muscle cross-bridges and inhibited velocity of the filaments at subsaturating myosin surface densities. At saturating myosin density neither cross-bridge force nor actin-tropomyosin velocity were affected by tropomyosin (8). This data corresponds to those of Lehrer et al. (10) who measured Mg-ATPase of skeletal myosin and found that at low concentration of myosin S1 skeletal tropomyosin inhibited the ATPase and stimulated it at high concentration. The authors explained the results by both steric and allosteric effects of tropomyosin on interaction of myosin with actin (8,10). Steric effect consists in that tropomyosin blocks myosin binding sites on actin filaments and so low myosin concentration is insufficient for activation of actin-tropomyosin filament. At high myosin concentration the filaments become fully activated and this demonstrates allosteric effect of tropomyosin.

Allosteric effect of tropomyosin can be explained by its ability to cause structural changes in F-actin. Rubenstein and colleagues using pyren-labeled actin have found a dependence of pyren fluorescence on the tropomyosin isoform type (11). It was recently found by Moraczewska and colleagues (12) that the degree and cooperativity of myosin-induced shift of tropomyosin localization was different for various of tropomyosin isoforms. All these assume that different isoforms of tropomyosin differently affect the interaction of myosin with actin filament.

Thus our results support reciprocal effects of myosin and tropomyosin on actin-myosin interaction in myocardium. This may play a significant role in maintenance of the effective heart work both during ontogenesis and in pathological conditions.

This work was supported by the grant RFBR #10-04-96065r-ural-a, RBRF #11-04-00750-a, Program 12-П-4-1042 of Presidium RAS and the Government of Sverdlovsk Region.

References

1. Perry, S. V. (2001) *J Muscle Res Cell Motil* **22**, 5-49
2. Izumo, S., Nadal-Ginard, B., and Mahdavi, V. (1988) *Proc Natl Acad Sci U S A* **85**, 339-343
3. Hoh, J. F., McGrath, P. A., and Hale, P. T. (1978) *J Mol Cell Cardiol* **10**, 1053-1076
4. Chizzonite, R. A., Everett, A. W., Prior, G., and Zak, R. (1984) *J Biol Chem* **259**, 15564-15571
5. VanBuren, P., Harris, D. E., Alpert, N. R., and Warshaw, D. M. (1995) *Circ Res* **77**, 439-444
6. Noguchi, T., Camp, P., Jr., Alix, S. L., Gorga, J. A., Begin, K. J., Leavitt, B. J., Ittleman, F. P., Alpert, N. R., LeWinter, M. M., and VanBuren, P. (2003) *J Mol Cell Cardiol* **35**, 91-97
7. Malmqvist, U. P., Aronshtam, A., and Lowey, S. (2004) *Biochemistry* **43**, 15058-15065
8. VanBuren, P., Palmiter, K. A., and Warshaw, D. M. (1999) *Proc Natl Acad Sci U S A* **96**, 12488-12493
9. Jagatheesan, G., Rajan, S., Ahmed, R. P., Petrashevskaya, N., Boivin, G., Arteaga, G. M., Tae, H. J., Liggett, S. B., Solaro, R. J., and Wieczorek, D. F. (2010) *J Muscle Res Cell Motil* **31**, 227-239
10. Lehrer, S. S., and Morris, E. P. (1982) *J Biol Chem* **257**, 8073-8080
11. Chen, W., Wen, K. K., Sens, A. E., and Rubenstein, P. A. (2006) *Biophys J* **90**, 1308-1318
12. Sliwinska, M., Zukowska, M., Borys, D., and Moraczewska, J. (2011) *Cytoskeleton (Hoboken)* **68**, 300-312

ALTERNATING MAGNETIC FIELDS EFFECTS ON CONTRACTIVE ACTIVITY OF NEWBORN RAT SKELETAL MYOTUBES OF DIFFERENT MATURITY IN THE PRIMARY CULTURE

V.S.Korkosh[1,4], B.F.Shchegolev[2,3], S.V.Surma[2,3], I.V.Nerubatskaya[1,3], G.B.Belostotskaya[1,3]

[1]I.M. Sechenov Institute of Evolutionary Physiology and Biochemistry of Russian Academy of Sciences;
[2]Pavlov Institute of Physiology of Russian Academy of Sciences;
[3] V.A. Almazov Federal Heart, Blood and Endocrinology Centre;
[4]St. Petersburg University, 199034, Universitetskaya nab., 7-9. St. Petersburg, Russia

There are a number of physical theories and hypotheses that describe the effect of weak magnetic fields (MF) on biological objects: magnetic parametric resonance [*1,2*], quantum interference [*3*], the precession of ions thermal vibrations [*4*]. However, until now we can't connect magnetobiological effects (MBEs) with specific targets, in which we may observe physical effects described by the proposed theories.

Taking into account that calcium ions play key role during contraction, muscle tissues and cells are attractive and adequate objects for different MBEs studies and especially mechanisms of probable MF influence on Ca^{2+} signaling.

It is well known that during in vitro development of rat skeletal muscle cells, calcium currents and spontaneous oscillatory contraction progressively appear after myoblast fusion, maturation of excitation-contraction coupling (ECC) and contractile mechanism. In the work of Fu at al. [5] it was shown that functional sarcoplasmic reticulum (SR) and control of ryanodine receptors (RyR) mediated SR Ca^{2+} release directly contribute to the spontaneous contraction of embryonic stem cell-derived cardiomyocytes, even at very immature stages of development. It is widely accepted that nicotinic acetylcholine receptor (nAChR) channel activity controls myoblast fusion into myotubes during myogenesis [6]. It has been suggested also that the temporal fluctuations of sarcomere shortenings in the isolated rat ventricular myocytes in the resting state are caused by spontaneous Ca^{2+} release from RyR [7]. Moreover it was shown that increased Ca^{2+} content inside SR was accompanied by increased frequency and amplitudes of spontaneous Ca^{2+} sparks [8], which then gives rise to the periodic nature of the calcium transients [9] and spontaneous contractions.

Goal and objectives. In this work we studied the effects of ultra-low frequency (0.01-2.0 Hz) alternating magnetic field (AMF) on the contractile activity of myotubes of different maturity in the primary culture of newborn rat satellite cells.

Material and methods. Satellite cells of newborn Wistar line rat legs muscle were obtained by destruction of muscular tissue with help of collagenase IA (2 mg/ml, Sigma) in Ringer's solution (146 mM NaCl, 5 mM KCl, 2 mM CaCl2, 1 mM MgCl2, 11 mM glucose, and 10 mM HEPES; pH 7.4) during 30-40 min at 37°C [*10*]. Satellite cells were cultivated in DMEM medium supplemented by 10% fetal serum, 50 U/ml penicillin and 50μg/ml streptomycin. After 3 days of cultivation the medium was changed for DMEM with 2% fetal serum and antibiotics. Fetal serum reduction allows to shorten the period of active myocyte proliferation and forward the process of myocyte fusion and myotube differentiation [*11*].

In order to measure the intracellular concentration of free calcium ions, $[Ca^{2+}]_i$, the cells were incubated in the Ringer's solution with the fluorochrome Fura-2AM (Sigma) at the concentration of 10 μM for 1 h at 24°C. $[Ca^{2+}]_i$ was recorded with the help of an Intracellular imaging and photometry system (US). The InCytIm^{TM} program was used to calculate the concentration of calcium ions as a ratio of fluorescence intensities (F340/F380) taking into account the calibration curve [*12*]. The maturity of myotubes was detected by Ca^{2+} transient in response to the action of agents starting up ECC: Ach (20 μM), K^+ (100 mM) and caffeine (Caf, 5mM). The use of caffeine allowed also estimating the SR Ca^{2+} content [*13*].

A special coil was constructed in order to form the AMF (10 cm in diameter and 6 cm long copper wire with a diameter of 1.5 mm and 0.8 Ohm general resistance). Signal generator G6-28 was used to power the coil (fre-

quency range: 0.001 Hz - 1 MHz, the main error of frequency: ± 1% (0.1 Hz - 100 kHz), ± 2% (0.001-0.1 Hz and 100 kHz to 1 MHz), output voltage: 500 mV - 5 V).

We used a 3-component magnetometer HB0302.1A (0.1-100μT) with a resolution of 0.1 μT to measure the magnetic field induction in the working volume of the coil. To register the variable components of magnetic field we used transducers (sensors) of magnetic field NV0303 and NV0303.1. PC-oscilloscope PCS-500 (Welleman, Belgium) was used to get the data from these sensors (digitization and signal input into the computer).

Special laboratory setup was constructed for the experimental purposes. It was used to observe the effects of the AMF on the cell culture. Cells were photographed with a digital camera Leica DFC300 FX (Germany) and the inverted microscope PIM-III (WPI, USA) with the objective x25.

Results. Ultra-low frequency MF (0.01 – 2.0 Hz) proved to have significant effect on the contraction rate of myotubes in early development stages, which might lead to the abnormality of contraction or the absolute cessation of myotube activity (Fig. 1a). In the same time, those AMFs have little or even no effect on myotubes of late development stages (that is 14-16 days old) (Fig. 1b).

It should be noticed also, that myotubes demonstrate different character of calcium level fluctuations in the different stages (Fig. 2). While 6-days-old myotubes revealed small Ca^{2+} oscillations (about 4-5 nM), 9-days-old myotubes demonstrate greater oscillations of calcium level (up to 25 nM). Besides, 6-day-old myotubes gave very weak Ca^{2+} answer (no more than twofold increase of the base level) on the Ach, K^+ and caffeine application, demonstrating the immaturity of the receptors, which take part in ECC (Fig. 3 a). However, the amplitude of Ca^{2+} transients on the Ach action in 8-day-old myotubes riched 360 nM, overdrawing initial level in 10-30 times (Fig. 3 b). These results are in agreement with the data of Cseri et al. [*14*] that the short-term response on Ach action grows by the increase in the number of nuclei inside myotubes.

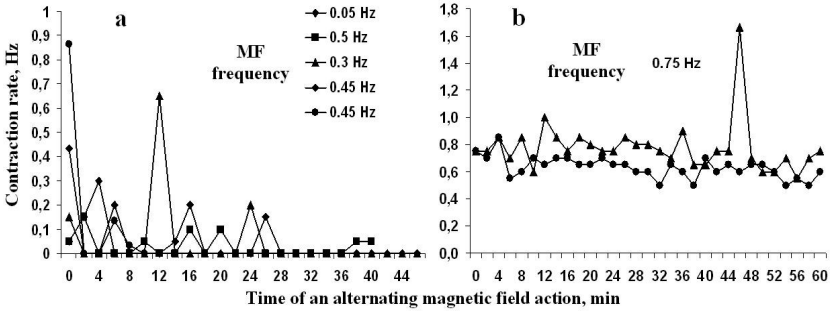

Fig. 1. The influence of an alternating magnetic field with different frequency characteristics on the contraction rate of myotubes of different maturity: a) 10-11-day-old myotubes; b) 14-day-old myotubes.

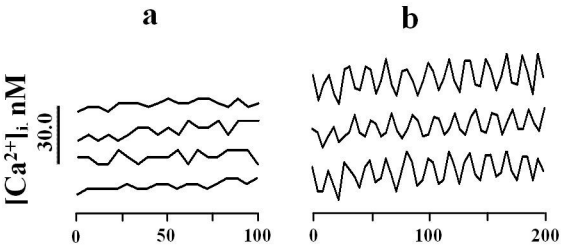

Fig. 2. Spontaneous oscillations of calcium level in 6- (a) and 9-day-old (b) myotubes.

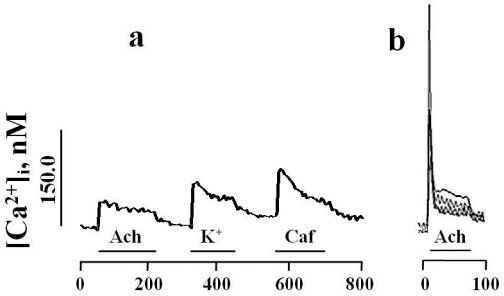

Fig. 3. Ca^{2+} transients after the action of Ach (20 μM), K^+ (100 mM) and caffeine (5 mM) in 6-day (a) and 8-day-old (b) myotubes.

Proceeding on our results we suppose that sensitivity to AMF of skeletal myotubes depends on their maturity. The weak AMFs insignificantly influence myotubes with finally formed ECC and mature contractile mechanism (as a rule on the late period of cultivation), but considerably disorganize the contractile activity of undifferentiated young myotubes. The similar MBEs were obtained in our previous studies with weak (60-400 mT) static magnetic field (SMF), which accelerated of myoblast division and the formation of hypertrophic myotubes, but gradually decreased (no more than 25% of a base level) the contraction frequency of mature myotubes and dramatically reduced (in the first minutes) the frequency of contractions (up to a full stop) of myotubes which were forming EMC [*11*]. Moreover, an attempt was made to connect revealed MBEs with Ca^{2+}-signaling processes. We have determined that stimulating action of SMF on skeletal muscle cell proliferation and differentiation is connected with MF–induced growth of $[Ca^{2+}]_i$ [*11*], but the late effect, in turn, suppress the activity of receptors, exercising ECC and muscle contraction [*15*].

Summary. Thereby, summarizing our new results with our previous data we can state that there is a straight connection between the effects of ultra-low frequency (0.01-2.0 Hz) AMFs and weak SMFs (60-400 mT) on

the proliferation and functioning of skeletal muscle cells in the primary culture against the stage of cell development and myotube's maturity, mediated by active intracellular Ca^{2+} signaling.

References

1. Lednev V.V., Biofizika 41 (1), 224 (1996).
2. Belova N.A., Lednev V.V. Biofizika 46 (1), 122 (2001).
3. Bingi V.N. Magnetobiology: experiments and models. M.: Milta, p.592 (2002).
4. Zhadin M.N, Biofizika 41 (4), 832 (1996).
5. Fu J.D., Li J., Tweedie D., Yu H.M., et al. FASEB J. 20(1), 181 (2006).
6. Bandi E., Bernareggi A., Grandolfo M. et al. J Physiol. 568, 171 (2005).
7. Sarai N., Kihara Y., Izumi T., et al. Jpn J Physiol. 52(4), 371 (2002).
8. Grandy S.A., Denovan-Wright E.M., Ferrier G.R., Howlett S.E.. Am J Physiol Heart Circ Physiol. 287 (3), H1029 2004.
9. Szentesi P., Zaremba R., Stienen G.J. J Muscle Res Cell Motil. 19(6), 675 (1998).
10. Beam K.G., Knudson M.J Gen Physiol . 91, 781 (1988).
11. Eldashev I.S., Shchegolev B.F., Surma S.V., Belostotskaya G.B. Biofizika 55 (5), 868 (2010).
12. Grynkiewicz G., Poenie M., Tsien R.Y. J. Biol. Chem. 260, 3440 (1985).
13. Overend C.L., Eisner D.A., O'Neill S.C.. J Physiol. 502 (3), 471 (1997).
14. Cseri J., Szappanos H., Szigeti P., et al. Eur. J. Physiol. 443, 731 (2002)
15. Belostotskaya G.B., Eldashev I.S., Surma S.V., Shchegolev B.F. Vestnik St. Petersburg University. 5 (4), 198 (2011).

INFLAMMATORY ENVIRONMENT CAUSES CYTOSKELETON REORGANIZATION IN HUMAN ADIPOSE-DERIVED MESENCHYMAL STROMAL CELLS

I.V. Korovina, O.A. Grigorieva, N.I. Kalinina, K.A. Rubina, V.Y. Sysoeva

Faculty of Basic Medicine, Lomonosov Moscow State University, 31-5, Lomonosovsky av., Moscow 119192, Russia

The most of adult organs and tissues including bone marrow, adipose tissue and skin contain mesenchymal stromal cells (MSCs). Many studies have demonstrated that these cells could play a central role in tissue regeneration due to activation of resident stem cells. However the mechanism of MSC activation during tissue damage has not been fully elucidated. Initial stages of tissue damage are characterized by inflammation associated with accumulation of immune cells, including neutrophils and macrophages. We suggest that pro-inflammatory milieu created by these cells activates MSCs. In this study, we examined how inflammatory factors affect MSC migration and cytoskeleton organization.

Materials and methods. To assess the effect of inflammatory environment on MSC we developed a non-contact co-culture model. MSCs were isolated from human fat and grown until 2 passage in medium supporting the growth of undifferentiated mesenchymal cells. Activated macrophages were derived from THP-1 human promonocyte cell line adhered to the permeable membrane (pore diameter 0,4 μm) by PMA treatment for 24 hrs. MSC were

cultured in the presence of activated promonocytes in transwell system, which provided the interchange of soluble factors between two cell types without direct contact. We have analyzed cell morphology, activity of cell center and organization of cytoskeleton by immunofluorescent staining of actin and tubulin. We also assessed directed migration of MSCs using Roche´s xCELLigence System for real-time cell analysis cell invasion/migration assays (RTCA DP) after 24 and 48 hours.

Results. We have observed that inflammatory milieu changes of MSC shape and cytoskeleton organization. The cells acquired elongated shapes and lost the active cell center. Microtubules have re-organized, the number of stress-fibers has increased at least 2 folds and the fraction of cells with mature focal contact has decreased comparing to untreated MSCs. Consistently with this observation, MSCs migrated 2,5 times faster towards activated macrophages versus untreated THP-1 cells. We have observed that mRNA content and surface expression of PDGFRβ and integrin β1 in MSCs increase under inflammatory conditions.

Conclusion. Our data suggest that during initial stages of tissue regeneration MSCs are activated by inflammatory milieu. This activation results in up-regulation of MSCs migration due to at least in part PDGFRβ-dependent signaling pathway.

HYPERCONTRACTION OF MUSCLE FIBRES IS ASSOCIATED WITH ACTIVATION OF POTENTIAL-DEPENDENT L-TYPE CALCIUM CHANNELS IN SATELLITE CELLS.

A.M. Krasnyi, V.A. Pochaev, N.D. Ozernyuk

Koltzov Institute of Developmental Biology RAS,
26 Vavilov Str., Moscow, 119991 Russia
alexred@list.ru

As a result of a strong tension/contraction or damage of muscle fiber quiescent satellite cells respond by entering the cell cycle. At the same time calcium-dependent processes occur, which require short-term Ca^{2+} concentration increase in cytoplasm. In our study we have shown that one of the mechanisms of Ca^{2+} influx into the cytoplasm of satellite cells localized on the muscle fiber is mediated by voltage-dependent L-type channels following activation of nicotinic acetylcholine receptors. Voltage-dependent L-type Ca^{2+} channels and nicotinic acetylcholine receptors in satellite cells are shown by us for the first time. Calcium activity of satellite cells, caused by carbachol (acetylcholine analog) treatment, can induce a Ca^{2+} flow into the muscle fiber at the contact region of the satellite cell and the fiber. Muscle satellite cells in normal conditions are mitotically inactive, but under stimulus condition (injury, physical activity) they start to proliferate. This is accompanied by irreversible local hypercontraction of the fiber. Later on the activation occurs differentiation, which ultimately leads to hypertrophy of muscle fibers (1-3).

In general data on physiological characteristics of satellite cells were obtained after their isolation and subsequent cultivation (4). In this paper cal-

cium activity of satellite cells localized on isolated single muscle fibers was evaluated. This experimental model allowed to study the mechanisms of calcium signaling in mitotically inactive satellite cells.

As an object for our research we used rat muscle fibers isolated from hindlimb muscles (*m. flexor digitorum brevis* - short flexor muscle of toes) by enzymatic digestion (collagenase type I, dispase) and cultured on plastic plates. Calcium imaging experiments were performed on Leica DMI6000 fluorescent microscope station. Muscle fibers were loaded with fluorescent dye Fluo-3. Each experiment was repeated at least 10 times.

There is a view that voltage-dependent calcium channels appear only during differentiation of satellite cells at the stage of myoblast fusion and myotube formation (5, 6, 7). However in our earlier studies we showed these channels are present in proliferating myoblasts C_2C_{12} cell line (8, 9). In various tissues Ca^{2+} entry through these channels occurs following the plasmalemma depolarization caused by the action of ionotropic nicotinic acetylcholine receptors. In quiescent satellite cells this type of receptors were not shown previously and were detected only at the stage of proliferating myoblasts (10, 11). Here we suggest for the conjugation of nicotinic acetylcholine receptors and voltage-dependent calcium channel in satellite cells.

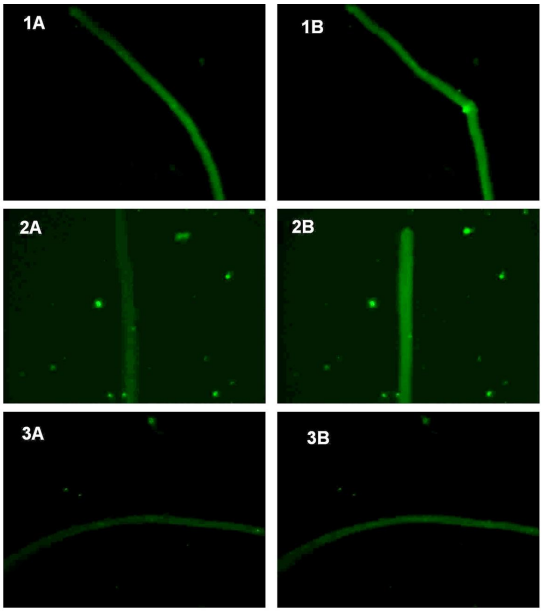

Fig. 1. 1A, 2A, 3A: intact fibres, loaded with Fuo-3 fluorescent dye; 1B: carbachol treatment; 2B: carbachol treatment in Ca^{2+} free medium; 3B: carbachol treatment, preincubation with verapamil (10uM).

For investigating the coupling process between nicotinic acetylcholine receptors, inducing plasmalemma depolarization, and potential-dependent calcium channels in satellite cells, localized on the muscle fibre, we used carbachol - acetylcholine analog. Figure 1.1 shows the result of carbachol (0.1 mM) treatment of muscle fibers. In our experiments heterogeneity in fluorescent cell responses as a result of carbachol adding was observed. As a rule only one cell has higher level of fluorescence, thus there is a strong input of Ca^{2+} into adjacent muscle fibre with the maximum input of Ca^{2+} in the contact region, causing local hypercontraction of the muscle fibre. Thus hypercontraction is correlated with the activity of satellite cells.

Carbachol also acts directly on the muscle fiber causing single reversible contraction. Carbachol action on isolated muscle fibers in Ca^{2+} free medium causes single contraction/relaxation process without fibre damage; Ca^{2+} comes out from the sarcoplasmic reticulum into the cytoplasm (Figure 1.2). At the same time in satellite cells cytoplasmic Ca^{2+} concentration is not increased.

In our previous study we used adrenaline for activation of calcium channels in C_2C_{12} myoblasts; Ca^{2+} entry was completely blocked by verapamil (L-type channels inhibitor) cells pretreatment (8). The action of verapamil on satellite cells doesn't block Ca^{2+} entry into the cytoplasm. However the action of carbachol induces Ca^{2+} influx in satellite cells. This effect is considerably blocked by verapamil and amlodipine, specific inhibitors of L-type Ca^{2+} channels (Figure 1.3).

Thus carbachol causes voltage-dependent Ca^{2+} channels opening following nicotinic acetylcholine receptors activation and plasmalemma depolarization. The emptying of the Ca^{2+} reticular stores in quiescent satellite cells doesn't occur. Multiple increase in cytoplasmic Ca^{2+} concentration associated with the voltage-dependent channels can irreversibly damage muscle fibers. This phenomenon may be the cause of muscle spasms.

References

1. Bischoff R. The satellite cell and muscle regeneration. In: *Myology: Basic and Clinical*, 2nd ed., edited by Engel AG and Franzini-Armstrong C. New York: McGraw-Hill, 1994, vol. 1, p. 97–118.
2. Hawke TJ, Garry DJ. Myogenic satellite cells: physiology to molecular biology. *J Appl Physiol* 91: 534–551, 2001.
3. Seale P, Rudnicki MA. A new look at the origin, function, and "Stem-Cell" status of muscle satellite cells. *Dev Biol* 218: 115–124, 2000.
4. Balan OV, Voroteliak EA, Smirnova TD, Ozerniuk ND. Specific features of satellite cells and myoblasts at different stages of rat postnatal development. Izv Akad Nauk Ser Biol. 2008 Mar-Apr;(2):151-5.
5. Varadi G, Orlowski J, Schwartz A. Developmental regulation of expression of the alpha 1 and alpha 2 subunits mRNAs of the voltage-dependent calcium channel in a differentiating myogenic cell line. *FEBS Lett.* 250(2):515-8, 1989.
6. Bidaud I., Monteil A., Nargeot J. et al. Properties and role of voltage-dependent calcium channels during mouse skeletal muscle differentiation // J. Muscle Res. Cell Motil. 2006. V. 27 (1) P. 75-80.
7. Zheng Z., Wang Z., Delbono O. Charge movement and transcription regulation of

L-type calcium channel a1S in skeletal muscle cells // J. Physiol. 2002, V.540. №2. P. 397–409.
8. Krasnyi AM, Ozerniuk ND. The expression of genes encoding the voltage-dependent L-type Ca^{2+} channels in proliferating and differentiating C2C12 myoblasts of mice. Izv Akad Nauk Ser Biol. 2011 May-Jun;(3):349-53.
9. Krasnyi AM, Sefikhanov TG, Ozerniuk ND. Regulation of Ca^{2+} influx in proliferating and differentiating myoblasts of mice with participation of L-type Ca^{2+} channels. Biofizika. 2011 Jan-Feb;56(1):74-7
10. Krause RM, Hamann M, Bader CR, Liu JH, Baroffio A, Bernheim L. Activation of nicotinic acetylcholine receptors increases the rate of fusion of cultured human myoblasts. J Physiol. 1995 Dec 15;489 (Pt 3):779-90.
11. Entwistle A, Zalin RJ, Warner AE, Bevan S. A role for acetylcholine receptors in the fusion of chick myoblasts. J Cell Biol. 1988 May;106(5):1703-12.

EXPRESSION OF MECHANICALLY GATED ION CHANNELS DURING XENOPUS EMBRYOGENESIS

S.V. Kremnyov[1*], D.A. Nikishin[2]

[1] Laboratory of Developmental Biophysics, Lomonosov MSU, Leniskie gory, 119234, Moscow

[2] Laboratory of Embryophysiology, Koltzof IDB RAS, Vavilova st.,119334, Moscow

[*] s.kremnyov@googlemail.com

Cell shape changes and collective cell migrations are key mechanisms of the morphogenesis of tissues and organs. During animal development, these cell behaviors is highly coordinated and regulated. The central mechanism of these coordinations and regulations is interaction between cell adhesion and mechanical stress. It was shown that main sensors during mechanically activated cell migrations or extracellular matrix synthesis are mechanically gated ion channels. But, practically all these data were obtain on *in vitro* models, and there are now evidences that these mechanisms could drive animal development *in vivo*.

The aim of our work was to explore expression of mechanically gated ion channels during *Xenopus tropicalis* embryogenesis and identify, which of them could be involved in mechanically regulated morphogenesis. So far, we have checked following ion channels: TRPV1, TRPV2, TRPV4, TRPM3, TRPM7, TRPC1-like, TRPC5, TRPC6, PKD2, Piezo1 and Piezo2. Maternally expressed following: TRPV4, TRPC5, TRPC6, TRPM3, TRPM7, Piezo1 and Piezo2. Relatively high expression level was detected for TRPV4, TRPM3, TRPM7 and Piezo1. But TRPV1, TRPV2, TRPC1-like and PKD2 started express late: from neurula or hatching stage.

We have shown that early morphogenesis could be regulated by mechanical stresses through mechanically gated ion channels and in future it should proved by gain- and loss- of function experiments.

DETAILS OF MORPHOLOGICAL STRUCTURE OF MUSCLE SYSTEM IN PLANARIAN *POLYCELIS TENUIS*

N.D. Kreshchenko

Institute of Cell Biophysics, Pushchino, Moscow region, 142290, Russia

In representatives of phylum Platyhelminthes musculature plays several important roles: it has a supportive function for different cell types of the organism in the absence of true skeleton, it serve for penetration and attachment to the host tissue in parasitic species, and for locomotion of free-living larval stages of parasitic and adult stages of non parasitic flatworms. Besides of that, in free-living worms the musculature is used for searching, capturing and holding their preys, food ingestion and for implementation of reproductive behavior. Investigation of the muscle structure by staining with fluorescently (TRITC) labeled phalloidin, specifically binding to F-actin of muscle filaments, revealed the details of morphological organization of the body musculature in planarian *Polycelis tenuis* (Turbellaria, Platyhelminthes). The elements of the nervous system were identified using immunostaining with antibody to neuropeptide FMRFamide.

Methods

Freshwater planarians *Polycelis tenuis* was collected in the vicinity of the Oka river (Pushchino, Moscow region). Animals were maintained in aquarium with tap and distilled water (2:1) at 20±1ºC, fed with mosquito larvae once a week and kept hungry for one week before the experiment. Animals 10 mm in length were flat fixed in 4% paraformaldehyde in 0.1 M phosphate-buffered saline (PBS, pH 7.4) for 4 h at room temperature, transferred in 10% sucrose in PBS for several days, embedded in Tissue Tek and sectioned by cryotom at -20ºC on frozen sections of 15-18μm thickness. Sections were collected on Polysine or Gold Super Frost Plus microscope slides (Menzel-Glaser), air dried and stored at -20ºC. For staining sections were washed 3 times for 5 min in PBST (PBS with Triton X-100, 0,3%), covered with primary antibodies to neuropeptide FMRFamide (1:1000, Sigma) and incubating for 24 h at 4ºC. They were washed again (3x5min) in PBST, immersed in FITC-labeled immunoglobulines (1:30, DACO) for 24 h at 4ºC in the dark. After next wash (3x5) in PBS the samples were stained with TRITC-labeled phalloidin (1:100, Sigma) for 4-6 h. After final wash they were mounted in 75% glycerol in PBS under the cover slips and examined with Leica DM600 and Leica TCS SP5 microscopes.

Results

Staining with TRITC-labeled phalloidin revealed muscular system structure in planarian *P. tenuis*. The developed body wall musculature include three layers of muscle fibres: circular, longitudinal and diagonal. Thin circular muscle fibres situated underneath the epithelium and basal membrane, diagonal fibres and thick longitudinal muscle fibres are tightly packed (Fig. 1A-D). Longitudinal muscle layers is organized by of 3-5μm thick bundels is consisted of 2-4 muscle fibres with the distance between them around 4-5 μm (Fig. 1D).

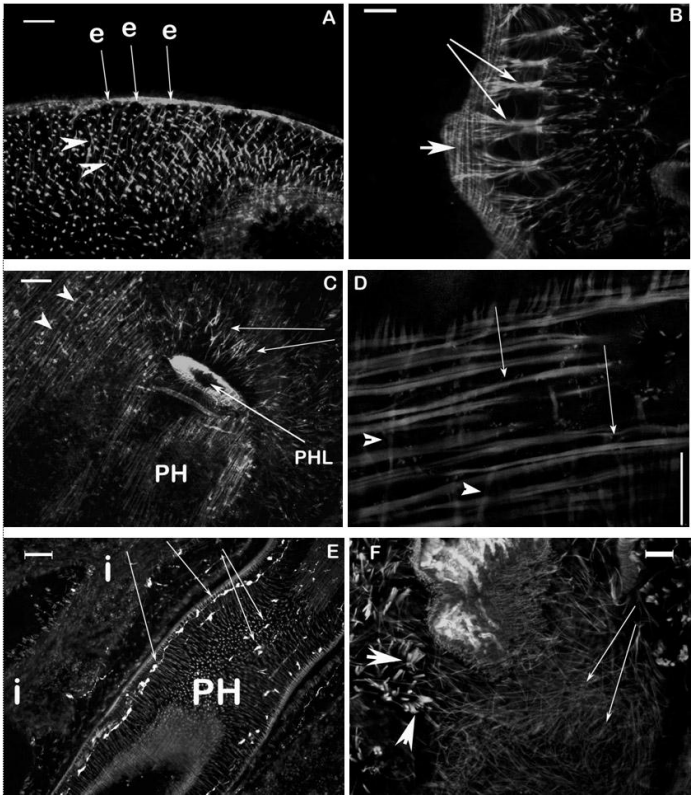

Fig. 1A-F. Musculature of *P. tenuis* stained with TRITC-labeled phalloidin (grey). **A** – Anterior body part with numerous eyes appeared as black circles (**e**, arrows) on the very edge of the body, diagonal (arrowheads) and circular (appear as grey dots on the section) muscle filaments of the body wall. **B** – Regularly situated bundles of transverse muscles connecting the dorsal and the ventral sides of the body (arrows), longitudinal muscle fibres (arrowhead). **C** – Longitudinal muscle filaments running along ventral body side (arrowheads), the anchoring muscles (arrows) secure the basal part of muscular pharynx (**PH**), pharyngeal lumen (**PHL)**. Note the longitudinal fibres running alone the pharynx tube. **D** – Close look of the longitudinal muscle layer (arrows) in the body wall under the epithelium, and transverse fibres underneath (arrowheads). **E** – Circular and longitudinal pharyngeal musculature, **i** – intestine branches; FMRF–immunopositive neurons in the pharynx wall appears in white (arrows). **F** – Irregularly organized thin muscle filaments in the wall of copulatory bursa (arrows). Arrowheads indicate bundles of body wall muscles comprising of thick muscle filaments.
Scale bars: on A, B, F – 50µm, on C, E – 100µm, on D – 25 µm. Top and right upper corner on each photo − to the head end of body.

Circular and diagonal layers usually contain single or doubled muscle fibres of 1,3-2,1 μm thick. Regularly, on the distance of 50-60μm, situated thick (10-20μm) transversal bundles composing of several muscle fibres were observed connecting the dorsal and the ventral body sides (Fig. 1B). Numerous small eyes situated on the anterior end of the body were surrounded with very thin muscle filaments (Fig. 1B). Thick muscle filaments running from the ventral to the dorsal body sides penetrated through tissue of the paired cephalic ganglion, not covered by any membrane (data not shown).

Cylindrical muscular pharynx is attached to the body musculature with its basal part by the anchoring muscles. Pharyngeal tube is comprised by circular, longitudinal and radial muscle fibres densely packed in the pharynx wall (Fig. 1C,E). Pharyngeal cavity where pharynx is located in the middle of the body is composed by the layers of circular and longitudinal muscle filaments having the same organization as in the body wall. FMRFamide–immunopositive neurons (cell bodies with size of 14-17μm and numerous nerve fibres) were found in the pharynx innervating musculature (appeared in white on photo, Fig. 1E). Branches of blind intestine were underlying by loosely packed very thin muscle filaments. The complex genital apparatus of sexually reproduced planarian *P. tenuis* include of several muscular organs: tubes, reservoirs, copulatory apparatus. On Fig. 1F the wall of the copulatory bursa are observed composing of a number of irregularly organized and running in different directions thin (0,8-1,5μm) muscle filaments.

Conclusions

Despite of some progress in the investigation of the musculature in Platyhelminthes the knowledge about its morphological structure are restricted in most of species. The anatomy of the muscular system had been described for two free-living turbellarian – *Dugesia japonica* (Orii et al., 2002) and *Girardia tigrina* (Bueno et al., 1997; Kreshchenko, 2010) and for several parasitic worms (Mair et al., 1998; 2003; Tolstenkov O.O., et al., 2011). Immunocytochemical method used in the study combined with fluorescent and laser scanning microscopy provide new information on muscle system organization in planarians. The results indicate that pattern of body musculature in *P. tenuis* share similarity with previously studied species (Mair et al., 1998; Kreshchenko et al., 2010; Tolstenkov O.O et al., 2011). The data on musculature organization in basal flatworm species is accumulating and can be useful for better understanding of major principles of the evolution of muscle system in animal kingdom, for further investigation of its functioning and regulation in model flatworm species and for the practical application of the information obtained in the development of novel anthelmintic drugs. Observations on innervations of musculature in *P. tenuis* by FMRF-immunopositive neurons may indicate a possible role for FMRFamide–like neuropeptides in the regulation of muscle function.

Author thanks M. Turovskaya for cutting of some samples by cryotome and to V.A. Yashin for the technical assistance with fluorescent and confocal microscopes. Study supported by RFBR grants 09-04-00243a and 12-04-01086-a.

References

1. Bueno D., Baguna J., Romero R. 1997. Histochem. Cell Biol., 107(2): 139-149.
2. Kreshchenko N.D. 2010. Biological motility: from fundamental achievements to nanotechnologies, Pushchino, P. 142-145.
3. Mair G.R., Maule A.G., et al. 1998. Parasitology. 117(1): 75-82.
4. Mair G.R., Maule A.G., et al. 2003. J. Parasitol. 89(3): 623-625.
5. Orii H., Ito H., Watanabe K. 2002. Zool. Sci. 19(10): 1123-1131.
6. Tolstenkov O.O., Akimova L.N. et al. 2011. Parasitol. Res., DOI 10.1007/s00436-011-2526-x.

DIFFERENTIAL EFFECTS OF THE CLORIDE CHANNELS BLOCKER 9-AC ON TWO TYPES OF EXTRACELLULAR ACTION POTENTIALS OF THE FROG (R. TEMPORARIA) SKELETAL MUSCLE FIBERS

I.V. Kubasov[1] and M.G.Dobretsov[2]

[1]- I.M. Sechenov Institute of Evolutionary Physiology and Biochemistry, Saint-Petersburg, Russia

[2]- Department of Anesthesiology, University of Arkansas for Medical Sciences, Little Rock, AR USA

It is known that skeletal muscle fibers have high Cl^- conductance (G_{Cl}), which constitutes up to 80-85% of overall ionic membrane conductance of these cells at rest. Remaining 15-20% of resting muscle fiber membrane permeability can be attributed to the potassium conductance G_K (1). High chloride conductance plays a critical role in the setting and maintaining of the resting membrane potential of muscle fibers and in determining the rate of repolarizing phase of the muscle fiber action potentials. Application of selective Cl^- channel blockers (anthracene-9-carboxylic acid (9-AC) results in generation of repetitive after-discharges of stimulated muscle fibers and in a substantial slowing of relaxation of contractile responses of the skeletal muscle (2, 3). Similar features of evoked electrical and contractile muscle responses are being observed in studies of animal models of myotonia and human subjects carrying CLCN1 gene mutation resulting in expression of CIC-1 chloride channels with suppressed conductivity (4). Despite that CIC-1 represents the major class of Cl^- channels expressed by skeletal muscles of vertebrates, the question about compartmentalization of these channels within the muscle fiber plasma membrane remains unsettled. Immunohistochemical studies suggest that CIC-1 channels are present on sarcolemma, but almost lacking on the membrane of t-tubules of the skeletal muscle fibers (5). This view however, is difficult to reconcile with electrophysiological data suggesting that nearly 80% of the skeletal muscle fiber Cl^- conductance should be attributed to the channels of its t-system (6, 7, 8). Activity of ion channels and transporters localized within the t-system has a critical significance for contractility of skeletal muscle fibers; therefore the question above is of importance for our understanding of skeletal muscle physiology and pathophysiology. Our previous studies indicated that the analysis of characteristics of the third phase of propagating muscle fiber action po-

tentials recorded extracellularly using narrow-tipped pipettes may provide a valuable information regarding currents generated within t-tubules located just under the rim of the pipette and, therefore, regarding the role of ion-transporting mechanisms of the t-system of skeletal fibers (9). Considering these data and the question above, the major aim of this work was the study of the effects of specific CIC-1 chloride channels blocker, 9-AC on characteristics of bi- and tri-phasic (sarcolemma and sarcolemma + t-tubular membrane, respectively) extracellularly recorded AP of fibers of the frog (Rana temporaria) sartorius muscle. As in our previous experiments, either bi-phasic (type 1, T1) or tri-phasic (type 2, T2) APs were recorded in muscle fibers with the pipettes containing control solution. Respective temporal and amplitude characteristics of first and second phases of T1 and T2 APs did not differ. The presence or absence of the late positive (third) phase was, therefore, the only characteristic distinguishing these two types of the signals.

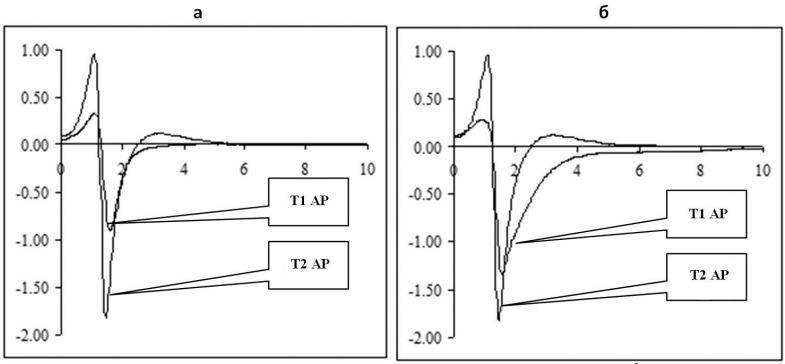

Fig. 1. T1 and T2 APs (labels) recorded immediately (a) and on 20th minute (b) after establishing the loose seal contact between the muscle fiber and pipette loaded with 100 μM of 9-AC. Horizontal axes – time (ms), vertical axes – voltage (mV).

As under control conditions, either T1 or T2 responses were recorded during first minutes after the muscle fiber was approached with the pipette loaded with 9-AC (100 μM) (Fig. 1a). The difference of behavior of these two types of responses became obvious with time of recording. On the 10-15th minutes of continuous recording with 9-AC filled pipette from the fiber generating T1 response, a significant ($p<0.05$) increase in the duration of half-decay time (by 69 ± 18 %) of the second phase of T1AP observed over the same time (27 fibers, 4 muscles; compare Fig.1a and b). Similar changes in temporal characteristics of T1 APs were also observed in experiments, in which 100 μM 9-AC was added to the bath solution. Unlike described above for the T1 type of responses, amplitude and temporal characteristics of either of phases of T2 APs did not change significantly during over than 20 minutes of continuous recording with 100 μM 9-AC loaded pipettes (38 fibers, 4 muscles; compare Fig. 1a and b). However with 9-AC present in the extracellular solution, the second phase of T2 APs was observed to split into multiple (2 to 4) peaks (Fig. 2).

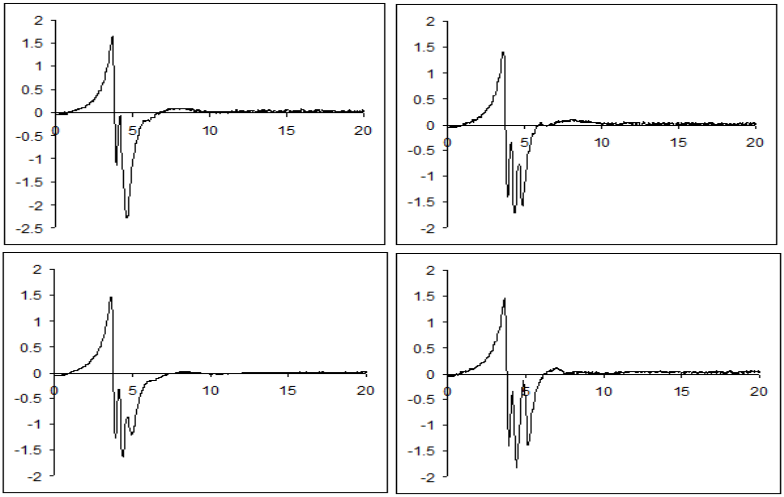

Fig. 2. The figure panels show four consecutive recordings of T2 APs, which were collected at from the same muscle fiber of the muscle stimulated at 0.1 Hz and incubated with 100 μM 9-AC for 20 minutes. Horizontal axes – time (ms), vertical axes – voltage (mV).

We did not observe multiple second phase responses generated in either of 27 recordings of T1 APs. Therefore, it is likely that these repetitive responses were generated in the t-tubules opened on the surface of the fiber under the rim of recording pipette and providing the outward current underlying generation of the third phase of this type of the signals.

Whether this suggestion is correct and whether these multiple peaks represent repetitive generation of inward spikes of Na current within a t-tubule or de-synchronization of Na currents generated in several t-tubules opened under the pipette remains to be determined. Whatever is the answer to the question above, we did not observe this type of responses in experiments with the Cl channel blocker included in the pipette solution. Thus the reason for putative repetitive or de-synchronized activity of Na channels of the t-tubular membrane should be attributed to some changes in electrogenesis of the sarcolemma of the muscle fiber, which could be associated with the fiber depolarization and prolongation of spreading on its surface AP, evidenced in prolongation of the second phase of T1 APs. Further experiments are needed to clarify these issues.

Conclusions

1. T1 and T2 APs, the action potentials presumably generated by currents originating in the skeletal muscle sarcolemma or both sarcolemma and t-system, respectively, respond differently to the selective block of C1C chloride channels with 9-AC.

2. Evaluation of the role of prolongation of T1 type of responses in generation of multiple peaks of the second phase (Na current) of T2 skeletal muscle APs requires further studies.

This work was supported by grant 02.740.11.5135 by Federal Program of the Ministry of Science and Education of the Russian federation and in part by the COM UAMS pilot grant program .

References

1. Bretag A.H. Muscle chloride channels. // Physiol. Rev. 1987; 67: 618–724.
2. Bryant S.H, Morales-Aguilera A. Chloride conductance in normal and myotonic muscle fibres and the action of monocarboxylic aromatic acids. // J. Physiol. 1971; 219: 367–383.
3. Conte Camerino D., Tortorella V., Bettoni G. et al. A stereospecific binding site regulates the Cl^- ion channel in rat skeletal muscle. // Pharmacol. Res. Commun. 1988; 20: 1077–1078
4. Rudel R., Ricker K., Lehmann-Horn F. Transient weakness and altered membrane characteristic in recessive generalized myotonia (Becker). // Muscle Nerve 1988; 11: 202–211.
5. Lueck J.D., Rossi A.E.,Thornton C.A., et al. Sarcolemmal-restricted localization of functional ClC-1 channels in mouse skeletal muscle. // J. Gen. Physiol. 2010;136:597–613.
6. Dulhunty A.F. Distribution of potassium and chloride permeability over the surface and T-tubule membranes of mammalian skeletal muscle. // J. Membr. Biol. 1979; 45:293–310.
7. Palade P.T, Barchi R.L. Characteristics of the chloride conductance in muscle fibers of the rat diaphragm. // J. Gen. Physiol. 1977; 69: 325–342.
8. Dulhunty A.F. The dependence of membrane potential on extracellular chloride concentration in mammalian skeletal muscle fibres. J. Physiol. 1978; 276: 67–82
9. Kubasov I.V., Dobretsov M.G. Characterisnics of spreading action potentials recorded in various sites of skeletal muscle fibers of the frog Rana temporaria. // J. Evol. Biochem. and Physiol.. 2011; V.47, №5: 414-416.

THE DIRECTION OF STEM CELLS MOVEMENT INTO THE BRAIN DEPENDS ON THE AREAS OF THEIR INJECTION INTO PERIPHERAL PARTS OF THE NERVOUS SYSTEM

V.A. Kulchitsky[1], Y.G. Shanko[2], P.G. Molchanov[3], S.N. Cherehkevich[3], M.O. Chotianovich[1], A.A. Denisov[1,3], S.G. Pashkevich[1], I.V. Strizhak[1], M.V. Andrievskaya[3], A.V. Rodich[2], T.N. Pitlik[3], P.M. Bulay[3]

[1]Institute of Physiology, National Academy of Sciences of Belarus, 28 Akademicheskaya Street, 220072, Minsk, Belarus
[2]Republican Research and Clinical Center of Neurology and Neurosurgery, 24 F. Skorina Street, 220114, Minsk, Belarus
[3]Belarusian State University, 4 Nezavisimosti Avenue, 220030, Minsk, Belarus

Motility is an inherent property of all living cells. Because of the motility various tissues and organs, including cell populations of different origin (which are topographically divided at different stages of ontogenesis) are

formed in the process of ontogenesis. After the formation of tissues, organs, systems and the whole organism the motility function is important for organization of behavioral and defensive reactions, delivery of regulatory substances and nutrients, providing interoperability between tissues, organs and cells, and realization of intracellular and intranuclear processes. In the current study the attention was not focused on the mechanisms of motility that is on those issues which are professionally elaborated by the organizers of the scientific forum. It is about the methods of stem cells delivery into various parts of the brain. The dominant methods are: systemic (intravenous) way of application or, conversely, the local way of stem cells placing into the damaged part of the brain after the preliminarily performed trepanation. According to the first way there are contradictory opinions based, on the one hand, on the relative simplicity and accessibility of the systemic approach, and, on the other hand, on the problems of blood-brain barrier overcoming and a certain diffuseness of stem cells allocation in the bloodstream and body tissues. The local way of stem cells delivery, as it was mentioned above, requires supplementary measures, for example, additional surgical intervention, that is not always possible in a number of situations [1].

There are some other ways; one of them is based on the well-known ability of stem cells to move via the perineural spaces. In this case, the injection of stem cells into the peripheral parts of cranial nerves must be accompanied by the migration of cells due to their inherent motility into the central parts of particular system of cranial nerves. As the stem cells have a certain tropism to regulatory substances (which are accumulated in damaged tissues) while moving, this factor was also taken into account when choosing targets for stem cells reparative potential use.

At the early stages the procedure was worked out and the series of experiments on stem cells injection to white rats conducted. The stem cells were previously obtained from the rats' adipose tissue and cultured (at least two passages) in a CO_2-incubator. FITC was used as a fluorescent label. Application of stem cells was performed into peripheral parts of the two cranial nerves. In the first series of experiments (n=8) cells were injected under the mucous membrane of the nasal cavity (i.e., into peripheral parts of the olfactory nerve). In the second series of experiments cells were injected into the Meckel's cave (i.e., into the trigeminal ganglion region) (n=5).

Such a choice of cranial nerves was due to the central representation of each nerve chosen. Information firstly goes by the olfactory nerve to the rostral brain regions (frontal lobes of the brain and surrounding areas of nervous tissue). The signaling to the brainstem goes by the trigeminal nerve.

The histological material capture was carried out in 10 minutes, 2 and 24 hours after the injection. The preparations for fluorescent microscopy were made with the "squashed drop" method. In 10 minutes FITC-labeled stem cells were found in the place of application and in olfactory filaments after the injection under the nasal mucous membrane, and in the trigeminal ganglion after the injection into the Meckel's cave, but were not found in the brain. In 2 and 24

hours after the application under the nasal mucous membrane FITC-labeled stem cells were found in the olfactory filaments, olfactory bulbs, basal ganglia, the optic nerve, tuber cinereous of the diencephalons, on the basis of frontal lobes). In 2 and 24 hours the fluorescence was seen in the spinal nucleus of the trigeminal nerve and reticular formation of the brainstem.

Thus, in the experiments carried out a peculiar topographic feature of stem cells was noted. It depends on the location of their injection into the peripheral parts of the cranial nerves. The injection of cells in the vicinity of the olfactory nerve is accompanied by their movement and distribution to the rostral brain areas. The injection of stem cells into the trigeminal nerve system is accompanied by their migration to the caudal parts of the brain. Such pattern of stem cells motility from the periphery to the brain may be taken into account on trying to enhance the reparative potential of neural tissue after injuries or strokes namely in those brain areas, that were affected after the pathological process development [2].

Acknowledgements: We thank Victor Boksha (Neurosyntek Modeling and Manufacturing Inc., Los Altos, CA.) for helpful discussions.

References

1. Kalyunov V.N., Kulchitsky V.A., Chernov A.N. Stem cells: reality, perspectives, illusions and myths // News of Biomedical Sci. 2011. Vol.3, No1, P.120-136.
2. Cherenkevich T.N., et al. The effect of electrical stimulation on the stem cells proliferation and differentiation // News of Natl. Acad. Sci. 2011. No2. P. 110-121.

ARACHIDONIC ACID METABOLISM INHIBITORS MODULATE THE EFFECT OF DRUG MOLIXAN ON INTRACELLULAR Ca^{2+} CONCENTRATION IN MACROPHAGES

L.S. Kurilova, Z.I. Krutetskaya, O.E.Lebedev, N.I. Krutetskaya, V.G. Antonov, V.V.Lastochkin, K.O. Vojtcehovitch, A.A.Naumova

Saint-Petersburg State University, 7/9 University emb., Saint-Petersburg, Russia

A number of disulfide-containing drugs affecting redox-state and having prominent physiological effect have clinical value. Thus, a synthetic analogue of oxidized glutathione (GSSG) pharmacological drug glutoxim® (GSSG disodium salt with platinum nanoaddition, PHARMA-VAM, Moscow, Russia), is applied as an immunomodulator and hemostimulator in therapy of bacterial and viral diseases, psoriasis , radio- and chemotherapy of oncological disorders. Another disulfide-containing drug molixan® (complex of glutoxim with inosine nucleoside) has the similar application. However, the cellular and molecular mechanisms underlying these drugs action are poorly understood.

Earlier we found that GSSG and glutoxim increase intracellular Ca^{2+}-concentration, $[Ca^{2+}]_i$, inducing Ca^{2+}-mobilization from thapsigargin-sensitive Ca^{2+}-stores and subsequent Ca^{2+}-entry in rat peritoneal macrophages [1]. Later we demonstrated that the same effect on $[Ca^{2+}]_i$ is observed in macrophages treated with molixan [2]. In addition, it was found that tyrosine kinases, tyrosine phosphatases [1], phosphatidylinositol kinases [3], small G-

ptoteins from Ras family as well as phospholipase C and protein kinase C, the key molecules of phosphoinositol signaling pathway [4] and actin cytoskeleton [5] are the critical components of the signaling cascade, triggered by GSSG and glutoxim and leading to $[Ca^{2+}]_i$ increase in macrophages. Also it was found that the metabolites of cyclooxygenase pathway of arachidonic acid (AA) metabolism are involved in the regulation of glutoxim effect on $[Ca^{2+}]_i$ in macrophages [6].

It is known that AA, released from membrane phospholipids, can be metabolized via both cyclooxygenase and lipoxygenase pathways, resulting in the formation of prostaglandins and leukotrienes in macrophages. AA itself has been shown to affect cell signaling elements in different types of cells. AA and its metabolites formed by the cyclooxygenase or lipoxygenase pathways play an important role in regulation of various physiological processes.

Therefore, the aim of the present work was to elucidate whether enzymes and/or products of AA metabolism are involved in the effect of molixan on $[Ca^{2+}]_i$ in rat peritoneal macrophages. Using Fura-2AM microfluorimetry, we have studied the influence of inhibitors of AA oxidation pathways on $[Ca^{2+}]_i$ rise induced by molixan in rat peritoneal macrophages. Evidence is obtained which indicates the involvement of AA metabolites, probably of the cyclooxygenase and lipoxygenase pathways, in the formation of the Ca^{2+}-response to molixan in macrophages; in the presence of AA metabolism inhibitors molixan induces no $[Ca^{2+}]_i$ increase.

In order to investigate the possible involvement of cyclooxygenase pathway of AA metabolism in the effect of molixan on $[Ca^{2+}]_i$ in macrophages we used two structurally different cyclooxygenase inhibitors aspirin (acetylsalicylic acid) and indomethacin. Control experiments, shown in Fig. 1a, demonstrate that preincubation of the cells with 100 μg/ml molixan in Ca^{2+}-free solution leads to a gradual increase of $[Ca^{2+}]_i$ in macrophages due to the mobilization of Ca^{2+} from the intracellular Ca^{2+}- stores. The addition of Ca^{2+} ions in the external medium causes the additional $[Ca^{2+}]_i$ increase mediated by Ca^{2+}-influx from the external medium.

Fig. 1b shows that the preincubation of macrophages with 40 μM indomethacin for 5 min before molixan addition almost completely suppressed Ca^{2+}-response induced by molixan. Fig. 1c demonstrates that preincubation of the cells with 100 μM aspirin for 5 min before molixan application has the same effect on Ca^{2+}-responses induced by molixan. The results suggest the involvement of cyclooxygenase pathway of AA metabolism in the effect of molixan on $[Ca^{2+}]_i$ in macrophages.

In order to investigate the possible involvement of enzymes and/or products of lipoxygenase pathway of AA metabolism in the effect of molixan on $[Ca^{2+}]_i$ in macrophages we used a well known lypoxygenase inhibitor nordihydroguaiaretic acid (NDGA). Fig. 2b shows that preincubation of macrophages with 10 μM NDGA for 5 min before 100 μg/ml molixan addition leads to the almost complete inhibition of Ca^{2+}-responses induced by molixan in comparison with control experiments (Fig. 2a).

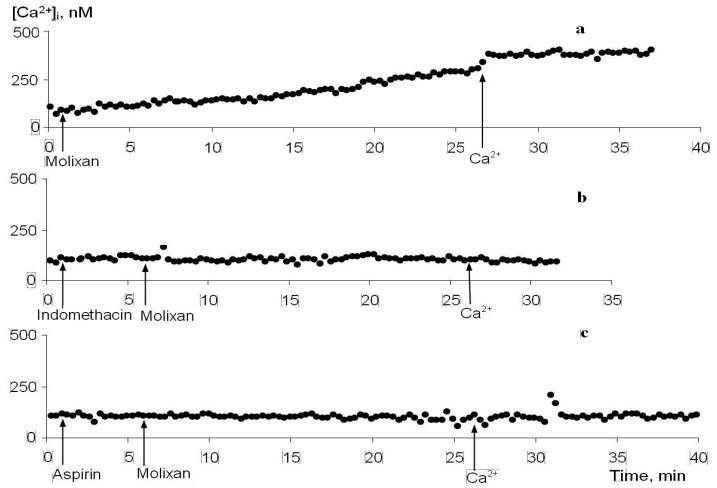

Fig 1. The effect of aspirin and indomethacin on Ca^{2+}-responses induced by molixan in macrophages.

Here and in Fig. 2 the abscissa axis shows time, min; the ordinate axis, Ca^{2+}-concentration in the cytosol, nM.

a - cells were incubated with 100 μg/ml molixan in Ca^{2+}-free medium for 25 min, then Ca^{2+}-entry was induced by addition of 2 mM Ca^{2+} to the external medium. b, c – cells were preincubated with 40 μM indomethacin (b) or 100 μM aspirin (c) in Ca^{2+}-free medium for 5 min, then 100 μg/ml molixan was applied; 20 min later 2 mM Ca^{2+} was added to the external medium.

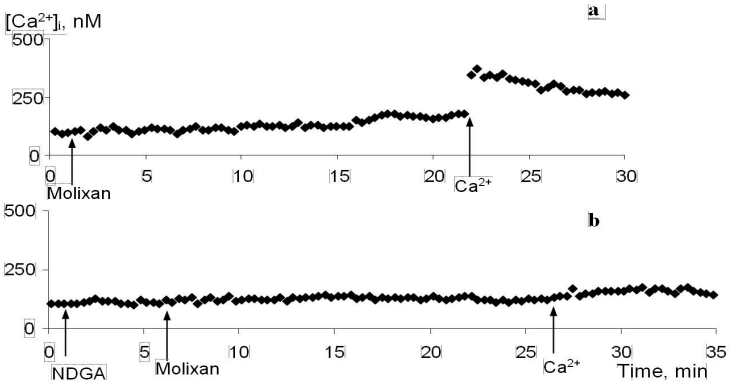

Fig. 2. The effect of nordihydroguaiaretic acid (NDGA) on Ca^{2+}-responses induced by molixan in macrophages.

a - cells were incubated with 100 μg/ml molixan in Ca^{2+}-free medium for 20 min, then Ca^{2+}-entry was induced by addition of 2 mM Ca^{2+} to the external medium. b – cells were preincubated with 10 μM NDGA in Ca^{2+}-free medium for 5 min, then 100 μg/ml molixan was applied; 20 min later 2 mM Ca^{2+} was added to the external medium.

The results suggest that lipoxygenase pathway of AA metabolism is also involved in the effect of molixan on $[Ca^{2+}]_i$ in macrophages.

Thus, the present study has shown that some interacting mechanisms between AA formation and molixan-induced Ca^{2+}-responses are present in rat peritoneal macrophages. NDGA, an inhibitor of lipoxygenase pathway of AA metabolism inhibits the Ca^{2+}-response to molixan. Cyclooxygenase inhibitors indomethacin and aspirin also completely eliminate the Ca^{2+}-response induced by the drug. The data presented indicate that in rat peritoneal macrophages AA metabolites, probably of cyclooxygenase and lipoxygenase pathways, are involved in the generation of the Ca^{2+} responses to molixan.

References

1. Kurilova L.S., Krutetskaya Z.I., Lebedev O.E., Antonov V.G. The effect of oxidized glutathione and its pharmacological anologue glutoxim on intracellular Ca^{2+} concentration in macrophages. Cell and Tissue Biology. 2008. V. 2. P. 322-332.
2. Крутецкая З.И., Курилова Л.С., Лебедев О.Е., Крутецкая Н.И., Войцехович К.О., Наумова А.А., Шамшев А.В. Влияние дисульфидсодержащего препарата Моликсан на внутриклеточную концентрацию Ca^{2+} в макрофагах. В. мат. VIII Международной конференции «Биоантиоксидант». Москва. 2010. С. 232-233.
3. Krutetskaya Z.I., Lebedev O.E., Kurilova L.S., Antonov V.G., Nozdrachev A.D. Possible involvement of phosphatidylinositol kinases in the effect of the oxidized glutathione and Glutoxim on the intracellular Ca^{2+} concentration in macrophages. Doklady Biol. Sci. 2008. V.422. P. 296-297.
4. Krutetskaya Z.I., Lebedev O.E., Kurilova L.S., Antonov V.G., Nozdachev A.D. The role of the key enzymes of the phosphoinositide signaling pathway in the effect of oxidized glutathione and glutoxim on intracellular Ca^{2+} concentration in macrophages. Doklady Biol. Sci. 2009. V. 428. P. 407-409.
5. Крутецкая З.И., Лебедев О.Е., Курилова Л.С., Антонов В.Г., Ноздрачев А.Д. Участие актиновых филаментов в действии окисленного глутатиона и препарата глутоксим на внутриклеточную концентрацию Ca^{2+} в макрофагах. ДАН. 2011.Т. 346. № 5. С. 705-708.
6. Наумова А.А., Курилова Л.С., Крутецкая З.И., Лебедев О.Е., Крутецкая Н.И., Игловикова О.И., Войцехович К.О. Влияние индометацина на Ca^{2+}-ответы, индуцированные окисленным глутатионом или препаратом глутоксим в макрофагах. В. мат. VIII Международной конференции «Биоантиоксидант». Москва. 2010. С. 317-318.

SYSTEMIC HAEMODYNAMIC CHANGES DURING ISOMETRIC RHYTHMIC CONTRACTIONS OF KNEE EXTENSORS WITH DIFFERENT PATTERNS OF FORCE DEVELOPMENT

S.Y. Kuznetsov, V.A. Makarov, A.S. Borovik, O.L. Vinogradova

SSC RF Institute for Biomedical Problems RAS, Moscow, Russia

10 young healthy male volunteers (23.7±2.8 yrs; 177.5±4.0 cm; 75.5±8.8 kg) with maximal knee extension torque 238.9±34.6 N·m performed isometric rhythmic contractions of knee extensors in regime 20 s contraction – 20 s rest till exhaustion at Biodex dynamometer (USA). Muscle contrac-

tions, blood pressure (BP), heart rate (HR) and respiratory rate were recorded continuously during experiment. This protocol made it possible to reveal not only dynamics of recorded indices during muscle contraction, but long-term changes associated with developing fatigue as well. Pattern of strength changes was plot on the computer display and the subject could control muscle tension comparing the current signal from the dynamometer with the plot. Respiratory rhythm was set by voice command from PC. Beginning of each contraction was ordered in turn in the middle of inspiration and expiration cycle. Three series of experiments were performed with different rates of force increment in each cycle of muscle contractions. In the first series the tension increased up to 30% of maximal voluntary contraction (MVC) approximately during 1 s and was maintained at this level to the end of contraction, in the second series the tension increased during 5 s and in the third – during 10 s. The experiment with evoked by electrical stimulation of *n. femoralis* 30% MVC muscle contractions were performed as well.

Coherent accumulation allowed us to reveal "fine structure" of BP and HR dynamics during muscle contractions. In the beginning of contraction BP and HR demonstrates on the background of general increase decaying oscillations with frequency near 0.1 Hz, that points to their baroreflex origin. With lower rate of tension increase, amplitudes of these oscillations become lower as well. Reaction of cardiovascular system to muscle contractions of the same intensity rises with the development of muscle fatigue. Dynamic behavior of BP and HR during contractions evoked by electrical stimulation practically does not differ from the reaction during voluntary contractions with the same pattern of strength development. The probable physiological mechanisms of the complex dynamic behavior of cardiovascular indices during muscle contractions are discussed.

THE MECHANISM OF ORIENTATION OF MOBILE CELLS *CHLAMYDOMONAS REINHARDTII* AT PHOTOTAXIS

V.G. Ladygin

Institute of Basic Biological Problems RAS,
Pushchino, Moscow region, 142290, Russia

It is known that many unicellular flagellant algae have good mobility. Ultrastructural organization, biochemical composition and the mechanism of functioning the flagella are well understood. However, structural- functional organization of a photosensible organ, the eyespot, or stigma of *Chlamydomonas reinhardtii*, determining the direction of cells' movement, has been studied insufficiently. The problem of formation and ultrastructural organization of the eyespot and its biochemical composition was of interest for us.

Direction and the rate of cells' movement at phototaxis have positive effect only in the blue light of 400-500 nm, i.e. in the range of carotenoids' absorption. Hence, we gave consideration to studying the composition of carotenoids in the globules of the eyespot. For the recent 10-15 years it has been established that the molecules of rhodopsin and all-trans, 9-cis-, 11-cis-

and 13-cis retinal function in the membranes surrounding the globules of the eyespot. However, the composition of lipid-carotenoids globules of the eyespot has not been studied.

With the help of pigment mutants we succeeded fist in studying all stages of biogenesis of the eyespot from formation of 1-2 globules up to formation of the well developed eyespot, consisting of 2-4 sequences of lipid-carotenoid globules.

With electronic microscopy it has been shown that the eyespot at cross sections consists of oval and subcircular lipid-carotenoid globules (Fig.1a).

With special technique of fixation it has been established that all globules of the eyespot were surrounded with the protein membranes (Fig.1b). Just in theses membranes rhodopsin and the isomers of retinal were localized.

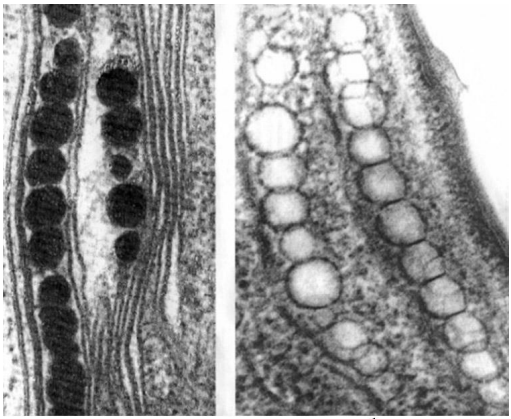

a b

Fig.1

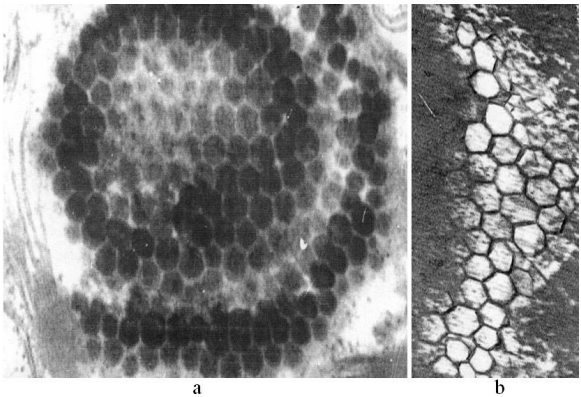

a b

Fig.2

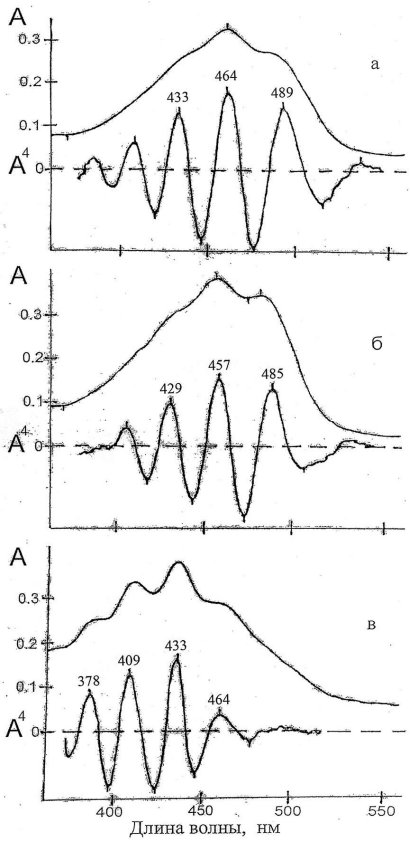

Fig. 3

At linear sections of the eyespot's globules it has been found that in every layer the globules were tightly packed between each other, forming hexagonal structures like bee honeycomb (Fig.2,a).

With the help of special fixation it has been shown that protein membranes of the eyespot form hexagonal structure (Fig.2, b).

The analysis of pigments isolated from the globules of the eyespot showed that β-carotene was, mainly, in the eye in the cells of the wild type *Chlamydomonas reinhardtii*. No xanthophylls were found in the globules of the eyespot (Fig.3, a).

It is important in principle to elucidate: can carotenoids' composition change in the eye of the mutants when changing their composition in photosynthetic membranes of the chloroplasts?

For these studies were taken the mutants, the first one with high content of α-carotene and the second one with high content of ζ-carotene. The analysis of the globules of the eyespot of the first mutant showed that carotenes' composition changed significantly in them. They started to accumulate mainly α-carotene (Fig.3, б).

Similar change of carotenoids at the 2-nd mutant, at which great content of ζ-carotene was accumulated in the globules of the eyespot have been found by us (Fig.3, в).

Thus, it has been established by us that only carotenes (without any xanthophylls) are available in the globules of the eyespot.

It is more important that we have managed to show first: the composition of carotenes can change in the globules of the eyespot.

It should be also considered that changes of carotenes' composition in the globules of the eyespot were observed only at mutants with genetic changes of the carotenes' composition in the chloroplasts' membranes.

A role of the eyespot in orientation and the rate of the cells' movement at phototaxis is being discussed.

SEASONAL CHANGES IN THE ISOFORM COMPOSITION AND FUNCTIONAL PROPERTIES OF HEAVY CHAINS OF MYOSIN FROM SKELETAL MUSCLES OF HIBERNATING GROUND SQUIRRELS *SPERMOPHILUS UNDULATUS*

M. V. Lazareva[1], I. M. Vikhlyantsev[2], A. G. Bobylev[2], N.N. Salmov[2], Z. A. Podlubnaya[2,3]

[1]Belgorod State National Research University, Russia
[2]Institute of Theoretical and Experimental Biophysics, Russian Academy of Sciences, Pushchino, Moscow region, Russia
3Pushchino State Institute of Natural Science, Pushchino, Moscow region, Russia

Among a wide range of physiological states of low vital activity, hibernation of mammals is the most pronounced form of the transient suppression of life. Because animals are immobilized for a long period of time during hibernation and are then capable to pass to a normal motor activity without pathological consequences, there is reason to expect that, in muscles of hibernators, reversible adaptative changes occur, which can contribute to the change in the physiological state of the animal. The studies showed that changes in the structural and functional properties of heavy and light chains of myosin and proteins bound to it (titin, MyBP-C) contributed to the adaptation of the myocardium of hibernators to environmental conditions [1−6]. There is evidence for adaptational changes in the composition of myosin light chains as well as MyBP-X and MyBP-C in skeletal muscles of ground squirrels during hibernation [2, 4, 7, 8]. In particular, it was found that the composition of fast isoforms of light chains in preparations of skeletal muscle myosin of ground squirrels *Spermophilus undulatus* during hibernation decreased about 1.5−2 times [4,7].

In the present work, we studied seasonal changes in the isoform composition of heavy chains of myosin and its functional properties (actin-activated ATP activity, Ca^{2+}-sensitivity of actin-activated ATPase) to determine the contribution of these changes to the adaptation of skeletal muscles of ground squirrels *Spermophilus undulatus* to hibernation conditions.

Skeletal muscles (*m. gastrocnemius*, *m. vastus lateralis*, *m. triceps brachii*, *m. longissimus dorsi u m. psoas*) in different physiological states: hibernation, arousal, winter and summer activity were used. The isoform composition of myosin heavy chains (MHC) was studied by 7% SDS-PAGE as described in [9]. The ATPase activity of reconstructed actomyosin of the ground squirrel was measured from the yield of inorganic phosphate using the colorimetric method [10].

In all muscles examined, a shift of the isoform composition of myosin toward an increase in the content of “slow” MHC was found during hibernation. Thus, the content of the “slow” isoform I in *m. longissimus dorsi*, *m. triceps*, and *m. gastrocnemius* increased three to four times, and the content of the fast isoform IIx/d of MHC considerably decreased (~5 times) as compared with the content of these isoforms in the muscles of active summer

animals. In *m. psoas*, the "slow" isoform I (of MHC) appeared during hibernation (to 26% of the total content of MHC), and the content of the fast isoforms IIa and IIx/d decreased ~ 1.5 times. Similar changes in the isoform composition of MHC were observed in *m. vastus lateralis* of ground squirrels during hibernation. It should be noted that the isoform composition of MHC in the skeletal muscles of arousing and active winter ground squirrels was similar to that in muscles of hibernating but not summer-active animals.

What is the physiological significance of the changes in the myosin phenotype of skeletal muscles of ground squirrels during hibernation? It is known that the enzymatic activity of myosin isoforms is different [11, 12]. At present it is generally accepted that the isoform IIb of myosin has the highest activity in the presence of actin; then the fast isoforms IIa and IIx/d follow; the slow isoform I shows the lowest ATPase activity [13]. If a filament contains only one type of MHC, the myofibrillar ATPase activity decreases in the series of isoforms in the same order: IIb>IIx/d>IIa>I [14]. Because the main strategy of hibernation is the most stringent economy of energy resources, it can be stated that changes in the isoform composition of MHC in skeletal muscles of ground squirrels, aimed at increasing the content of slow MHC isoforms during hibernation are adaptational changes. Based on these results and the literature data, we assumed that the actin-activated ATPase activity in myosin from skeletal muscles of torpid ground squirrels would decrease *in vitro*. Indeed, it was found that the actin-activated ATPase activity in myosin isolated from skeletal muscles of torpid ground squirrels was twofold lower compared with that in summer-active animals. Interestingly, the actin-activated ATPase activity of myosin from skeletal muscles of winter-active ground squirrels was also lower (~1.3 times) than that in summer-active animals. How can this difference be explained? It is known that not only heavy chains of myosin but also its light chains contribute to actomyosin ATPase. In particular, it was shown that the phosphorylation of light chains 2 of myosin enhances its ATPase activity [15]. Considering that light chains of skeletal myosin of torpid ground squirrels are dephosphorylated [4], it can be stated that the lower ATPase activity of myosin from skeletal muscles of active winter ground squirrels, as compared with that of myosin from skeletal muscles of active summer ground squirrels is due to the higher content of the "slow" isoform I of MHC.

It should be noted that the Ca^{2+}-sensitivity of actin-activated ATPase of myosin [16] from skeletal muscles of torpid and active winter ground squirrels was lower than that of myosin from skeletal muscles of active summer ground squirrels. How great is the need for a decrease in the Ca^{2+}-sensitivity of myosin during hibernation? It is known that low temperatures suppress the activity of enzymatic systems, including ATP-dependent membrane pumps generating a Ca^{2+} gradient on opposite sides of inner and outer membranes [17]. It may happen that the concentration of free Ca^{2+} ions in the cytosol of resting myocytes would approach the threshold of the activation of the myofibrillar apparatus. This may lead to spontaneous contractile activity.

Therefore, the decrease in the Ca^{2+}-sensitivity of myosin can be considered as an adaptation factor that prevents the undesirable activity of the myofibrillar apparatus of skeletal muscles of ground squirrels during hibernation.

Thus, adaptative changes in the isoform composition of MHC of skeletal muscles of ground squirrels during hibernation and in the enzymatic and regulatory properties of myosin are directed at suppressing the contractile activity of these muscles, which is necessary in this period.

This work was supported by the Russian Foundation for Basic Research (grant No. 11-04-01026) and a grant of the Federal Targeted Program "Scientific and Scientific-Pedagogical Personal of Innovative Russia", State Contract No. 02.740.11.0710.

REFERENCES

1. Morano I., Adler K., Agostini B., Hasselbach W. // J Muscle Res. Cell Motil. 1992. V. 13(1). P. 64-70.
2. Vikhlyantsev I.M., Alekseeva Yu.A., Shpagina M.D., Udaltsov S.N., Podlubnaya Z.A. // Biofizika. 2002. V. 47(4). P. 701-705.
3. Osipova D.A., Khalina Y.N., Podlubnaya Z.A. // In book: "Biological motility". Pushchino. 2004. P. 231-233.
4. Zuikova O.V., Osipova D.A., Vikhlyantsev I.M., Malyshev S.L., Udaltsov S.N., Podlubnaya Z.A. // Biofizika. 2005. V. 50(5). P. 797-802.
5. Malyshev S.L., Osipova D.A., Vikhlyantsev I.M., Podlubnaya Z.A. // Biofizika. 2006. V. 51(5). P. 929-933.
6. Karaduleva E.V., Vikhlyantsev I.M., Tutukina M.N., Podlubnaya Z.A. // Vestnik Biotechnol. and Phys.-Chem. Biol. Yu. A. Ovchinnikova. 2010. V. 6(4). P. 5-12.
7. Lukoyanova N.A., Ignat'ev D.A., Kolaeva S.G., and Podlubnaya Z.A. // Biophysics. 1997. V. 42. P. 323-328.
8. Shumilina Yu.V., Karaduleva E.V., Vikhlyantsev I.M., Podlubnaya Z.A. // Pathogenesis. 2008. V. 3. P.97.
9. Tikunov BA, Sweeney HL, Rome LC // J Appl Physiol. 2001 V. 90(5). P. 1927-1935.
10. Lanzetta P.A., Alvarez L.J., Reinach P.S., Candia O.A. // Analyt. Biochem. 1979. V. 100. P. 95-97.
11. Syrový I. // Prog. Biophys Mol. Biol. 1987. V. 49(1). P. 1-27.
12. Seidel J., Sreter F., Thompson M., Gergely G. // Biochem. Biophys. Res. Communications. 1964. V. 17(6). P. 662-667.
13. Sieck G.C., Zhan W.Z., Prakash Y.S., Daood M.J., Watchko J.F. // J Appl Physiol. 1995. V. 79(5). P. 1629-1639.
14. Bottinelli R., Canepari M., Reggiani C., Stienen G.J. // J. Physiol. 1994. V.481(3). P. 663-675.
15. Sweeney H.L., Bowman B.F., Stull J.T. // Am. J. Physiol. 1993. V. 264(5 Pt 1). P. C1085-1095.
16. Malyshev SL, Freidina NA, Vikhliantsev IM, Bledzhiants DA, Karaduleva EV, Shumilina IuV, Udal'tsov SN, Marsagishvili LG, Bobylev AG, Podlubnaia ZA. Biofizika. 2010. V. 55(5). P.790-802.
17. Wang S.Q., Lakatta E.G., Cheng H., Zhou Z. // J. Exp. Biol. 2002. V. 205. P. 2957-2962.

EXPRESSION OF IGF-I AND PROTEIN DEGRADATION MARKERS DURING HINDLIMB UNLOADING AND GROWTH HORMONE ADMINISTRATION IN RATS

T.A. Leinsoo, O.V. Turtikova, B. S. Shenkman

SRC, Institute for Biomedical Problems, RAS, Moscow, Russia

It is well established that hindlimb unloading produces atrophy in rat postural muscles and a number of phenotypic alterations in skeletal muscle. Many of these processes are triggered by the axis growth hormone (GH)/insulin-like growth factor I (IGF-I). However GH and IGF-I expression relationship in rodent models of gravitational unloading is weakly investigated.

Thirty-two 2.5-mo-old rats were assigned randomly and equally to one of four groups: *1*) control, saline injected (C+S); *2*) control, GH injected (C+GH); *3*) hindlimb suspended, saline injected (HS+S); *4*) hindlimb suspended, GH injected (HS+GH). In the present study we examined the IGF-I expression by RT-PCR assay in the rat soleus, tibialis anterior and liver after 3 day of hindlimb suspension with GH administration. Simultaneously were studied expression levels of MuRF-1 and MAFbx/atrogin as a key markers of intracellular proteolysis.

Real time PCR analysis was performed using two reference genes, the large

ribosomal protein P0 (RPLP0) and GAPDH; in the study RPLP0-to-GAPDH ratio was stable.

We demonstrated the IGF-I expression in the group HS+S was decreased by 68% as compared to control C+S. GH administration for suspended animals slightly prevented decrease of IGF-I expression (58% compared to C+S). IGF-I expression in tibialis anterior for both suspended groups decreased by ~30%. At the same time changes of IGF-I expression in liver were minimal. Differences of IGF-I expression in liver among experimental groups were minimal (84±4%).

Hindlimb suspension increased activity of ubiquitin-proteasome system in soleus up to 8 fold in groups HS+S and HS+GH. No differences were found between control groups C+S and C+GH in soleus. For MuRF-1 levels in tibialis anterior were demonstrated 2.5 fold increasing for HS+S and 1.7 fold increasing for C+GH. MuRF-1 expression decreased by 38% in group HS+GH. So excess of exogenous GH prevent protein degradation in tibialis anterior in suspended hindlimb.

We conclude GH administration no prevent IGF-I expression decreasing under the conditions of simulated weightlessness. There are separated mechanisms of action of GH and IGF-I for protein metabolism in skeletal muscles. Gravitational unloading activate proteolysis independently from growth hormone activity.

Supported by RFBR Grant 11-04-02048.

A RELATIONSHIP BETWEEN THE THERMAL STABILITY OF MONOMERIC G-ACTIN AND THE CONFORMATIONAL STATE OF THE NUCLEOTIDE-BINDING CLEFT IN ITS MOLECULE

D.I. Levitsky [1,2]

[1] *A.N. Bach Institute of Biochemistry, Russian Academy of Sciences, Moscow, Russia;*

[2] *A.N. Belozersky Institute of Physico-Chemical Biology, Moscow State University, Moscow, Russia*

Actin is one of the most abundant and highly conserved cell proteins and it is involved in many cellular processes that are essential for growth, differentiation and motility. Actin molecule consists of two domains, separated by two diametrically opposed clefts, each domain being subdivided into two subdomains. The larger cleft, between subdomains 2 and 4, is the nucleotide-binding cleft (so named because it constitutes the nucleotide-binding site), whereas the smaller cleft, between subdomains 1 and 3 (also known as the hydrophobic cleft), is a primary target for most actin-binding proteins (ABPs) and therefore it is also called "target-binding cleft" [1]. The nucleotide-binding cleft was suggested to exist in two main states, closed and open. A large body of biochemical data shows that different ABPs may have opposite effects on rate of nucleotide exchange on actin monomers: e.g., profilin enhances the nucleotide exchange, whereas twinfilin inhibits the exchange. The opposite effects of these ABPs on the rate of nucleotide exchange can be explained by their different effects on the conformational state of the nucleotide-binding cleft. The atomic structure of the actin-profilin complex showed that the binding of profilin to the hydrophobic cleft leads to the opening of the nucleotide-binding cleft [2]. In contrast, the crystal structure of the G actin complex with C-terminal ADF-H domain of twinfilin suggested that binding of twinfilin to the hydrophobic cleft may ''lock'' the nucleotide-binding cleft in a closed conformation [3]. Thus, the effects of ABPs on the rate of nucleotide exchange on actin monomers, increase or decrease, seem to be determined by ABP-induced opening or closing of the nucleotide-binding cleft.

There is, however, some discrepancy between the actin crystal structures and the data of solution studies on the nucleotide exchange. For example, the solution studies are consistent with the opening of the nucleotide-binding cleft upon the transition from the ATP– to ADP–G-actin, whereas only the closed conformation of this cleft was observed in the crystal structures of ADP–G-actin [4]. Another example is G-actin specifically cleaved within the DNase I-binding loop (D-loop) in subdomain 2, which demonstrated the increased nucleotide exchange rate in solution [5], but its crystal structure showed the nucleotide-binding cleft in a typical closed conformation [6]. It seems possible therefore that crystallization favors a closed state for G-actin even though the state of the nucleotide-binding cleft in solution may vary. To avoid ambiguity, it seems important to apply some other additional approach to examine the nucleotide-binding cleft conformation, open or closed. In our opinion, the thermal stability of G-actin can be successfully used for this purpose.

In previous studies, we have shown using differential scanning calorimetry (DSC) that both replacement of actin-bound ATP by ADP and specific cleavage of G-actin within the D-loop (i.e., the changes for which the transition of the nucleotide-binding cleft to its open state was predicted from solution studies) strongly decrease the thermal stability of G-actin [7]. Thus, it seems highly possible that the thermal stability of G-actin is mainly determined by the conformational state of the nucleotide-binding cleft: the actin molecule is stable when the cleft is closed, while an opening of the cleft leads to significant destabilization of G-actin.

More recently, we continued these studies and applied DSC to characterize and compare the effects of two different ABPs, twinfilin and profilin, on the thermal unfolding of G-actin in its different states, with either ATP or ADP as a bound nucleotide. Our results showed that twinfilin strongly stabilizes ADP–G-actin (i.e., it increases the maximum temperature of its thermal transition by almost 8°C, from 50.8°C to 58.6°C), thus making its thermal unfolding very similar to that characteristic for ATP–G-actin in the absence of twinfilin, but it has no significant effect on the thermal stability of ATP–G-actin, in which the nucleotide-binding cleft is already exists in the closed conformational state. By contrast, profilin strongly decreased in a concentration-dependent manner the thermal stability of ATP–G-actin. At rather high profilin/actin molar ratio (1.5:1) we observed on the DSC profiles an appearance of a new peak with maximum at lower temperature (52.5°C) than those for isolated ATP–G-actin (61°C) or profilin (56°C), and the maximum of this peak shifted to higher temperature when the profilin/actin molar ratio decreases from 1.5 to 0.125. A noticeable destabilizing effect of profilin was also observed with ADP–G-actin (in this case, the thermal stability of G-actin decreased by 5–6°C in the presence of profilin). These results confirm the assumption that the thermal stability of G-actin is mainly determined by the conformational state of the nucleotide-binding cleft, more open or more closed, and therefore it may be used as a marked characteristic for the conformation of the cleft.

This work was supported in part by RFBR (grant 12-04-00441) and by the Program “Molecular and Cell Biology” of Russian Academy of Sciences.

References

1. Dominguez, R. and Holmes, K.C. (2011) Actin structure and function. *Annu. Rev. Biophys.* **40**, 169–186.
2. Chik, J.K., Lindberg, U., and Schutt, C.E. (1996) The structure of an open state of β-actin at 2.65 Å resolution. *J. Mol. Biol.* **263,** 607–623.
3. Paavilainen, V.O., Oksanen, E., Goldman, A., and Lappalainen, P. (2008) Structure of the actin-depolymerizing factor homology domain in complex with actin. *J. Cell. Biol.* **182**, 51–59.
4. Otterbein, L.R., Graceffa, P., and Dominguez, R. (2001) The crystal structure of uncomplexed actin in the ADP state. *Science* **293**, 708–711.
5. Khaitlina, S.Yu and Strzelecka-Gołaszewska, H. (2002) Role of the DNase-I-binding loop in dynamic properties of actin filament. *Biophys. J.* **82,** 321–334.
6. Klenchin, V.A., Khaitlina, S.Yu and Rayment, I. (2006) Crystal structure of po-

lymerization-competent actin. *J. Mol. Biol.* **362**, 140–150.
7. Pivovarova, A.V., Khaitlina, S.Yu and Levitsky, D.I. (2010) Specific cleavage of the DNase-I binding loop dramatically decreases the thermal stability of actin. *FEBS J.* **277**, 3812–3822.

AGE-SPECIFIC CHANGES IN CARDIOMYOCYTE ULTRASTRUCTURE OF JAPANESE QUAIL COTURNIX JAPONICA

T.V. Lipina, M.S. Duhinova, N.B. Serezhnikova, L.S. Pogodina, Yu.S.Chentsov

Lomonosov Moscow State University Biology department; Moscow, Vorobjevy gory, 119992, Russia

Aging is inevitable process, leading to dramatic changes in majority of organs, including cardiovascular system. Many heart diseases are known to be connected with aging. Nowadays this process is under active investigation in mammals, at the same time it is less studied in other vertebrates. But some non-mammal organisms are used as model objects for studying of aging changes in man, so their study has both fundamental and practical interest. For example, Japanese quail C*oturnix japonica* has natural quick aging; aging of its retina is regarded as an adequate model for studying of age-related process in human retina, as retinas of man and quail have similar structure and metabolism (Zak et al., 2010). However age-specific changes in quail myocardium remain undescribed. Their investigation can help to discover general features of senescent heart in different vertebrates and to compare aging processes in various tissue types, which often undergo oxidative stress (for example, retina and myocardium).

The purpose of the present study was to compare morphological features of ventricle cardiomyocytes in quails of two ages. The opportunity to get quail hearts was generously afforded by P.P. Zak (Emanuel Institute of Biochemical Physics of Russian Academy of Sciences). So, two age groups were studied: 8 weeks (young birds) and 48 weeks (old birds). Following parameters were analyzed: 1) at light-microscopic level - cross-section diameters of cardiomyocytes, as it is known that aging in mammals lead to increase in cardiomyocyte sizes - their hypertrophy (Anversa et al., 1986), 2) at electron-microscopic level – relative volumes of myofibrils and mitochondria, as their ratio shows the proportionality of changes in contractile and energy production systems in cardiomyocytes.

Samples from left ventricle myocardium of quails were fixed by 4% glutaraldehyde and postfixed by 1% osmium tetraoxide, further processed following standard techniques and embedded in Epon 812. On the semi-thin sections cross-section diameters of cardiomyocytes (in nuclear zone) were analyzed with program ‘ImageJ’. Ultrathin sections of oriented lengthwise cardiomyocytes were analysed by transmission-electron microscopes JEM-100B and JEM-JEOL100c. On photonegatives and computer images the relative volumes of myofibrils and mitochondria were detected by standard point test system. Statistical analysis was done with “STATISTICA 6.0” by nonparametric Mann-Whitney U-test. Differences were estimated as significant at $p < 0.05$.

We revealed no differences in myocardial tissue structure between analyzed groups at light-microscopic level. Morphometric analysis showed that there was no statistical difference in cardiomyocyte diameters also between 8 and 48 weeks. So aging in quail myocardium is not associated with cell hypertrophy, as it is known in mammal myocardium. It is likely that age of 48 weeks is not enough for significant changes in heart muscle cell size of Japanese quail. Perhaps marked changes at heart structure, including hypertrophy, appear at older age, as it is known that at some conditions quails can live up to 4 years (Fite, Bengston, 1989).

At electron-microscopic level we found that cardiomycytes in both age groups characterized by nuclei with irregular borders, predominately located at the cell centre; myofibrils had sarcomeres of classical structure, there were local edemas of sarcoplasm. As a rule, mammalian cardiomyocyte nuclei have even regular borders in young animals, their shape became irregular and with invaginations at aging and at pathology, including apoptosis (Lushnikova et al., 2004).

Mitochondria in heart muscle cells of 48 week-old quails had several peculiarities as compared with young birds: less-oriented cristas, intracrista incisions in some organellas. Some mitochondria were elongated (their length exceeds 3 sarcomeres). Elongated mitochondria were previously described in cardiomyocytes of different mammals in conditions of functional overload. Rarely in this study we found mitochondria of unusual form, in particular ring-shaped in cardiomyocytes of both age groups. It is interested to note that such mitochondria significantly increased in number in retina of the same birds at age 48 weeks, but not at age of 8 weeks (Serezhnikova et al., 2011).

Granules of lipofuscin, known as aging pigment, were shown rarely in heart muscle cells of both age groups. It should be noted, that retinal pigment epithelium of the same quails (48 weeks old) had statistically significant increase in lipofuscin granules (Serezhnikova et al., 2011). So lipofuscin accumulation has remarkably different rates in retina and myocardium. On the other hand it can not be excluded that rates of aging differ dramatically in these organs in birds. It is interestingly, that in aging rat and human heart lipofuscin is found quite often. It is important to note that cardiac muscle lipofuscin is regarded as the result of mitochondria desruption (Perennec, Hatt, 1990), but accumulation of retinal lipofuscin originates from phagocytosed outer photoreceptor segments (Sparrow, Boulton, 2005). Different origin of this pigment agrees with our results of its different amount in heart and retina of quails.

Mitochondria and myofibril relative volumes remained unchanged in cardiomyocytes of 48-week-old birds in comparison with 8 weeks-old birds, so balance between contractile apparatus and energy-production system is kept at this age interval.

Thus, revealed features of quail myocardium of 8- and 48-week-old birds differ from changes of this age period observed in the same birds in retina; and they markedly differ from aging animal myocardium as well. Further investigations, including material of older quails, are necessary to understand reasons of such sharp distinctions.

Authors are sincerely grateful to colleagues from Emanuel Institute of Biochemical Physics of Russian Academy of Sciences, P.P. Zak and N.M. Trofimova, for the afforded opportunity to study quail hearts.

References

1. Zak P.P, Zikova A.V., Trofimova N.N., Abu Hamidah A.E., Fokin A.E., Eskima E.N., Ostrovsky M.A // Doklady Biological Sciences. 2010. 434. №2. p. 272-274.
2. Anversa P., Hiler B., Ricci R., Guideri G., Olivetti G. // J Am Coll Cardiol, 1986. 8(6): p.1441-1448.
3. Fite K.V., Bengston L. // Current Eye. Res. 1989. Vol. 8. №10. P. 1039-1048.
4. Lushnikova E.L., Nepomnyashchikh L.M., Rozenberg V.D. // Morphological and molecular-genetic bases of dilated cardiomyopathy. 2004. Moscow. Publ. House RAMS. 192p.
5. N.B. Serezhnikova, M.S. Duhinova, L.S. Pogodina, T.V. Lipina, Trofimova N.N., Zak P.P. // II international scientific-practical conference " High tech, fundamental and application studies in physiology and medicine", 2011r. S-Petersburg, P. 292-293.
6. Perennec J., Hatt P.Y. Myocardial morphology in cardiac hypertrophy and failure: electron microscopy and experimental data // Cardiac hypertrophy and failure. Ed. by B. Swynghedauw, 1990. P. 251-266.
7. Sparrow J.R., Boulton M. // Exp.Eye Res. 2005. Vol. 80. P. 595-606.

VISCOELASTIC PROPERTIES OF PAPILLARY MUSCLE UNDER MONOCHROTALINE INDUCED PRESSURE OVERLOAD

R.V. Lisin, A.T. Smoluk, L.T. Smoluk, Y.L. Protsenko

Institute of Immunology and Physiology of the Ural Branch of the RAS, 620049, Pervomayskaya st., building 106, Ekaterinburg, Russia

Diastolic heart failure develops when pressure overload hypertrophy alters the viscoelastic properties of the myocardium. These properties could be altered by changes in any of the components of the composite myocardium, such as cardiac muscle cells, fibroblast, blood vessels, and the extracellular matrix that surrounds these structures [**8**]. In addition, myocardial material properties can be altered by factors extrinsic to the myocardium such as hemodynamic load, heterogeneity, and neurohumoral activation. Changes in any one of these myocardial and extramyocardial determinants, either singly or in combination, may alter cardiac muscle material properties and may change diastolic function. Therefore studying of mechanical properties at pressure overload hypertrophy is an actual problem. In our work we aim to analyze viscoelastic properties of rat papillary muscle under monochrotaline induced pressure overload.

Experimental animals are Wistar rats of the age 3.5-4 month of both sexes and mass ~300g. The development of pressure overload hypertrophy was obtained by subcutaneous introduction of monocrotaline (MCT, Sigma-Aldrich). It is adequately known the monochrotaline effects on rats. Many studies of monochrotaline influence have shown the development of the pulmonary artery hypertension and proliferative pulmonary vasculitis [**2-4**]. Also it has been mentioned hepatocirrhosis, hydroperitoneum and pleural effusion

in some studies [**2**]. These signs indicate significant hypertrophy of right ventricle induced by pressure overload. The changes are adequately developed at 30-35 day [**4**]. We chose the following method of the MCT use [**1**]. After 4 weeks MCT effect resulted in appearance of the signs of right ventricular hypertrophy, pulmonary artery hypertension, pulmonary edema and after 6 weeks it resulted in significant evidence of these signs.

Papillary muscles were isolated from rat right ventricle and had diameter up to 500 micrometer, length up to 3 millimeter. To study viscoelastic properties of the muscles we used early described method [**6, 7**]. The papillary muscle was put into temperature-controlled bath (25^0C) with flowing Krebs-Ringer solution. One end of the preparation strip was tied to the stock of the force transducer and the second end to the rod of the length servomotor. Before the starting the experiment a papillary muscle was electrically stimulated in normal solution within ~60 minutes until steady-state contractility has been reached. After establishing steady-state contractility we determined two control lengths: L_0 and L_{max}. Length L_0 corresponded to zero-level of passive tension of the papillary muscle. Length L_{max} corresponds to maximum active tension of the muscle. Then we assessed functional condition of the papillary muscle. It was stretched until L_{max} and released to so called "work" length that was approximately equal $0.95L_{max}$. Subsequently we calculated relation between passive tension (F_p) and active tension (F_A) provided that $F_p/F_A < 0.10$. Greater value of the relation F_p/F_A suggested that the muscle was damaged and it was excluded from the analysis. Next electrical stimulation was switched off and the relationship "length-force" of passive muscle was assessed. Then the muscle was returned to L_0 and we recorded the force relaxation in response to stepwise stretching with increment equal 2% of L_0 (fig. 1). Each subsequent deformation was carried out by length servomotor after disappearing of evident relaxation of passive tension in response to previous deformation.

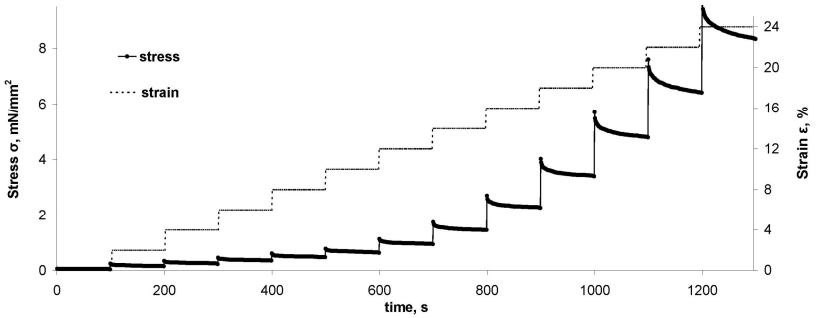

Fig. 1. Stress relaxation of hypertrophied muscle (solid line, left scale) in response to stepwise stretching (dotted line, right scale)

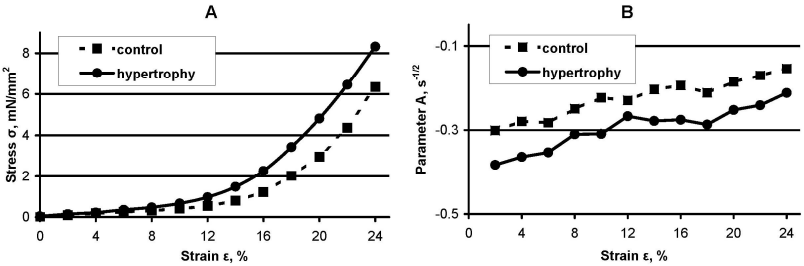

Fig. 2. (A) Stress-strain dependence; (B) Strain dependence of A-parameter, qualitative characteristic of muscle viscosity. Hypertrophied muscle - solid line, control muscle - dotted line.

We compared elastic and viscous properties of hypertrophied muscle and control muscle (fig 2) according to methods [5]. It is show that viscoelastic properties of hypertrophied muscle significantly differ from viscoelastic properties of control muscle. Thus we suggest that monochrotaline induced pressure overload results in increase of muscle stiffness and some reduce of muscle viscosity.

This work is supported by RFBR Grant 10-04-00601-a and Project 12-Y-4-1009 of USC of the Ural branch of the RAS

References

1. Frasch H.F., Marshall C., Marshall B.E. Endothelin-1 is elevated in monocrotaline pulmonary hypertension. // Am J Physiol. 1999. V. 276(2 Pt 1). P. L304-10.
2. Ghodsi F., Will J.A. Changes in pulmonary structure and function induced by monocrotaline intoxication. // Am J Physiol. 1981. V. 240(2). P. H149-55.
3. Lamberts R.R., Caldenhoven E., Lansink M., Witte G., Vaessen R.J., St Cyr J.A., Stienen G.J. Preservation of diastolic function in monocrotaline-induced right ventricular hypertrophy in rats. // Am J Physiol Heart Circ Physiol. 2007. V. 293(3). P. H1869-76.
4. Meyrick B., Gamble W., Reid L. Development of Crotalaria pulmonary hypertension: hemodynamic and structural study. // Am J Physiol. 1980. V. 239(5). P. H692-702.
5. Smoluk L.T. Experimental and theoretical study of viscoelastic properties of papillary muscle: Author's abstract of diss. cand. of phys-math science. in russian. 2011. Puschino. 20 C.
6. Smoluk L.T., Protsenko Y.L. Mechanical properties of passive myocardium: experiment and mathematical model. // Biophysics. 2010. V. 55(5). P. 796-799.
7. Smoluk L.T., Protsenko Y.L. Viscoelastic hysteresis of papillary muscle. // Russian Journal of Biomechanics. 2011. V. 52(2). P. 24-31.
8. Stroud J.D., Baicu C.F., Barnes M.A., Spinale F.G., Zile M.R. Viscoelastic properties of pressure overload hypertrophied myocardium: effect of serine protease treatment. // Am J Physiol Heart Circ Physiol. 2002. V. 282(6). P. H2324-35.

CELL RESISTS HYPOXIA BY ENHANCING OXIDATIVE POWER AND REDISTRIBUTION OF MITOCHONDRIA

K.G. Lyabakh

International Scientific Training Center for Information Technologies and Systems Nathional Academy of Sciences of Ukraine, prosp. Acad.Glushkova, 40, Kiev, 03680, Ukraine

While adapting to environmental changes, cells tend to eliminate energy imbalance. Being at the core of cellular energetic process, mitochondria monitor O_2 supply and play central role in cell resistance to hypoxia. Apparently, a cell, and even its mitochondria, has the ability to sense O_2 and to activate adaptive processes that will enhance the survival in anticipation that oxygen availability might become limiting. Mitochondria move within the cell, their fission, fusion, motility, proliferation, and redistribution may change their oxidative power qO_2 and affect the cell oxygen regimen [1,2]. Our goal is to examine the enhancement of oxidative power and redistribution of mitochondria as a regulator of cell oxygen regimen under hypoxia.

Methods

To test some of mitochondria abilities to meet the oxygen lack challenge we used mathematical modeling of transport and utilization of O_2 in skeletal muscles under hypoxia [3]. The model describes steady state of capillary blood flow and three-dimensional oxygen diffusion - reaction in the myocyte. Solving the equation system, we get the distribution of pO_2 mm Hg and VO_2 (ml/min/100g tissue) in muscle fiber and mean values of tissue pO_2 (P_tO_2), pO_2 in capillary (P_aO_2, P_vO_2) and mean value of tissue VO_2. Muscle blood flow F (ml/min/100g), oxygen concentration in arterial blood C_aO_2 (ml O_2/l), and mitochondria oxidative power qO_2 (ml/min/100g tissue) serve as input variables. Oxidative power qO_2 may be defined as mitochondrion number per unit of cell volume multiplied by their oxidative potential. The calculated values of the ratio $S(x,y,z) = VO_2(x,y,z)/qO_2$ describe the degree of hypoxia at (x,y,z). They set up a field of hypoxia where $pO_2<pO_2crit$. We refer to a hypoxia if $VO_2< 0.9\ qO_2$. The variation of S from 1 to 0 shows gradual decline of cellular VO_2. The zone where $VO2/qO_2 < 1$ represents the picture of hypoxia of varying severity. The computational experiments take into account hypoxic influence - various values of C_aO_2 and regulatory impact – values of oxidative power of mitochondria qO_2, with which mean value of VO_2 could stay approximately constant. C_aO_2 varied within the range of 100-195mlO_2/l, the F varied within the range of 10 - 70 ml / min/100g of tissue, at the selected minimum value qO_2=3 ml/min/100g tissue. In the first series of calculations, we considered homogeneous distribution of qO_2; in the second series qO_2 was assumed to be proportional to values of VO_2 obtained in the first series. We supposed that certain mitochondria may move from areas of poor oxygen supply to the region of better oxygenation where oxygen demand would be satisfied. Parameters of both oxygen regimens were compared.

Results

It is obvious that inadequate O_2 delivery results in lower muscle oxygen consumption rate VO_2, but carrying out the work with required intensity necessitates keeping VO_2 at a required level. According to our calculations, if oxidative power of mitochondria qO_2 increases, VO_2 can remain unchanged despite increasing hypoxemia (Fig.1). We can see that maintain a constant level of VO_2 is possible only within definite range of qO_2. At a certain value of C_aO_2, the curve VO_2 (qO_2) goes abruptly upwards. Further increase of qO_2 becomes ineffective because O_2 cannot be extracted from blood. To keep a constant VO_2 at hypoxia by increasing qO_2 it is necessary to enhance O_2 delivery. Thus regulatory resource of increasing qO_2 can be limited by the level of blood flow F (Fig. 1).

Calculated values oxygen mode parameters in muscle under arterial hypoxemia and increased oxidative power are listed in Table 1. It is shown that with decreasing of C_aO_2 qO_2 have to be increased to get VO_2=const on a background of certain F_i. With further decrease in C_aO_2, F must be increased in order to regain the possibility of regulating VO_2 by varying qO_2. We represented the limiting values of F and qO_2 at C_aO_2 = 130 and 110ml/l in Table 1 Maximum value of qO_2 ≈6ml/min/100g. As can be seen, hypoxia area in the myocite grows (S decline to 0.61) , but VO_2 stays unchanged provided F is at an appropriate level.

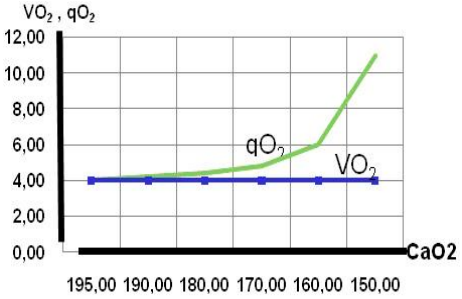

Fig. 1. Cell VO_2 remains constant under arterial hypoxemia due to the increase of qO_2.

Table 1 Oxygen mode parameters in the cell under arterial hypoxemia: homogeneous distributed qO_2 in the cell is increased. P_{min} is pO_2 in the dead corner

C_aO_2	195	160	150	130	110
F	30	30	30	40	60
qO_2	4	4.7	6	5.7	6
P_aO_2	105	52	47	38	31
P_vO_2	22	14	11	14	16
P_tO_2	20	8	4.3	4	3
P_{min}	2.8	0.3	0	0.2	0.2
S	0.92	0.78	0.62	0.65	0.61
AVD	123	121	123	92	61
VO_2	**3.7**	**3.7**	**3.7**	**3.7**	**3.7**

Based on the results of mathematical modeling and literature data [1, 2, 4, 5], we assume that mitochondrial oxidative power may be redistributed inside a cell by increasing individual oxidative power of each mitochondrion and by their migration inside a cell. Using previously obtained values of VO_2, we redistribute qO_2 according to cell gradient of VO_2 and calculate parameters of a new oxygen regimen (Table 2).

Table 2 Oxygen mode parameters in the cell under hypoxic hypoxia: qO_2 is increased and redistributed to avoid hypoxia

C_aO_2	195	160	150	130	110
F	30	30	30	40	60
qO_2	3.7	4.7	6	5.7	6
P_aO_2	105	52	47	38	31
P_vO_2	23	16	13	15	17
P_tO_2	20	11	7.3	7	6.2
P_{min}	5.8	4	3.4	3.6	3.7
S	0.95	0.94	0.95	0.94	0.93
AVD	117	113	117	86	57
VO_2	**3.5**	**3.5**	**3.5**	**3.5**	**3.5**

Migration and increase of oxidative capacity create such distribution of mitochondria power inside a cell that hypoxia is reduced or eliminated ($S \geq 93\%$, $P_{min} > P_{crit}$) and mean value of cell VO_2 achieves the required level (Table 2).

Thus for convenience we may assume: that the first step of tissue adaptation process is an increase of mitochondrial oxidative power. This step permits to maintain VO_2=const. Perhaps it will not be enough and the cell will have to send signals about O_2 deficit and "to ask for" a change of blood flow level. Next step in adaptation is redistribution of mitochondria according to VO_2 gradient. This will require a certain reconstruction of mitochondrial system, which implies not just increase of oxidative power but also parallel relocation of mitochondria inside the cell and increasing their number. According to [4], mitochondrial clusters eliminate cell hypoxia. Our results show that inhomogeneous distribution of mitochondria can improve oxygen regimen even without clusters. As a result, hypoxia is eliminated, and a new energetic level is attained.

Conclusion

Augmentation of oxidative power of mitochondria in a cell enables to keep constant mean value of oxygen consumption rate under hypoxia. Redistribution of oxidative power of mitochondria may improve tissue oxygen regimen by decreasing or elimination tissue hypoxia.

References

1.Загускин С.Л., Загускина Л.Д., Загускина С.С. Внутриклеточная регуляция потребления кислорода в нейроне рецептора растяжения речного рака // Цитология .— 2007. — 49 ,10. —С. 832-838.

2.Li Y, Rempe D. During hypoxia, HUMMR joins the mitochondrial dance// Cell Cycle.—2010. — 9 , 1. — P. 50-57.

3.Lyabakh K. Mathematical modeling of oxygen transport in skeletal muscle during exercise: hypoxia and VO_2 max // Adv. Exper. Med. Biol. — 1999. —471. — P. 585-593.

4.Mainwood, G.W, and Rakusan K. A model for intracellular energy transport // Can. J. Physiol. Pharmacol. — 1982. —60, 1. — P.98-102.

5. Лябах Е.Г., Маньковская И. Н. Снабжение кислородом мышц человека при работе в горах // Спортивная медицина.— 2008. —1. —С.120-126.

MODIFICATION OF FUNCTIONAL STATE OF MUSCLE TISSUE UPON INFLUENCE EXTREMELY LOW FREQUENCY OF ELECTROMAGNETIC FIELD

V.S. Martynyuk, Yu.V. Tseyslyer, O.V. Tsymbalyuk, O.V. Shelyuk, N.E. Nurishenko

Taras Shevchenko National University of Kyiv,
64, Volodymyrs'ka St., Kiev, 01061, Ukraine;
E-mail: mavis@science-center.net, yuliya.tseysler@gmail.com

Search of mechanisms of the effect of weak electromagnetic fields of extremely low frequency (EMF ELF) on biological objects is one of the intriguing problems of modern biophysics. The action of ELF EMF on biological objects is realized though different primary and system mechanisms and depended on frequency and amplitude of EMF, exposure, biological nature of experimental objects and its initial physiological state [1], as well as concomitant physical factors and chemical agents [2]. It is known that different functional systems of humans and animals demonstrate unequal sensitivity to the influence of EMF ELF. Analysis of published data shows that the muscle tissue and its components are regarded as one of the targets of EMF [3], but this question remains poorly understood. In this regard it should be noted that the greatest number of papers devoted to studying the effect of EMF ELF on the activity of the myocardium and functional status of the cardiovascular system [4]. At the same time, there are small amount data that testified on direct effects of EMF on smooth muscle tissue and structural-functional properties of contractile proteins.

Smooth muscles are part of shells of internal organs: the intestines, blood vessels, respiratory tract, excretory and sexual organs, and many glands. Smooth muscles play an important role in regulating the functional activity of these organs.

The actomyosin complex is basic contractile element of muscle proteins. Its ATPase activity is the key property of the muscle elements to carry out their contractile function. The basis of functional disorders of muscle contrac-

tility can be changes of activity of the myosin ATPase that is the main mechano-chemical energy converter. Violation of actin-myosin interaction can lead to changes in ATP utilization in muscle tissue and, as a consequence, to changes in the rate of contraction of myofibrils. Physical factors of different nature are able to influence on the ATPase activity of actomyosin. Among these factors the EMF ELF are considered, but its effects are poorly understood on the level of muscle tissue and its components.

Therefore, the aim of our study was to investigate the effect of EMF ELF on some functional parameters of smooth muscle and ATP-ase activity of skeletal muscle actomyosin. In particular, the effects of ELF EMF on spontaneous and K^+-induced and also acetylcholine-induced contraction of smooth muscle strips of rat *caecum* were studied. At the same time the influence of the EMF ELF on the ATPase activity of actomyosin *in vitro* that isolated from rabbit skeletal muscle was estimated.

Materials and methods. The smooth muscle contractile activity of circular smooth muscles of the rat's *caecum* was evaluated in this study. Strips of smooth muscles were placed in the chamber 2 ml with flow Krebs' solution (the flow rate is 4 ml/min) at 37°C. Contractions was measured by using an electric potentiometer H339. Contractions were induced by application of acetylcholine (ACh, 10 μM) in Krebs' solution, as well as hyper-potassium solution (K^+, 80 mM). The contractile responses of smooth muscle strips were analyzed by the method of kinetic analysis proposed by T.V. Burdyga and S.O. Kosterin [5].

The actomyosin of skeletal muscle from rabbit was isolated by the Perry's method modified by A.D. Tartakovsky [6] and us. Actomyosin was purified additionally by centrifugation at 20 000g for an hour. The Mg^{+2}/Ca^{+2} - and K^+-ATPase activity of actomyosin evaluated by the method described in [7]. The exposure of actomyosin solutions (2 mg/ml) in EMF ELF was 1, 2 and 3 hours at 37^oC.

EMF (meander wave) with frequency 8 Hz and 25 μT was created by using the special generator G6-28 and Helmholtz coils.

Student's test was used for estimation of statistical significance of differences between independent statistical samplings.

Results. In the first part of this research the study of the spontaneous activity of smooth muscle strips showed that the effect of EMF ELF exposure caused a statistically significant ($p<0.05$) increase of frequency of contractions and tends to increase the amplitude of spontaneous contractions. Simultaneously, the electromagnetic treatment organizes a rhythmic activity. One of the causes of such changes can be synchronizing effect of EMF on the pacemaker activity of Cajal cells that play key role in the spontaneous activity of smooth muscles in different organs.

EMF ELF caused inhibition of K^+-induced contractions (23%, $p<0.001$) and also significant increase in the duration of the contraction and slowdown of relaxation (32.5%, $p<0.01$) in smooth muscle strips (fig. 1).

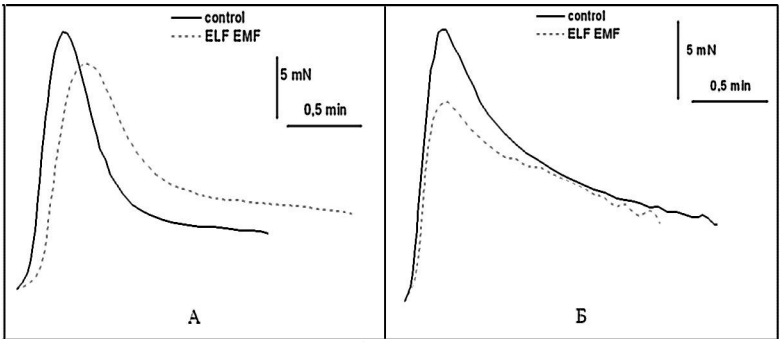

Fig. 1. Examples of recordings of K^+-induced (80 μM) (A) and acetylcholine-induced (10 μM) (B) contraction of smooth muscle strips of rat's *caecum* upon influence of EMF 8 Hz 25 μT.

Acetylcholine-induced contraction was less sensitive to the EMF-influence, however, the statistically significant decrease of the maximum power of contraction on average 11% was revealed (fig. 1). The other mechanic-kinetic parameters of acetylcholine-induced contractions remained at control values. EMF-induced changes in acetylcholine contractions were significantly weaker compared with the responses to K^+-depolarization, and no changes of ratio phase and tonic components was revealed in this case. The appearance of ordered cyclic tonic components was the feature of the EMF influence on the acetylcholine-induced contraction.

The effect of EMF ELF on the protein contractile elements of skeletal muscle, in particularly on ATPaase activity of actomyosin, was evaluated in the second part of the study. The analysis of the effect of EMF ELF on the ATPase activity of actomyosin showed that this process is characterized by certain dynamics. During first two hours of exposure of the protein solutions the EMF ELF inhibited the ATPase activity in comparison with control samples that are not exposed to the EMF for all other equal conditions. This fact confirms data previously obtained by Lednev V. et al. [3]. However, the significant ($p<0.05$) increase of ATPase activity of actomyosin on the third hour of EMF-exposure was revealed but unexpected. Moreover, it is necessary to note that a similar pattern of change of enzyme activity was universal both for media with ions Mg^{+2} and Ca^{+2}, and for the absence of these ions in the buffer (fig. 2). So, Mg^{+2}/Ca^{+2}- and K^+-ATPase activity for one hour exposure to EMF were almost identical and were decreased by 16.5% and 16.3% relative to control samples. Two hours later, Mg^{+2}/Ca^{+2}-ATPase activity decreased by 19.5%, and K^+-ATPase by 15.5%. After three hours of EMF exposure stimulate the Mg^{+2}/Ca^{+2}-ATPase activity by 33.6%, whereas the K^+-ATPase activity by 50.3% (see Fig. 2). In our opinion, such effect of the EMF ELF exposure evidences on dynamic changes in the structural-functional properties of actomyosin in solution during long time that is feature of nonequilibrium system.

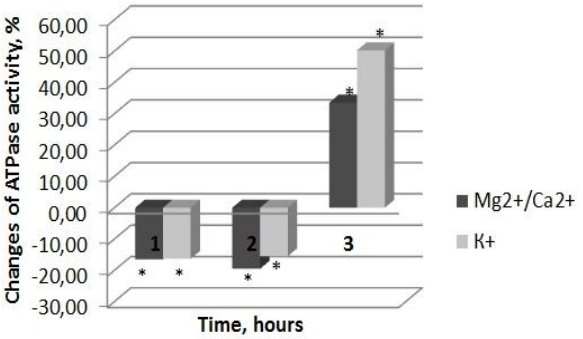

Fig. 2. Change the Mg^{2+}/Ca^{2+}- and K^{+}-ATPase activity (%) upon the influence of EMF (n=30) during 3 hour exposure.

Conclusions. Thus, our findings suggest that extremely low frequency EMF can alter both the contractile activity of smooth and skeletal muscle tissues. The direction and magnitude of the EMF-induced changes depends on the chemical agents that induce contraction and also on time of exposure. The Ca^{+2}, Mg^{+2}-independent effects of the EMF ELF are intriguing and opens the prospect of learning a new primary mechanisms of action of this physical factor that based on sensitivity of magnetic moments of the nuclear spins of the hydrogen atom and diamagnetic currents of electrons in molecules [8].

References

1. Грабовская Е.Ю. / Автореф. дис… канд. биол. наук: 03.00.13 / Симферопольский гос. ун-т. – Симферополь, 1992. – 23 с.
2. Цейслер Ю.В., Калиновский П.С., Мартынюк В.С. // Ученые записки ТНУ им. В.И.Вернадского. Серия «Биология, химия». – 2003. – Т.16 (55), № 3. – С. 8–12.
3. Lednev V.V., Malyshev S.L. / Abstract of Annual Meeting on Bioelectromagnetics Society, June 10–14, 2004. St Paul, Minisota, USA. 2004. P. 2–3.
4. Митрофанова Т.А., Гурфинкель Ю.И., Митрофанова Е.В., Петров А.Ю., Тедорадзе Р.В. / Материалы конференции «Космическая погода: ее влияние на человека и биологические объекты», Москва, 17-19 февраля 2005. – Москва, 2006. - С. 55-56.
5. Burdyga Th.V., Kosterin S.A. // Gen. Physiol. Biophys. – 1991. - № 10. – P. 589-598.
6. Тартаковский А.Д. / Сб.: Биофизические и биохимические методы исследования мышечных белков / Под ред. Г.Р. Иваницкого. - Л.: Наука, 1978. – С. 55-76.
7. Fiske C.H., Subbarow G. // J.Biol.Cem.-1925.-V.66.,N1.- P.375-400.
8. Леднев В. В. // Моделирование геофизических процессов. – 2003. – С. 5-12.

ISOFORM-SPECIFIC EFFECTS OF HINDLIMB UNLOADING ON Na,K-ATPASE IN THE RAT SOLEUS MUSCLE

V. Matchkov[2], I.A. Razgovorova[1], V.V. Kravtsova[1], B.S. Shenkman[3], I.I. Krivoi[1]

[1]St. Petersburg State University, St. Petersburg, Russia;
[2]Aarhus University, Aarhus, Denmark;
[3]RAS Institute for Biomedical Problems, Moscow, Russia

The Na,K-ATPase is a p-type ATPase which catalyzes the active transport of K^+ into and Na^+ out of the cell, thereby maintaining the steep Na^+ and K^+ gradients that provide electrical excitability and the driving force for many other transport processes. The Na,K-ATPase composed of alpha-catalytic and beta-glycoprotein subunits. Four isoforms of the alpha subunit are known to exist in tissues of vertebrates. It is generally accepted that the ubiquitous alpha1 isoform plays the main "house-keeping" role while the other isoforms expressing in a cell- and tissue-specific manner possess additional regulatory functions that are still poorly understood. The largest pool of Na,K-ATPase in a vertebrate's body is contained in the skeletal muscles where the alpha1 and alpha2 isoforms of alpha-subunit are expressed [Orlowski, Lingrel, 1988]. The Na,K-ATPase is critically important for excitability, electrogenesis and contractility of skeletal muscle. Although the alpha2 isoform is expressed in high abundance in skeletal muscle, the functional role and mechanisms of regulation of this isoform remain unclear and are now being intensively investigated. It is well known that content of Na,K-ATPase strong depends on skeletal muscle activity: muscle inactivity decreases Na,K-pump concentration while activity increases it [Clausen, 2008]. Some data indicates that increased skeletal muscle activity differently regulates alpha1 and alpha2 isoforms of the Na,K-ATPase [Kristensen et al., 2008]. Earlier it was shown that disuse induced by hindlimb unloading (HU) leads to progressive atrophy of postural skeletal muscle; the muscle undergoes a number of dramatic remodeling events. The isoform-specifity of HU effects on the Na,K-ATPase are not studied. In the present study, the effect of HU on the resting membrane potential (RMP), the electrogenic activity of the Na,K-ATPase $\alpha1$ and $\alpha2$ isoforms as well as their expression in the rat soleus muscle were investigated.

Experiments were performed on male Wistar rats (210–230 g). To induce muscle unloading, the animals were tail suspended individually in special cages for 3 days. Control animals were not suspended. At the end of the period of unloading, soleus muscles were removed from the animals under deep anesthesia. Isolated muscles were perfused in a chamber with normal physiological solution aerated with a mixture of 95% O_2 and 5% CO_2 at 28°C (pH=7.4). The RMPs were recorded intracellularly in nonsynaptic region of muscle fibers using standard microelectrode techniques. Since in rodents the alpha1 isoform of the Na,K-ATPase is ouabain-resistant whereas the alpha2 isoform is highly ouabain-sensitive, we used ouabain at different concentrations to separate electrogenic contributions of these isoforms. We estimated the electrogenic contribution of the alpha2 isoform to RMP by administration

of 1 μM ouabain, a concentration selectively blocking alpha2 isoform in rodents without effect on ouabain-resistant alpha1 isoform [Heiny et al., 2010]. The electrogenic contribution of the alpha2 isoform was estimated as a difference between RMP before and during 15–30 min of 1 μM ouabain action. Then, for complete block of the alpha1 isoform an ouabain concentration of 500 μM was used. The electrogenic contribution of the alpha1 isoform was estimated as a difference between RMP during 15–30 min of 1 μM ouabain action and during 15–30 min after 500 μM ouabain addition.

Western blots were performed using lysates of frozen muscles. The alpha1 and alpha2 isoform expressions were identified using specific antibodies. Membranes were then stripped for antibodies and stained for pan-actin which served as a house-keeping protein. Detected protein was quantified as a ratio to pan-actin. The mRNA expression was estimated with quantitative PCR using Taqman probe (FAM) technology. Gene expression was normalized to two house-keeping genes, GAPDH and transferrin receptor.

After 3 days of HU RMP value in soleus muscles (–66.8±0.7 mV, 187 fibers) was significantly more positive (by 4.2±0.9 mV; $p<0.01$) than in control rats (–71.0±0.5 mV, 222 fibers). RMP distributions were close to normal; in experimental rats the distribution was shifted to more depolarized RMPs as compared with control rats. In control rats, electrogenic activities of the alpha1 and the alpha2 isoforms were 4.6±0.6 mV and 6.2±0.6 mV, respectively. The total Na,K-ATPase electrogenic contribution in control rats was 10.8±0.6 mV. After 3 days of HU, electrogenic activity of the alpha1 isoform decreased to 2.6±0.6 mV ($p<0.01$) compare to the control; the activity of the alpha2 isoform was not detectable (0.5±0.8 mV). The total electrogenic Na,K-ATPase contribution after HU was 3.1±0.9 mV ($p<0.01$ vs. control).

3 days of HU did not significantly changed the whole-muscle protein content of Na,K-ATPase alpha1 subunit, while alpha2 subunit protein content decreased to 48±7% ($p < 0.01$) of the control. At the same time, there was not seen any changes in Na,K-ATPase alpha1 and alpha2 subunits mRNA expression.

It was previously been shown that HU leads to accumulation of Ca^{2+} in myoplasm as well as increases the level of μ-calpains, Ca^{2+}-dependent protease [see for review: Kachaeva, Shenkman, 2012]. Our results suggest that the decreased alpha2 subunit content in muscle after HU might be due to increased protein degradation rather than alteration in the expression of Na,K-ATPase alpha subunits. The translocation mechanism by which Na,K-ATPase subunits are recruited to plasma membrane from intracellular compartments [Benziane, Chibalin, 2008] could also be involved in HU responses of skeletal muscle. Our data provide further evidence that in the rat skeletal muscle the alpha1 isoform of Na,K-ATPase serves to maintain basal electrogenesis and contractility while the alpha2 isoform seems to provide some regulatory function(s) and more adjustable under functional unloading.

Supported by RFBR #10-04-00970; Saint-Petersburg State University research grant #1.37.118.2011; the Danish Research Council and the Novo Nordisk Foundation.

References

[1] Benziane B., Chibalin A.V. Skeletal muscle sodium pump regulation: a translocation paradigm. Am. J. Physiol. Endocrinol. Metab. 295: E553–E558. 2008.

[2] Clausen T. Role of Na^+,K^+-pumps and transmembrane Na^+,K^+-distribution in muscle function. Acta Physiol. 192: 339–349. 2008.

[3] Heiny J.A., Kravtsova V.V., Mandel F., Radzyukevich T.L., Benziane B., Prokofiev A.V., Pedersen S.E., Chibalin A.V., Krivoi I.I. The nicotinic acetylcholine receptor and the Na,K-ATPase a2 isoform interact to regulate membrane electrogenesis in skeletal muscle. J. Biol. Chem. 285(37): 28614–28626. 2010.

[4] Kachaeva E.V., Shenkman B.S. Various jobs of proteolytic enzymes in skeletal muscle during unloading: facts and speculations. J. Biomed. Biotech. doi:10.1155/2012/493618. 2012.

[5] Kristensen M., Rasmussen M.K., Juel C. Na^+–K^+ pump location and translocation during muscle contraction in rat skeletal muscle. Pflugers Arch. – Eur. J. Physiol. 456: 979–989. 2008.

[6] Orlowski J., Lingrel J.B. Tissue-specific and developmental regulation of rat Na,K-ATPase catalytic alpha isoform and beta subunit mRNAs. J. Biol. Chem. 263(21): 10436–10442. 1988.

REORGANIZATION IN TUBULIN CYTOSKELETON MODULATES THE EFFECT OF GLUTOXIM ON Na^+ TRANSPORT IN FROG SKIN

A.V. Melnitskaya., Z.I. Krutetskaya, S.N. Butov, N.I. Krutetskaya, V.G. Antonov

Saint-Petersburg State University, 7/9 University emb., Saint-Petersburg, 199034, Russia

Amphibian skin and other isolated epithelial systems are classical models to study the mechanisms of ion transport across biological membranes. Na^+ transport in osmoregulated epithelia is a complex multicomponent system that creates and maintains electrolytic and water homeostasis. Various protein components of this system may be the targets for oxidative stress. The influence of oxidizing and reducing agents was demonstrated for a number of epithelial tissues. However, molecular mechanisms of oxidizing and reducing agents effect on various components of Na^+ transepithelial transport are poorly studied. Novel binuclear catalytic agents containing nanoadditions of d-metals currently are widely used in clinical practice. Glutoxim® (FARMA-VAM, Russia) is a synthetic biologically active compound, disodium salt of oxidized glutathione (GSSG) with platinum nanoaddition. Glutoxim is widely applied as an immunomodulator and hemostimulator for the therapy of bacterial and viral infection, psoriasis and the radio- and chemotherapy of oncological diseases. Another GSSG analogue, NOV-002 (GSSG in combination with cisplatin in ratio 1000:1), is a GSSG mimetic and induces the receptor-mediated activation of proteins involved in hematopoiesis. Previously, we found that Na^+ transport in the frog skin is modulated by various oxidizing agents, such as cystamine, cystine, GSSG and glutoxim [1]. It was demonstrated for the first time that GSSG and glutoxim applied to the basolateral surface of the frog skin imitated the insulin effect and stimu-

lated transepithelial Na^+ transport. However, the mechanisms underlying GSSG and glutoxim stimulation of Na^+ transport remain obscure.

It is known that cytoskeleton proteins such as actin and tubulin are highly redox sensitive and are easily glutathionylated [2]. Therefore, it seems reasonable to examine whether microtubules are involved in glutoxim regulation of Na^+ transport in the frog *Rana temporaria* skin. Two structurally distinct microtubule disrupters nocodazole and colcemid, and taxol (paclitaxel), the agent that promotes tubulin polymerization, were used in the experiments.

Materials and methods. Experiments were performed on frog *Rana temporaria* males. The skin from the frog abdomen was removed and placed in Ussing chamber (World Precision Instruments, Inc., Germany) with 12 mm inner orifice. Frog skin electrical parameters were measured with the automatic device for voltage-clamp and registration of current-voltage relations (I-V relations). To measure I-V relations, transepithelial pothential, V_T was changed periodically to a series of nonzero values. In intervals between measurements of I-V relations skin V_T was kept at 0 mV (short-circuit regime) or at open-circuit potential V_{OC} ($V_{OC}=V_T$ at transepithelial current $I_T=0$). Skin electrical parameters were determined from I-V relations: short-circuit current I_{SC} ($I_{SC}=I_T$ at $V_T=0$), V_{OC} and transepithelial conductance g_T. Na^+ transport was evaluated as amiloride-sensitive I_{SC}. To ensure that Na^+ transport was the source of I_{SC}, the blocker of epithelial Na^+- channels (ENaC), amiloride (20 (μM)) was added to the solution washing the apical skin surface. It is known that amiloride (20—100 μM) selectively blocks ENaC. The reagents were purchased in Sigma company (United States). The agents, producing microtubule reorganization were added 30 - 40 min before glutoxim application. Statistical analysis was performed using Student's t-test. The data are presented as $x \pm s_x$. Figure illustrates the results of typical experiments.

Results and discussion. The mean values of frog skin electrical characteristics in control (from 10 experiments) are: $I_{SC} = 14.58 \pm 0.91$ μA; $V_{OC} = -38.01 \pm 2.74$ mV; $g_T = 0.38 \pm 0.01$ mS. 100 μg/ml glutoxim applied to the basolateral surface of the intact frog skin like insulin stimulated Na^+ transport. After glutoxim application I_{SC} increased in average by 31.24 ± 8.32 % whereas V_{OC} enhanced by 38.04 ± 5.15 % (the data from 10 experiments). g_T value was not altered. It is shown that nocodazole almost completely prevented stimulatory effect of glutoxim on Na^+ transport in the frog skin (Figure, *curve 2*). On average (the results of 10 experiments), after the preincubation of skin apical surface with 25 μM nocodazole for 30 min before application of 100 μg/ml glutoxim to the frog skin basolateral surface, I_{SC} increased by 9.01± 1.02 %, and V_{OC} increased by 10.12 ± 1.21 %. g_T value was not changed. It was found that preincubation of apical surface of frog skin with another microtubule disrupter colcemid (25 μM for 30-40 min) not only drastically inhibited glutoxim stimulation of Na^+ transport, but induced the significant reduction of frog skin electrical parameters (Figure, *curve 3*). After colcemid application, I_{SC} decreased by 20.12 ± 3.18 %, and V_{OC} decreased by 23.14 ± 4.05 %. g_T value was not changed. Pretreatment of frog skin apical

surface with microtubule stabilizer taxol (50 μM for 30-40 min) also leads to attenuation of the stimulatory effect of glutoxim on Na^+ transport in the frog skin: I_{SC} increased only by 5.06 ± 0.93 %, and V_{OC} increased by 7.12 ± 1.02 %. g_T value was not changed.

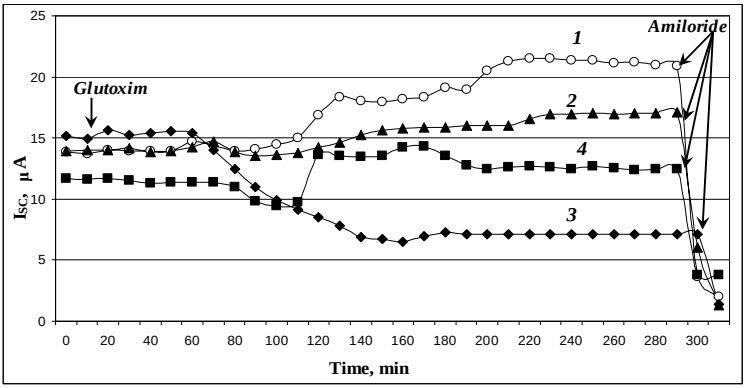

Dependence of glutoxim-induced changes in the short circuit current I_{SC} on the tubulin cytoskeleton integrity. *Curve 1* — I_{SC} after intact skin basolateral surface exposure to 100 μg/ml glutoxim; *curve 2* — I_{SC} after preliminary treatment for 30 min of the skin apical surface with 25 μM nocodazole; *curve 3* — I_{SC} after pretreatment for 30 min of the skin apical surface with 25 μM colcemid; *curve 4* — I_{SC} after pretreatment for 30 min of the skin apical surface with 50 μM taxol. At the end of each experiment 20 μM amiloride, a ENaC blocker, was added to the solution washing the skin apical surface.

We reported earlier that Na^+ transport in the frog skin was dependent on the functional and structural organization of actin and tubulin cytoskeleton [3, 4]. It was demonstrated that antimitotic drugs (colchicine, colcemid, vinblastin) inhibited I_{SC} in the skin of *R. temporaria* frog. Here, we demonstrated that structural rearrangements of the tubulin cytoskeleton modulate glutoxim effect on Na^+ transport in the frog skin. It is known that microtubule structure reorganization with antimitotic agents reduced hormone (aldosterone, vasopressin) induced stimulation of transepithelial Na^+ transport. Microtubules, probably, play an important role in exo- and endocytosis by regulation of ENaC density in the apical membrane. Microtubule disruption also attenuates insulin effect on cellular processes. However, there is evidence that tubulin cysteine residues are targets of oxidants. It was shown that GSSG in physiologically higher concentrations inhibited microtubule assembly. Our results support the idea on the tubulin cytoskeleton involvement in glutoxim regulation of Na^+ transport in the frog skin.

It is known that various Na^+ transporting proteins contain numerous cysteine residues which are the targets for intra- and extracellular oxidizing and reducing agents. In reabsorbing epithelia ENaC play a critical role in the Na^+ transport. Numerous cysteine residues localized in various ENaC segments determine its redox sensitivity and are the targets for intra- and extracellular

oxidizing and reducing agents. Addition of 20 μM amiloride, a ENaC blocker, into the solution washing the apical surface of the frog skin at the end of each experiment almost completely inhibited I_{SC} (Figure). It implies that glutoxim affects Na^+ transport primarily by modulation of ENaC activity.

Thus, our results show that any changes in the tubulin cytoskeleton structure reduce glutoxim-induced Na^+ transport stimulation in the frog skin. These as well as our previous data [4–7] allow to suppose that glutoxim may interact with cysteine-rich domains of the insulin receptor in the basolateral membrane of epithelial cells, induce its transactivation and trigger the signaling cascade including tyrosine kinases, phosphatidylinositol kinases, protein kinase C and cytoskeleton elements that results in stimulation of Na^+ transport in the frog skin.

References

1. Krutetskaya Z.I., Lebedev O.E., Melnitskaya A.V., Antonov V.G., Academician Nozdrachev A.D. 2008. Doklady Biol. Sci. 421: 235-238.
2. *Wanq J., Boja E.S., Tan W., Tekle E., Fales H.M., English S., Mieyal J.J., Chock P.B.* 2001. J. Biol. Chem. 276: 47763–47766.
3. Krutetskaya Z.I., Lebedev O.E., Melnitskaya A.V., Antonov V.G., Academician Nozdrachev A.D. 2006. Doklady Biol. Sci. 410: 367-369.
4. Мельницкая А.В., Крутецкая З.И., Лебедев О.Е. 2006. Цитология. 48 (10): 817–840.
5. Krutetskaya Z.I., Lebedev O.E., Melnitskaya A.V., Antonov V.G., Academician Nozdrachev A.D. 2009. Doklady Biol. Sci. 428: 416 – 417.
6. Melnitskaya A.V., Krutetskaya Z.I., Lebedev O.E. 2009. Biochemistry (Moscow) Supplement Series A: Membrane and Cell Biology. V.3. N.3. P. 323.
7 Melnitskaya A.V., Krutetskaya Z.I., Lebedev O.E., Kurilava LS., Antonov V.G., Butov S.N. 2010. Cell and Tissue Biology. V. 4. N. 3. P. 273-279.

A MECHANISTIC MODEL OF Ca-REGULATION OF THIN FILAMENTS IN STRIATED MUSCLE

N.A. Metalnikova

Institute of Mechanics, Moscow University,
1 Mitchurinsky prosp., Moscow, 119992, Russia

The force-calcium curve that describes activation of striated muscles by calcium ions is much steeper than one would expect from stoichiometry of calcium binding to troponin (Tn). The Ca-activation curve is usually approximated with the Hill equation:

$$V = \frac{[C]^n}{[C]_{50}^n + [C]^n},$$

where V is normalized response (tension, ATPase activity, a signal from troponin *etc*.); $[C]$ is molar Ca^{2+} concentration; $[C]_{50}$ is Ca^{2+} concentration that provides half-maximal response; n is a cooperativity constant, called Hill parameter. As two and one Ca^{2+} ions are needed to activate skeletal and cardiac Tn, respectively, n is expected to be between 1 and 2. In reality it is

much higher and even in cardiac muscle is 3 or higher [1], [2]. It was believed that the high cooperativity of Ca-activation of muscle results from a shift of tropomyosin by myosin heads strongly bound to actin. However full blocking of actin-myosin interaction by blebbistatin does not reduce the steepness of the calcium activation curve [2] indicating that the steepness is an intrinsic property of the thin filaments themselves.

Here we describe a mechanistic model that explains high steepness of the Ca-activation curve for the thin filaments in the absence and in the presence of myosin heads and also suggest a mechanism that may explain stress- or strain-dependence of Ca-activation that is the basis of the Frank-Starling Law of the heart [3]. The model is based on works [4], [5], [6] where tropomyosin (Tm) is modeled by a continuous elastic chain in a harmonic potential well on the surface of an actin filament. A new expansion of this model is that we additionally assume that Tm chain has some tension that may also effect its configuration.

In the absence of Ca^{2+} inhibitory domain of TnI can bind actin and shift the whole Tm chain to a state where it covers myosin binding sites on actin. This corresponds to Blocked states in terms of the three-state models [7]. Ca^{2+} binding to TnC opens hydrophobic 'pocket' where to the switch domain of TnI can bind. When this happens, the inhibitory domain of TnI cannot reach actin and Tm is in actin-free state that corresponds to the Closed state [7]. Strong binding of myosin head shift Tm further and opens myosin binding region of neighbor actin filaments (Open state in the McKillop, Geeves model).

Model

Mathematical model of the Tm chain. Following [4] we consider tropomyosin as a elastic bar with bending stiffness k, in a harmonic potential well with stiffness α and under tension F. Then equilibrium equation for Tm is: $k\varphi''''(s) - F\varphi''(s) + \alpha\varphi(s) = 0$, where φ is azimuthal angle ($\varphi = 0$ in equilibrium that corresponds to the Closed state of Tm) and s is the position of a Tm point along the axis of the actin filament. We introduce dimensionless coordinate $x = \frac{s}{\xi}$, where $\xi = (\frac{4k}{\alpha})^{\frac{1}{4}}$ is the persistence length [4]. Then dimensionless equilibrium equation is:

$$\varphi'''(x) - 4\beta\varphi'(x) + 4\varphi(x) = 0,$$

where $\beta = \frac{F}{\alpha\xi^2}$ is dimensionless tension. Two other dimensionless parameters are $\lambda = \frac{c}{\xi}$ where c = 38.5 nm is the distance between two neighbor troponins on a Tm chain and $\gamma = \frac{\sqrt{2}\varphi_0^2 k^{\frac{1}{4}} \alpha^{\frac{3}{4}} \sqrt{1+\beta}}{k_B T}$, the ratio of elastic energy resulting from a pinning the Tm chain to angle φ_0 to thermal energy $k_B T$ where k_B is the Boltzmann constant and T is the absolute temperature. Tm

can be pinned to actin to $\varphi = \varphi_0$ with TnI or to $\varphi = -\chi\varphi_0$ with a myosin head strongly bound to actin (here $0 < \chi < 1$ is a constant). The additional boundary conditions across each pin point are continuous first and second derivatives of φ over *x*. The second condition means the absence of a concentrated torque in a pin point. Dimensional elastic energy of segment of the Tm chain between points *a* and *b* is:

$$E(a,b,\beta) = \int_a^b (\frac{1}{4}(\varphi''(x))^2 + \varphi^2(x) + \beta(\varphi'(x))^2)dx.$$

Mathematical model of Ca-regulation of troponin complex. A kinetic scheme used to describe interaction of troponin components, TnI and TnC, with Ca^{2+} and actin was based on structure of troponin complex [8] and for cardiac muscle is as follows:

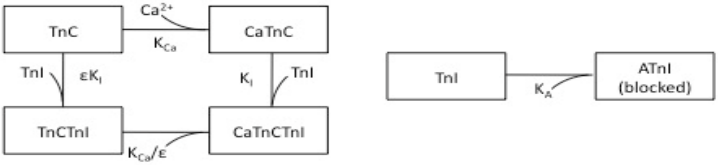

Here K_{Ca}, K_I and K_A are equilibrium constants for Ca^{2+} binding to TnC; for binding of switch segment of TnI to TnC and binding of inhibitory domain of TnI to actin, respectively; $\varepsilon < 1$ is a constant. Let $C = K_{Ca}[Ca^{2+}]$, *y*, *z* are dimensionless Ca^{2+} concentration and probabilities of free (unbound) states of TnC and inhibitory/switch domain of TnI, respectively. Then for steady-state processes the probability of being in states CaTnC, CaTnCTnI, TnCTnI are Cy, $CyzK_I$ and $y\varepsilon zK_I$, respectively, and obey equations:

$$\begin{cases} y + y\cdot C + y\cdot C\cdot z\cdot K_I + y\cdot \varepsilon\cdot z\cdot K_I = 1 \\ z + z\cdot K_A + y\cdot \varepsilon\cdot z\cdot K_I + y\cdot C\cdot z\cdot K_I = 1. \end{cases}$$

If the inhibitory domain of TnI is detached from actin ($K_A = 0$) the equation can be solved for any given calcium concentration, *C*. If TnI is attached to actin, then $z = 0$ and $y = 1/(1+C)$.

Monte-Carlo simulation. We considered a 1001 nm long thin filament with 27 troponin complexes separated by the axial distance *c*. Potential actin binding sites for myosin heads are separated by distance $a = 5.5$ nm. The heads cannot bind actin sites just against troponin complex, so that the number of available sites is 26×6 = 156. The Monte-Carlo simulation procedure was organised as follows. For a given *C* we moved from one end of the chain to another from one potential pinning point (Tn or actin) to the next one and calculated the probability of pinning or unpinning. The unpinning probability for troponin was set to $1 - e^{-k_-}$ where k_- is a constant (=0.1 for most calculations). The pinning probability for an unpinned troponin site i_n was taken as $1 - e^{-k_+}$ where $k_+ = k\_zK_A exp(-\gamma\Delta E)$, $\Delta E = E(i_{n-1}, i_n, \beta) + E(i_{n+1}, i_n, \beta) - E(i_{n-1}, i_{n+1}, \beta)$, i_{n-1} and i_{n+1} are pinned sites

closest to i_n on the left and right. The unpinning probability for myosin heads was set to $1-e^{-k_M}$- where k_{M-} is a constant (also taken as 0.1) and pinning probability was calculated as $k_{M+} = k_{M-}\rho\exp(-\gamma\chi^2\Delta E)$ where ρ is a constant density of the myosin heads distribution. The energy change was calculated assuming that energy $E(a,b,\beta)$ between two pinned points a and b depends only on a and b, not on pinning outside this range. For each C repeated 10^7 times calculation of the state of all 27 troponin and 156 actin binding sites using pseudorandom numbers and than calculated average values for each parameter: fraction of CaTn complexes, the fraction of actin-bound troponins, the fraction of actin-bound myosin heads.

Results and discussion

The basic set of dimensionless parameters was chosen as K_I =700, K_A =500, γ=4.5, ε=0, χ=0.4. Some results of the calculations are shown in figure. On the left side the calculated Ca-dependence of the probability of formation of CaTn complex without myosin heads are shown for different Tm tension (β) and in rigor ($K_A = 0$). On the right side the probability of formation of CaTn complex with in absence (ρ=0) and the presence of myosin heads are shown against dimensionless calcium concentrations, *C*.

Model describes high cooperativity of Ca^{2+}-activation with an apparent Hill coefficient of 3-4 observed experimentally [1-3] and fits well experimental data [2] where Ca^{2+} binding to TnC without myosin heads was shown to be cooperative and much less strong than in rigor. We show that tension of tropomyosin chain can modulate calcium sensitivity of the thin filaments. The binding of myosin heads in our model strongly affects calcium sensitivity as was demonstrated in [9].

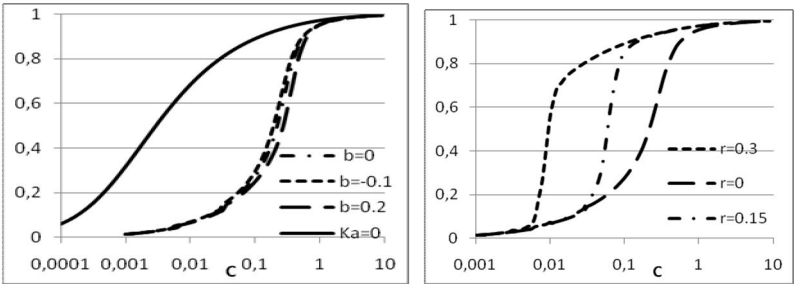

Calculated Ca^{2+} curves for probability of CaTn complexes for different model parameters. Left: β = –0.1,0, 0.2 and K_A=0 at ρ=0. Right ρ=0, 0.15, 0.3 at β = 0.

The author thanks her supervisor, Dr. A. Tsaturyan and Russian Foundation for Basic Research for support.

References

1. Gordon A.M., Homsher E., Regnier M. // Physiol. Rev., 2000, **80** (2): 853-924.
2. Sun Y.B., Irving M. //J. Mol. Cell. Cardiol , 2010, **48** (5): 859-865.

3. de Tombe P.P., Mateja R.D., Tachampa K. *et al*. // J. Mol. Cell. Cardiol., 2010, **48**(5): 851-8.
4. Smith D.A. // J. Phys. Math. Gen., 2001, **34**: 4507–4523.
5. Smith D.A., R. Maytum, M. A. Geeves. // Biophys. J., 2003, **84**: 3155–3167.
6. Smith D.A., M. A. Geeves. // Biophys. J., 2003, **84**: 3168–3180.
7. McKillop D.F., M.A. Geeves. // Biophys. J., 1993, **65**: 693–701.
8. Vinogradova M.V., D.B. Stone, R.J. Fletterick. *et al*. // Proc. Natl. Acad. Sci. USA, 2005, **102**: 5038–5043.
9. Farman G.P., Allen E.J., Schoenfelt K.Q. *et al*. // Biophys J., 2010, **99**(9):2978-86.

EFFECTS OF ADAPTOGEN "EXTRALIFE" ON THE PEROXIDE HYDROGEN PRODUCTION AND FUNCTIONING OF THE ATP – DEPENDENT POTASSIUM CHANNEL IN MITOCHONDRIA

S.V. Murzaeva [1], S.P. Belova, [1,2] E.I. Lezhnev, [1,2] K.N. Belosludtsev[1], G.D. Mironova [1,2]

[1] Institute of Theoretical and Experimental Biophysics, Russian Academy of Sciences, Pushchino, Moscow Region, 142290 Russia; [1,2] Pushchino State natural - Institute of Science, Pushchino, Moscow Region, 142290 Russia
svmurzaeva@rambler.ru

Mitochondria are the main suppliers of ROS in the cell, production of which is enhanced by hypoxia [1-3]. Important role in protecting the heart from hypoxia belong to mitochondrial potassium channels [4, 5-8]. It is assumed that the opening of channels mitoK_{ATP}, activates the entry of potassium in the inner mitochondrial membrane, thus the work of the respiratory chain is stimulated, ATP synthesis is recovered, the accumulation of ROS is reduced and the homeostasis of cells returns to normal [4, 8, 9]. The application methods of therapies hypoxia based on the use of modulators mitoK_{ATP} channels, allows to protecting organs during ischemic injury by preventing heart attacks heart and brain [4, 13].

In our laboratory conducted a systematic search for natural modulators to the activation of mitoK_{ATP} channels in mitochondria. We have previously shown that the herbal adaptogen "Extralife" (ELF) - containing flavonoids, at low concentrations (0.005-1μg/ml) activates a mitoK_{ATP} channel [8, 9]. However, high concentrations of ELF (3-10 μg/ml) resulted in inhibition of the channel, what coincides with the emergence of prooxidant properties of this drug [1, 9]. As you know prooxidants, favor the formation of ROS, which in turn can lead to induction of oxidative stress in mitochondria and other negative consequences, up to cell death [1, 2].

The aim of this work was to obtain direct evidence of the influence of different concentrations of ELF at the rate of formation H_2O_2 in mitochondria and to establish a connection this process with the functioning mitoK_{ATP} channels (activation / inhibition) in order to confirm the ELF of participation in the mechanisms of adaptation to hypoxia.

Mitochondria were isolated from rat heart using conventional differential centrifugation. The formation of H_2O_2 in mitochondria was

determined using the dye Amplex Red (AR) with horseradish peroxidase [10]. ELF has been used in the concentration range 0.005 - 10 μg/ml at the 0.100-0.150 μg of mitochondrial protein.

In this paper we found that the drug "Extralife" at concentrations of 0.005-10 μg/ml dose-dependently increases H_2O_2 of formation in rat heart mitochondria in the presence of respiratory substrates. The increase in the rate H_2O_2 of formation in mitochondria during oxidation of NAD-dependent substrates of a glutamate-malate occurred in 1.7-3.5 folds and of a succinate, in the presence of the inhibitor rotenone, in 1.4-2 times (Fig. 1).

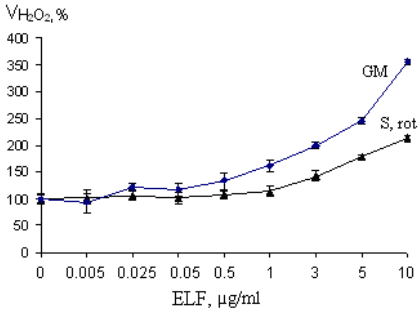

Fig. 1. Effect of ELF on the rate H_2O_2 of formation (%) with glutamate + malate (GLM), and succinate + rotenone (S, rot) in rat heart mitochondria. Incubation medium contained 120 mM KCl, 5 mM KH_2PO_4, 2 mM $MgCl_2$, 1 mM EGTA, 10 mM HEPES, pH 7.3; 2 μM oligomycin, 0.1% BSA, 1 ed. horseradish peroxidase/ml, 10 μM AR, 0.1-0.15 mg/ml of mitochondrial protein, and, where indicated: 2 μM rotenone, 5 mM succinate, 2.5 mM glutamate, 2.5 mM malate. The average values of 4 independent experiments (n = 4) ± standard deviation are indicated.

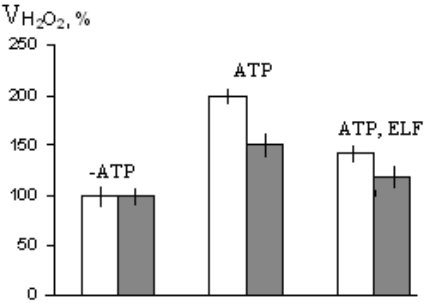

Fig. 2. Effect ELF on the ATP - induced H_2O_2 of formation (rate, %) in rat heart mitochondria with glutamate + malate (open bars) or succinate + rotenone (dark bars). Additions to the incubation medium: 200 μM ATP and 0.5 μg/ml ELF.

However, under certain conditions ELF reduces the rate H_2O_2 of formation in mitochondria.

It is known that the addition of ATP in the mitochondria promotes the closure of potassium channels and increases the rate H_2O_2 of generation, which partially removed channel by activators [5]. In fact, addition of ELF

(0,005-1 μg/ml) of low concentrations leads to reduced H_2O_2 of formation induced by ATP, but the concentration (5-10 μg/ml) increase the rate. Figure 2 shows the effect of one of the most effective concentrations of ELF removing ATP - induced formation of hydrogen peroxide. During the oxidation NAD-dependent substrates, this effect reached 57%, and during the oxidation of succinate in the presence of rotenone - 30%.

The facts that low levels of ELF may reduce the formation of H_2O_2, and it may be associated with activation of the mitoK_{ATP} channel indicate experiments with the specific inhibitor of this channel 5-hydroxydecanoate (5-HD) (table). The rate H_2O_2 of formation in the absence of ELF at the close of mitoK_{ATP} channel 5-HD increases. Adding of the adaptogen in concentrations of 0.05-3 μg/ml reduces the rate H_2O_2 of formation to the control level.

Effect of ELF on the rate H_2O_2 of formation (%) with glutamate-malate in the mitochondria of the heart in the presence of a blocker of the channel mitoK_{ATP} 5-HD

ELF, μg/ml	5-HD, 208 μM
0	134±4
0.05	128±6
1	125±11
3	101±3

Since the activating effect of ELF on the mitoK_{ATP} channel, obtained earlier in [8, 9] and inhibition of rate H_2O_2 of formation induced by inhibitor channel ATP and 5-HD are strictly dose-related and occur at the same concentrations of adaptogen it is likely that these processes are interrelated. In the literature there is a perception of the mutual regulation of the activity of the mitoK_{ATP} channel and of the formed hydrogen peroxide in the mitochondrial respiratory chain [6, 11], which indicates the possibility of participation of ELF in these processes due to the antioxidant activity. Nevertheless, we tend to believe that ELF - containing flavonoids, activates the channel mitoK_{ATP} as redox modulators [14], influencing directly on SH-groups of proteins that play an important role in the activity of channel. On this basis, in this study we are received a confirmation, that in microdoses ELF plays a role of the modulator mitoK_{ATP} channel and of the reduction of H_2O_2 production in the mitochondria.

This work was supported by RFFI grant № 10-04-009-20-a; grant "Development of Scientific Potential of Higher Education» № 2.1.1/11950; DPDS and T № 4.3010.2011; grant Russian President for supporting Russian scientists (MK-145.2012.4).

References

1. Лукьянова Л.Д., Германова Э.Л., Лыско А.И. // Вестн. РАМН. 2007. № 2. С. 55-62.
2. Скулачов В.П. Энергетика биологических мембран. М., 1989.
3. Korshunov S.S., Skulachev V.P., Starkov A.A. // FEBS Lett. 1997. Vol. 416, N 1. P.15-18.
4. Миронова Г. Д., Качаева Е. В., Крылова И. Б. и др. // Вестн. РАМН. 2007. № 2. С. 44-50.
5. Ferranti R., da Silva M. M., Kowaltowski A. J. // FEBS Lett. 2003. Vol. 536, N 1-3. P.51-55.

6. Fornazari M., de Paula J.G., Castilho R.F., Kowaltowski A.J. // J. Neurosci. Res. 2008. Vol. 86. P.1548-1556.
7. Garlid K.D., Paucek P. // Biochem. Biophys. Acta. 2003. Vol.1606, N 1-3. P. 23-41.
8. Mironova G.D., Shigaeva M.I., Gritsenko E.N. et al. // J. Bioenerg. Biomembr. 2010. Vol. 42, N 6. P. 492-503.
9. Миронова Г. Д., Шигаева М.И., Белослудцева Н.В. и др. // Бюл. экспер. биол. 2008. Т. 146, № 8. С.195-199.
10. Zhao M., Diwu Z., Panchuk-Voloshina N., Haugland R. // Anal.Biochem. 1997. V. 253, 162-168.
11. Avshalumov M.V., Rice M.E. // Proc. Natl. Acad. Sci. USA. 2009. Vol. 100, N 20. P. 11729-11734.
12. Zhang D., Chen Y., Campbell W. et al. // Circ. Res. 2001; 81,177-1173.
13. Krylova I. B., Kachaeva E. V., Rodionova O. M., Negoda A. E., Evdokimova N.R., Balina M. I., Sapronov N. S., Mironova G. D. // Exp. Gerontology. 2006. 41. N. 7. P. 697-703.

COMPARISON OF THE CHARACTERISTICS OF THE SINGLE INTERACTIONS OF RABBIT MUSCLE PROTEINS ISOFORMS

S.R. Nabiev, D.V. Schepkin, G.V. Kopylova, S.Y. Bershitsky

Institute of Immunology and Physiology, Ural Branch of the Russian Academy of Sciences, Yekaterinburg, 620041, Russia

During muscle contraction myosin molecules of the thick filaments in sarcomere cyclically interact with actin of the thin filaments. This interaction is lead to either sliding of the filaments with respect to each other or force generation.

There are six different isoforms of actin in higher mammals: two of striated muscle, two of smooth muscle and two of non-muscle types [1]. Actin isoforms of striated muscle type (α-actin) contain α-cardiac and α-skeletal actin. Their expression patterns are species specific and change at organism development. For example, in a normal adult mouse α-cardiac actin predominates in the heart and is also found in slow skeletal muscle, while α-skeletal actin predominates in fast skeletal muscle [2] There is a cross-expression of isoforms in different tissue types during development. Furthermore α-skeletal actin is often found in the fetus heart but after the birth its content in the heart is greatly reduced. Expression of different isoforms also varies in human cardiac tissue [3].

Although structurally actin isoforms are slightly different from each other (by 4 neutral amino acid residues of 375) functionally they may differ significantly because 3 of 4 different amino acids are in the myosin binding site. It has been demonstrated that certain actin isoforms activate myosin ATPase preferably in the presence of specified isoforms of myosin [3].

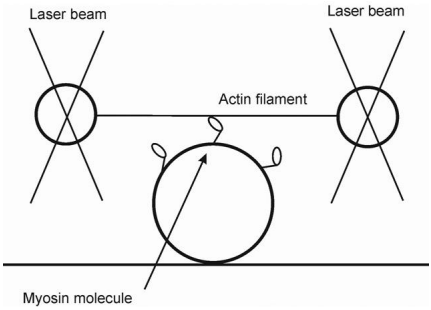

Fig. 1. The ends of actin filament are attached to 1-micron polystyrene beads held by two laser beams near the myosin coated surface of a two-micron glass pedestal.

Studies on the hearts of BALB/c mice showed sustained elevated contents of α-skeletal actin (~50%) in the normal adult hearts. It was shown that the increase of α-skeletal actin in the heart obviously correlated with an increase in cardiac contractility BALB/c mice in compare with α-cardiac actin [4].

Here we recorded single interactions of isolated molecules of two cardiac myosin isoforms V1 and V3 with skeletal and cardiac actin isoforms by using the optical trap technique. Pure protein isoforms were prepared from rabbit muscle with standard procedures [5]. In experimental flow cell two independent beams of IR laser held two polystyrene beads (~1 μm), a fragment of cardiac or skeletal actin filament was attached to those beads. Two-micron glass beads ('pedestals') were fixed on the cell surface and covered by single molecules of cardiac myosin isoforms V1 or V3 (fig. 1).

The average step size and duration of attached state for all isoforms of actin and myosin are shown in table 1.

Besides we measured average force of myosin isoforms interacting with actin filament. Position of one of the beads, 'motor', was feedbacked by tiny change in the position of the other bead, 'sensor', to compensate its shift due to step of myosin molecule (fig. 2).

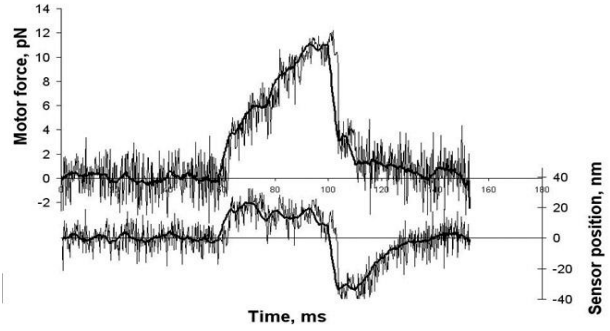

Fig. 2. Example of experimental record. Upper trace is a signal of force on "motor" bead, the lower one is – a position of "sensor" bead.

Table 1

	V1 myosin		V3 myosin	
	step size, nm	duration, ms	step size, nm	duration, ms
Skeletal actin	11.6±2.0 (n = 1723)	54.2±1.3	12.5±2.7 (n = 773)	62.1±2.73
Cardiac actin	9.5±2.0 (n = 835)	55.8±1.93	12.5±2.5 (n = 699)	66.8±2.93

Table 2

	V1 myosin		V3 myosin	
	average force, pN	duration, ms	average force, pN	duration, ms
Skeletal actin	1.82±0.7 (n = 835)	34.77±1.42	2.07±0.5 (n = 614)	37.1±1.50
Cardiac actin	1.84±0.6 (n = 382)	36.5±1.87	2.03±0.5 (n = 373)	35.3±1.83

The average force for different isoforms of actin and myosin is shown in table 2.

As it seen from the tables, there are no any significant differences in average step size, interaction force and duration of the events for the different isoforms of actin. Characteristics of single interactions of isolated molecules of contractile proteins cannot explain the correlation between the content of skeletal actin and cardiac contractility. In this experiment we did not investigate the function of regulatory proteins and so cannot exclude that the key reason of these differences is the regulation of contraction process.

Work was supported by RFBR and Presidium of RAS.

References

1. Vandekerckhove J, Weber K. At least six different actins are expressed in a higher mammal: an analysis based on the amino acid sequence of the amino terminal tryptic peptide. J Mol Bio. 1978; 126: 783-802.
2. Swynghedauw B. Developmental and functional adaptation of contractile proteins in cardiac and skeletal muscles. Physiol Rev. 1986; 66: 710-771.
3. Rubenstein P. The functional importance of multiple actin isoforms. Bioessays. 1990; 12: 309-315.
4. Hewett et al. Alpha-skeletal actin is associated with increased contractility in the mouse heart. Circulation Research. 1994; 74: 740-746.
5. VanBuren, D.E. Harris, N.R. Alpert, D.M. Warshaw, Cardiac V1 and V3 myosins differ in their hydrolytic and mechanical activities in vitro, Circ Res. 1995; 77: 439-444.

POSSIBLE REASONS FOR THE VARIABILITY OF THE INOTROPIC INSULIN EFFECT IN PAPILLARY MUSCLES OF GROUND SQUIRREL MYOCARDIUM

O.V. Nakipova [1], N.A. Chumaeva [2], L.A. Andreeva [1], A.I. Anufriev [3], N.I. Kukushkin [1]

[1] Institute of Cell Biophysics, Russian Academy of Sciences, Pushchino, Moscow Region, 142290 Russia;

[2] Institute of Behavioural Sciences, University of Helsinki, P.O. Box 9, 00014 Helsinki, Finland;

[3] Institute of Biology, Yakutsk Branch, Siberian Division, Russian Academy of Sciences, Yakutsk 677891, Russia

e-mail:olga.nakipova@gmail.com

The main findings of the present study are that insulin induces positive, negative or no inotropic effects in papillary muscles of ground squirrels myocardium. The character of the effects of insulin depends on the physiological state of animals; time and concentrations of the hormone applied; affected by conditions that alter cellular Ca^{2+} loading and the ratio of protein-tyrosine kinases/phosphatases activity.

1. Introduction

The majority of studies report a positive inotropic effect of insulin in the heart ventricle of different mammal species and in human myocardium. However, some investigators described patterns of two-phase and even three-phase insulin action depending on species and age of animals being under different pathologies and experimental conditions [1-4]. Earlier we have shown that the type of insulin-induced inotropic effect in the ground squirrel heart tissue significantly varies over the annual cycle of animals [5]. In a group of deeply hibernating animals (rectal temperature about 1–3^{0}C) insulin causes no changes in contractility of papillary muscles (at 30^{0}C of perfusion medium and 0.5 Hz stimulation). In active animals of different seasonal periods and in arousal animals insulin at the same conditions induces both cardiostimulating and cardiodepressive effects depending on the time and concentrations of the hormone applied and stages of arousal [5-7]. The main goal of the present study is to elucidate the possible reasons for the variability of insulin action in the myocardium of hibernators.

2. Methods

The effects of insulin (0.1-50 nM) on isometric twitch force (0.1 to 1.0 Hz; 30 ± 1ºC; 1.8 mM Ca^{2+}) were studied in right ventricular papillary muscles from active ground squirrels of different seasons (summer, n = 14; autumn, n = 16 and winter interbout, n = 16) in control conditions and after 1 hr pretreatment of PM with 2 mkM nifedipine (an L-type Ca^{2+}-channel inhibitor) and 1.0 mM orthovanadate (a tyrosine phosphatase inhibitor).

3. Results

In active animals of different seasonal periods insulin causes both positive and negative inotropic effects. At low frequencies (0.1–0.5 Hz), insulin of low concentrations (0.1–1.0 nM) induces a transient (within the first 20 min after ap-

plication) positive effect (about 15–25 %) comparable to the effects reported in isolated rat [3] and human [1, 2] hearts. Application of high hormone concentration (10 nM) in a low range of stimulation frequencies causes a biphasic effect (a small initial positive inotropic effect followed by a marked negative one). At frequencies above 0.5-Hz stimulation, insulin of 10 nM concentration causes presumably a negative inotropic effect which magnitude varies in different preparations (from 15 to 55%) and depends on the initial character of force-frequency relationship. In PM with the pronounced force-frequency relation the effect of insulin is significantly higher than in those exhibiting small frequency responses.

Earlier we have shown that insulin suppresses a slow inward calcium current through L-type Ca^{2+} channels (I_{CaL}) in frog atrium cells [8, 9]. It was proposed that I_{CaL} is possibly involved in the insulin-induced negative inotropy in ground squirrels hearts. Nifedipine (1-1.5 hr pretreatment), a blocker of L-type calcium channel, reduces the inhibitory effect of insulin in autumn and winter animals, and on the contrary intensifies it in summer animals. This fact indicates that different mechanisms must be involved in insulin actions in animals of summer and winter periods.

Alteration of protein phosphorylation in tyrosine residues is known to be a major link in mechanism of insulin action [10]. We performed a study on orthovanadat action (a known inhibitor of tyrosine phosphatase) on insulin effect. In the group of summer animals the pretreatment of papillary muscles with orthovanadate (100 mkM) does not change the negative inotropic effect of insulin in a low range of stimulation frequencies but almost completely removes this effect at stimulation frequencies above 0.3 Hz (n=4).

4. Discussion

The present results clearly show that the pattern of inotropic effect of insulin observed in PM of ground squirrel ventricle is affected by physiological state of animals, stimulation frequencies and activity of L-type Ca^{2+}-channels. All of these conditions alter the Ca^{2+} load in myocardial cells. The obtained results together with data [3] allow us to assume that the state of Ca^{2+} loading myocardial cells might be involved in the variability of insulin effects on contractility of the ground squirrels heart. The relative importance of various Ca pools in contractile activation depends on animal species, thus potentially contributing to data conflict on inotropic effects of insulin.

Another possible reason for insulin action variability in myocardium of hibernators may lie in the change of protein-tyrosine kinases and protein-tyrosine phosphatases ratio which is altering during the development of cell response to insulin [10]. In accordance with this suggestion the results of the present study with orthovanadat indicate that tyrosine phosphatase is critical for a negative inotropic effect of insulin in ground squirrels hearts.

5. Conclusion

The conducted investigations clarify to a large extent the contradictory picture of insulin influence on myocardium contraction demonstrate the new perspective ways which the use of hibernating animals heart offers for elucidation of the machinery determining a direction of insulin inotropic action.

The authors are grateful to L.S. Kosarskii for the technical help in carrying out of experiments.

References

1. Von Levinski D, Bruns S, Walther S, Kogler H, Pieske B. Insulin causes [Ca^{2+}]i-dependent and [Ca^{2+}]i-independent positive inotropic effecs in failing human myocardium. *Circulation.* 2005;111:2588-2595.
2. Chih-Hsueng Hsu, Jeng Wei, Yao-Chang Chen, Shih-Ping Yang, Chien-Song Tsai, and Cheng-I Lin. Cellular mechanisms responsible for the inotropic action of insulin on failing human myocardium. *The Journal of Heart and Lung Transplantation.* 2006; 25 (9): 1126-34.
3. Schmidt HD, Koch M. Influence of perfusate calcium concentration on the inotropic insulin effect in isolated guinea pig and rat hearts. *Basic Res Cardiol*. 2002 Jul;97(4):305-11.
4. Sviglerova J, Kuncova J, Stengl M. Negative inotropic effect of insulin in papillary muscles from control and diabetic rats. *Physiol Res.* 2005;54:661-670.
5. Nakipova OV, Gainullin RZ, Andreeva LA, Safronova VG, Kosarskii LS, Kolaeva SG, Solomonov NG, Kukushkin NI. Effect of insulin on the myocardium of the active, hibernating and awakening Ground squirrels Citellus undulates. *Biophysics.* 2000;45(2):335-342.
6. Nakipova OV, Andreeva LA, Chumaeva NA, Anufriev AI, Kosarskii LS, Kolaeva SG, Kukushkin NI, Solomonov NG. Frequency-dependent effect of insulin on myocardial contractility in active ground squirrel Citellus undulatus in different seasons. *Dokl. Biochem. Biophys.* 2001; 380:361-363.
7. Nakipova OV, Andreeva LA, Chumaeva NA, Zakharova NM, Semenova TP, Solomonov NG. Dependence of the Inotropic Effect of insulin on the peculiarities of force–frequency relationship in the papillary muscles of the Siberian ground squirrel heart *Dokl. Biochem. Biophys*. 2006; 408: 122-124.
8. Nakipova OV, Kokoz YuM, Freidin AA, Safronova VG, Lazarev AV. Effect of insulin on calcium current in frog myocardium. *Fiziol Zh SSSR (in russion).* 1987; 73(4):492-498.
9. Nakipova OV, Kokoz YuM, Lazarev AV, Freidin AA, Krupenin VA. Modification by cycloxehimide of the effects of insulin on sarcolemmal calcium transport. *Fiziol Zh SSSR (in russion).* 1988;74(3):420-427.
10. Fantus IG, Deragon G, Lai R, and Tang S. Modulation of insulin action by vanadate: evidence of a role for phosphotyrosine phosphatase activity to alter cellular signaling. *Molec Cell Biochem*. 1995;153:103–112.

SIGNALING ROLES OF NNOS AND HSP90 IN SKELETAL MUSCLE UNDER GRAVITATIONAL UNLOADING

T.L. Nemirovskaya[1,2], Y.N. Lomonosova[2]

[1]Faculty of basic medicine, Moscow state university, 117192, Lomonosovskii prospect 31/5 Russia;
[2]Institute for bio-medical problems, 123007, Moscow, Khoroshevskoe sh. 76a; Russia

It is known that gravitational unloading lead to skeletal muscle atrophy and breakdown of cytoskeletal proteins, which results in muscle functional impairment. It was demonstrated that neuronal NO synthase (nNOS), heat shock proteins (HSP) 90 and HSP70 are μ-calpain substrates and its

contents decrease during the unloading. We supposed that increase of NO level and HSP90, HSP70 expression in time of gravitational unloading condition can maintain soleus protein turnover. In earlier studies it was shown that increase of nNOS activity inhibits μ-calpain activity and reduces cytoskeletal proteins destruction in cultured myotubes. HSP90 in turn is essential to proper Akt function (involved in protein turnover regulating), since reduced HSP90 - Akt binding causes Akt inactivation. Moreover, HSP90 protects nNOS from ubiquitination, increases NO formation, intensifying catalytic function of nNOS. To test the hypothesis, concerning involvement of nNOS and HSPs in maintenance of skeletal muscle metabolism, NO precursor L-arginine (HSA group) and HSP90, HSP70 expression inducer 17-AAG (HSG group) were applied under the unloading. We observed that L-arginine prevented NO decrease, HSP90 mRNA expression drop and reduced atrophy degree during the unloading. 17-AAG prevented HSP90, HSP70 mRNA level drop and atrophy completely under the unloading. The calcium-dependent proteases, μ-calpains, contribute to skeletal muscle atrophy regulating ubiquitin-proteasome pathway, namely E3-ligases MAFbx and MuRF1 which expression increased significantly under the unloading. Both NO and the HSPs mRNA level maintenance at the control level (C group) led to decrease of μ-calpains content in time of the unloading. MAFbx, MuRF1 mRNA expression in the HSA group and ubiquitin-conjugated proteins content in the HSG group were as low as those in the C group. The translocation and activity of Foxo3 transcription factor is required for upregulation of MAFbx and MuRF1. In addition, Foxo3 transcription factor is excluded from the nucleus being phosphorylated by Akt. Both NO and the HSPs mRNA level maintenance at the control level resulted in growth of phosphorylated Foxo3 content as compared to that in unloaded group. Increased NO content under the unloading in the HSA group maintained P-p70S6k, p70S6k contents at the control level, as regards to induced HSPs mRNA expression in the HSG group, it prevented drop of pAkt content under the unloading. To sum up, activations of nNOS- and the HSPs-dependent systems under the rats unloading prevent atrophy development. It might be associated with μ-calpain and pFoxo expression maintenance at the control level as well as activation of protein synthesis system (Akt-mTOR-p70S6k).

When analyzed expression of I type myosin heavy chain (MHCI) mRNA, we observed that L-arginine administration maintained the MHCI mRNA content at the control level, but inhibition of nNOS by L-NAME led to as low the MHCI mRNA content as that in the hindlimb suspended group. Hereby, nNOS can take part in the regulation of slow MHC mRNA expression.

FIBRIL FORMATION OF COLLAGEN *IN VITRO* AT TEMPERATURES CLOSE TO PHYSIOLOGICAL

T. I. Nikolaeva[1], S. M. Kuznetsova[1], V. V. Rogachevskii[2]

[1]Institute of Theoretical and Experimental Biophysics, Russian Academy of Sciences, Pushchino, Moscow region, 142290 Russia

[2]Institute of Cell Biophysics, Russian Academy of Sciences, Pushchino, Moscow region, 142290 Russia

Collagen of type I forms part of fibrils and fibers of most connective tissues. The structure of collagen fibrils of the skin and internal organs (the heart, lungs, liver, kidney) is composed of complexes of type I collagen with collagens of types III and V. Fibrils in the skin of an adult organism that possess both rigidity and flexibility have a relatively small diameter (about 60 nm). In the skin derma, collagen fibrils form a mobile and flexible network, which fulfils the mechanical function and is involved in the functioning of cells. The structure of collagen fibrils is determined not only by the diversity of types of macromolecules entering into their composition but also the conditions of fibrillogenesis. Temperature affects the conformation of collagen molecules and thus the self-assembly of collagen into fibrils [1]. The formation of native collagen fibrils begins after the microunfolding of local regions of the triple helix, which have a low stability [2, 3]. It follows from the literature data that the unfolding of labile regions at the ends of the triple helix of collagen from the skin of animals occurs in the temperature range of 28–41°C [4–6]. Studying the formation of fibrils *in vitro* by the action of temperature gives an insight into the molecular mechanisms of the collagen fibril formation *in vivo*.

The goal of the present work was to study the formation of collagen fibrils at temperatures of the close physiological. We developed a system of fibrillogenesis, which consisted of collagen from the skin of two-month-old pigs and phosphate-buffered saline (PBS), pH 7.0, I = 0.145 M. The fibril formation was recorded from changes in the optical density (D) of collagen solutions in thermostated quartz cuvettes on a Specord UV VIS spectrophotometer (Karl Zeiss, Germany) at a wavelength of 400 nm. The time of fibril formation was defined as the time the curve of changes in optical density reaches a plateau.

For the electron microscope examination, pieces of collagen gel were fixed for 2 h in a solution containing 2.5% glutaraldehyde and 3% paraformaldehyde in Na cacodylate buffer. Slices were obtained from blocks of high hardness on a Leica EM UC6 microtome using a diamond cutter and placed on carbon-fixed support films, contrasted with uranyl acetate and lead citrate, and analyzed on a JEOL 1200EX microscope. The diameter of fibrils was measured at the centre of their longitudinal section on negatives scanned with a resolution of 2400 dpi using the program IGL Trace 1.26b.

The study of the kinetics of collagen fibril formation depending on temperature shows that, as temperature increases from 28.5 to 38.5°C, the rate of fibril formation and the time of the formation of the stable structure of

fibrils increases two- to threefold. The optical density of the collagen gel in the plateau phase decreases, which may indicate changes in the number of fibrils and/or their sizes. The results of the electron microscope examination of the structure of collagen fibrils formed at different temperatures show that the diameter of fibrils is the greatest (58–68 nm) at T = 28.5–32.5°C. An increase in temperature to 34.5°C leads to a decrease in the diameter to 41 nm. As temperature to increases to 36.5°C, the diameter of fibrils decreases to 28 nm. We showed that, by creating temperature conditions close to physiological, it is possible to significantly affect the diameter of fibrils, which fulfils an important functional role. The number of fibrils of certain diameter also depends on the temperature of their formation. Fibrils of minimal diameter, obtained at 36.5°C, compile more homogeneous population of fibrils as compared with the fibrils formed at temperatures lower (34.5°C) and higher (38.5°C) by two degrees than physiological. At T = 28.5–32.5°C, an inhomogeneous population of fibrils is formed.

Thus, we found that an optimal temperature for the formation of fibrils from this collagen is 36.5°C. Physiological temperature stimulates a strong intermolecular binding of collagen molecules from the pig skin into fibrils. We found conditions for the formation of homogenous fibrils of a minimal diameter (about 28 nm): PBS, pH 7.0, I = 0.145 M, T = 36.5°C, C = 1.5 mg/ml.

Collagen fibrils reconstructed in the present work can find application in cell and tissue engineering. On the basis of collagen fibrils from the pig skin, it is possible to create analogues of various connective tissues: skin derma, heart valves, and blood vessels.

References

1. V. Ya. Aleksandrov. Cells, macromolecules and temperature. (L. Nauka, 1975).
2. K. E. Kadler, Y. Hojima Y., and J. Prockop., J. Biol. Chem., **263**, 10517 (1988).
3. Y. Xu. Meth. Enzym., **466,** 211 (2009).
4. P. L. Privalov, E. I. Tiktopulo, and V. M. Tischenko, J. Mol. Biol, **127**, 203 (1979).
5. H. P. Bächinger., and J. M. Davis, Int. J. Biol. Macromol., **13**, 152 (1991).
6. E. Makareeva, W. A. Cabral, J. C. Marini, and S. Leikin, J. Biol. Chem., **281**, 6463 (2006).

PIRIMILPHOS-METHYL EFFECT ON SKELETAL MUSCLE CONTRACTION DYNAMICS

D.M. Nozdrenko, L.V. Korchinska, V.M. Soroka

Taras Shevchenko Kyiv National University, Department of Biophysics, Volodimirska Str., 64, 01033, Kyiv, Ukraine

Pesticides are an permanent ecology factor. Environment saturation with potentially dangerous substances cause numerous pathologies. Organophosphorus pesticides as a high-performance agent against broad variety of insects and low persistence substance are widely used in nowaday agronomi-

cal practice (more than 40%). High prevalence and availability of organophosphorus pesticides provoke large number of poisonings among human population. Yet no uniform opinion about pathological changes in skeletal muscles function is present. Also, non cholinergic effects of organophosphates remain unknown.

The investigation of the influence of organophosphorus insecticides such as pirimilphosmethyl, diazinon and chlorpyrifos on the contraction dynamics of skeletal muscle fibers from m.tibialis anterior of frog Rana Temporaria was performed. Concentration range from 10^{-7} to $5 \cdot 10^{-5}$ mol/dm^3 was used. During the experiments the strength of contraction, the change of the length, the ambient solution temperature and the stimulation signal parameters were fixed. Experiments were carried out in an instantly circulating and thermostated Ringer solution with 3 minutes relaxation time.

Result showed that pirimiphosmethyl at 10^{-5} mol/dm^3 after 9 minutes of stimulation almost completely suppresses muscle function, at 10^{-8} mol/dm^3 no effect was present. For more detailed analyses concentration dependent influence of pirimiphosmethyl a number of concentrations were used 10^{-7}, $2{,}5 \cdot 10^{-7}$, $5 \cdot 10^{-7}$, $7{,}5 \cdot 10^{-7}$, 10^{-6}, $2{,}5 \cdot 10^{-6}$, $5 \cdot 10^{-6}$ mol/dm^3.

Test result showed that decrease of force productivity and muscle contraction lengths with pirimiphosmethyl in concentration 10^{-7} mol/dm^3 was 73,7±1,6% ($p<0{,}05$) and 72,6±0,9% ($p<0{,}05$) in comparison to control (Fig.1, pic.2).

The maximum effect of pirimiphosmethyl was achieved 60 minutes after the pesticide application. With more prolonged pesticide application no extra loses in muscle contraction dynamics was present.

During the research of pirimiphosmethyl impact at concentration of 2,5·10-7 mol/l it was found that the inhibiting effect of the insecticide on the dynamic parameters of contraction increased as compared with the previous concentration. The maximal decrease of muscle strength and reduction of the length alterations of muscle fibers was 54,5±1,8% ($p<0{,}05$) and 52,6 ± 2,3% ($p < 0.05$) from control and was stable after about 69 minutes of insecticide action. It should be noted that in action of pirimiphosmethyl at concentrations 10-7 and 2,5·10-7 mol/l any significant difference between the maximal decrease of muscle contraction strength and lengths of fibers was not observed.

The level of suppression in contractile dynamics parameters of skeletal muscles under pirimiphosmethyl action in concentration of 5·10-7 mol/l did not significantly differ from the respective decrease in contractile activity obtained at concentration 2,5·10-7 mol/l (Fig. 1 , Fig. 2).

The maximal reduction of strength and length changes of muscle in such conditions amounted 45,3 ± 2,3% ($p < 0.05$) and 44,2 ± 1,2% ($p < 0.05$) from control values, respectively. But such loses in forth-lengths productivity was induced at 45 minute after insecticide application.

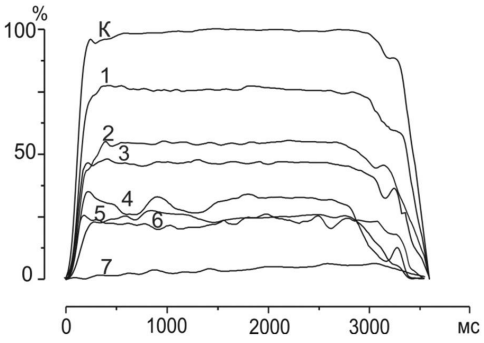

Fig. 1. Changes in contraction force induced by electrical stimulation at 30 Hz duration 3000 ms with pirimiphosmethyl concentration ranged from 10^{-7} to $5 \cdot 10^{-5}$ mol/dm^3 . x – time y – force production. Relaxation time 3 minutes. K – control 1- 7 force curves after pirimiphosmethyl application 10^{-7}, $2{,}5 \cdot 10^{-7}$, $5 \cdot 10^{-7}$, $7{,}5 \cdot 10^{-7}$, 10^{-6}, $2{,}5 \cdot 10^{-6}$, $5 \cdot 10^{-6}$ mol/dm^3.

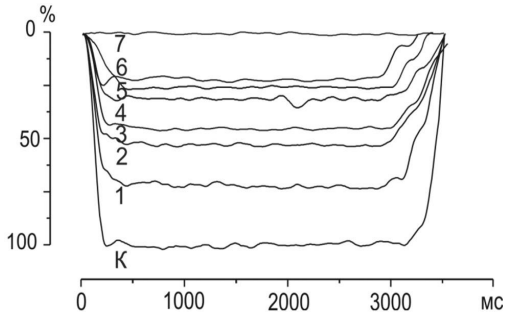

Fig. 2. Contraction lengths changes induced by 30 Hz stimulation 3000 ms duration with pirimiphosmethyl concentrations ranged from 10^{-7} to $5 \cdot 10^{-5}$ mol/dm^3. Same marcs as in Fig. 1.

After pirimiphosmethyl concentration increase up to $7{,}5 \cdot 10^{-7}$ mol/dm^3 insecticide potentiation of the suppressive effect on muscle fibers contraction activity was observed, maximum force and lengths lowering was 38.7±2.6% ($p<0{,}05$) and 31.6±2.3% ($p<0{,}05$) from control. This maximum contraction depression was gained at 30 minutes after reagent application. Force response at pirimiphosmethyl concentration 10^{-6} mol/dm^3 was only 26.7±2.3% ($p<0{,}05$) from control, at the same time muscle contraction length lowering was to 23.3±2.1% ($p<0{,}05$) from control. Contraction force and lengths measurements after effect of pirimiphosmethyl in the concentration of 2,5·10-6 mol/dm3 did not show any significant difference from the values of the test at the previous concentration. Maximum lowering in force and length of muscle contraction process was 23,4±2,3% ($p<0{,}05$) and 22,6±2,2% ($p<0{,}05$) from control. Stationary level in contraction was reached 36 minutes after application.

The most apparent influence of pirimiphosmethyl on skeletal muscle activity among used concentrations was at 5·10-6 mol/dm3 . Under these experimental conditions muscle force productivity reached stationary level at 33 minutes from pesticide application and was 3,9±1,3% ($p<0{,}05$) from control, at the same time muscle length was not different from 21 minutes after pirimiphosmethyl application. Therefore as a result of pirimiphosmethyl in-

fluence at 5·10-6 mol/dm3 virtually full fiber contraction activity suppression was observed.

Changes in contraction dynamics depending on time of pirimiphos-methyl application did not always show linear characterisctcs. In some cases time delay in dynamics parameters changing was present. After the delay we observed quick change in contraction measurements with next switch to a new level of contraction at 5·10-7, 5·10-7, 7,5·10-7, 10-6, 2,5·10-6 mol/dm3. Effect of high concentrations of insecticide manifested in gradual decrease in contraction dynamics with the next rapid decay. Time delay before change in contraction measurements was smaller at higher insecticide concentrations.

Because used insecticides are lipophilic substances they are able to penetrate into the cell by dissolving in the lipid phase of the plasma membrane and subsequently affect the functional activity of the cellular structures, concentration and time dependence of decrease of contraction dynamic parameters. We believe, this can be explained by an increasing number of substances that penetrate through the plasma membrane of muscle fibers and its effects on cellular processes.

As the experiments were made on isolated bundles of muscle fibers, which were stimulated by electrical impulses, it could be arguing that concentration-dependent inhibition of contractile activity of skeletal muscles occurs as a result of non-cholinergic effects of pirimiphosmethyl.

TRANSVERSAL STIFFNESS AND SOME CYTOSKELETAL PROTEINS CONTENT IN RAT'S LEFT VENTRICLE CARDIOMYOCYTES UNDER ANTIORTHOSTATIC SUSPENSION OF VARIOUS DURATION

I.V. Ogneva, T.M. Mirzoev, N.S. Biryukov, O.M. Veselova, I.M. Larina

SSC RF Institute of Biomedical Problems RAS, Russian Federation, 123007, Moscow, Khoroshevskoyoe shosse, 76a

Cephalic fluid shift under antiorthostatic suspension of rat causes an increase of the volumetric load on the heart, at least at the early stages. The goal of the research was to identify the structural and functional characteristics of the rat's left ventricle under antiorthostatic suspension by the tail using the Moley-Holton method within 1, 3, 7 and 14 days.

The transversal stiffness has been determined for various parts of the contractile apparatus and the membrane with the cortical cytoskeleton of the cardiomyocyte using the atomic force microscopy and the relative content of desmin, beta-actin, gamma-actin, alpha-actinin-1 and alpha-actinin-4 in the membrane and cytoplasmic fraction of proteins has been determined by Western blotting.

The results of AFM measurements of the stiffness of the myofibrillar apparatus of rat's left ventricle cardiomyocytes suggest that transversal stiffness of the Z-disk and M-line in the relaxed state was 16.0±1.3 pN/nm and 9.9±0.6 pN/nm respectively, which is close to the results described in Zhu et

al. (2009) that have been obtained by analyzing bunches of myofibrils from the left ventricle of adult cows, where the stiffness of the Z-disk was 18±2.5 pN/nm, and that of the M-line was 11±0.5 pN/nm. In the rigor state, the transversal stiffness of the Z-disk and the M-line, according to our data, was 24.5±0.9 pN/nm and 16.4±0.5 pN/nm respectively, while in Zhu et al. (2009) they were at 25±2 pN/nm and 17±0.5 pN/nm respectively. In the course of antiorthostatic suspension, the transversal stiffness of the contractile apparatus of the rat's left ventricle cardiomyocytes near the Z-disk and the M-line remained unchanged. The transversal stiffness of the contractile apparatus near the semi-sarcomere increased after 3 days and remained increased up to the 14th day of antiorthostatic suspension.

AFM results suggest that in the relaxed state, the transversal stiffness of the membrane with adjacent cortical cytoskeleton increased near the middle of the semi-sarcomere, i.e. between the projections of the Z-disk and M-line after 1 day, and continued to increase during antiorthostatic suspension. The stiffness of the membrane in the Z-disk and M-line projection also grew, but somewhat later, i.e. after 14 and 3 days of suspension, respectively. Increased stiffness of all parts of the membrane during activation of contraction and rigor of fibre remained the same as in the control group, which was expected because desmin content remaned unchanged, as desmin enables transfer of tension from the contractile apparatus to the membrane of the cardiomyocyte.

Similarly to the results of Costa et al. (2006) obtained using human aortic endotelium cells, it can be suggested that changes in transversal stiffness of cardiomyocytes are related to changes of the submembrane actin cytoskeleton, which is consistent with the data of Collinsworth et al. (2002). The increased transversal stiffness of the cortical cytoskeleton of cardiomyocytes may be related to increased content of non-muscle actin isoforms (beta and gamma) and actin-binding proteins, particularly alpha-actinin-1 and alpha-actinin-4. Thus, it is known that alpha-actinin-1 is expressed in cardiomyocytes (Velez C. et al., 1995) and in skeletal muscle cells, along with alpha-actinin-4, at various stage of differentiation (Goffart S. et al., 2006).

In order to verify this assumption (that increased transversal stiffness of the cortical cytoskeleton of cardiomyocytes may be linked to increased content of non-muscle actin isoforms), we have analyzed relative content of these proteins in the cytoplasmic and membrane fractions. Our results suggest that beta-actin content in the cytoplasmic and membrane fraction remained unchanged during antiorthostatic suspension and subsequent reloading. Gamma-actin content in the cytoplasmic fraction of proteins also remained the same as the control group level during suspension and reloading. However, gamma-actin content in the membrane fraction of proteins increased significantly on the first day of antiorthostatic suspension and continued to increase up to the 14th day, following the same trend as that of transversal stiffness. It should be noted that the increase of non-muscle F-actin (beta-

actin) was observed in cat's cardiomyocytes during stimulated hypertrophy (Balasubramanian S. et al., 2010), although gamma-actin content was not measured.

At the same time, alpha-actinin-1 content in the cytoplasmic fraction of proteins decreased after 7 days of suspension, but increased in the membrane fraction. Alpha-actinin-4 content in the membrane fraction of proteins grew on the first day of antiorthostatic suspension and continued to increase up to the 14th day, and starting from the third day, its content in the cytoplasmic fraction exceeded the control group level.

It should be noted that hardly anything is known about the role of non-muscle forms of alpha-actinin in skeletal muscle cells and cardiomyocytes. Nevertheless, there is evidence that the increase of relative alpha-actinin-4 content in the cytoplasmic fraction is linked to decrease of alpha-actinin-1 content there and formation of a cancer pattern of fibroblasts (Honda K. et al., 1998). There also exist results suggesting that cancer transformation of cells, particularly lymphocytes, is accompanied by increased stiffness thereof, measured by an AFM (Cai X. et al., 2009). Consequently, increased stiffness of the cells is related to the development of their submembrane cytoskeleton, reduction of alpha-actinin-1 content and increase of alpha-actinin-4 content in the cytoplasmic fractions of proteins.

In the conclusion, to sum up our experimental results and the above discussion, we can hypothesize the following sequence of events in cardiomyocytes at early stages of antiorthostatic suspension. Increased volumetric load on the heart at early stages of antiorthostatic suspension causes deformation (stretching) of the cardiomyocyte, involving coordinated stretching of the contractile apparatus and the cortical cytoskeleton. Stretching of the contractile apparatus may cause smaller inter-filament spacing and, consequently, the observed increase of myofibrill stiffness, which can be the reason for reduced contractility of the cardiomyocyte. Furthermore, we can suggest a hypothesis (that has to be proven experimentally) that stretching of the cortical cytoskeleton will cause dissociation of alpha-actinin-1 from sub-membrane actin, and initiate overexpression of non-muscle actin and alpha-actinin-4, since the content of these two non-muscle isoforms of alpha-actinin is interrelated. Increased content of non-muscle actin in the membrane fraction will require increased content of both isoforms of alpha-actinin in the membrane fraction as well to form the structure of the cortical cytoskeleton, which will be reflected in its increased stiffness that we observed in our experiments.

The financial support of the Russian Foundation for Basic Research (RFBR grant 10-04-00 106-a) and program of fundamental research of SSC RF - IBMP RAS is greatly acknowledged.

EFFECT OF 12-DAY SPACE FLIGHT ON THE TITIN ISOFORM COMPOSITION AND SARCOMERIC ORGANIZATION OF SKELETAL MUSCLE OF MONGOLIAN GERBIL (*MERIONES UNGUICULATES*)

A.D. Okuneva [1,2], I.M. Vikhlyantsev [1], V.V. Rogachevsky [3], N.N. Salmov[1], Z.A. Podlubnaya [1,2], A.I. Grigor'ev[4]

[1]*Institute of Theoretical and Experimental Biophysics, Russian Academy of Sciences, Pushchino, Russia;*

[2] *Pushchino State Institute of Natural Sciences; Pushchino, Russia;*

[3] *Institute of Cell Biophysics, Russian Academy of Sciences, Pushchino, Russia*

[4]*SSC RF Institute for Biomedical Problems, Russian Academy of Sciences, Moscow*

The locomotory system of animals and humans develops under gravity conditions and organized with regard to the action of gravitational forces. The absence of support loads in microgravity conditions is accompanied by changes in the functions of vestibular and locomotor systems [1]. In particular, it leads to the development of structural and functional changes in skeletal muscles, known as "hypogravitational muscle syndrome" (HMS) [1]. HMS manifests in the reduction of muscle tone, decrease of strength of muscle contractions, muscle hyperreflection and coordination disorders in the short-term (2-5 days) influence of microgravity. These disorders are accompanied by the development of atrophy of muscle fibers when the influence of microgravity is more long. Atrophy is accompanied by destructive changes in the thick and thin filaments, in particular, the degradation of myosin heavy chains is increased, the content of titin, nebulin, X-protein is decreased, integrity of dystrophin layer of sarkolemmal membrane is disturbed, myosin phenotype is transformed toward to the increase the proportion of fast isoforms of myosin heavy chains. Later the muscle tone, endurance and the general muscle performance are reduced. The most changes are observed in the muscle soleus, because it consists of slow fibers by 85-90%.

In earlier studies we observed decrease in the content of N2A and a more high molecular weight (NT) titin isoforms in m. soleus of human and rat under conditions of simulated microgravity [2,3]. These changes contribute to the development of the HMS.

In this paper we present the results of the study of changes in titin isoform composition and sarcomeric structure in *m. soleus, m. tibialis anterior* and *m. gastrocnemius* of Mongolian gerbils (*Meriones unguiculates*) after the 12-day flight on the Russian spacecraft "Photon M3".

Methods. 2.0-2.3% SDS-PAGE with the addition of agarose (0.5-0.6%) were used for electrophoretic studies of titin isoformes composition by method [4]. The content of titin was evaluated in relation to the content of myosin heavy chains. Western blotting of titin was performed by the method [2]. Antibodies AB5 to titin was used as the primary antibodies. These

antibodies bind to the titin molecule in the A-disk around the M-line of the sarcomere. Muscle tissue samples were fixed for 2 hours in 1.25% glutaraldehyde with 3% formaledgide in 0.1 M Na-kakodilat buffer for electron microscopic studies. The samples were transferred to 1% solution of OsO4 for 1 hour. Dehydration of the samples was carried out by ethanol of different concentrations and the acetone. Fixed and dehydrated samples were filled by a mixture of Araldite M. and Epon 812 resins. Cutting of samples was carried out on ultratome with slope angle of the knife 5˚. Negative staining of samples was performed by 1%-aqueous solution of uranyl acetate and lead citrate.

Results and discussion. Taking into account that the content of N2A and NT isoforms in m. soleus of human and rat decreased under conditions of simulated microgravity [2,3,5], we expected to find a similar decrease of the titin content in skeletal muscles of Mongolian gerbils after space flight. However, electrophoretic studies was found the increase of NT-titin isoform content in m. tibialis anterior, m gastrocnemius, m.soleus at 1,12-2,0 times after space flight. At the same time in m. tibialis anterior was observed conservation of the N2A-titin isoform content, but in m. soleus and m gastrocnemius was found reduction (in 1,2-1,25 times) of N2A-titin (figure). In all these muscles the content of T2-titin fragment was decreased in 1.3-1.4 times (table).

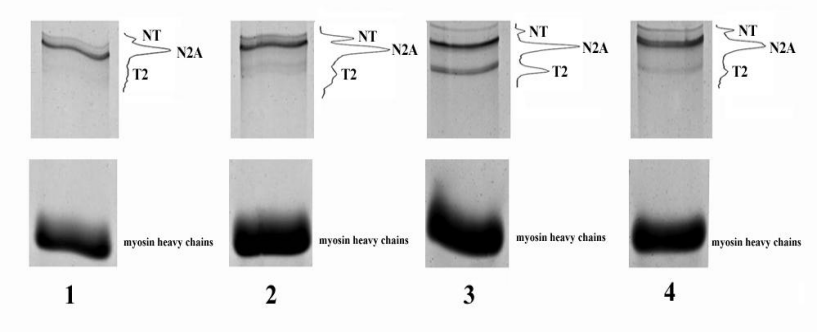

The changes in titin isoform composition in skeletal muscles of Mongolian gerbils under real microgravity conditions. Electrophoresis was performed in a vertical mini-gel containing 0.55% agarose and polyacrylamide 2.1-2.3%.
1 - m.soleus of control group gerbils, 2 - m. soleus of flight group gerbils, 3 - m. tibialis anterior of control group gerbils, 4 - m. tibialis anterior of flight group gerbils.

It is known that the decrease of N2A-titin isoform content is accompanied by disruption of the structure and contractile properties of rat soleus muscle under conditions of simulated microgravity [5]. Similar abnormalities of structure and functional properties of muscles as well as the decrease of titin content were observed in muscles after the influence of ionizing radiation [6]. We hypothesized that decrease of the titin content in m. soleus of gerbils after

Content of titin isoforms in gerbil skeletal muscles

Muscle	Group	NT/ТЦМ	N2A/ТЦМ	T2/ТЦМ	NT/N2A
m.soleus	control	0,025	0,127	0,020	0,188
	flight	0,028	0,102	0,015	0,247
m. tibialis anterior	control	0,016	0,146	0,071	0,108
	flight	0,031	0,145	0,051	0,126
m. gastrocnemius	control	0,015	0,157	0,087	0,101
	flight	0,030	0,133	0,062	0,163

space flight (table) could lead to a damage of muscle sarcomeric organization, because atrophic changes in this muscle were observed [7]. However, the results of our studies did not reveal any disorders of highly ordered sarcomeric structure in m. soleus of gerbils after space flight. It should be noted that the decrease of contractile ability and the reduction of the Ca2+-sensitivity of force development of m. soleus fibers of gerbils flight group was not found [7].

It is interesting that the changes in titin isoform composition in atrophied skeletal muscles of hibernating ground squirrels (Spermophilus undulatus) are similar to those in muscles of gerbils in conditions of space flight. In particular, it was found the preservation of the content of NT-titin isoform with a decrease in 1.3-1.5 times the content of N2A-titin isoform in ground squirrel skeletal muscles during hibernation [8,9]. These changes are not accompanied by disturbances of structural and functional properties of the skeletal muscle of ground squirrel [9-11]. Taking into account our results and published data about that the decrease of titin content is accompanied by disruption of the structure and contractile properties of muscle [5,6], we conclude that a main role in supporting of structural and functional properties of muscle plays the NT-isoform titin but not N2A-isoform of this protein. It is interesting that the decrease in N2BA- and N2B-titin isoformes content in ~ 1.5 times with preservation of the NT-isoform content in cardiac muscle of hibernating ground squirrels [8] did not lead to disturbances of the sarcomeric structure [9] and contractile properties of myocardium [12]. These data confirms our conclusion.

So, the changes in titin isoform composition in skeletal muscles of gerbils after a 12-day space flight have adaptive nature and are aimed at preserving the content of high molecular weight NT-titin isoforms for the support an ordered sarcomeric structure and contractile activity of muscles.

This work was supported by the Russian Foundation for Basic Research (grant No. 11-04-01026 and a grant of the Federal Targeted Program “Scientific and Scientific-Pedagogical Personal of Innovative Russia”, State Contract No. 02.740.11.0710.

References

1. Grigoriev A.I., Kozlovskaya I.B., Shenkman B.S. // Ros. Fiziol. Zh. im. Sechenova. 2004. V. 5. P. 508-521.

2. Vikhlyantsev I.M., Podlubnaya Z.A., Shenkman B.S., Kozlovskaya I.B. // Dokl. Biochem Biophys. 2006. V. 407 (5). P. 88-90.
3. Vikhlyantsev I.M., Podlubnaya Z.A. // Biofizika. 2008, V. 53(6). P. 1058-1065.
4. Vikhlyantsev I.M., Podlubnaya Z.A., Kozlovskaya I.B. // Doklady AN. 2004. V. 395(6). P. 828-831.
5. Udaka J., Ohmori S., Terui T., Ohtsuki I., Ishiwata S., Kurihara S., Fukuda N. // J. Gen. Physiol. 2008. V. 131(1). P. 33-41.
6. Horowits R., Kempner E.S., Bisher M.E., Podolsky R.J. // Nature. 1986. V. 323. P. 160-164.
7. Lipiec E.N, Ponomareva E.V. Ogneva I.V., Vikhlyantsev I.M, Karaduleva E.V., Kuznecov S.L., Podlubnaya Z.A, Shenkman B.S. // Aviakosm. i ecol. Med. 2009. V. 43. №3. P. 34-39. 8. Vikhlyantsev I.M., Karaduleva E.V., Podlubnaya Z.A. // Biofizika. 2008. V. 53(6). P. 1066-1072.
9. Trapeznikova K., Vikhlyantsev I., Kokoz Yu., Okuneva A., Rogachevsky V.,. Khutsyan S., Salmov N., Podlubnaya Z. // In book: Biological Motility: Fundamental and Applied Science, 2012.
10. Khromov A.S., Srebnickaya L.K., Rozdestvenskaya Z.E., Orlova A.A., Lednev V.V. // In book:"Mechanisms of hibernation", 1987, Pushchino, ONTI, P. 95-101.
11. Steffen J.M., Li Y., Steele P.S., Klueber K.M., Milsom W.K. // In: "Life in the Cold. Ecological, physiological, and molecular mechanisms" (edited by C. Carey, G. Florant, B. Wunder, B. Horwitz), Westview Press, Boulder, San Francisco, Oxford, 1993. p. 511-518.
12. Wang S.Q., Lakatta E.G., Cheng H., Zhou Z. // J. Exp. Biol. 2002. V. 205. P. 2957-2962.

CRYOELECTRON MICROSCOPY OF ACTIN: NEW INSIGHTS AND CONTROVERSY

Albina A. Orlova, Vitold E.Galkin, Edward H. Egelman

Department of Biochemistry and Molecular Genetics, University of Virginia Health System, Charlottesville, Virginia, USA

Electron cryo-microscopy has established itself as a valuable method for the structure determination of protein molecules, protein complexes, and cell organelles. Cryo-observation of vitrified samples allows the ultrastructural study of macromolecules, molecular assemblies and cells in their natural environment. Cryoelectron microscopy combined with single-particle reconstruction methods is a powerful technique to study the structure of biological assemblies at molecular resolution of 3-10A, it provides a means of capturing different conformational states and dynamic interactions of such assemblies. When the components of a macromolecular complex are known to atomic resolution, then the fitting and docking of X-ray coordinates into the lower-resolution cryo-EM maps can provide new insights into the structure of the complexes and their functions.

In cryo-EM the specimen, typically an unstained protein embedded in vitreous ice, is held at cryogenic temperatures while images are formed in the electron microscope. A modern cryo-EM specimen consists of aqueous film that spans holes in the thin carbon film. The protein film is blotted to very

thin thickness and the grid is rapidly plunged into liquid ethane. The image of protein molecules in ice has much lower contrast than negative-stained image because the protein elements produce only a weak phase-shift signal. And this is why for high-resolution work a microscope with highly coherent “field emission” electron source is required.

In addition to technical advances in specimen preservation and data collection, improvements in both computer hardware and image processing algorithms have been fundamental to the success of three-dimensional structure determination. At near-atomic resolution many detailed features in secondary structure can be resolved.

Actin was discovered more than 60 years ago and has been extensively studied because of its crucial roles in many functions, such as cell shape, movement and polarity and force generation in mucle. Actin is one of the most abundant eukaryotic proteins, and its activities in vivo are modulated by >150 different actin binding proteins. Because the active form of actin is the filament, a significant effort has been made to obtain a high-resolution structure of F-actin in the last two years. Two papers were published where cryo-EM images of skeletal F-actin were analyzed using improved single-particle method for helical objects (1). Japanese group has reported the F-actin structure at 6.6A resolution, using some advances in cryo-EM. In contrast to the large literature showing that the helical twist of F-actin can be quite variable, authors concluded that F-actin is quite homogeneous structurally and that “F-actin is not so flexible” (2). Our results which were obtained by the same image analysis approach showed that F-actin is structurally polymorphic and it cannot be described using only one atomic model and must be understood as an ensemble of different states (3).

How can these very different observations, of variable twist and polymorphic filaments versus relatively fixed twist and single structure be reconciled? We think that the answer lies in specimen preparation for cryo-EM, when the filaments can be subjected to very large forces due to both fluid flow and transverse compression. The understanding the differences between the results is likely to have great biological significance. We suggested that F-actin itself may function as a highly dynamic tension sensor. This property may help explain the unusual conservation of actin’s sequence, as well as shed further light on actin’s essential role in structures from sarcomeres to stress fibers (4).

References

1. E.H.Egelman (2000). Ultramicroscopy, 85, 225.
2. T. Fujii et al. (2010). Nature, 467, 724.
3. V.E.Galkin et al. (2010). Nature Struct. Biology, 17, 1318.
4. V.E.Galkin et al. (2012). Current Biology, 22, R96.

NUCLEOTIDE-INDUCED STRUCTURAL CHANGES IN THE MYOSIN HEAD PREVENT INTERMOLECULAR INTERACTIONS OF THE N-TERMINAL EXTENSION OF THE ESSENTIAL LIGHT CHAIN 1

Nikolai S. Padalko[1,2], Olga P. Nikolaeva[3], Denis I. Markov[1], and Dmitrii I. Levitsky[1,3]

[1] A.N. Bach Institute of Biochemistry, Russian Academy of Sciences, Moscow, Russia;

[2] Department of Biophysics, School of Physics, Moscow State University, Moscow, Russia;

[3] A.N. Belozersky Institute of Physico-Chemical Biology, Moscow State University, Moscow, Russia

In the previous work, we compared the thermal aggregation properties of two isoforms of the isolated myosin head (myosin subfragment 1, S1) containing different "essential" (or "alkali") light chains, A1 or A2 [1]. A significant difference between these S1 isoforms was revealed in the temperature dependencies of their aggregation measured by the increase in turbidity at low ionic strength. Under these conditions, the aggregation of S1 containing a light chain A1 (but not A2) was strongly dependent on protein concentration, the increase of which (from 0.125 to 2.0 mg/ml) shifted the aggregation curve by ~10 degrees towards the lower temperatures. It was concluded that the aggregation properties of this S1 isoform at low ionic strength is basically determined by intermolecular interactions of the N-terminal extension of the A1 light chain (which is absent in the A2 light chain) with other S1 molecules, and these interactions seem to be independent of the S1 thermal denaturation as they may take place even at low temperature. It was proposed that these intermolecular interactions reflect the ability of the A1 N-terminal extension to form intramolecular interactions with the motor domain of the same S1 molecule [1], which are thought to play an important role in muscle contraction [2, 3] (e.g., during the ATPase reaction, which is accompanied by considerable conformational changes in the myosin head).

To check this assumption, in the present work we compared the temperature dependencies of aggregation of the S1 isoforms S1(A1) and S1(A2) in their ternary complexes with ADP and orthovanadate (V_i), which are stable analogues of the S1 ATPase intermediate state $S1^{**}$-ADP-P_i. No appreciable differences in the aggregation properties were observed between the two S1 isoforms in their ternary complexes S1-ADP-V_i. We can explain these results as follows. We propose that the intramolecular interaction between the A1 N-terminal extension and the motor domain of S1 (presumably, the SH3 subdomain located near the N-terminus of the heavy chain [3]) naturally occurs during the ATPase reaction, due to global conformational changes in the $S1^{**}$-ADP-P_i intermediate. These structural changes are accompanied by the rotation of the regulatory domain relative to the motor domain leading the A1 light chain to a close proximity with the S1 motor domain. In the absence of nucleotides, the A1 N-terminal extension is located rather far from the motor domain

and is unable to intramolecular interaction; under these conditions, it interacts with other S1 molecules, and this intermolecular interaction is expressed in unusual aggregation of S1. Formation of the S1-ADP-V_i ternary complex, which mimics the $S1^{**}$-ADP-P_i intermediate of the ATPase reaction, decreases the probability of intermolecular interactions of the A1 N-terminal segment thus preventing unusual aggregation of S1(A1) isoform at low ionic strength.

This work was supported in part by RFBR (grant 12-04-00441) and by the Program "Molecular and Cell Biology" of Russian Academy of Sciences.

References

1. Markov, D.I., Nikolaeva, O.P., and Levitsky, D.I. (2010) Effects of myosin "essential" light chain A1 on the aggregation properties of the myosin head. *Acta Naturae* **2**(2), 77–81.
2. Borejdo, J., Ushakov, D.S., Moreland, R., Akopova, I., Reshetnyak, Y., Saraswat, L.D., Kamm, K., and Lowey, S. (2001) The power stroke causes changes in the orientation and mobility of the termini of essential light chain 1 of myosin. *Biochemistry* **40**, 3796–3803.
3. Lowey, S., Saraswat, L.D., Liu, HJ., Volkmann, N., and Hanein, D. (2007) Evidence for an interaction between the SH3 domain and the N-terminal extension of the essential light chain in class II myosins. *J. Mol. Biol.* **371**, 902–913.

CYTOSOLIC G-ACTIN AS A SUPPOSED THERAPEUTIC TARGET FOR DOPAMINE ACTION.

E.Yu. Parnyshkova, L.L. Pavlik, D.A. Moshkov

Federal State Budget Institution of Science Institute of Theoretical and Experimental Biophysics Russian Academy of Science, Institutskaya st. 3, Pushchino, 142290 Russia

Many structural elements of the cytoskeleton can easily decay and appear again, changing their location or morphology. These features are based on the properties of its main structural proteins to polymerize/depolymerize and on their interactions with other cytosolic structural and regulatory proteins. The principal component of the system of microfilaments in cellular matrix is actin presenting in the cell in globular (G-) and fibrillar (F-) aggregation forms. Changes in the environmental conditions lead to shifts in vital activity of the cells which accompany by changes in proportion between G- and F-actin in each event in accordance with certain, normal or changed status of the cells [1]. Under pathological conditions the contents of G-actin greatly and firmly increases, in particular at neoplastic transformations. We have conjectured that since the aggregation state of actin is a peculiar feature and in some extent a measure of cell "healthy", one of the therapeutic ways against maligned cells can be induced polymerization of their cytosolic G-actin by means of exogenous penetrating substances, for example dopamine (DA). The premise for such investigations have served the experimental results on interaction of DA with alive cells and with G-actin in model solution and membranous systems, have been getting in our laboratory recently [2], which indicate that DA penetrates into cytosole and interacts with G-actin, transforming it into actin filaments, intercalating and remaining in them as inte-

gral component. The present work is dedicated to study the role of cytosolic actin in morphofunctional organizations of alive normal (healthy), maligned and tumorous (cancerous) cells of different origin; and the possibility to use DA as oncotherapeutic drug and also as diagnostic tool.

In this work the following cellular cultures were studied: model system of normal (3T3) and maligned, transformed by virus mouse fibroblasts (3T3-SV40), the malignant cells of two types, able to attach and spread on substrate (Hep-2, human larynx cancer) and developing in suspension *in vitro* (acute mononuclear human leukemia, line THP-1) and *in vivo* (Erlich ascite carcinoma in mice, EAC). The influence of DA on viability, histology and ultrastructure of these cells were studied as well as a content of G-actin, polymerized and transformed into filaments under the influence of DA, was determined within their cytosole by means of cytochemical Flack's reaction revealing the catecholamine.

It was shown that DA did not influence noticeably upon normal healthy cells, possessed the full-fledged actin cytoskeleton. At the same time it manifested gradually increasing cytotoxicity at the interaction with truly tumorous cells with different degree of malignancy (fig. 1). It was revealed that survivability of spread fibroblasts transformed by viruses SV-40 and attached to substrate (cells 3T3-SV40) became 44% as compared with 100% in control normal fibroblasts (3T3 line), in malignant spread cells HEp-2 it was 12%, in leukemic cells growing in suspension (TNR-1) it made up only 9% [3, 4]. Thus, it is seen that the more malignant were the cell the more disastrous under nearly equal concentration was the action of DA on them. One can assume that difference in degree of toxicity of DA for studied types of the cells is connected with differences in contents of G-actin in their cytosole.

Besides, the study of viability of the ECA cells have revealed that their number in ascitic fluid of experimental mice received injections of 1 ml DA during 6 days was nearly 24-times less than in control animals got only saline injections that is to say the survivability decreased from 100% in control till 4% in experimental conditions (fig. 2). It should be noted that in connection with quick metabolizing of DA *in vivo* (the period of semiejection is about 10 minutes) the heightened concentrations ($1{,}7x10^{-2}$ – 10^{-3}M) and multiple (2 time per day) intraperitoneal injections of DA were used [5].

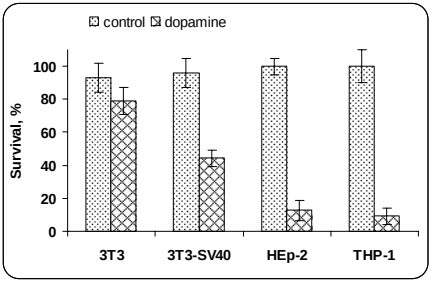

Fig. 1. Survivability of spread (3T3, 3T3-SV40, HEp-2) or developed in suspension (THP-1) cells after incubation with dopamine [10^{-4} M, $5x10^{-4}$ M] *in vitro*.

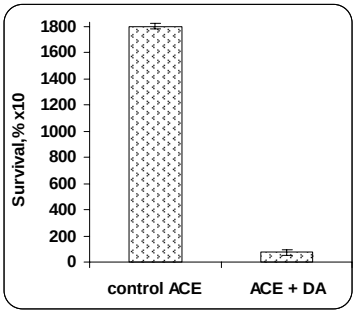

Fig. 2. Survivability of mice EAC cells after intraperitoneal injections of 1 ml DA *in vivo* during 6 days. Initial inoculums contained 1 million cells.

Subsequent histological investigations of all c examined cells have revealed that data on survivable of cells with different malignancy correlates rather well with their histological structural states. It became obvious that the more malignant were the tumour cells the more heavily they were damaged on light-optical level. One of the prominent structural changes were gradually increasing with growing concentrations of DA and duration of its influence the vacuolization of cytoplasm and considerable reduction of the cells dimensions. Measurements of cells diameter made from smears and histological sections of cells grown in suspension, such as THP-1 and EAC, have shown that incubation with DA reduced the diameter of the cells by 25% and 37%, correspondingly, as compared with controls (fig. 3).

As it was established the cause of cells diameter decrease under the influence of DA was polymerization of G-actin induced by this catecholamine since the following depolimerization of F-actin, formed by interaction with DA, by glutamate or cytochalasine practically entirely (up to 95%) restored former size of the cells observed in controls.

Further analysis of ultrastructure of the same normal and malignant cell cultures in controls and experience (before and after DA action) has revealed that normal, healthy fibroblasts attached to substrate (cell culture 3T3) had fully formed rather well differentiated developed cytoskeleton composed of thick cortical layer just beneath the plasmatic membrane, bundles of actin filaments (so called stress-fibers), obliquely or transversally situated within cytosole, and the network of scattered single threads. In suspension cultures the cells had less developed cytoskeleton pre-

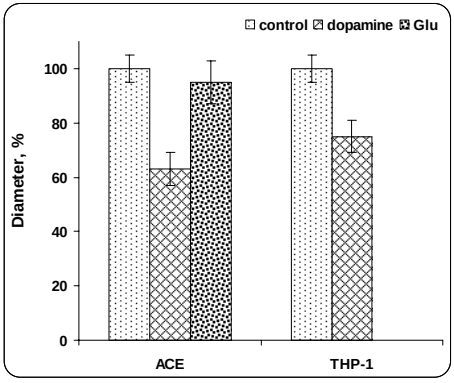

Fig. 3. Changes of cells diameter in suspension cultures (THP-1 and EAC) treated by dopamine.

sented by narrow cortical layer and weakly developed network of single actin threads, substantially, there were no visible stress-fibers in cytosole of such cells. It became obvious that the more malignant were studied cells, the less developed was their actin cytoskeleton. In leukemia and AKE highly malignant cells none the cytoskeleton was revealed throughout the cytosole except narrow cortical layer around the cell surfaces. , except кортикального layer, he practically is not. Under influence of DA one common feature of its effect on cells was detected: an appearance of filaments bundles and dense network of actin threads in cytosole loci where they were absent before DA treatment. Described ultrastructural effect of DA was practically negligible in a case of normal healthy cells (3T3) and it became more and more pronounced with strengthening of cells malignancy. Obviously that cellular target of DA action is G-actin, localized in cortical and subcortical layers and in deep loci of cytoplasm, which after interaction with DA transform into the network of fine threads and narrow bundles of filaments. Analyzing the ultrastructural data it is difficult directly to assert that newly formed actin threads are induced by DA action on living cells. However there is approach to prove this assumption taking into consideration that if it is so then the newly formed actin threads within cytosole should be built simultaneously of actin and dopamine molecules according to our recent data obtained in *in vitro* experiments and to results of highly effective liquid chromatography of actin/dopamine filamentous complexes induced by interaction of G-actin and DA. The possibility to visualize these complexes within cytosole by means of florescent microscopy by using the Falck method especially elaborated for detection of catecholamines in cells. This method applied to cultured cells in control and experimental preparations after treatment of DA have shown that in malignant cells after their incubation in cultural medium containing DA the fluorescence of cytosole in loci with the former most concentration of G-actin increased manifold as compared with controls. It was noted that the more malignant were the cells the more intensive was the glow of cytoplasm. At the same time the fluorescence of the normal healthy cells was negligible. It is important that in normal cells (3T3) after treatment by DA the cytosole exhibited only diffuse glowing. Meantime, it is generally known that just that very case beside such fibroblasts in cytoplasm are revealed massive stress-fibers visible in luminescent microscope after their staining with fluorescently labeled phalloidine specifically interacting with F-actin. Uniform glowing of cytosole after treatment of cells by DA implies that this catecholamine does not interact with already formed F-actin cytoskeleton, but is incorporated only in newly formed actin threads. The latest opens the prospect of the development of a novel method for qualitative and quantitative detection of G-actin in cytosole of any living cell. The obtained results unambiguously give evidence concerning the much greater contents of G-actin in tumour cells than in normal, healthy ones. All above stated facts on the influence of dopamine *in vitro* and *in vivo* on cellular cultures in whole show that this catecholamine could be consider as a prototype of the novel class of

the compounds possessing antitumor activity, acting on the basis of direct influence of DA on G-actin, pathological high contents of which is characteristic for malignant cells, and which manifests itself as a basic cellular therapeutic as well as diagnostic target for dopamine.

References

1. Ujihara Y., et al., J. Physiol. Sci. 2008, vol. 58. №7, p. 499-506.
2. Moshkov D.A., et al., Biophysics, 2010, vol. 55, № 5, p. 850 – 856.
3. Parnyshkova E.Yu., et al., Morphology, 2011, vol. 140, №6, p. 69-74.
4. Parnyshkova E.Yu., et al., Biological Membranes, 2012, vol. 29, №3, p. 18-28.
5. Moshkov D.A., et al., Bull. Exp. Biology and Medicine, 2012, vol. 153, № 5, p. 308-312.

INTERACTION OF FULLERENE C_{60} WITH LIPIDS AND PROTEINS

L.B. Piotrovskiy

Science Research Institute of Experimental Medicine, North-West Branch of RAMS, 12 acad.Pavlov str., Saint Peterburg, 197376, Russia

In biological systems fullerenes, in particular, fullerene C_{60}, can act as a photosensitizer, antioxidant or membranotropic agent. In the first case, the active principle is singlet oxygen, which is formed by the interaction of fullerene irradiation with visible light and triplet oxygen. The action of singlet oxygen is nonselective, as it destroys all available biological systems. Antioxidant action is also non-selective - C_{60} molecule captures all the available free radicals (up to 34 radical per molecule) [1]. Membranotropic action is stipulated by the very high lipophilicity of the fullerene molecule, for which the partition coefficients octanol/water and toluene/water are equal to 6.67 and 8.44, respectively [2]. And only it can be called selective (or specific), since in this case, the fullerene molecule (or aggregate of fullerene molecules) interact with specific biological structure (or molecule).

Lipophilicity of the fullerene is expressed primarily in its relatively high solubility in nonpolar media. Therefore, fullerene molecule C_{60} from water soluble inclusion complexes can be easily transferres into a hydrophobic phase. In particular, the simple mixing of an aqueous solution of the C_{60}/PVP complex with toluene fullerene quantitatively transferred into the organic layer. However, this does not happen if the fullerene C_{60} molecules in the aqueous phase exist in the form of aggregates (nanoC60), which are hydrophobic in nature. In other words, only in the low aggregated state of fullerene molecule can penetrate into the lipid membrane or form inclusion complexes with lipophylic domains of proteins.

The molecules of fullerene C60 from the complexC_{60}/g-CD are transferred into the liposomes while keeping their photodynamic activity [3]. Though the fullerene molecules are not only loosing their photodynamic action, but start to protect the cells from the UV irradiation while they are transferred into the cells from the C_{60}/PVP complex in the cultural media [4, 5]. Significant differences are also observed in the interaction of individual

molecules of fullerene C_{60} with lipid- and protein-rich membranes. Cell cultures grow normally in the presence of C_{60}/PVP complex in culture medium, but the same complex has a strong virucidal effect, destroying the influenza virions [5, 6].

Separate experiments shows that the fullerene can interact with different proteins, but again the interaction depends on the degree of aggregation of the fullerene molecules. From the water-soluble forms with a low degree of aggregation (C_{60}/PVP and C_{60}/g-CD complexes) the fullerene molecule embedd in a various protein molecule, e.g. albumin [7]. A molecule of C_{60} from the C_{60}/PVP complex can also be incorporated into the molecules of green fluorescent protein (GFP) and transthyretin, not causing the dissociation of the subunits of the last [8]. Our experiments with albumin, containing fatty acids. demonstrated that a fullerene molecule displaces some molecule of fatty acids the protein. At the same time highly aggregated form, nanoparticles, on the contrary, adsorbs protein molecules on the surface [9].

Fullerene itself is a nanoparticle, especially when it is in the aggregated state. We should always bear in mind that such water soluble aggregated form of the fullerene as nanoC60, obtained by different methods, are not stable in aqueous medium at relatively high ionic strength [10].

Therefore, the question of interaction of C_{60} molecules with different biological structures and formations requires a detailed study, and it is mandatory to take into account the possible conversion of used water-soluble form in biological media.

References

1. Krusic P.J., Wasserman P.N., Keizer P.N. et al. Science, 1991, v.254, p.1183-1185.
2. Jafvert C.T., Kulkarni P.P. Environ. Sci. Technol. 2008, v.42, p.5945-5950
3. Ikeda A., Sato T., Kitamura K. et al. Org. Biomol. Chem., 2005, v.3, p.2907–2909.
4. Xiao L., Takada H., Gan X., Miwa N. Biorg. Med. Chem. Lett., 2006, v.16, p.1590-1595.
5. Piotrovsky L.B., Dumpis M.A., Litasova E.V. et al. Fullerenes, Nanotubes and Carbon Nanostructures, 2011, v.19, p.147-153.
6. Sirotkin A.K., Piotrovsky L.B., Poznyakova L.N., Kisekev O.I., Voprosi biol. med. farm. khimii, 2005, №3, p. 21-24.
7. Benyamini H., Shulman-Peleg A., Wolfson H.J. et al. Bioconjugate Chem. 2006, v.17, p.378-386.
8. Shavlovsky M.M., Solov'ev K.V., Dumpis M.A. et al. In sb. "Nanotehnologii v biologii I meditsine", E.V. Shlykhto red. S. Petersburg, 2008, p. 101-106.
9. Deguchi S., Yamazaki T., Mukai S. et al. Chem. Res. Toxicol., 2007, v.20, p.854-858.
10. Brant J., Lecoanet H. Wiesner M.R. J. Nanoparticle Res., 2005, v.7, p.545–553.

ABOUT THE FUNCTIONAL ROLE OF AMYLOIDS OF MUSCLE PROTEINS OF THE TITIN FAMILY

Z.A. Podlubnaya[1,2], I.M. Vikhlyantsev[1], S.N. Udaltsov[1,3], M.D. Shpagina[1]

[1] Institute of Theoretical and Experimental Biophysics, Russian Academy of Sciences, 142290 Pushchino, Moscow Region, Institutskaya str. 3

[2] Pushchino State Natural Science Institute, 142290, Pushchino, Moscow Region, Prospect Nauki 3;

[3]Institute of Physicochemical and Biological Problems in Soil Science, Russian Academy of Sciences, 142290 Pushchino, Moscow Region, Institutskaya str. 2

In 2002 we discovered the capability of the muscle X-protein (a protein of the titin family) to form amyloids *in vitro* [1, 2] and later of other proteins of this family [3-9]. This result was not unexpected since molecules of titin family proteins (titin, proteins X, C and H) of skeletal and cardiac muscles contain about 90% of the β-pleated sheet structure necessary for the formation of amyloids. For many proteins, this structure is reached in vitro under very severe conditions. The high initial percent of the β-pleated structure ensured a high velocity of amyloid formation by the titin family proteins under mild conditions near physiological ones. Later the amyloid properties were discovered by us also for an other protein of the titin family, namely, for smitin, a protein of smooth muscles of vertebrates [10].

Studies on the antiamyloid properties of different substances (antibiotics, nootrops, fullerene C60 and its water soluble derivatives) have also carried out. Their destructive action on amyloids of the above muscle proteins and brain Abeta-peptides and the action preventing the formation of new amyloids have been demonstrated. [11]

Studies on the toxicity of amyloids formed by the above proteins *in vitro* and of preparations disrupting these amyloids in different cell cultures showed its absence. The toxicity of water-soluble derivatives of fullerene C60 was registered only for the sodium salt of the fullerene C60 derivative [12]. This stimulates further successful search of the most effective antiamyloid substances in particular, among the nanoderivatives of fullerene C60.

In spite of the absence of toxicity of amyloids of muscle proteins *in vitro*, their unlimited growth in the cell will result in its death. Evidently, these amyloids can be considered as pathological. However, other amyloid fibrils were revealed, which were not associated with diseases. They are formed for the performance of different biological functions. Therefore, they were referred to as functional amyloids [13-18]. These papers describe some examples of living organisms in which the inherent ability of proteins to form such structures in order to generate novel and diverse biological functions.

In regard to functional amyloids formed by proteins of the titin family, this supposition was made by us long ago when we revealed heightened ability of X-protein isolated from skeletal muscles of hibernating ground squirrels Spermophilus Undulatus to form amyloid helical fibrils, in comparison with that characteristic for awake animals [19-21]. It has been shown that such a heightened ability to aggregate correlates with the increase in the extent of phosphorilation of proteins of the titin family during hibernation. Moreover, during hibernation of these animals, the displacement of the acid-base equilib-

rium towards acidic medium takes place. This leads to acidosis when the processes of CO_2 adoption by cells are accelerated and hypoxia develops. We showed that X-, C- and H-proteins isolated from skeletal muscles of hibernating ground squirrels formed amyloid fibrils in greater amounts than the proteins from muscles of active animals. These proteins are connected with myosin filaments and take part in contraction. Changes in intracellular medium upon hibernation can reduce the affinity between X-, C-, H-proteins and myosin filaments. In addition, the decrease of pH in the medium during hibernation would stimulate the formation of amyloid aggregates by these proteins, which would inhibit the muscle contraction. This is supported by our *in vitro* data on the inhibitory effect of X-, C- and H-proteins on ATP-азе of actomyosin [22]. Thus, the formation of amyloid fibrils upon hibernation along with the increase in the level of phosphorylation of these proteins will contribute to the inhibition of the muscle contractile activity, which is necessary for the survival of the animal in this period. This is one of examples of the possible functional significance of reversible formation of amyloids by proteins of the titin family. In future *in vivo* studies will be directed toward the demonstration of amyloid deposits in muscles of hibernating ground squirrels.

This work was supported by a grant of the Presidium of RAS «Basic Research for Medicine», 2012 and by a grant of RFBR № 10-04-00141-a.

References

1. Alekseeva Yu.A., Shpagina M.D., Vikhlyantsev I.M., Podlubnaya Z.A. // Proc. of conf. “From modern fundamental biology to new science intensive technologies”, Pushchino, 2002, p. 46-47.
2. Alekseeva Yu.A., Shpagina M.D., Vikhlyantsev I.M., Petropavlov N.P., Podlubnaya Z.A. // Collector: “Gorizonti biofiziki: ot teorii k praktike” (Red. G.R. Ivanitsky), G.P. Serpukhov, 2003, p. 83-86.
3. Marsagishvili L.G., Vikhlyantsev I.M., Emel’yanenko V.I., Podlubnaya Z.A. // Tezisi IX-Mezdunarodnoy Pushchinskoy shkoli-konferentsii molodikh uchenikh (Pushchino, 18-22 April 2005), p. 155.
4. Marsagishvili L.G., Emel’yanenko V.I., Shpagina M.D., Podlubnaya Z.A. // Nauchnie trudi I S’ezda fiziologov SNG (Sochi, 19-23 sept. 2005), v. 1, p. 14.
5. Marsagishvili L.G., Vikhlyantsev I.M., Shpagina M.D., Emel’yanenko V.I., Podlubnaya Z.A. // Tezisi dokl. XVII zimney molodeznoy naychnoy shkoli «Perspektivnie napravleniya fiziko-himicheskoy biologii i biotehnologii», Moskva, 7-10 feb. фев. 2005, p. 7.
6. Marsagishvili L.G., Vikhlyantsev I.M., Shpagina M.D., Podlubnaya Z.A. // Tezisi dokl. III Vserossiyskoy shkoli-konferentsii po fiziologii mishts i mishechnoy deyatel’nosti (Moskva, 1-4 feb. 2005.), p. 21.
7. Marsagishvili L.G., Shpagina M.D., Emel’yanenko V.I., Podlubnaya Z.A. // Biofizika, 2005, v. 50, № 5, p. 803-809.
8. Marsagishvili L.G., Shpagina M.D., Podlubnaya Z.A. // Sbornik. "Stress i vistseral’nie sistemi" (pod red. V.A. Kul’chitskogo, L. Navratila, K. Messlingera), Minsk, Belarus 2005, «Biznesofset», 2005, p. 146-148.
9. Podlubnaya Z.A., Marsagishvili L.G. // Tehnologii jivih sistem, 2008, v. 5, № 5-6, p. 11-21.

10. Okuneva A.D., Bobylev A.G., Bobyleva L.G., Podlubnaya Z.A. // Abstract of the 40th European Muscle Conference, 14-18 September, 2011, p. 37.
11. Bobylev A.G., Marsagishvili L.G., Shpagina M.D., Podlubnaya Z.A. // Tehnologii jivih sistem, 2009, № 7, v. 6, p. 46-53.
12. Bobylev A.G., Kornev A. B., Bobyleva L. G., Shpagina M. D., Fadeeva I. S., Fadeev R. S., Deryabin D. G., Balzarini J., Troshin P. A., Podlubnaya Z. A. // Organic & Biomolecular Chemistry, 2011, v. 9, p. 5714-5719.
13. Chiti F. and Dobson Ch. M., // Annu. Rev. Biochem., 2006. v. 75, p. 333–366.
14. Uversky V.N. and Fink A.L. // Biochim. Biophys. Acta 2004, v. 1698, p. 131–53.
15. Chapman M.R., Robinson L.S., Pinkner J.S., Roth R., Heuser J., et al. // Science, 2002. 295, p. 851–855.
16. Claessen D., Rink R., de Jong W., Siebring J., et al. // Genes Dev., 2003. v. 17, p. 1714–1726.
17. Berson JF, Theos A.C., Harper D.C., Tenza D., Raposo G., Marks M.S. // J. Cell Biol. 2003. v. 161, p. 521–533.
18. Maji S.K., Perrin M.H., et al. // Science, 2009, v. 325, p. 328-332.
19. Vikhlyantsev I.M., Alekseeva Yu.A., Shpagina M.D., Podlubnaya Z.A. // Tezisi III Vseross. konf. «Mekhanizmi funktsionirovaniya vistseral'nih sistem» (Sankt-Peterburg, 29 sent - 1 okt 2003 .), p. 57-58.
20. Vikhlyantsev I.M., Podlubnaya Z.A. // Biofizika, 2003, v. 48, № 3, p. 499-504.
21. Podlubnaya Z.A., Alekseeva Y.A., Vikhlyantsev I.V., Malyshev S.L., Shpagina M.D. // J. Muscle Res. & Cell Motil., 2004, v. 25(3), p. 263-264.
22. Marsagishvili L.G., Podlubnaya Z.A.. // Mater. 4-th Ros. Konf. «Gipoksiya: mehanizmi, adaptatsiya, korrektsiya», Moskva, 12-14 okt., 2005, p. 75.

THE MYOGENIC GENES EXPRESSION IN HUMAN SKELETAL MUSCLE AFTER DIFFERENT RESISTANCE EXERCISE PROTOCOLS

D. Popov[1], I. Kravchenko[2], V. Furalyov[2], A. Bachinin[1], N.Kurochkina[3], A.Moroz[3], T. Miller[1], O.Vinogradova[1]

[1] SRC of RF – Institute for Biomedical Problems Russian Academy of Sciences, 76A Khoroshevskoye shosse, Moscow, 123007, Russia
[2] A. N. Bach Institute of Biochemistry, Russian Academy of Sciences, 33, build. 2, Leninsky prospekt, Moscow, 119071, Russia
[3] Lomonosov Moscow State University, 31-5 Lomonosovsky Prospekt, Moscow, 117192, Russia

Choosing an optimal contractile activity protocol associated with resistance exercise for improving an increase in muscle mass is an important task for a rehabilitation medicine and a sporting activities. The aims of the present study were to compare an expression of myogenesis regulators in human skeletal muscle 1) after moderate-intensity resistance exercise with (MI) and without (with blood flow restriction) relaxation (MIWR) and 2) after high-intensity (HI) and MI resistance exercise.

Methods

Seven men adapted to strength training performed three resistance exercise sessions three times on separate days in a randomized order: 1) MIWR (8 x 12 knee extensions without relaxation, 50% 1RM, 7 min recovery), 2) MI (8 x 12 knee extensions, 50% 1RM, 7 min recovery), 3) HI (8 x 12 knee extensions, 75% 1RM, 7 min recovery). The duration of muscle activity during exercise in different sessions was equalized. The venous blood samples were taken before, during and 15 min after exercise sessions for determination of lactate, glucose, cortisol (C), testosterone (T), growth hormone (GH), insulin (I) and insulin-like growth factor 1 (IGF-1) concentrations. The vastus lateralis muscle biopsies were collected before, 40 min, 5 and 22 h after the exercise session and analyzed by qPCR for mRNA expression of *IGF-1EA*, *IGF-1EC (MGF)*, *Myostatin*, *MyoD*, *p21* and *MyHC-2x*.

Results

The lactate concentration after MIWR was 7.9(6.6-8.7) mM that was significantly higher ($p<0.05$) than after both HI: 5.8(5.0-7.3) mM and MI: 2.6(2.5-4.3) mM sessions. The concentrations of glucose, I, IGF-1 after exercise did not change and did not differ between sessions. The concentrations of C after HI and after MIWR were higher ($p<0.05$) than after MI. The decrease ($p<0.05$) of T concentration was found after MIWR only.

MIWR led to a decrease ($p<0.05$) of Myostatin mRNA abundance at 40 min and 22 h of recovery: 0.35(0.23-0.78)- and 0.2(0.01-0.5)-fold relative to initial level, respectively. Myostatin mRNA abundance decreased ($p<0.05$) 22 h after HI: 0.1 (0.08-0.23)-fold relative to initial level, and did not change during recovery after MI session. Difference ($p=0.06$) of myostatin mRNA abundance was found between HI and MI at 5 h of recovery: 0.6(0.16-1.27)- and 1.3(0.28-6.6)-fold relative to initial level, respectively. MyHC-2x mRNA abundance increased at 5 h of recovery after MIWR: 2.75(0.88-16.7)-fold relative to initial level, and did not change during recovery after HI and MIWR. The expression of IGF-IEA, IGF-IEC (MGF), MyoD and p21 mRNA did not change during recovery and did not differ between exercise sessions as well.

Discussion

The current study demonstrated that in skeletal muscle of men adapted to strength training 1) the decrease of myostatin mRNA abundance after MIWR was comparable with the decrease of myostatin mRNA abundance after HI. 2) Myostatin mRNA expression during recovery was associated with intensity of resistance exercise, if it was performed without blood flow restriction.

The work is supported by the RFBR grant # 12-04-01668-a.

3D MATHEMATICAL MODEL OF THE STRUCTURE AND FUNCTION OF THE HUMAN HEART LEFT VENTRICLE

S.F. Pravdin[1,2], L.B. Katsnelson[2,4], O.E. Solovyova[2,4], A.V. Panfilov[3], V.I. Berdyshev[1,4], V.S. Markhasin[2,4]

[1]Институт математики и механики УрО РАН,
[2]Институт иммунологии и физиологии УрО РА),
[3]Гентский университет (Бельгия),
[4]Уральский Федеральный Университет
sfpravdin@imm.uran.ru

Ventricular myocardium is a twisted thick muscular band. To simulate the electrophysiological and mechanical activity of the myocardium, it is important to have not only information about the properties of cardiomyocytes, and the shape of the heart, but also data about the direction of muscle fibers in the heart wall.

In the classic work [4] Streeter proposed the idea of constructing a mathematical model of the geometry of the heart left ventricle with the help of a family of surfaces uniformly filled with curves. However, this idea has not yet been completed, ie there are no formulas describing these surfaces and curves.

We propose an analytic realization of the Streeter's idea. With the help of geometric transformations, we map a flat semi-circle with the given chords on it, parallel to its diameter, to the twisted surface, simulating the muscular layer. At the same time images of the chords come into the model muscle fibers on one layer. By turn one surface around the axis of symmetry of the ventricle, one can obtain all other layers filling the ventricle. The ventricle is generally a body of rotation of the original surface around the axis of symmetry. In other words, this body of revolution is filled with curves that simulate muscle fibers.

We compared the angles of inclination of fibers in our model with measurements in vitro from the same paper [4]. The comparison was carried out in the upper and middle parts of the left ventricle along a segment perpendicular to the epicardium. The results of verification showed that our model and experimental data agree well both qualitatively and quantitatively.

Based on this model of the LV structure, we modelled the propagation and damping of the waves (including spiral ones) of electrical excitation in the anisotropic myocardium. To describe the propagation of excitation, we used models of cardiac cells [1] and [5] with the addition of the diffusion term.

We also used the Jarrousse's method [3] of the calculation of the mechanical activity of the myocardium to our model, and calculated one LV cycle. As a model of the passive stiffness we used the formula from [2]; blood pressurization was modelled by application of pressure, dependent in some way on time, along the normal to certain nested LV layers. In addition, we took into account the gravity and the force of viscous friction.

One of the important results of the calculations is that, as in the real heart, ejection fraction 60% is provided by not only shortening of the fibers (in our model it is 2-20%), but also torsion of the LV (twist angle of the individual fibers is 0.5-10%).

The work is supported by grant 12-M-14-2009 of the Presidium of UrB RAS and grant 1F2B8M/JDW/2010-2011/10-BTL-RUS-01 of the Flemish Society of Belgium.

References

1. R.R. Aliev, A.V. Panfilov. A simple two-variable model of cardiac excitation. In *Chaos, Solitons and Fractals*, volume 7(3), pages 293-301, 1996.
2. P. Hunter, M.P. Nash, G.P. Sands. Computational Biology of the Heart. Ch. Computational Electromechanics of the Heart. Chichester: John Wiley & Sons, 1997. Pages 345-408.
3. O. Jarrousse. Modified Mass-Spring System for Physically Based Deformation Modeling. PhD Dissertation. Karlsruhe, 2011.
4. D. Streeter. Handbook of physiology. Sec. 2. Vol. I. The Heart. Ch. Gross morphology and fiber geometry of the heart. Bethesda, Maryland: Am. Physiol. Soc., 1979. Pages 61-112.
5. K.H.W.J. Ten Tusscher, D. Noble, P.J. Noble, A.V. Panfilov. A model for human ventricular tissue. In *Am J Physiol Heart Circ Physiol*, volume 286, pages H1573-H1589, 2003.

A COMPARATIVE ANALYSIS OF THE STRATEGY OF THE BLOOD CELLS MOVEMENT IN SOME INVERTEBRATES

A.A. Prisny, T.A. Pigaleva, S.V. Kulko, E.A. Grebcova

Belgorod State University, 85, Pobeda str., Belgorod, 308015, Russia

A variety of forms and diversity of functions performed by hemocytes (cellular elements of hemolymph), discussed and shown in a number of russian and foreign scientists. It was studied the morphology of cellular elements of the hemolymph of different clams. In the most investigations particular attention is paid to phagocytic activity and connection between hemocytes and immune reactions in the clam body. It was shown that the phagocytic cells that have the ability to form pseudopodia, can self-navigate through the substrate. However, the regularities of pseudopodia formation, the pattern of their formation by certain type of cells, and capacity for independent movement on the substrate not so full revealed, what causes the relevance of this study.

To conduct the study were used adult clams Helix pomatia and Stenomphalia ravergieri, annelids Lumbricus terrestris and Hirudo medicinalis, insects Lucanus cervus and Gryllus assimilis. Hemolymph and coelomic fluid were collected using standard methods. The collected hemolymph was placed using the micropipette in a plastic petri dish, and then investigated on an inverted optical microscope Nikon Digital Eclipse Ti-E.

Analysis of the hemolymph by an inverted optical microscope revealed the presence in the hemolymph of snails H. pomatia several cell types, namely: Type 1 – the large amorphous cells (average size 36,9 μm), which characterised with high phagocytic activity, adheres well to glass and form a large number of pseudopodia, looks like a lobopody and long thin filopodia. Cells of this type are capable to active movement by the substrate by means of pseudopodia. Was shown evident chemotactic response to the introduction of supernatant of yeast Saccharomyces cerevisiae, when phagocytes purposefully moves towards en-

thetic cells. Without the supernatant cell make circular motions with a small radius. Type 2 – medium size cells (average size – 31,6 μm), without a stable shape, can release a small amount of pseudopodia, have limited capacity for phagocytosis. Cells of this type adheres to the glass, and within a short time with the help of filopodia moves toward similar hemocytes. Formed aggregate produces a large number of pseudopodia and able to move to small distances, limited, obviously, the dimensions of the outside cells. Type 3 – round or oval cells (average size – 18.1 μm) are not phagocytic cells, not attached to the substrate. Cells of this type are capable of forming a thin short pseudopodia, in form and arrangement resembling aksopodia.

Similar results were obtained in the study of S. ravergieri hemolymph. Type 1 – the large cells (average size – 41,7 μm), without a stable shape, forming numerous pseudopodia. Cells of this type are attached on the substrate, but continue to move across the surface by amoeboid-like movement. Produce pseudopodia of the lobopody form, and sometimes long thin filopodia. Show a moderate phagocytic activity and low level of response to the introduction of the supernatant of yeast S. cerevisiae. Sometimes this type of hemocytes coalesce into aggregates, and then lose their mobility. Type 2 – rounded cells (average size – 25,17 μm), forming a thin aksopody-like pseudopodia, not fixed to the substrate. Phagocytic activity did not shows, but capable to move with a current of fluid to foreign cells and "grope" them with pseudopodia. Type 3. – small amorphous cells (average size – 19,51 μm): small size, capable of forming pseudopodia – mainly short lobopody. Hemocytes of this type actively moves across the glass and aggregate with similar cells, produced aggregates may show phagocytic activity. It is also capable to chemotactic movement toward the introduced cells of S. cerevisiae. Type 4 – the fourth cell type is different from the cells of the third type only by the size (average – 11,75 μm), and probably is not an independent type of cell, only an intermediate phase of the growth of third type hemocyte. Cells of this type form a small lobopodia and use them to actively move on the substrate.

Coelomic fluid of annelids contain more diverse cells in morphological terms. For Hirudo medicinalis identified four types of coelomocytes. Type 1 – Is the most common type of cells in the coelomic fluid Hirudo medicinalis, the rounded shape and small size cells with a homogeneous cytoplasm and uniformly stained nucleus displaced to the cells periphery. This type of coelomocytes is not able to perform active linear movement, but at the expense of long filopodia, and rizopody cells often rotates and perform small spontaneous shift. Type 2 – larger cells with an eccentrically located nucleus, vacuolated cytoplasm, sometimes with the granules. Cells are able to produce long filopodia and phagocytize foreign objects. Also was observed directed motion of this type of hemocytes. Type 3 – large cells that in intravital observation, shows rapid changes of cell shape, and the directional movement to foreigh objects (S. cerevisiae). Hemocytes move due the produce of broad lobopody and quite not capable of the formation of filopodia. Type 4 – round or oval cells with clear margins, which, depending on the size were divided into two subtypes great

(4a) with a large nucleus, and the smaller (4b), with a small nucleus. This cells do not actively move and do not form pseudopodia.

Blood of Lumbricus terrestris contains seven different types of coelomocytes. Type 1 – large amoeboid cells, their cytoplasm is filled with a large number of vacuoles. The nucleus is a relatively small, eccentrically located. Cells performs different active movement, not attached to glass. Type 2 – large amoeboid cells, the cytoplasm is filled with large vacuoles. Nucleus is small, peripherally located. Cells attach to the glass, after which no longer capable of active movement. Type 3 – the big cell, oval in shape with sharp contours, completely filled with granules (dark and light). Sometimes granules hide a small core, which is located eccentrically. The cells are not able to form pseudopodia. Type 4 – average amoeboid cells, the cytoplasm is filled with large and small dark granules. The core is located in the center or on the periphery. The cells are capable to adhesion to the glass, there is no active movement Type 5 – rounded cells with clear margins. The nucleus is oval, peripheral positioned. The cytoplasm contains dark granules and light vacuoles. These cells are not able to active move, but are able to produce long filopodia. Type 6 – rounded cells with clear margins. The kernel is oval, relatively large, on a peripheral position. The cytoplasm is homogeneous. The cells are capable of producing filopodia. Type 7 – small round cells, the cytoplasm is homogeneous. Pseudopodia not form. For insects, we have identified three types of cells.

On the basis of their locomotor behavior of hemocytes of insects can be divided into two groups: the fast moving cells, fixed cells, fixed cells with high phagocytic activity. Type 1 – elongated, spindle-shaped cells. Migration potential of these hemocytes is high. They form several long thin filopodia, as well as demonstrate the ability to phagocytosis. Type 2 – fixed small round cells. They do not form pseudopodia. Type 3 – polymorphic cells type, round, oval, sometimes irregular in shape. This type of hemocytes produce many short branched pseudopodia (rizopodia) and lobopodia, show high phagocytic activity, but the cells are fixed.

Based on the above described types, we constructed a summarizing table:

	H. pomatia	S. ravergieri	L. terrestris	H. medicinalis	L. cervus	G. assimilis
Type 1	F*\L**\R***	F\L\R	F\R	F\R	F	F
Type 2	F	F	L	F	-	-
Type 3	F	L	-	L	F\L	F\L
Type 4			L	-		
Type 5			F			
Type 6			F			
Type 7			-			

*F – filopodia, **L – lobopodia ***R – rizopodia.

The table shows that the cells of the immune system of each of the presented invertebrates produce almost all types of prolegs. This explained by the need for the presence of cells with different motor activity, for the effective implementation of the immune response. The greatest number of shown cell types produce long and thin filopodia. Hemocytes with rizopodia represented by single types.

Our investigation describes three types of cells in the hemolymph of H. pomatia, four cell types S. ravergieri, four types of H. medicinalis, 7 types of hemocytes L. terrestris and three types of cells of the hemolymph L. cervus and G. assimilis.

MODELLING THE AUTOOSCILLATORY CALCIUM DYNAMICS IN SINOATRIAL NODE CELL IN THE FRAMEWORK OF ELECTRON-CONFORMATIONAL THEORY OF RYR-CHANNELS ACTIVITY

A.M. Ryvkin[1,2], A.S. Moskvin[1,2], O.E. Solovyova[1,2], V.S. Markhasin[1,2]

[1]Institute of Immunology & Physiology, UB RAS;
[2]Ural Federal University

We report the results of the studies of oscillatory dynamics of isolated Ca^{2+} release unit (RU) in sinoatrial node cell (SANC) in frames of electron-conformational model (ECM) of ryanodine (RyR) channels[1,2]. The RU includes junctional compartment (jSR) of the sarcoplasmic reticulum network (nSR), cluster of coupled RyR-channels, and sub-sarcolemmal space (subspace , SS) (Fig. 1).

As it was argued recently [3] the isolated from sarcolemmal voltage oscillator (membrane "clock") RU can operate as a self-sustained oscillator (SR Ca^{2+} "clock"), described by a simple "release-pumping-delay" mechanism when a small spontaneous Ca^{2+} release from jSR to the subspace occurs as the primary or initiating event. When Ca_{SS} increases to a sufficient level, it amplifies the Ca^{2+} release via the mechanism of the Ca^{2+}-induced Ca^{2+} release (CICR) [4]; this relatively strong, secondary Ca^{2+} release simultaneously depletes (i.e., resets) jSR. The released Ca^{2+} is pumped into the nSR. The delay between releases is determined by the Ca^{2+} pumping rate and Ca^{2+} diffusion from the subspace to cytosol and also from nSR to jSR. As Ca_{jSR} slowly increases, RyR's are restituted, and the next release is ultimately initiated, etc.

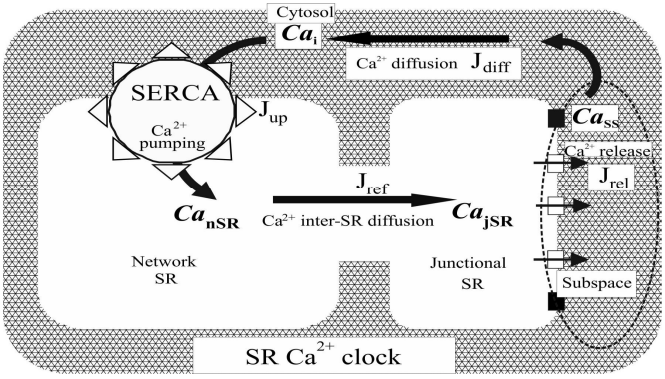

Fig. 1. Schematic illustration of the cell compartments and Ca^{2+} fluxes in the SR Ca^{2+} "clock" model. SERCA is a sarco/endoplasmic reticulum Ca^{2+}-ATPase that transfers Ca^{2+} from the cytosol to the SR (J_{up}). J_{ref} is the refill flux from SR-network (nSR) to SR-lumen (jSR). J_{rel} is the release flux to subspace through opened RyR-channels (white rectangles). J_{dif} is the diffusion flux from subspace to cytosol.

We assumed that the Ca^{2+} flux through the RyR-cluster follows the formula:

$J_{rel} = N_{open} k_{rel} \left(Ca_{jSR} - Ca_{SS} \right)$, where k_{rel} is a release rate constant through a single channel, N_{open} is the number of opened channels, $\left(Ca_{jSR} - Ca_{SS} \right)$ is the difference between Ca^{2+} concentrations in jSR and SS, respectively.

It is known that RyR-channels are arranged on the SR membrane in closely packed clusters such that their large cytoplasmic domains contact each other [5]. In our model we take into account nearest RyR neighbors inter-channel conformational coupling [2].

Fig. 2 shows the computer simulation results which demonstrate the Ca^{2+} SR "clock" activity as a function of interaction between RyR channels in a 9x9 RyR's square lattice. We see that coupling influences strongly the stability of oscillatory dynamics, as well as fluctuations of frequency and amplitude. Puzzlingly, given low Ca^{2+} release rate and strong enough RyR-RyR coupling we observed the emergence of stable clusters of opened channels and steady-state Ca^{2+} leakage to subspace. The RU oscillatory regime can be restored by external membrane stimuli, so a self-consistent dynamics of SR Ca^{2+} "clock" and membrane oscillator ensures the stability of the whole SANC in a wide range of parameters.

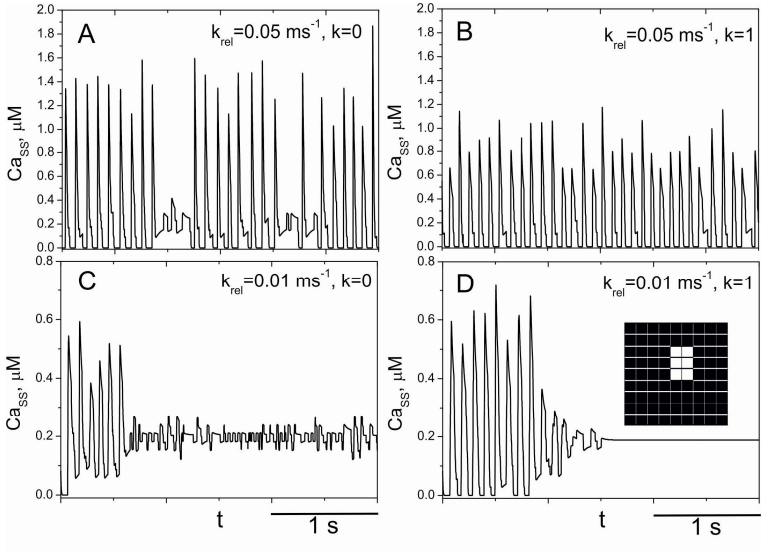

Fig.2. $Ca_{SS}(t)$ dependence given several values of parameters k_{rel} and *k* (inter channel conformational coupling constant). A, B: under conditions of fast releas the RyR-RyR coupling provides the stability of oscillations. C, D: under condition of law k_{rel} value the RyR-RyR coupling causes a steady-state release through th stable cluster of opened RyRs. (white 2x3 rectangle group in insert).

Supported by: the UB RAS Project 12-П-4-1067 (RAS Presidium Program), Junior Scientists' Grant of the UB RAS (Ryvkin).

References

[1] *Moskvin A.S., et al.* // JETP Letters. 2011. V. 93. No. 7. P. 403–408.
[2] *Moskvin A.S., et al.* // Progress in Biophysics and Molecular Biology. 2006. V.90 P. 88-103.
[3] *Maltsev V.A., Lakatta E.G.* // Am. J. Physiol. Heart Circ. Physiol. 2009. V. 296. P. 594-615.
[4] *Bers D.M.* // Excitation-Contraction Coupling and Cardiac Contractile Force. Second Edition, Kluwer Academic Publishers, New York. 2002. P. 420.
[5] *Marx O. et.al.* //Circ. Res. June 8 2001 P. 1151-1158.

QUANTITATIVE ANALYSIS OF STRESS GRANULES IN CELLS WITH INTACT OR DEPOLYMERIZED MICROTUBULES USING A NEW ALGORITHM FOR IMAGE PROCESSING

A.A. Sablina[1], E.M. Chudinova[2], P.A. Ivanov[3], E.S. Nadezhdina[2]

[1]Faculty of Bioengineering and Bioinformatics, M.V. Lomonosov Moscow State University, 1-73 Leninskie Gory, Moscow, 119991, Russia
[2]Institute of Protein Research Russian Academy of Sciences, 4 Institutskaya ul., Pushchino, 142290, Russia
[3]Faculty of Biology, M.V. Lomonosov Moscow State University, 1-12 Leninskie Gory, Moscow, 119991, Russia

Stress granules (SGs) are dense bodies occurring in the cytoplasm of eukaryotic cells in response to stress (heat shock, oxidative stress, UV irradiation). They play an important role in ensuring the viability of cells under extreme conditions, so the knowledge of the mechanisms of their formation can be applied in the development of drugs selectively targeting malignant cells. SGs contain mRNAs, mRNA-associated proteins, small ribosomal subunits and several translation initiation factors. It is shown that the treatment of cells with nocodazole, an agent that disassembles microtubules, has a significant influence on the formation of the SGs, their disassembly after termination of the stress, as well as their motility. At the same time, nocodazole does not affect the phosphorylation of eIF2a, which is generally an important step in the formation of SGs, therefore, the effect of nocodazole on the SG is likely to be mediated by microtubules. In our work sodium arsenite in concentrations of 50 - 625 micromol/l was used as stressing factor, and nocodazole at a concentration of 6 mg/ml was used to disassemble of microtubules. In the experiments we used cell lines CV-1 (derived from green monkey kidney epithelium) and HeLa (human cervical carcinoma). The curve of dependence of fraction of cells with SGs from the concentration of arsenite is S-shaped and lies above for intact cells as compared to cells with disassembled microtubules (reaches saturation and zero at lower concentrations than for cells treated with nocodazole). The curves of dependence of the proportion of cells with SGs on the concentration of arsenite in cells with intact and disassembled microtubules roughly coincide with the displacement along the axis

of concentration. An algorithm for counting SGs and their parameters, such as amount of fluorescent substance, has been developed and implemented as a plugin for ImageJ program. Usage of the algorithm greatly reduces subjectivity. The principle of its work consists in the subtraction of image after smoothing from the original image to make possible counting of granules after thresholding. This happens because at the edge of the cell granules may be paler than the background in the center, which is especially characteristic of the large CV-1 cells. As a control, we used cells treated with cycloheximide, which causes a complete disassembly of the SGs in a concentration of 10 mcg/ml in the culture medium. We have shown that there is more SGs in cells treated with nocodazole, and they are smaller. Paclitaxel, a substance that stabilizes microtubules, has another effect on SGs. The curve of dependence of fraction of cells with SGs from the concentration of arsenite for paclitaxel-treated cell almost coincides with one for intact cells. But data for amount of granules in cells and their size are more similar to those for nocodazole-treated cells. The average distance from a granule to the centre of cell nucleus is bigger in nocodazole-treated cells than in intact ones, indicating that probably SGs move along microtubules towards the centre of the cell, that facilitates their enlargement. All the data concerning amount of granules in cells, their size and position have been obtained using our algorithm. Thus, microtubules play an important role in the assembly and enlargement of SGs. The role of microtubules in the formation of SG needs further study.

The work was supported by RFBR grant 10-04-01107-a.

THE POSSIBILITY OF USE OF THE GREEN FLUORESCENT PROTEIN FOR CREATION OF 2-CELL CHIMERICAL MOUSE EMBRYOS WITH HELP (ASSISTANCE) OF LASER BEAM FOR THE INVESTIGATION OF EARLY MAMMAL DEVELOPMENT

N.Yu. Sakharova[1], A.K. Shakhbazyan[1,2], A.A.Smirnov[1], E.F.Vikhlyantseva[1], O.M. Sarkisov[2], B.K. Gavrilyuk[1]

[1]Institute of Theoretical and Experimental Biophysics, Russian Academy of Sciences, Pushchino, Russia

[2]N.N.Semenov Institute of Chemical Physics, Russian Academy of Sciences, Moscow, Russia

The important pecularities of development of early mammalian embryos are the asynchronous division of two first blastomeres and their division spindles lie in different perpendicular planes. It is supposed that these pecularities are connected with complex cytoplasmic processes which occur in egg before or after fertilization. It is known that there is different cytoplasm in two blastomeres that are result of first zygote division.

The different quality of cytoplasm of two first blastomeres may be consequence of cytoplasmic segregation, when the certain factors of cytoplasm are distributed in different cells. The finding out of mechanisms of first morphogenetic processes in early embryo is an important problem of modern experimental embryology, because these early processes determine all future

pattern of development of pre-implantation embryo. However by the present time there are many results obtained in different laboratories that compose the contradictory picture of development processes.

This contradiction is obliged to the methods that applied for elucidation of the fate of a concrete blastomere. It is considerated that interference, that is inevitable for all modern methods, influences the results of experiments. That all prevent the correct explanation of the initial stages of development.

We offer the new experimental approach which helps to avoid the negative effects that provoke the mechanical damage of embryos. It is appropriate to use the mice with a transgene of green fluorescent protein (GFP). We have studied the early development of mice C57BL/6-Tgn(ACTbEGFP)1Osb/J. As was shown in our investigation all eggs of hemizygous females give the green fluorescence of cytoplasm that can be found with the help of the fluorescent microscope. This fluorescence doesn't demand any other influense on the alive cells and served in all early embryos that were obtained from mating of females -/egfp and males -/- independently from own genotype of embryos.

For the investigation of influence of cytoplasmic factors, that determine the fate difference of blastomeres on a 2-cell stage, we offer to use the 2-cell chimaeres in which one of blastomeres has a "green" protein. The cell fusing may be made with help of optico-laser setting, that includes a laser capture, laser perforator and laser scalpel (Shakhbazyan et al, 2009).The using of laser helps to avoid the damage that can be made during the mechanical procedures which influense the results of experiments.

The mobility of separate component of cell has a principal significance for the process of cell construction. In preliminary experiments we have shown that during the cell fusing the protein GFP gradually spreads over all volume of the constructed cell. It is necessary to make a detail investigation of this phenomenon and its connection with the state of donor cell for elucidation of significance of cytoplasmic differences in blastomeres of early embryos.

NEUROPROTECTION THROUGH ASTROCYTE SHAPE TRANSFORMATION ON ACCOUNT OF CYTOSKELETON

N.V. Samosudova,[1] V.P. Reutov [2]

[1]Inst. Information Transmission Problems RAS,
Moskow, B. Karetni per.19, 127954, Russia
[2]Inst. High. Nervous Activity and Neurophys. RAS,
Moscow, Butlerova, 5, 117485, Russia

The ultrastructure of the frog cerebellar molecular layer was studied under model insult, which was induced by high concentration of two natural neuromediators: glutamate (Glu) and nitric oxide (NO). These substances are the main damage factors of the natural insult [1]. An insult is local interruption of blood current to neuronal and glial cells. Isolated frog cerebellum was incubated in Ringer solution with addition of Glu or NO (1mM). The behavior of astrocytes (one type of the glial cells) relative to synapses of the frog cerebellar molecular layer was investigated by routine method of electron microscopy.

In vertebrates a cytoskeleton of astrocytes is characterized by mass of intermediate filaments, containing different proteins. The main mass of glial filaments consist of "glial fibrillar acidic protein"(GFAP); the other filaments may contain different proteins such as actin, vimentin and some others. GFAP as well as actin provide the maintaining of the astrocyte mechanical strength and cell shape. At the same time, actin filaments are responsible for astrocyte movement. Besides, the astrocyte cytoskeleton also includes of another elements such as microtubules (MTs). As it is known MTs interact with tau-protein, which is responsible for MT- stabilization and flexible.

In our study under the strong injury (insult model) we have observed changes of the astrocytic process shape. In some cases these processes can swell and loss all cytoplasmic elements, in the others- the most cytoplasmic elements were preserved. In this case it was observed a transformation of astrocytic processes. Processes extended, became narrow, an interval between two their sides decreased and cross bridges appeared inside of each process. They were be able to wrap around injured synapses and to form the likeness of capsule. Each capsule consisted of many rows (from 4 to 5). Undoubtedly actin filaments are responsible for change of the process form and structure, leading to the capsule formation. This fact suggest about the neuroprotective possibilities of astrocytes and coincide with the recent data [2] also concerning to astrocytic neuroprotection. It is known that disfunction of tau-protein is cause of neurodegeneration and dementia. It was showed that astrocytes have neuroprotective mechanisms against tau-toxicity. This mechanism is connected with presence of four proteins, which were identified in astrocytes under neurodegeneration and dementia. As a rule, the concentration of these four proteins was increased in astrocytes, which infiltrated the area with numerous accumulations of hiperphosphorylated (damage) tau- protein and neuronal loss.

So, our suggestion about neuroprotective ability of astrocytes was confirmed by the cited study [2]. It ought to indicate on the main role of cytoskeleton in neuroprotective action of astrocytes.

References

1.Olney J.W., Annu. Rev. Pharmacol. Toxicol. 1990. V. 30. P.47-71.
2.Yata K., Oikava S., Sasaki R., Shindo A., Yang R. et al., Brain Res. 2011. 1410:12-23.

CIRCADIAN AND CIRCANNUAL RHYTHMS OF THE EFFECT OF MONOAMINES ON THE PLASTICITY OF THE CENTRAL NERVOUS SYSTEM OF HIBERNATORS

T.P. Semenova, L.A. Spiridonova

Institute of Cell Biophysics, Russian Academy of Sciences, Pushchino, Istitutskaya str.3, Moscow region, 142290 Russia

Any phenomenon in biological systems develops in a particular spatial and temporal continuum, which requires evolutionarily formed and fixed adaptation mechanisms. One of these mechanisms is the temporal organization of biological processes [Halberg et al., 1989; 2009]. In a wide spectrum of

biological rhythms inherent in animal organisms, circadian rhythms have been studied most extensively. By contrast, circannual rhythms and the relationships between these rhythms and circadian rhythms are poorly understood [Bitting et al., 1999; Toitou, 2008; Karatsoreos et al., 2011]. Hibernators are a unique model for studying the role of circannual rhythms in the mechanisms of adaptive behavior [Heller a. Ruby, 2004]. The functional state of the CNS of hibernators and their adaptive behavior during the annual cycle undergo drastic changes in a wide range, from their complete suppression during hibernation in the winter period to the restoration of normal activity in summer (Semenova et al., 2001).

In view of the foresaid, a comparative study of the role of circadian rhythms in the regulation of plasticity of the CNS of hibernators in different phases of the yearly cycle is of great importance for understanding the basic mechanisms of the functioning of the brain under extreme conditions. Adaptive rearrangements in response to extremal environmental factors occur at the whole organism, cellular, and molecular levels of organization [Bitting et al., 1999; Semenova, Kolaeva, 1999; Kalmykov et al., 2002; Onufriev et al., 2002]. It should be emphasized that hibernators exhibit significant seasonal changes in the metabolism, biochemical and hormonal status, and behavior. These changes and the processes of entry of animals into hibernation and exit from it are under the control of a number of endogenous factors among which neurotransmitters, neuropeptides, and hormones deserve special attention [Halberg et al., 1989; Popova et al., 1993; Semenova a. Kolaeva, 1999; Naumenko et al., 2006; Zuikov et al., 2008].

The main goal of this communication was to reveal biorhythmological features of the plasticity of the CNS in long-tailed Yakutian ground squirrels (*Spermophylus undulatus*), which are the representatives of hibernating animals. For this purpose, a 24-h monitoring of seasonal changes in the exploratory behavior of animals was performed, and seasonal features of the action of the precursors of monoamines on their exploratory activity in the morning and evening hours were studied.

Experiments were performed on 54 mature ground squirrels weighing 600—800 g. For the time of experiments, ground squirrels were housed (placed) in a laboratory chamber with a constant temperature of 18–20°C under a 12-h light-dark regime. A comparative analysis of seasonal features of the exploratory activity was performed on eight groups of ground squirrels: four groups in the morning hours (8.00–11.00) and four groups in the evening hours (20.00–23.00). The experiments were carried out using a hole board and an open field facilities; in the former, the number of head dips and the number of rearings were recorded, and in the latter, the number of rearings and crossed squares. Experimental animals received the precursor of serotonin synthesis 5-hydroxytryptophan (5-HTP, Sigma) at a dose of 10 mg/kg body weight or the precursor of noradrenalin synthesis L-dioxyphenylalanine (L-DOPA, Sigma) at a dose of 20 mg/kg body weight intraperitoneally 30 min before the beginning of the experiment. Control

animals were injected with an equivalent volume of the physiological solution. The statistical processing of the experimental data was carried out using the programs Excel 97 and Sigma Plot 4.0.

The results of observations showed that the level of the exploratory activity of hibernators in the hole board and open field in the summer period is higher than in the other seasons, which agrees with the previously obtained data (Semenova et al., 2001). A comparison of the results obtained over a period of 24 h by the two methods revealed differences between the exploratory activity of the animals in the morning and evening hours. It was found that the activity in the evening hours is by 61–78% lower in the open field ($P < 0.05$) and by 32–56% lower in the hole board ($P < 0.05$) compared with the morning hours throughout the year.

Similar manifestations of the exploratory activity over a period of 24 h were observed against the background of changes in the level of monoamines in the brain, which play an important role in the regulation of both the hibernation process and behavior of animals. The number of crossed squares in the open field (indicator of horizontal exploratory activity) and the number of rearings (indicator of vertical exploratory activity) in the evening hours in animals injected with precursors of monoamines were less throughout all seasons of observation compared with the morning hours. This regularity is also observed in the hole board, although it is less pronounced.

The specific effects of 5-HTP and L-DOPA on the exploratory activity of hibernators are season-dependent. Thus, the significant suppression of the exploratory activity in animals with the increased level of serotonin in the brain occurs in autumn. The number of crossed squares in the open field decreases 2.5 times ($P < 0.05$), and the number of rearings, 1.6 times ($P < 0.05$). In the spring and summer periods, the administration of 5-HTP is also accompanies by the suppression of the exploratory activity; however, it is less pronounced and shows up as a tendency. The number of rearings in the hole board after the administration of 5-HTP in autumn decreases 2.7 times ($P < 0.05$), and the number of head dips decreases 5.7 times ($P < 0.05$); in the spring and summer periods of the annual cycle, the effect of serotonin is less pronounced. After the administration of L-DOPA, a significant increase in the exploratory activity is observed in spring. The values of both components of the exploratory activity in the hole board and an open field increase 1.7–3 times ($P < 0.05$) compared with the control. In summer and autumn periods, these parameters increase in animals injected with L-DOPA only by 5–34%, and the effect of this mediator shows up as a tendency. The diurnal monitoring of the activity showed that the inhibitory effect of 5-HTP on the behavior of ground squirrels is most distinct in the morning hours, and the activating action of L-DOPA is most clearly pronounced in the evening hours. The level of the exploratory activity in the hole board and open field in the morning hours is higher than in the evening hours. This regularity manifests itself most clearly in the period the maximum activity of animals in summer and characterizes the behavior of not only intact animals but also animals with the altered activity of monoaminergic systems.

Thus, we revealed circadian and circannual rhythms in the level of the activity of the CNS in hibernating Yakutian ground squirrels (*Spermophylus undulatus*), which are retained even after directed interference into the functioning of neurotransmitter systems. The activation of the serotonergic system of the brain in ground squirrels is accompanied by the season-dependent inhibition of the exploratory activity, which is most clearly pronounced in autumn. The increase in the level of the exploratory activity against the background of the activation of the noradrenergic system is most distinct in spring. In other words, the specific effects of the interference into the activity of serotonin- and noradrenergic systems of the brain of hibernators and the influence of this interference on the exploratory behavior are determined by the circadian and circannual rhythms of their vital activity.

References

1. Bitting L., Watson F.L., O'Hara B.F. et al. HSP70 expression is increased during the day in a diurnal animal, the Golden-mantled ground squirrels *Spermophilus lateralis*. // Molecular and Cellular Biochemistry. 1999.199: 25-34.
2. Halberg F., Lakatua D., Lodeiro C. Chronobiology, growth hormone and healthy and malignant growth. // J. Endocrinol. Invest. 1989. 12 (8 Suppl.3): 41-47.
3. Halberg F., Cornelissen G., Wilson D. et al. Chronobiology and chronomics: detecting and applying the cycles to nature. // Biologist (London) 2009. 56 (4): 209-214.
4. Heller H.C., Ruby N.F. Sleep and circadian rhythms in mammalian torpor. //Annual Review Physiology. 2004. 66: 275-289.
5. Kalmykov V.L., Anoshkina I.A., Semenova T.P. et al. An effective method of combined quantitative analysis of phospholipid and natural lipid fraction in neocortex of ground squirrels (*Citellus undulatus*). //Neurokhimia. 2004. 4: 243-247.
6. Karatsoreos J.N., Bhagat S., Bloss E. et al. Disruption of circadian clocks has ramifications for metabolism, brain, and behavior.// PNAS. 2011. 108(4): 1657-1662.
7. Naumenko V.S., Tkachev S.E., Kulikov A.V., Semenova T.P. et al. // Genes, Bain and Behavior. 2008. 7: 300-305.
8. Onufriev M.V., Semenova T.P., Kolaeva S.G. et al. The activity of NOS in the different regions of brain of ground squirrels *Citellus undulatus* in the different fazes of annual cycle. //Neurokhimia. 2002. 19(4):264-268.
9. Popova, N.K., Voronova, I.P., Kulikov, A.V., Involvement of brain tryptophan hydroxylase in the mechanism of hibernation. Pharmacology Biochemistry and Behavior, 1993. V.46**.** P. 9-13.
10. Semenova T.P., Anoshkina I.A., Khomut BH., Kolaeva S.G. Seasonal peculiarities of behavior of Yakutian ground squirrels *Citellus undulatus* in the hole board and open field tests.// Physiological Processes. 2001. 56: 195-200.
11. Semenova T.P., Kolaeva S.G. Role of endogenous factors in the regulation of the central nervous system functional states in the hibernators. // In: "Ecological Physiology". Eds. V.A. Trufakin, K.A Shoshenko. Novosibirsk. Publ. House of Siberian branch of RAMS.1999. P.213-219.
12. Toitou Y. Dysfunction of biological clocks and their treatments. // Ann. Pharm. Fr. 2008. 66 (3): 146-157.
13. Zuikov A.V., Semenova T.P., Kozlovsky I.I. et al. The seasonal peculiarities of tuftsin family derivative heptapeptide effects on the CNS plasticity of the hibernators. //«Biological Motility: basic research and practice». Pushchino. 2008. 130 – 132.

APPLICATION OF THE MEDICAL PRODUCT OF NUCLEOTIDES IN NEUROLOGICAL PRACTICE

M.E. Shabanova, M.M. Baurina, L.P. Grinio

D.I. Mendeleyev University of Chemical Technology of Russia, 9 Miussky sq., Moscow, 125047 Russia

At present the pancreatic hydrolysate of yeast ribonucleic acid, the preparation encad [1], is a medical product of a wide-spectrum action. On the date of the Helmholtz Moscow Research Institute of eye diseases using encad since 1970, this preparation is practically a unique remedy detaining the progressing of dystrophic process at pigmentary abiotrophy of a retina – the heavy hereditary disease, resulting in impaired vision and loss of sight. Several decades ago in neurological practice encad also started to be applied for treatment for such heavy disease leading to a lethal outcome as lateral amyotrophical sclerosis. In the treatment of the group of patients with lateral amyotrophical sclerosis the authors used the preparation encad containing a complex of mono- and oligoribonucleotides. It was noticed improvement of the condition in 60% cases observed. The treatment was realized under biochemical control (the assessment of the uric acid in the blood serum and urine and the excretion of oxypurine in the urine). It was possible to depict definite clinic-biochemical correlations. The conclusion was made that encad could be used in the early stages of the disease and mainly in focal segmentary-nuclear lesions. The preparation is contraindicated in generalization of the process and in impetuous development of the disorder [2]. In this early research it has already been revealed the regulating action of this complex of nucleotides on the nucleic exchange in tissues at the positive clinical result. In experiments it has been demonstrated that encad has decreased mortality in brain ischemia, and it possesses nootrophic and anti-stressor action. In general, the wide spectrum of encad function is founded on its ability to regulate metabolism of nucleotides, including the cyclic nucleotides.

Relation between disorders of purine metabolism and disfunction of the immunity is well known. It is necessary to notice that we have obtained the convincing clinical data about efficiency of using encad in autoimmune diseases: Shegren disease [3] and multiple sclerosis; it can be caused by desensitizing properties of the medicine. Recently it has been shown that so-called terminating codons exist as a result of a definite point mutation in a gene. These mutations have a consequence such as synthesis of the truncated variants of the proteins, which are incapable of fulfilling the inherent functions. Mutations of this type underlie many genetic diseases, including some forms of Duchenne muscular dystrophy. At distal Duchenne's myopathies there is no dystrophin in muscles, which provides maintenance of integrity of muscular cells. Their destruction leads to atrophy of skeletal, cardiac and breathing muscles, and then premature death of patients. The dystrophin gene is the longest human gene known, covering 2.4 megabases, and located at locus Xp21. In the significant part of cases the disease is caused by the presence of a premature terminating codon in this gene. Recently the preparation encad has been used in

a large group of patients with the primary Duchenne's muscular dystrophy. The results of the treatment were estimated both by clinical (the increase in functionality of the patient) and by biochemical parameters of muscular dystrophy. An efficiency of the treatment for such a severe hereditary disease reached up 73 %. Increasing the concentration of protein-bound and free hydrocortisone is particularly revealed under the influence of the medicine encad. As far as glucocorticoid hormones of adrenal glands reflect the basic adaptable possibilities of an organism, a change in increasing their concentration testifies to increase of adaptation of patients under the influence of the treatment at the first stages of disease. In overwhelming majority of cases the increase in strength and mass of muscles was also noticed at patients and their functionality extended due to this [4].

Recently the method of treatment for such a form of muscular dystrophy has been offered by H.L. Sweeney's group. The drug developed by this group has appeared to be capable to interact selectively with ribosomes of all types of cells of the mice with Duchenne muscular dystrophy model. As a result ribosomes didn't react to a premature terminating codon at dystrophin synthesis and they made functionally inherent protein. In muscles of sick mice under the influence of this preparation enough functionally inherent dystrophin is formed and their functions were completely restored. Thin mechanism of medical influence of the encad at Duchenne's muscular dystrophy should be investigated in humans in future.

The analysis of this medical product with the method of a high-performance liquid chromatography gives an idea of its complex multicomponent composition. The quantitative determination of separate components of purine and pyrimidine compounds shows that in the purine derivatives a big part is made up of adenosine (56%) and adenosine monophosphate (38%); guanosine monophosphate is 100% among guanine nucleotides. In case of pyrimidines, uracil has not been identified, and a share of uridine monophosphate reaches 26%. So, this analysis of encad has revealed separate fractions of nucleotides, nucleosides and nitrogenous bases in certain ratios. The preparation suits necessary product quality ratings at maintenance of the low-molecular fraction up to 25%, defined with a method of a thin-layer chromatography [5].

Method of preparing nucleotides was awarded by a medal at the IX International specialized exhibition 'Biotechworld 2011'.

References

1. A.I. Bogoslovski, L.A. Katsnelson, T.I. Milyavskaya, K.V. Trutneva, B.B. Fuks, M.E. Shabanova, S.F. Shershevskaya. Method of preparing the nucleotides. Patent SU 663403, 1979.
2. T.L. Bunina, O.A. Khondkarian, T.S. Korshunova, E.G. Larsky, B.B. Fuks, M.E. Shabanova, A.S. Niyazbekova. The treatment of lateral amyotrophic sclerosis by ribonucleotides. S.S. Korsakov Neuropathology and psychiatry journal LXXVI: 166-74, 1976, Moscow, Medicine.
3. M.M. Pozharitskaya, O.V. Makarova, T.N. Kop'eva, B.B. Fuks, M.E. Shabanova, L.M. Voronina. Method of treatment Shegren disease and syndrome. Patent SU 1673123, 1991.

4. L.P. Grinio, B.B. Fuks, M.E. Shabanova, N.I. Korabelnikova. Medical agent for curing degenerative diseases of the neuromuscular system. Patent SU1703113, 1992.
5. M.M. Baurina, A.A. Krasnoshtanova, I.A. Krylov, M.E. Shabanova. Method of preparing pancreatic ribonucleic acid hydrolyzate. Patent RU 2274658, 2006.

CONTRUBTION OF ACTIN ISOFORMS AND CARDIAC MYOSIN ISOFORMS TO CALCIUM REGULATION

D.V. Shchepkin, G.V. Kopylova, L.V. Nikitina

Institute of Immunology and Physiology, Ural Branch of the Russian Academy of Sciences, Ekaterinburg, 620041, Russia

Recent extensive studies shown that the experimental heart pathologies lead to changes either isoforms or phosphorylation status of myofibrillar proteins. These changes play significant role for maintenance contractile activity of myocardium at pathology. For example, isoforms of myosin heavy chains and actin alter during pressure overload hypertrophy or hypertension in the rat hearts. Expression of myosin and actin isoforms also changes during ontogenesis (1).

In myocardium of mammals there are two isoforms of myosin heavy chains: α and β (2). In ventricle together with ventricular isoform of light chains they form two main isomyosins: V1 and V3, homodimers consisting of α- and β-heavy chains, respectively. The myocardium of mammals has two isoforms of α-actin: skeletal and cardiac. These isoforms are coded different genes. These two isoforms are almost identical, differing by only four amino acids over 375 residues. Two of the four differences are located at the amino terminus, the region of the protein that binds myosin (3). There is inhomogeneous distribution of actin and myosin isoforms in myocardium. V1 is predominant in subepicardium while V3 prevails in subendocardium (4). According to recent published data actin isoforms also nonuniformly locate in the left ventricular wall. All pathologies is perturbed this irregularity (5).

The most studies of isoforms changes were carried out on intact myocardium or isolated myocardium preparations (6,7). These not allow accurate view about role of these isoforms in cardiac output. The methods of optical trap and an *in vitro* motility assay throw light on the interaction of contractile and regulatory proteins and contribution of isoforms of contractile and regulatory proteins in myocardium contractility.

To assess contribution of actin and cardiac myosin isoforms to calcium regulation of cardiac contraction we used the *in vitro* motility assay. For this we studied the '*p*Ca-velocity' relationship for regulated thin filament consisting of either cardiac or skeletal isoforms of α-actin and regulatory proteins (tropomyosin and troponin) over cardiac rabbit myosin isoforms V1 and V3. Troponin and tropomyosin were obtained from left rabbit ventricles. According to gel electrophoresis tropomyosin extracted from rabbit myocardium is α-chain homodimer. Cardiac and skeletal actins were isolated from left ventricles and *psoas* muscle of rabbit respectively.

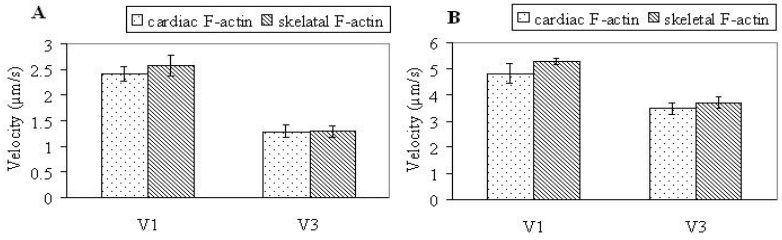

Fig. 1. Velocity of skeletal and cardiac F-actin (A) and regulated thin filaments with skeletal and cardiac F-actin (B) over cardiac myosin isoforms V1 and V3 in the *in vitro* motility assay.

The results of our experiments showed that the sliding velocity of both F-actin filaments and regulated thin filaments at maximal calcium (pCa 4) over cardiac isomyosins V1 and V3 in the *in vitro* motility assay did not depend on actin isoforms of thin filaments (fig. 1). In our laboratory using an optical trap method it was shown that actin isoforms did not affect kinetic and mechanical characteristic of cardiac myosin isoforms V1 and V3.

Martin with coworkers have shown using isolated preparations of transgenic mouse myocardium that γ-actin expression (no expression γ-actin in normal heart) led to a decrease in Hill cooperativity coefficient and calcium sensitivity of 'pCa–force' relation (8). Therefore we performed a series of experiments to obtain the dependence of movement velocity of regulated thin filaments with either skeletal or cardiac α-actin isoforms on calcium concentration (pCa 5–pCa 8) for cardiac isomyosins. The Hill coefficient (*h*) and calcium sensitivity taken as *p*Ca50 were estimated from the 'pCa–velocity' relations for cardiac myosin isoforms V1 and V3 (Table). The Hill coefficient and calcium sensitivity did not differ for isomyosins V1 and V3 in the case of the thin filament with the skeletal α-actin isoform (table).

At the same time the Hill coefficient and calcium sensitivity appreciably differed for V1 and V3 isoforms in the case of the thin filament with the cardiac α-actin isoform (table, fig. 2), where these characteristics were higher

Comparison of Hill equation parameters of the 'pCa–velocity' relationships for regulated thin filaments with either cardiac or skeletal F-actin over cardiac isomyosins V1 and V3 obtained in the in vitro motility assay.

isomyosin	*h*	V_{max}, *μm/s*	pCa_{50}
V1 with cardiac F-actin	1.29 ± 0.54	4.80 ± 0.40	8.52 ± 0.33
V3 with cardiac F-actin	0.68 ± 0.02	3.47 ± 0.21	7.69 ± 0.17
V1 with skeletal F-actin	0.94 ± 0.43	5.28 ± 0.11	7.75 ± 0.10
V3 with skeletal F-actin	0.63 ± 0.11	3.70 ± 0.23	7.80 ± 0.17

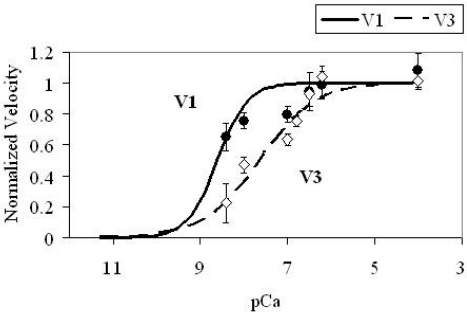

Fig. 2. The '*p*Ca–velocity' relationships for regulated thin filaments with cardiac F-actin over cardiac isomyosins V1 (circles, solid line) and V3 (rombuses, dashed line) in the *in vitro* motility assay. The data were fit with the Hill equation. Each data points represent mean ± SD of three experiments.

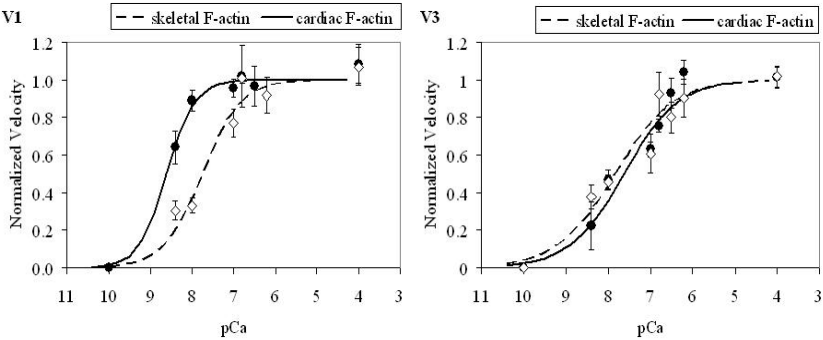

Fig. 3. The '*p*Ca–velocity' relationships for regulated thin filaments with cardiac (rombuses, dashed line) and skeletal (circles, solid line) F-actin over cardiac isomyosins V1 and V3 in the *in vitro* motility assay. The data were fit with the Hill equation. Each data points represent mean ± SD of three experiments.

for isomyosin V1. The Hill coefficient and calcium sensitivity significantly differed for both actin isoforms when V1 isomyosin was used, and did not differ when V3 was used (fig. 3). Thus cardiac isomyosin V1 was found to be most sensitive to change of actin isoforms in the thin filament.

This work was supported by the grant RFBR #10-04-96065r-ural-a, RBRF #11-04-00750-a, Program 12-П-4-1042 of Presidium RAS and the Government of Sverdlovsk Region.

References

1. Izumo, S., Nadal-Ginard, B., and Mahdavi, V. (1988) *Proc Natl Acad Sci U S A* **85**, 339-343
2. Hoh, J. F., McGrath, P. A., and Hale, P. T. (1978) *J Mol Cell Cardiol* **10**, 1053-1076

3. Vandekerckhove, J., Bugaisky, G., and Buckingham, M. (1986) *J Biol Chem* **261**, 1838-1843
4. Eisenberg, B. R., Edwards, J. A., and Zak, R. (1985) *Circ Res* **56**, 548-555
5. Suurmeijer, A. J., Clement, S., Francesconi, A., Bocchi, L., Angelini, A., Van Veldhuisen, D. J., Spagnoli, L. G., Gabbiani, G., and Orlandi, A. (2003) *J Pathol* **199**, 387-397
6. Suzuki, T., Palmer, B. M., James, J., Wang, Y., Chen, Z., VanBuren, P., Maughan, D. W., Robbins, J., and LeWinter, M. M. (2009) *Circ Heart Fail* **2**, 334-341
7. Hewett, T. E., Grupp, I. L., Grupp, G., and Robbins, J. (1994) *Circ Res* **74**, 740-746
8. Martin, A. F., Phillips, R. M., Kumar, A., Crawford, K., Abbas, Z., Lessard, J. L., de Tombe, P., and Solaro, R. J. (2002) *Am J Physiol Heart Circ Physiol* **283**, H642-649

SIGNALING PATHWAYS INVOLVED IN THE RECOVERY OF THE ATROPHIED MUSCLE

B.S. Shenkman

SSC RF Institute for Biomedical Problems, RAS

The search of the signaling mechanisms underlying the disuse muscle atrophy is still one of the important problems of the modern physiology. However, the functional capacity of the muscular system after injury or after exposure to unloading will depend on the efficiency of the recovery process. But there are only few published reports dedicated to this area. It particularly regards the early acute period of reloading. In our studies it was shown that the dry (protein) mass growth was very slight during the first 3-7 days of reloading after simulated unloading. At the same time the elevated tissue hydration was observed [Litvinova et al, 2007, Kachaeva et al, 2011]. We also observed the absence of changes or even decline of single fiber contractility and myofibrillar transverse stiffness [Litvinova et al, 2006; Trappe et al, 2010, Ogneva, 2011]. The revealed data should be based upon the characteristics of the signaling pathways in muscle fibers. As a matter of fact, the elevated phosphorylation of the ribosomal kinase p70S6K after 2 days of reloading [Sugiura et al, 2002] suggesting the activation of anabolic pathways is balanced with the steady maintaining the high calpain activities [Enns et al, 2008] and higher expression level of E3 ubiquitin ligases after 3 days of reloading [Kachaeva et al, 2011]. And the increase of IGF-I expression in rat soleus was shown only after a week of reloading. It can not be excluded that the maintaining and even increase of catabolic activities during acute stage of reloading might be associated with the inadequately elevated eccentric loading of the initially atrophic muscle. Some countermeasures could be discussed to diminish the destructive processes in muscle during the acute recovery stage.

PROTEOMICS OF HUMAN MUSCULAR PROTEINS: DATABASE «PHMP» AND APPROACHES TO STUDY OF NORMAL DEVELOPMENT AND SOME DISEASES

S.S. Shishkin [1], M.A. Kovaleva [1], , L.I. Kovalev [1], M.V. Serebryakova [1], E.V. Khryapova [2], A.V. Ivanov [1], L.S. Eryomina [1], K.V. Lisitskaya [1]

[1] A.N. Bach Institute of Biochemistry RAS, Leninsky prosp., 33, build. 2, Moscow, 119071, Russia

[2] V.N.Orekhovich Institute of Biomedical Chemistry RAMS, Pogodinskay 10, Moscow, 119121, Russia

At the beginning of post-genomic era it has been established, that in the human nuclear genome is present more than 2000 genes which provide various motor functions, including muscular constrictions [1]. Thus, became obvious, that for the systematic studying of protein products of these genes is necessary to use in complex the methods of proteomics and bioinformatics. Moreover the muscular cells, tissues and organs as objects for proteomic studies attract attention of investigators for a number of reasons. First, certain alterations of gene expression occurring in the course of development and aging as well as the functioning of muscular tissues and organs should be reflected in so-called protein profiles that proteomic analysis can precisely characterize [2– 4]. Second, a significant number of muscular tissue diseases is known to date, in which proteomic analysis opens the way to elucidation of their pathogenesis and also favors the determination of diagnostically important molecular markers [2,5,6]. Third, because of differences in muscle cell differentiation and peculiarities of muscular organ morphology, proteomic technologies are used for the search for tissue-specific proteins, among which new protein isoforms or proteins can be found, which represents a significant item for study and seems to be important for realization of human proteome programs [4,7].

Recently we have published results of proteomic study of proteins from bioptates and autoptates of human skeletal muscle m. vastus lateralis [8]. Protein extracts were separated by O'Farrell two-dimensional gel electrophoresis (2DE). MALDI-TOF MS and MS/MS enabled identification of 89 protein spots as expression products of 55 genes. A modification of the O'Farrell's method including non_equilibrium electrophoresis in a pH gradient allowed detection – among major sarcomeric, mitochondrial, and cytosolic proteins – of several proteins, such as PDZ- and LIM domain-containing ones (pI > 8.70), fragments of known proteins, and a stable complex of heavy and light ferritin chains. The data underlie further studies of human skeletal muscle proteins in terms of molecular mechanisms of some physiological and pathological processes.

In parallel, the changes in the protein profile in cultured human myoblasts after induction of differentiation was studied by proteomic techniques (2DE and subsequent protein identification by MALDI-TOF MS and MS/MS analyses) [9]. Forty-one proteins have been identified, 25 of which were present in both proliferating and differentiating myoblasts, which allows them to be considered as myoblast housekeeping proteins. The changes in the distribution of some isoforms of tropomyosins, S100 proteins, cofilin, etc. have been revealed. The pos-

sible role of these changes in the cell protein profile in the realization of the program of skeletal muscle cell differentiation is discussed.

Later for the decision of the problems connected with proteomic study of low-abundance proteins the special approach has been developed. This approach included preliminary isolation of nuclear proteins from cultivated muscular cells (normal non-differentiated and differentiated myoblasts, rhabdomyosarcoma cells too) and their subsequent analysis by methods 2DE, MALDI-TOF MS and MS/MS. The obtained results became a basis for the beginning works on construction nuclear proteomes for some human cells. Thus microheterogeneity of histones has been shown and changes of H2B isoforms, correlating with changes proliferative activity of analyzed cells are revealed.

Undoubtedly, one of the most important and interesting objects for proteomic researches of muscular proteins is the cardiac muscle. Typical 2DE analysis allows to reveal 300-500 protein fractions at studying of bioptates and autoptates from human myocardium. In a separate series of researches we managed to study changes of protein profiles in specimen of human embryonic myocardium (6-36 weeks) and to compare these data to results proteomic studying of specimen from adult myocardium. It is detected, that embryos have the different changes in abundance of some «major» myocardial proteins, 15 from which have been identified by MALDI-TOF MS and MS/MS. Among such proteins were identified isoforms of tropomyosins, and also an alpha- and beta- subunits of ATP synthase, enolase 1 and some heat shock proteins (in particular, HSP27). Apparently, these proteins can serve as biomarkers of the normal or abnormal development of human cardiac muscle.

At present our results of a proteomic study of some human muscular cells, muscular tissues and organs were summarized and the database «Proteomics of human muscular proteins» has been created («PHMP», http://mp.inbi.ras.ru). «PHMP» consists of 7 interrelated modules, each containing four levels of proteomic and biomedical data on the proteins in corresponding tissues or cells. The first data level, onto which each module is based, is a 2DE proteomic reference map where proteins separated by 2D electrophoresis, and subsequently identified by mass-spectrometry, are marked. The results of proteomic experiments form the second data level. The third level contains protein data from published articles and existing databases. The fourth level is formed with direct Internet links to the information on corresponding proteins in the NCBI and UniProt databases. Up to now «PHMP» contains data on 259 proteins in total, including 19 muscular tissue-specific proteins, which can be used as potential biomarkers. In conclusion, the database «PHMP» will be useful in a wide range of applications, including studies of molecular mechanisms of the pathogenesis for some muscular diseases, and the search new diagnostic markers, etc.

References

1. Venter C.J., Adams M.D., Myers E.W., et al. (2001) *Science*, **291**, 1304-1351.
2. Perry, S.V. (2001) *J. Muscle Res. Cell Motil.*, **22**, 5–49.
3. Shishkin S.S., Kovalyov L.I., Kovalyova M.A. (2004) *Biochemistry (Moscow)*, **69**, 1283-1298.
4. Gannon J., Ohlendieck K. (2012) *Mol. Med. Report.* **5,** 993-1000.

5. Cieniewski-Bernard C., Acosta A., Dubois E., et al. (2008) *Clin. Exp. Pharmacol. Physiol.*, **35**, 362-366.
6. Barboro P., Rubagotti A., Orecchia P., et al. (2008) *Cell Oncol.*, **30**, 13-26.
7. Barry S.P., Jayasinghe S.N., Pericleous C., et al. (2008) *Biotechnol. J.*, **3**, 530_535.
8. Kovalyova M.A., Kovalyov L.I., Toropygin I.Yu., et al. (2009) *Biochemistry (Moscow)*, **74**, 1524-1538.
9. Makarov A.A., Kovalyova M.A., Kovalyov L.I., et al. (2009) *Russian Journal of Developmental Biology*, **39**, No.2, 83–89.

THE MATHEMATICAL FORMULATION OF A.F. HUXLEY'S MUSCLE CONTRACTION PHYSICAL MODEL

M.L. Shur, F.A. Blyakhman

Physics Dept., Ural Federal University and Biomedical physics Dept., Ural State Medical Academy, 3 Repin Str., Ekaterinburg 620219, Russia; e-mail: msh@sky.ru

Current concepts on the mechanism of muscle contraction are based on the model suggested by A.F. Huxley in 1957 [1] and developed later in [2]. Generally, this model is commonly accepted and formulated mathematically. Meanwhile, there are experimental data that haven't been explained theoretically so far. The author by himself pointed to this fact in his latest publication: *"It will be evident from what I have said that there are still great uncertainties in our knowledge of the mechanical aspects of the contraction process. Apart from such quantitative uncertainties, there is always a possibility – indeed, a probability – that our present concepts are seriously incomplete or even wrong."* [3].

Alternatively to well known description of the A.F. Huxley's model, in this paper we present the mathematical formulation of his model with the Newton's equation use. From our point of view, it looks reasonable since a muscle is a mechanical system.

Figure below demonstrates the A.F. Huxley's model in the form of a simple scheme where crossbridges are denoted by arrows. They represent elastic elements pulling the actin filament with a force $f = -k(x-h)$. All crossbridges are attached to the actin filament in one and the same position $x = 0$ (the leftmost arrow) where they produce an isometric force $f = kh$ and then move together with the actin filament at an equal velocities.

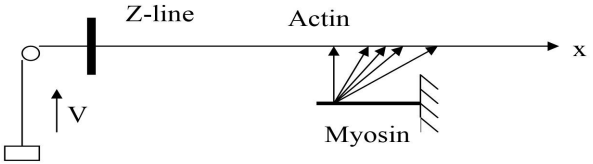

Let at a moment t the sarcomere force be $T(t)$. Then, by the time instant $t+\delta t$ the following would happen:

- All the attached crossbridges (in the amount $n(t)$) would shift with the actin filament by one and the same distance $\delta x = v\delta t$ and their force become equal to $T(t) - n(t)kv\delta t$.

- During this small time interval some part of crossbridges would detach. The rest amount is equal to the amount of crossbridges at the moment t multiplied by the probability for a crossbridge to not get detached. It has been shown by Poisson that the probability is equal to $e^{-g\delta t}$ (here g – the rate constant for the reaction that undo the connection of crossbridge with actin). Therefore, the force created by the crossbridges for a small time interval δt becomes equal to:

$$T_1(t+\delta t) = [T(t) - n(t)kv\delta t]e^{-g\delta t} \approx T(t) - n(t)kv\delta t - gT(t) \quad (1)$$

We expanded the exponent in a series with respect to the small parameter $g\delta t$ and restricted ourselves only to terms in $g\delta t$ of the first order.

- In exchange for the detached crossbridges, $J\delta t$ crossbridges would get attached ($J = [N - n(t)]f$ - this equality follows from the physical sense of the constant *f – rate constant for the reaction that make the connection between crossbridge and actin*)), according to the assumption after A.F. Huxley (and ours as well), in the state of the isometric tetanus and produce force:

$$T_2 = J\delta tkh = (N - n(t))\, f\delta tkh = n(t)gk\delta th = gT_0\delta t \quad (2)$$

Thus, the sarcomere force at a time instant $t + \delta t$ is equal to $T(t+\delta t)=T_1 + T_2$. From this equality a differential equation for the sarcomere force $T(t)$ is derived provided that the constants $(f;g)$ and consequently n do not depend on time.

$$\frac{dT}{dt} = -g(T - T_0) - Kv\,; \quad (3)$$

where K = nk; T_0 = Kh is the isometric force.

The velocity of a load v obeys the Newton's equation:

$$M\frac{dv}{dt} = T - P\,; \quad (4)$$

where $P=MG$ are the mass and weight of the load.

The system of equations (3) and (4) for T and v is reduced to the differential equation for v:

$$\frac{d^2v}{dt^2} + g\frac{dv}{dt} + \varpi^2 v - \varpi^2\frac{g}{K}(T_0 - P) = 0 \qquad \varpi^2 = \frac{K}{M} \quad (5)$$

The solution of this equation has the form:

$$v = C_1e^{a_1t} + C_2e^{a_2t} + \frac{g}{K}(T_0 - P)\,; \qquad a_{1,2} = -\frac{g}{2} \mp \sqrt{\left(\frac{g}{2}\right)^2 - \varpi^2} \quad (6)$$

$$C_1 = -\frac{gMa_2 + K}{MK(a_2 - a_1)}(T_0 - P)\,; \qquad C_2 = \frac{gMa_1 + K}{MK(a_2 - a_1)}(T_0 - P) \quad (7)$$

Let us specify that the oscillation mode of contraction be absent, that is, the expression under the square root in (6) be positive.

$$\left(\frac{g}{2}\right)^2 - \varpi^2 = \left(\frac{g}{2}\right)^2 - \frac{K}{M} = \frac{1}{4\tau_{at}^2} - \frac{KG}{\alpha T_0} = \frac{1}{4\tau_{at}^2} - \frac{G}{\alpha h} \geq 0; \qquad \alpha = \frac{P}{T_0} \tag{8a}$$

$$\text{or} \quad \tau_{at}^2 \leq \frac{4\alpha h}{G}. \tag{8b}$$

We employed the equality, known from the theory of random processes, $\tau_{at} = \frac{1}{\varpi}$; τ_{at} is the average time of staying of the crossbridge in the attached state. It is known that the crossbridge length is of the order of 10 nm and, therefore, it is evident that $L_{0C} \sim 10$ nm as well. Hence, it can be found from (8b) that $\tau_{at} \leq 0{,}01ms$ for the load weighing P=0,5T_0 (α=0.5; G = 10m/s^2 = 10^4 nm/(ms)^2). However, τ_{at} is independent of the load weight. It depends on concentrations of Ca^{++}, ATP, and other chemicals, as well as on temperature. Therefore, the obtained inequality, if invalid, implies that sarcomere contracts oscillatory rather than monotonically. It is conventionally considered that $\tau_{at} \approx 1{,}0ms$. Then it follows from (8b) that the expression under square root in (6) is negative even if

$$\alpha = \frac{P}{T_0} \geq 1 \cdot$$

This means that if a load exceeds the isometric force of the sarcomere, the latter would stretch in the oscillatory model.

Figure on the right schematically presents mechanical interaction of the pre-stretched sarcomere with a myofibril in the process of force generation. Spring with a stiffness k_m simulates the remaining part of the myofibril with a mass m.

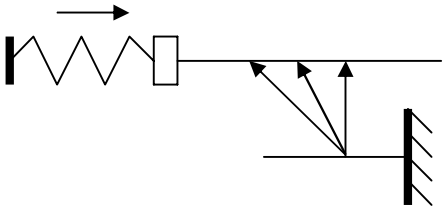

In this case the load experiences the sarcomere force and spring force; therefore, equation (4) will take the form:

$$m\frac{dv}{dt} = T + k_m(x - L); \tag{9}$$

The system of equations (3) and (9) is reduced to a differential equation of the third order in v, which in its turn is reduced to a cubic equation. It has three roots – one real and two complex conjugates. The force of such a myofibril will take the form:

$$T(t) = C_1 e^{-a_1 t} + C_2 \sin(\varpi t + \varphi) + C_3 \tag{10}$$

Thus, the mathematical description suggested herein for the A.F. Huxley's model allows an exact calculation of the force dynamics of actin-myosin interaction in sarcomere. It is important to underline that to this end it was necessary to employ Newton's equation. The analysis of the solutions gained allows explanation of a number of the experimentally observed phenomena.

1. As it was assumed in the A.V. Hill's work [4], the contracting muscle behaves as a system with damping. To explain this damping there is no need to introduce additional damping elements. It is related to the fact that crossbridges are constantly detaching and taking away energy.

2. Sarcomere is an unstable mechanical system which under a weak disturbance turns to an oscillating mode (see, for example, [5]).

3. The myofibril contraction proceeds in two phases. The first phase is quick and is described by the first term in the right part of (10).

4. Minding that the actin-myosin system possesses oscillatory degrees of freedom, one can qualitatively explain the facts on the step-like sarcomere length change [6].

References

1. Huxley A.F. A Theory of Muscular Contraction. *Prog. In Biophys. And Biophys. Chem*, 1957, v.7: 255.
2. Huxley A.F, Simmons R.M. Proposed Mechanism of Force Generation in Striated Muscle. *Nature* (London), 1971, v. 233: 533-538.
3. Huxley A.F. Mechanics and models of the myosin motors. *Phil. Trans. R. Soc. London*, 2000, v.355: 433-440.
4. Hill A.V. The heat of activation and the heat of shortening in a muscle twitch. *Proc. R. Soc.* 1938, 126B:136-195.
5. Telley I.A., Stehle R, Ranatunga K.W et al. Dynamic behavior of half-sarcomeres during and after stretch in activated rabbit psoas myofibrils: sarcomere asymmetry but no 'sarcomere popping'. *J Physiol*, 2006, 573(Pt 1): 173–185.
6. Blyakhman F.A., Shklyar T.F., Pollack G.H. Quantal length changes in single contracting sarcomeres. *J Muscle Res Cell Motil.*, 1999; (5-6): 529-538.

STRUCTURAL BASIS OF MUSCLE CONTRACTION

L. Skubiszak

Nałęcz Institute of Biocybernetics and Biomedical Engineering of the Polish Academy of Sciences, Ks. Trojdena 4, 02-109 Warszawa, Poland

An original computer program has allowed reconstruction of the bipolar hexagonal lattice of the vertebrate striated muscle sarcomere. It is demonstrated that the unambiguous reconstruction is impossible on the basis of gathered so far experimental data. There are a few structures which agree well with those established by different experimental methods. The structure has been finally selected by analysis of geometrical conditions indispensable for muscle contraction.

From the point of view of the biochemical data, according to which each crown consists of three myosin cross-bridges, 52 configurations of the myosin cross-bridge crowns can be taken into consideration. The thick filaments computed on the basis of these configurations are running in the interactive Table at the site http://sarcomere.ibib.waw.pl. In all cases, the arrangement of myosin tails has been used identical, along the helical trajectory.

From the point of view of arrangement of the myosin heads on the filament surface and the mass distribution within the thick filament, 5 configurations, denoted by 1L, 1M, 2L, 2M, and 4D have been found as consis-

tent with that observed by electron microscopy. In these cases, all myosin heads are arranged on the filament surface along the helical paths axially distanced by 43 nm, and the projection of mass density on a plane parallel to the filament axis can be extrapolated by the three symmetrically originated helical paths each of the 3 x 43 nm pitch. The analysis has revealed that in the case of the first four configurations, called asymmetrical, the agreement with the experimental data is nearly ideal. But in the case of widely accepted configuration, denoted as 4D, there are quite essential differences. According to the prevailing now concept, the three myosin cross-bridges are aligned in each crown symmetrically, i.e. at the angles of 0°, 120°, 240°, and the successive crowns are rotated by 40°. The mass distribution in such filament is usually described by three symmetrically originated helical paths each of the 3 x 43 nm pitch. The computer simulation confirms this concept, the mass distribution can be precisely described in this way. But in all published so far micrographs, the mass distribution can be only extrapolated by the three symmetrically originated helical paths. Moreover, in the case of symmetrical crowns, 4D configuration, the inclination of the helical paths differs from experimental, it is 71°. But in the case of filaments with asymmetrical crowns, it is exactly such as that observed experimentally, 68°.

On the basis of the five crown configurations, the bipolar filaments of the type 1L-1L, 1L-1M, 1L-2L, 1L-2M, 1M-1L, 1M-1M, 1M-2L, 1M-2M, 2L-1L, 2L-1M, 2L-2L, 2L-2M, 2M-1L, 2M-1M, 2M-2L, 2M-2M, and 4D-4D have been analyzed. The angles of rotation between the two filament halves have been considered following: 0º, 30º, 40º, 60º, 90º, 120º, 180º, and 240º.

The independent localization of each of the used elements has allowed to simulate the three specific muscle states: relax, rigor and different phases of contraction. The relaxed thick filament has been simulated by arrangement of all myosin heads on its surface. The relaxed thin filament has been computed by genetic helix in which each actin monomer is rotated with respect to the next one through 166.15° about the axis and is translated along the axis by about 2.75 nm; the Tm-Tn complexes have been arranged along the two gaps between the two strands of superhelix built from the actin monomers. In rigor, all myosin heads have been localized on the surface of surrounding thin filaments, and the actin monomers have been shifted axially up to 2.86 nm and angularly up to 168º. The contraction has been simulated by unwrapping of the myosin heads from the thick filament surface towards the surrounding thin filaments. The parameters for arrangement of actin monomers during contraction have been taken the same as for the rigor and have been found as those indispensable for stereo-specific interaction with myosin heads.

Each mode of the sarcomere structure has been verified by comparison of the calculated Fourier spectrum with actual diffraction patterns. It is worth noting that the actual diffraction patterns are dominated by the arrangement of myosin heads within the bipolar hexagonal lattice of the sarcomere. The computer simulation gives a possibility to calculate Fourier spectrum for different number of elements, for instance, only for one myosin filament or for

seven ones arranged into the hexagonal lattice, for 12 thin filaments arranged around a thick filament, or for seven myosin filaments and 12 thin filaments arranged into the hexagonal lattice. In this way, the role of thin filament in muscle contraction has been given to thorough examination.

The computer simulation has revealed the following important relationships:

1. The correct, three-fold rotational symmetry of the bipolar thick filament can be reconstructed only if its crowns have one of the four asymmetrical configurations, i.e., 1L, 1M, 2L, or 2M and the two filament halves are rotated around the angles of 0º, 90º, 120º, and 240º. In the cases of the angles of 30º, 40º, 60º, and 180º, the filament symmetry is six fold. The filament with symmetrical crowns and the 40º rotation between two halves, i.e. 4D-4D, has nine fold symmetry, i.e. it is nearly cylindrical. Calculation of the mass distribution along the filament axis has allowed to directly demonstrate the relation between the both symmetries.

Conclusion: The widely accepted view, that the symmetries of crown and filament are identical, three-fold rotational, is wrong.

2. In the calculated Fourier spectra the features specific for the actual diffraction patterns of the relaxed muscles, i.e., the prominent meridional reflections at the 3-d, 6-th, 9-th, etc. layer-lines, have been observed independently of the filament symmetry; it has been enough if the successive crowns were axially 14.3 nm apart and the identically oriented cross-bridges were at the distance 43 nm. The so-called “forbidden” for the 9/3 helical symmetry meridional reflections at the 1-st, 2-d, 4-th, 5-th, 7-th, etc. layer lines have been observed in all considered cases after introduction of slight differences in the axial distances between three successive crowns.

*Conclusion***:** The diffraction patterns can not be considered as decisive for verification of the structure of vertebrate striated muscle thick filament.

3. The splitting of the M3 reflection similar to that experimentally observed for living muscle in the conditions of contraction has been observed when the five conditions were simultaneously fulfilled. First, the bipolar structure of the thick filament was taken into consideration. Second, the two heads of the same myosin molecule were taken into consideration. Third, the two heads of the same myosin molecule were slightly spaced. Forth, the rotation between the left and right halves of the filament was 120º or 90º. Finally, the three successive cross-bridge crowns were unwrapped with a specific phase shift. It has been also revealed that the splitting did not depend on: (1) the mutual alignment of the two heads and (2) the configuration of myosin cross-bridge crown.

*Conclusion***:** The splitting of the M3 reflection can not be considered as an incontrovertible evidence for correctness of the tilting lever-arm mechanism of muscle contraction.

4. The differences in diffraction patterns from the F-actin filament and from the thin filament as: (1) the significant increasing of a number of layer lines, (2) the shifting of first meridional reflection from 1/35.86 to 1/37.91 nm^{-1}, and (3) the appearance of distinct second meridional reflection at

1/18.97 nm^{-1}, are caused by Tm-Tn complexes covering the F-actin superhelix. Any displacement of the complex in relation to the filament axis without changing the mutual arrangement of the actin monomers has not an effect on the spectrum. At the same time, the Tm-Tn shifting around the filament axis is determined by a change in arrangement of the actin monomers. The change in rotation of the successive actin monomers from 166.15 to 168º leads to: (1) decreasing in relative intensities of the first, second and third meridional reflections; (2) shifting of the first meridional reflection from 1/37.91 to 1/36.86 nm^{-1}; (3) shifting of the off-meridional reflection at first layer-line from 1/34.86 to 1/40.31 nm^{-1}; (4) decreasing in intensities of the specific reflections, called L6 and L7; (5) shifting of the L6 and L7 reflections from 1/5.94 to 1/5.89 nm^{-1} and from 1/5.1 to 1/5.16 nm^{-1}, respectively. The shifting of reflections: (1) the first meridional reflection to 1/41.61 nm^{-1}, (2) the second meridional reflection to 1/19.85 nm^{-1}, (3) the reflections L6 and L7 shift, respectively, to 1/6.17 and 1/5.38 nm^{-1}, (4) the reflection L13 from 1/2.75 to 1/2.867 nm^{-1}, as well as the appearance of: (1) the distinct off-meridional reflections at: 1/43, 1/21.5, 1/14.33, 1/10.75, 1/8.60, 1/7.12 nm^{-1}, and (2) the prominent meridional reflection at 1/2.867 nm^{-1} have been observed after increasing of the axial distance between the neighboring actin monomers from 2.75 nm to 2.867.

*Conclusion***:** The F-actin filament helix should not be regarded as a rigid rod. In the conditions of transition from relax into contraction, the neighbouring actin monomers within the genetic helix probably rotate in result of stimulation by Ca^{2+}-ions from 166.15º to 168º and shift from 2.75 to 2.867 nm probably in result of the strong interaction with myosin head. So, the hypothesis of steric blocking seems to be unreal.

Summary: The stereo-specific interaction between hundreds of myosin heads and actin monomers during contraction is possible only within the sarcomere in which: 1) each of the myosin filament is a tube-like backbone built from the twisted LMM subfragments and covered by the wrapped around myosin cross-bridges; 2) the three pairs of myosin heads are arranged within the cross-bridge crowns asymmetrically, at angles of 0º, 120º, 180º, and the successive crowns and the two filament halves are rotated at 120º; 3) all thick filaments are identically oriented within the hexagonal lattice and act synchronously; 4) the myosin cross-bridges act by cyclical unwrapping and wrapping of the thick filament backbone; 5) the coordination exists in action of the cross-bridges belonging to the same thick filament, namely, the three cross-bridges belonging to the same crown as well as those belonging to the crowns axially distanced by 43 nm work simultaneously, and the cross-bridges belonging to the crowns axially distanced by 14.333 nm work with a phase shift; 6) the six thin filaments surrounding a thick filament in a sarcomere half are rotated by 180º; 7) the axial distance and the rotation between neighbouring actin monomers within the genetic helix change, respectively, from 2.75 nm to 2.867 and from 166.15º to 168º.

The force for muscle contraction is probably generated not only by cy-

clical unwrapping and wrapping the myosin cross-bridges but also by elongation of the actin filaments. Lengthening of the actin filament (or microtubule) seems to be universal mechanism of force generation in living cells.

THE EXTERNAL AFFECTS AND THE WATER STRUCTURE: EMULONS. AN INFLUENCE THEM ON THE METABOLISM

A.N. Smirnov

Moscow State Technical University Radiotechnics, Electronisc and Automatics, 78 Vernadsky prosp., Moscow, 119454, Russia.
E-mail a.n.smirnov@mail.ru

In previous studies [1] it was shown that liquid water has a very complex structure. Using optical methods, acoustic emission and by thermal analysis of the water supramolecular complexes sized from 1 to 100 μm (micrometre) were found in "continuous" aqueous systems. Basing on the characteristic properties of these supramolecular formations we have named them "emulons". Sizes and spatial organization of supramolecular complexes depend on the composition of aqueous solutions, temperature and prehistory of the water. Size specters of emulons reveal five fractions with characteristic sizes:1-3 μm,10-12 μm,30-35 μm, 70 μm и100 μm.

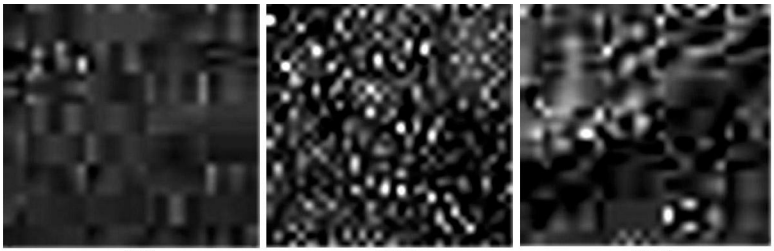

Fig. 1. Influence of temperature on the structure of water. Each image corresponds to the cross-sectional area 2x2 mm.

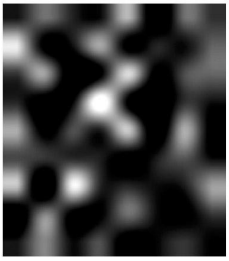

Fig. 2. Spatial distribution of emulons of water. Top side of the image is 400 μm.

Complex organization of water structure as a unite ensemble, that includes - emulons, result in the fact that properties of aqueous system are not simply the sum of properties of its different structural elements, but are explained by cooperation phenomenon .This makes it possible to make a conclusion that liquid water is not a homogeneous substance that consists of minimum five microstructural formations with different properties. The most exciting thing about this is that all these threshold temperatures coincide with characteristic temperatures of water, in example, at which sound speed in water is maximum, adiabatic compressibility of water is minimum, water density is maximum, minimum of heat capacity, and with other “abnormal” points of water that is no coincidence. The polydisperse structure of the emulons formed of the water, ensuring polymodalnost reply by the external affects, appearance hysteresis,considderable times relaxation. It is shown, that liquid water very easily change the structure. For example, on the fig. 3 bring change of the emulons at the “melt water” in time during.

Since the water, in at many cases is a primary target for faint exercise influence on the biology systems, it is posssible the structure of water modification in the time investigation pay attention very much.

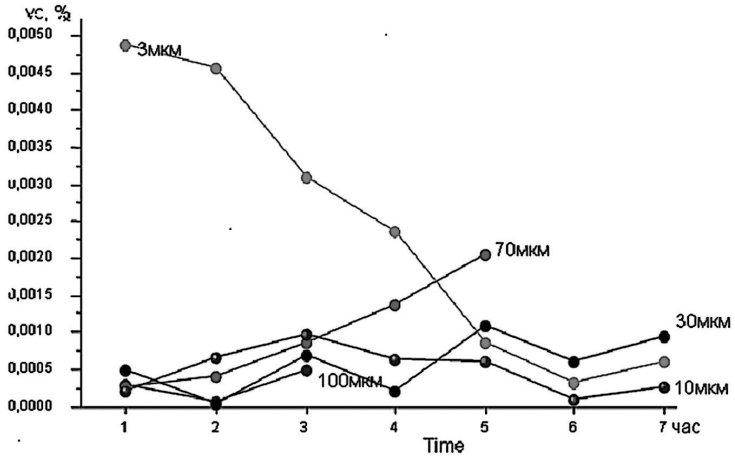

Fig. 3. Quantity of emulons at the “melt water” in time during.

References

1. Smirnov A.N., Water structure: new experimental data.// Science and Technologies for the industry, - 2010, -№ 4, p.41-45

2 Smirnov A.N., The new water structures: emulons // MOLECULAR BIOPHYSICS, Physics of the Alive, 2010,v.18, № 2, p.5-17.

STRESS RELAXATION OF HETEROGENEOUS MYOCARDIAL TISSUE. NUMERICAL EXPERIMENTS WITH 3D MODEL

A.T. Smoluk, L.T. Smoluk, Y.L. Protsenko

Institute of Immunology and Physiology of the Ural Branch of the RAS, 620049, Pervomayskaya st., building 106, Ekaterinburg, Russia

Space-time inhomogeneity of biomechanical and biochemical properties of the myocardium has significantly effect on the heart function [**2**]. Especially the heterogeneity is important at pathology when it increases substantially. Though the presence of heterogeneity in myocardium is an established fact, the significance of heterogeneity of viscoelastic properties remains an open question. Some occurrences of the contractile function of heterogeneous myocardium were established in the laboratory of biological motility and laboratory of mathematical physiology of Institute of Immunology and Physiology [**3, 4**]. But the heterogeneity of viscoelastic properties of myocardial tissue hasn't been investigated.

It is well known that viscoelastic properties of cardiac tissues play a crucial role in the heart function maintenance. Passive tension is an important factor in cardiac muscle mechanics because it determines the extent of filling of the heart and its subsequent stroke volume [**1**]. It is also important in the contracting myocardium because it has been shown that shortening velocity of cardiomyocytes depends on the passive tension [**7**]. Stress relaxation in the myocardium is an important dynamic characteristic of viscoelastic behavior of myocardial tissue sample. Experimental data of the stress relaxation allow to estimate elasticity as well as viscosity of the muscles under different load conditions.

But the experimental study of the influence of heterogeneous viscoelastic properties on the resulting mechanical response of the myocardial tissue sample is a difficult task. Therefore it is reasonable to use model approach. We aim to analyze stress relaxation of heterogeneous myocardial tissue sample in the framework of structural-functional three-dimensional model of morphological unit of myocardial tissue.

We have developed structural-functional model describing heterogeneous viscoelastic properties of myocardial tissue. The model is based on our early developed model of morphological myocardial unit [**5, 6**]. The presented model consists of two sequentially connected blocks with different geometry parameters and mechanical properties. Each block consists of longitudinal and transverse elastic elements, inclined viscoelastic elements connected pivotally without friction. The masses of the elements are not taken into account [**5, 6**]. The model behavior is described by the system of equation below:

$$
\begin{cases}
2\cdot l_1^{(1)}\cdot\left(F_2^{(1)}+F_{WLC}^{(1)}\right)-\left(L^{(1)}-l_2^{(1)}\right)\cdot F_1^{(1)}=0\\
2\cdot l_1^{(1)}\cdot F_3^{(1)}-\left(l_3^{(1)}-h_3^{(1)}\right)\cdot F_1^{(1)}=0\\
2\cdot l_1^{(1)}\cdot F_4^{(1)}-\left(l_4^{(1)}-h_4^{(1)}\right)\cdot F_1^{(1)}=0\\
\left(l_3^{(1)}-h_3^{(1)}\right)^2+\left(l_4^{(1)}-h_4^{(1)}\right)^2+\left(L^{(1)}-l_2^{(1)}\right)^2=4\cdot\left(l_1^{(1)}\right)^2\\
2\cdot l_1^{(2)}\cdot\left(F_2^{(2)}+F_{WLC}^{(2)}\right)-\left(L^{(2)}-l_2^{(2)}\right)\cdot F_1^{(2)}=0\\
2\cdot l_1^{(2)}\cdot F_3^{(2)}-\left(l_3^{(2)}-h_3^{(2)}\right)\cdot F_1^{(2)}=0\\
2\cdot l_1^{(2)}\cdot F_4^{(2)}-\left(l_4^{(2)}-h_4^{(2)}\right)\cdot F_1^{(2)}=0\\
\left(l_3^{(2)}-h_3^{(2)}\right)^2+\left(l_4^{(2)}-h_4^{(2)}\right)^2+\left(L^{(2)}-l_2^{(2)}\right)^2=4\cdot\left(l_1^{(2)}\right)^2\\
L^{(1)}+L^{(2)}=L\\
F_2^{(1)}=F_2^{(2)}
\end{cases},
$$

$$
\begin{aligned}
F_1^{(1)} &= k_1^{(1)}\cdot\left(l_1^{(1)}-l_{10}^{(1)}\right)+\eta_1^{(1)}\frac{d}{dt}l_1^{(1)}\\
F_2^{(1)} &= k_2^{(1)}\cdot\left(l_2^{(1)}-l_{20}^{(1)}\right)\\
F_3^{(1)} &= k_3^{(1)}\cdot\left(l_{30}^{(1)}-l_3^{(1)}\right)\\
F_4^{(1)} &= k_4^{(1)}\cdot\left(l_{40}^{(1)}-l_4^{(1)}\right)\\
F_1^{(2)} &= k_1^{(2)}\cdot\left(l_1^{(2)}-l_{10}^{(2)}\right)+\eta_1^{(2)}\frac{d}{dt}l_1^{(2)}\\
F_2^{(2)} &= k_2^{(2)}\cdot\left(l_2^{(2)}-l_{20}^{(2)}\right)\\
F_3^{(2)} &= k_3^{(2)}\cdot\left(l_{30}^{(2)}-l_3^{(2)}\right)\\
F_4^{(2)} &= k_4^{(2)}\cdot\left(l_{40}^{(2)}-l_4^{(2)}\right)
\end{aligned}
$$

where
$l_{i0}^{(j)}$ initial lengths of model elements of (j)-block;
$l_i^{(j)}$ actual lengths of model elements of (j)-block;
$k_i^{(j)}$ elastic coefficients of corresponding elements;
$\eta_1^{(j)}$ viscous coefficient of (j)-block;
$F_i^{(j)}$ forces applied to corresponding elements.

The first step of the analysis of stress relaxation in heterogeneous myocardial tissue was the introduction of geometrical heterogeneity of parameter $l_2^{(1)}$. The parameter was reduced by 2% as compared with $l_2^{(2)}$ (see table 1). Consequently stress relaxation curve and stress-strain curve were moved up (dashed curve, fig. 1). To equilibrate that geometrical heterogeneity the elastic and viscous parameters of both blocks of the model were changed (table 1). Thus curves of stress relaxation and stress-strain dependence took the initial forms (solid curve, fig. 1).

Table shows that to equilibrate that negligible geometrical heterogeneity by viscoelastic heterogeneity the values of viscoelastic parameters should be significantly decreased. Notably to obtain the same level of the tension as

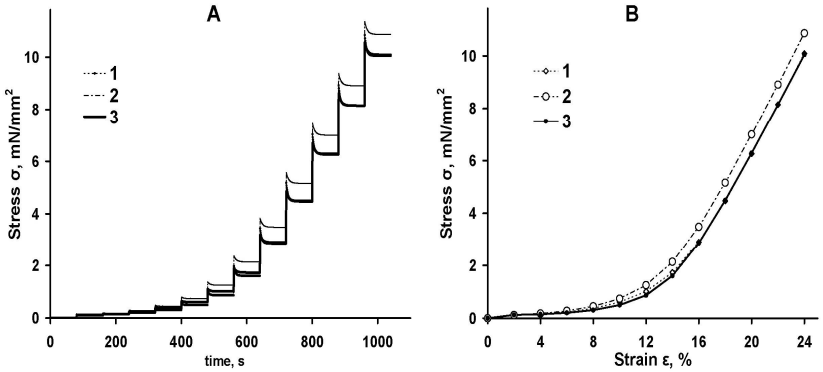

Fig. 1. Stress relaxation of the model under stepwise stretching with increment equal 2% (A). Stress-strain dependence (B). Uniform model - dotted curves (1); geometrical non-uniform model - dashed curves (2); geometrical and viscoelastic non-uniform model - solid curves (3).

Parameters of structural elements of the model

	Uniform model		Geometrical non-uniform model		Geometrical and viscoelastic non-uniform model	
	(1)	(2)	(1)	(2)	(1)	(2)
k_1, mN/mm^2	5.00	5.00	5.00	5.00	2.40	1.4
k_2, mN/mm^2	10.00	10.00	10.00	10.00	10.21	9.25
k_3, mN/mm^2	0.50	0.50	0.50	0.50	0.50	0.20
k_4, mN/mm^2	0.50	0.50	0.50	0.50	0.50	0.20
η_1, mN/mm^2·s	2.00	2.00	2.00	2.00	0.50	0.50
l_2/l_0	0.95	0.95	0.93	0.95	0.93	0.95

in the case of uniform model the less stiff and viscous heterogeneous elements are required. This result suggests that the presence of heterogeneity in myocardium supports more efficient structural organization of slices in the myocardium.

This work is supported by RFBR Grant 10-04-00601-a and Project 12-Y-4-1009 of USC of the Ural branch of the RAS.

References

1. Brady A.J. Mechanical properties of isolated cardiac myocytes. // Physiol Rev. 1991. V. 71(2). P. 413-28.
2. Brutsaert D.L., Rademakers F.E., Sys S.U. Triple control of relaxation: implications in cardiac disease. // Circulation. 1984. V. 69(1). P. 190-6.
3. Markhasin V.S., Solovyova O., Katsnelson L.B., Protsenko Y., Kohl P., Noble D. Mechano-electric interactions in heterogeneous myocardium: development of fundamental experimental and theoretical models. // Prog Biophys Mol Biol. 2003. V. 82(1-3). P. 207-20.

4. Protsenko Y.L., Routkevitch S.M., Gur'ev V.Y., Katsnelson L.B., Solovyova O., Lookin O.N., Balakin A.A., Kohl P., Markhasin V.S. Hybrid duplex: a novel method to study the contractile function of heterogeneous myocardium. // Am J Physiol Heart Circ Physiol. 2005. V. 289(6). P. H2733-46.
5. Smoluk L.T., Protsenko Y.L. Mechanical properties of passive myocardium: experiment and mathematical model. // Biophysics. 2010. V. 55(5). P. 796-799.
6. Smoluk L.T., Protsenko Y.L. Viscoelastic hysteresis of papillary muscle. // Russian Journal of Biomechanics. 2011. V. 52(2). P. 24-31.
7. Sweitzer N.K., Moss R.L. Determinants of loaded shortening velocity in single cardiac myocytes permeabilized with alpha-hemolysin. // Circ Res. 1993. V. 73(6). P. 1150-62.

NOVEL APPROACH TO STUDYING RELATIONSHIP OF 3D STRUCTURE AND MECHANICAL PROPERTIES OF BIOLOGICAL TISSUE

L.T. Smoluk, A.T. Smoluk, Y.L. Protsenko

Institute of Immunology and Physiology of the Ural Branch of the RAS, 620049, Pervomayskaya st., building 106, Ekaterinburg, Russia

Biological tissues exhibit a highly complex nonlinear mechanical behavior which includes active, quasi-incompressible, fibre-reinforced, viscoelastic and hyperelastic behavior [**2**]. The spatial organization of biological tissues largely determines mechanical properties and functions performed by these tissues. In our work we aim to develop a novel approach to studying of the relationship of three-dimensional internal structure and mechanical properties of myocardial tissue as an example of living biological tissue.

By our early developed mathematical model of viscoelastic properties of the myocardium samples it has been shown the spatial reorganization effect of myocardial structural parts under the strain of the sample could be significant [**5, 6**]. Also in numerical experiments it is established that the viscoelastic properties of real myocardial tissue samples are determined by geometry of the sample. By the model it is predicted that myocardial tissue should show structural elasticity and viscosity causing by the changing of relative position of the main sources of passive tension in the myocardium. Myocardium has complex composite structure but the main sources of passive tension in the myocardium are connective tissue matrix and cardiac myocytes. It should be noted that myocytes in the myocardium can connect to each other sequentially, parallel or angularly. Thereby the myocytes form certain groups surrounded by common connective tissue – perimysium. Herewith the myocytes are surrounded by endomysium – meshwork of single collagen fibers diameter of 10-40 nm [**4**].

We present here a novel approach to study the relationship of three-dimensional internal structure and mechanical properties of living biological tissue as example of myocardial tissue. It is well known that mechanical properties of the myocardium would be changed strongly with various pathologies like hypertrophy, ischemia, myocardial infarction and others [**1, 3, 7**]. It is also known that for example at hypertrophy the structural organization of the myo-

cardium is changed considerably too. Therefore the studying of relationship of internal structure and mechanical properties of the myocardium is an urgent problem. It is significant to note that there are no experimental data about changes of internal structure of myocardial tissue samples under the strain as we know. To get the goal of the study it should be developed an experimental set allowing record mechanical properties and three-dimensional image of the internal structure of the biological tissue sample simultaneously.

The subjects of our investigation are isolated right ventricular papillary muscles depth up to 200 micrometer, length up to 3 millimeter. Experimental animals are Wistar rats of the age 2.5-3 month of both sexes. The papillary muscle is put into temperature-controlled bath (25^0C) with flowing Krebs-Ringer solution. One end of the preparation strip is tied to the stock of the force transducer and the second end to the rod of the length servomotor (Muscle Research System, Scientific Instruments GmbH, Heidelberg, Germany). Comparatively low temperature of the solution allows to decrease the velocity of fluorescence dye (Direct Red, Sigma-Aldrich) degradation and to improve the stability of biomechanical properties of the samples.

Biomechanical properties of the muscles could be record under different strains. Simultaneously the scan series of the images of internal structure of the samples is recorded by the confocal laser scanning microscope LSM-710 (Carl Zeiss, Germany). Our pilot experiments have shown that the condition of the samples remains stable in steady-state during a few minutes. Using 40x objective the scanning area will be 350 to 350 micrometers along x and y axis. The scanning area is up to 200 micrometers along z axis regardless of the selected objective. Thus Z-axis scanning range imposes constraints on the muscle depth and we should select rather thin preparations. Z axis displacement will be 1 micrometer (it is possible to change the displacement if needed). Scan speed will be up to 5 frames per second at the frame resolution 512 to 512 pixels. It is possible to increase the frame resolution up to 6144 to 6144 pixels if needed (in this case the scan speed will be decrease proportionally). The combination of the frame series will be carried out by special software 3D for LSM (Carl Zeiss, Germany). Using the combination of the Muscle Research System and LSM-710 complex it could be recorded the spatial three-dimensional internal structure of the preparation under different strains.

Thus the proposed approach to study the relationship of three-dimensional internal structure and mechanical properties of the myocardial tissue allows to define the amount of influence of structural alterations in the tissue to its mechanical response. In additional the approach permits to understand more profoundly the mechanisms of the tension development and deformation of any living soft tissue.

This work is supported by RFBR Grant 10-04-00601-a and Project 12-Y-4-1009 of USC of the Ural branch of the RAS.

References

1. Bing O.H., Matsushita S., Fanburg B.L., Levine H.J. Mechanical properties of rat cardiac muscle during experimental hypertrophy. // Circ Res. 1971. V. 28(2). P. 234-45.

2. Fung Y.C. Biomechanics: mechanical properties of living tissues. B 2nd ч. 1993. New York. Springer C.
3. Jalil J.E., Doering C.W., Janicki J.S., Pick R., Shroff S.G., Weber K.T. Fibrillar collagen and myocardial stiffness in the intact hypertrophied rat left ventricle. // Circ Res. 1989. V. 64(6). P. 1041-50.
4. Robinson T.F., Cohen-Gould L., Factor S.M., Eghbali M., Blumenfeld O.O. Structure and function of connective tissue in cardiac muscle: collagen types I and III in endomysial struts and pericellular fibers. // Scanning Microsc. 1988. V. 2(2). P. 1005-15.
5. Smoluk L.T., Protsenko Y.L. Mechanical properties of passive myocardium: experiment and mathematical model. // Biophysics. 2010. V. 55(5). P. 796-799.
6. Smoluk L.T., Protsenko Y.L. Viscoelastic hysteresis of papillary muscle. // Russian Journal of Biomechanics. 2011. V. 52(2). P. 24-31.
7. Stroud J.D., Baicu C.F., Barnes M.A., Spinale F.G., Zile M.R. Viscoelastic properties of pressure overload hypertrophied myocardium: effect of serine protease treatment. // Am J Physiol Heart Circ Physiol. 2002. V. 282(6). P. H2324-35.

THE MOTILITY OF RATS IN THE OPEN FIELD TEST UNDER THE CONDITIONS OF ALTERED PHOTOPERIOD

I.Yu. Sopova, I.I. Zamorskii

Bukovinian State Medical University,
Teatralnaya pl. 2, Chernovtsy, 58002, Ukraine

The rats' motility in the open field test under the conditions of an altered photoperiod has been studied. The research was executed on the 48 juvenile male rats. In the open field within 3 minutes the next parameters were registered: horizontal activity, vertical locomotor reactions, mink reflex. The animals were contained during one week in conditions of usual (natural conditions of illumination) and altered (constant darkness, constant light) photoperiod after preliminary passage of the open field test. Then the behavior of animals was studied again in the open field.

Preliminary research has been shown that all 3 groups of animals authentically did not differ in parameters of the behavior reactions: horizontal activity was 20-30 squares, vertical locomotor reactions were 5-10 racks. The differences in the motility rates in the groups under study were observed after different lighting conditions.

In conditions of normal photoperiod the motor activity of animal remained similar to previously fixed parameters. The physical activity of rats in the darkness was declined: the horizontal activity in 2.3 times ($F_{1,12}$=90,24, p=0,00001), vertical movements in 3.7 times ($F_{1,12}$=76,56, p=0,000001), mink reflex in 2-fold ($F_{1,12}$=30,27, p=0,0001). The correlation parameters of locomotor activity with previous data was changed in animals that were in the continuous light: horizontal locomotion increased in 1.5 times ($F_{1,12}$=44,42, p=0,00002) and horizontal activity decreased in 1.7 times ($F_{1,12}$=17,47, p=0,013). Thus, the analysis of dynamics of components of locomotor activity in experimental animals shows that under the influence of the altered photoperiod there is an adaptive reorganization of behavior which

depends on character of illumination. The exploratory components of behavior were depressed in animals in the constant darkness. The adaptation of spontaneous locomotor activity was changed by balance of components of motility in animals in the constant light.

NONLINEARITY OF MUSCLE LENGTH ALTERATIONS UNDER CONTROLLED CHANGES OF EXERTION AND EFFERENTS STIMULATION FREQUENCY

V.M. Soroka, D.M. Nozdrenko, I.I. Bardadym

Taras Shevchenko Kyiv National University, Department of Biophysics, Volodimirska Str., 64, 01033, Kyiv, Ukraine

Muscle is the most inertial element of the motion system, so its dynamics largely underlines properties of real movements. Based on many experimental data there it no doubt that the dynamics of muscle contraction is nonlinear, firstly due to the hysteresis of muscle contraction which in some cases causes the differences in establishing of the muscle length equilibrium.

Experiments were performed on adult rats weighing from 0.2 to 0.3 kg. During preparations for experiments anesthesia was carried out by intraperitoneal nembutal injections (40 mg / kg). Standard preparation includes also dissection, cannulation (for drugs injections and measurement of pressure), tracheotomy, laminectomy at the lumbar level of the spinal cord. For preparations to modulated efferent stimulation, ventral nerve roots were cut at the segments L7-S, directly in sites of their brunching out from the spinal cord. Force changes were measured by four strain gauges, glued on both sides of the steel plate and included in the measuring circuit. Measurements of muscle length was performed by precision potentiometer sensor.

Muscle contraction is characterized by prolonged aftereffect, which leads to dependence of the movement, directly associated with the initial external conditions, to this external conditions changes, that affect the contractile properties of muscle. This important property of movement reactions is shown in Fig. 1, where changes of steady-state level of external exertion are shown that allowed to explore a wide physiological range of the length changes. In the range of lengths that exceed the length of the relaxed muscle, component of the length changes was decreased, and its average level shifted toward stretching. Comparison of the muscle response to external exertion changes with frequency-modulated afferent trapezoidal stimulation showed that corresponding points of length changes inflections didn't match with motion character in linear disturbance of external exertion.

Change of the external exertion caused asymmetric motor reaction with fast first phase of contraction and subsequent slow decline. With increasing of exertion almost always an increase of residual muscle strain was observed, features of such behavior of active muscle can be explained by asymmetry of lengthening and shortening in time, and also hysteretic effects of muscle contraction.

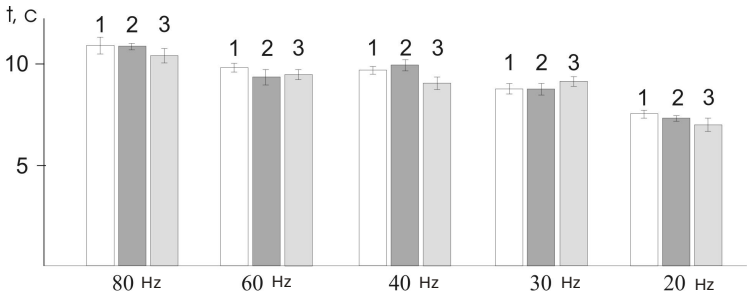

Fig. 1. Chart shows the changes of the time requred to achieve equilibrium steady contraction state. 1, 2, 3 - level of external exertion. 0.4, 0.3 and 0.2 N / m.

It should be noted that another important nonlinear property of described muscle contraction was present, which was revealed in the following changes of the external exertion. It is known that for linear dynamic systems principle of superposition is valid which states that system reaction on the amount of interactions should coincide with the sum of responses to each input applied separately. If this principle applies to the described dynamic systems, an external exertion - muscle length, the response to the second exertion cycle would be summed with the reaction to the first cycle and the amplitude of the second reaction stretching would cause greatly larger output level. Instead, an almost complete coincidence of the amplitudes of successive cycles of muscle stretching was observed.

The difference between the movement behaviors was more pronounced under conditions of muscle unloading. On the one hand side, this may be caused by the differences in shortening and elongation dynamics development, what should result to more prominent delays of movement in phases of shortening, but on the other hand side, movement differences in the shortened muscle could be increased by reducing steepness of static characteristics: length - force. Therefore, we believe that nonlinear dependence of steepness of static characteristics: length – force such as reducing the length of muscle, was the main cause of the observed harmonic fluctuation oscillations in the range of short lengths.

Thus Fig. 2 shows dependence of the rat soleus muscle rate from external exertion at reduced stimulation frequency from max (80 Hz) level to the stationary level of ther stimulating signal (20 Hz).

The absence of summation of active muscle reactions during linear changes of efferent stimulation can be explained by hysteretic properties of muscle contraction. This characteristic of motion reactions is pronounced when using modulated efferent stimulation in combination with previous changes of external exertion. Slight increase of growth speed of efferent stimulation signal frequency on phases of its sinusoidal site led to the forming of another movement character with different contraction velocity, which was dependent on the direction of the previous movement.

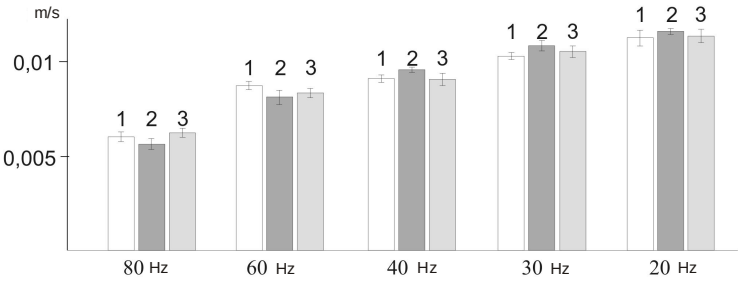

Fig. 2. The dependence of rat soleus muscle rate from external exertion at reducing of stimulation frequency from max (80 Hz) level to the stationary level of the stimulating signal (20 Hz). 1, 2, 3 - levels of external exertion 0.4, 0.3, 0.2 N/m.

Thus, stable non-linear changes in muscle strength, consisting from its increase during the previous extension and decrease in shortening, leading to differences in establishing of equilibrium muscle length depending from the previous history of its movement.

These results suggest that hysteresis of muscle contraction is characterized by prolonged aftereffect, which results in dependence of motion character on changes in external exertion and efferent stimulation, from motion prehistory and prehistory of muscle exertion. Development of hysteretic effects at various lengths in the physiological range of muscle contraction was unequal. With the shortening of muscle length the distance between the static characteristics of shortening and lengthening was decreased, which later manifested itself in features of muscle motion response formation when changing pyramidal efferent signal.

Nonlinear effects arising in the muscle as a result of exponential changes in length, leading to phase advance of force: extreme values of force was significantly ahead of those corresponding extreme values of lengths. Thus, stable non-linear changes in muscle strength, consisting of its increase during the previous extension and decrease in shortening, leading to differences in establishing of equilibrium muscle length depending on the previous history of its movement.

INTERACTION OF 14-3-3 WITH COFILIN AND PROBABLE PARTICIPATION OF SMALL HEAT SHOCK PROTEIN HSPB6 AND 14-3-3 IN REGULATION OF SMOOTH MUSCLE CONTRACTION

M.V. Sudnitsyna, A.S. Seit-Nebi, N.B. Gusev

Department of Biochemistry, School of Biology, Moscow State University, Moscow 119991, Russia

Object. The small heat shock protein HspB6 is recognized as potential modulator of smooth muscle contraction. Phosphorylated HspB6 and its cell-penetrating phosphorylated peptide are considered as therapeutically important smooth muscle relaxant. The molecular mechanism of relaxation induced by

HspB6 remains elusive. In order to explain the mechanism of HspB6-induced relaxation C. Brophy et al. put forward the following hypothesis. Phosphorylated cofilin tightly interacts with universal adapter protein 14-3-3 which protects cofilin from dephosphorylation. Hormonal stimulation induces HspB6 phosphorylation. Phosphorylated HspB6 displaces cofilin from its complex with 14-3-3. Liberated cofilin is rapidly dephosphorylated by protein phosphatases and induces reorganization of actin filaments leading to smooth muscle relaxation. This hypothesis might be correct only in the case if both phosphorylated cofilin and phosphorylated HspB6 possess comparable affinities to 14-3-3. However, direct interaction of cofilin with 14-3-3 was not analyzed in detail and was not compared with interaction of HspB6 with 14-3-3.

Methods. The method of far western blotting (overlay) was utilized for analysis of binding of baits (cofilin and HspB6) with 14-3-3 immobilized on nitrocellulose. Direct interaction of unphosphorylated and phosphorylated cofilin with 14-3-3 in solution was analyzed by means of native gel electrophoresis, chemical crosslinking and size-exclusion chromatography. Effect of 14-3-3 on the binding of phosphorylated and unphosphorylated cofilin to F-actin was analyzed by means of cosedimentation. Interaction of cofilin with G-actin and effect of 14-3-3 on this interaction was investigated by native gel electrophoresis.

Results. Recombinant human 14-3-3ζ was spotted on nitrocellulose and after drying the nitrocellulose strips were incubated with either HspB6 phosphorylated by cAMP-dependent protein kinase or with cofilin phosphorylated by activated LIM-kinase. Phosphorylation was performed in the presence of radioactive ATP and therefore both bait proteins carried radioactive phosphate. After incubation with bait protein which was performed in the presence of large excess of bovine serum albumin the strips of nitrocellulose were thoroughly washed and subjected to autoradiography. At low protein concentration neither HspB6 nor cofilin were bound to immobilized 14-3-3, however at bait concentration of 0.4 mg/ml both proteins interacted with immobilized 14-3-3 with comparable affinities. Although all precautions were undertaken in order to prevent non-specific binding, we cannot exclude that interaction detected reflects binding of analyzed protein-partners to immobilized on nitrocellulose and therefore non-native 14-3-3. Therefore different methods were used for investigation of direct interaction of 14-3-3 and cofilin in solution. By using native gel electrophoresis or chemical crosslinking we were unable to detect tight interaction of either unphosphorylated or phosphorylated cofilin with 14-3-3. At the same time both native gel electrophoresis and chemical crosslinking clearly demonstrated formation of tight complexes of phosphorylated HspB6 and 14-3-3. Size-exclusion chromatography failed to detect formation of complexes formed by 14-3-3 and either unphosphorylated or phosphorylated cofilin, whereas the same technique revealed formation of equimolar complexes of phosphorylated (but not unphosphorylated) HspB6 with 14-3-3. Moreover dimer-deficient mutant of 14-3-3 formed equimolar complexes with phosphorylated HspB6, however was not able to form tight complexes with either

unphosphorylated or phosphorylated cofilin. If cofilin interacts with 14-3-3, then it should affect binding of cofilin to F- and/or G-actin. Using the method of cosedimentation we analyzed effect of 14-3-3 on the binding of cofilin to F-actin. Under different conditions used (pH 6.5 and 8.0, different ionic strength and different molar ratio cofilin/actin) we were unable to detect any significant effect of 14-3-3 on the binding of cofilin to F-actin. In all experiments 14-3-3 remained in supernatant and did not affect distribution of cofilin between the supernatant and pellet containing F-actin. Phosphorylated cofilin weakly interacted with F-actin, however even in this case 14-3-3 was not able to retard cofilin in the supernatant and equal small portion of phosphorylated cofilin was detected in F-actin pellet independent on the presence or absence of 14-3-3. Native gel electrophoresis performed in the presence of ATP clearly indicated that unphosphorylated cofilin interacts with G-actin, whereas 14-3-3 under condition used was not able to interact with G-actin and did not affect formation of G-actin-cofilin complex.

Conclusions. Cofilin weakly binds to 14-3-3 immobilized on nitrocellulose. However, native gel electrophoresis, chemical crosslinking and size exclusion chromatography failed to detect formation of tight complexes between 14-3-3 and unphosphorylated or phosphorylated cofilin, whereas the same techniques clearly demonstrated interaction of phosphorylated HspB6 with 14-3-3. Thus, tight complexes of phosphorylated cofilin and 14-3-3 are not formed in the cell and therefore phosphorylated HspB6 cannot directly induce dissociation of these complexes, as it was suggested by Brophy et al. 14-3-3 did not affect interaction of cofilin with either F- or G-actin. Therefore, the data presented exclude participation of direct interaction of cofilin and 14-3-3 in regulation of smooth muscle contraction. However, 14-3-3 and HspB6 can be involved in the indirect cofilin-dependent reorganization of actin cytoskeleton. It is well-known that 14-3-3 binds and inhibits slingshot phosphatase dephosphorylating cofilin. Taking into account that concentration of HspB6 is much higher than that of slingshot phosphatase we can suppose that phosphorylated HspB6 can displace slingshot phosphatase from its complex with 14-3-3 and by this means activate cofilin dephosphorylation leading to smooth muscle relaxation. Further investigations are needed to confirm or reject this suggestion.

Acknowledgements. This investigation was supported by Russian Foundation for Basic Science.

HELICITY OF FLAGELLAR FILAMENTS IN DIFFERENT HALOARCHAEA CAN BE PROVIDED BY DIFFERENT MECHANISMS

A.S. Syutkin, M.G. Pyatibratov, S.N. Beznosov, O.V. Fedorov

Institute of Protein Research, Russian Academy of Sciences, Pushchino, Russia

Bacteria and Archaea use a rotation of helical flagellar filaments for motility in liquid media. Flagellar filament of Enterobacteria consists of only

one type of protein (flagellin) arranged into 11 longitudinal rows and each row consists of subunits in only one (R or L) conformational state. For most of known archaea their flagella are composed of several types of protein subunits named “flagellins” also. Archaeal flagellins have remarkable homology with each other and have not homology with bacterial flagellins.

Flagellar filaments of haloarchaea *Halobacterium salinarum* consist of five flagellins (A1, A2, B1, B2 and B3) which are encoded by five different genes located tandemly in two loci. Earlier we have demonstrated that two different *H. salinarum* flagellins (A1 and A2) of are necessary and sufficient to form a longitudinal and spiral filament. The cells of mutant strains with only one flagellin(A1 or A2) had straight flagella. Thus, the multicomponent nature of flagella from *H. salinarum* may be explained by the requirement of two flagellins for the formation of a flagellar filament with a spiral shape (Tarasov et al., 2000). Additional flagellins (B1-B3), probably, play an accessory role, taking part in the final stage of flagellar assembly.

In presented work we investigated a protein composition of flagellar filaments of other haloarchaea Haloarcula marismortui. The genome of haloarchaea Haloarcula marismortui carries two flagellin genes, flaA2 and flaB. Previously, we demonstrated that the helical flagellar filaments of H. marismortui are composed primarily of single flagellin (FlaB) molecules and the second flagellin (FlaA2) is present in minor amounts (Pyatibratov et al., 2008).

In this study we describe insertional mutant *H. marismortui* strains with inactivated A2 and B flagellin genes. It was shown that inactivation of the *flaA2* gene does not lead to changes in cell motility and helicity of filaments, while the cells with inactivated *flaB* lose their motility because of their flagella synthesis is stopped. The results shown that functional helical flagella of haloarchaea can consist of only one flagellin. Using trypsin digestion we found two FlaB flagellin forms having different sensitivities to proteolysis in the flagellar filament structure and having different chromatographic properties. We hypotesized that these flagellin forms can enshure the helical filament formation.

Moreover, we investigated a protein composition of flagellar filaments of psychrotrophic haloarchaea *Halorubrum lacusprofundi.* Formerly, this microorganism was considered as motionless, but recently after its full genome sequencing, the motility-related genes were identified. In contrast to most archaea only one flagellin gene (*flaB*) is present in *H. lacusprofundi* genome. We succeeded in finding conditions favorable for *H. lacusprofundi* motility and have purified and characterized their flagellar filaments. The results of electron microscopy shown that *H. lacusprofundi* produce helical flagella. It is an additional evidence that helical l flagella of haloarchaea can assembly from only one flagellin. Ion-exchange chromatography showed, like *H. marismortui,* the presence of severalforms of FlaB.

The results suggest that the mechanisms of flagellar helicity may differ in different haloarchaea and the presence of two flagellin genes is not strongly necessary (as in the case of *Halobacterium salinarum*) condition for the formation of functional helical flagellum.

This work was supported by grant No. 09_04_0110 from the Russian Foundation for Basic Research.

References

1. Tarasov VY, Pyatibratov MG, Tang SL, Dyall-Smith M, Fedorov OV. Mol Microbiol 2000; 35(1):69-78.
2. Pyatibratov MG, Beznosov SN, Rachel R, Tiktopulo EI, Surin AK, Syutkin AS, Fedorov OV. Can J Microbiol 2008; 54(10):835-44.

ADAPTABLE FEATURES OF CYCLIC WORK AS HANDS AND FEET

R.V.Tambovtseva

Institute of age physiology of the Russian Open Society, Pogodinsky street 8, Moscow, 119435, Russia

For the purpose of an estimation of age features of reaction of physiological systems on loading for the top and bottom extremities, investigated ergometric indicators at cyclic work of different capacity at boys from 7 till 17 years, and also reaction of vegetative systems and indicators of power production at boys 10-11 and the young man of 16-17 years. During research it has been shown that time of deduction by hands of cyclic loadings in a zone of the big capacity at 5-20 time exceeded a limiting operating time in a zone of the submaximum capacity. Accordingly, the same distinctions are registered in volume of the performed work. If to consider relative sizes the volume of the performed work in a zone of the submaximum capacity till 13 years appears above at work as hands, and after 14 years – at work as feet. In a zone of the big capacity working capacity of hands above till 16 years, and only after that age working possibilities of muscles of feet become more. Thus, at younger school age of a hand appear rather more developed, and only at the closing stages of puberty of a muscle of feet reach such level of development at which their working possibilities appear above. The dimensionless factor "and" Müller's equations at work as hands in the majority of age groups has appeared above, than at work as feet. It means that dependence of limiting time of deduction of loading on its capacity for muscles of hands, as a whole, more strongly, than for muscles of feet. Dynamics of an indicator maximum anaerobic the capacity calculated on the equation of Müller for muscles of hands sharply contrasts with its rather uniform increase with the years for muscles of feet. The sharp peak having on age of 12 years, testifies to sharp reorganizations in a power profile of muscles of the top extremities in puberty. After its end the given indicator for hands it becomes authentic more low, than for feet. Such parity can mean some prevalence in muscles of hands of aerobic processes anaerobic, except the puberty period. Size W40 characterizing capacity anaerobno-glikoliticheskogo of an energy source, counting on unit of muscular weight of hands in the majority of age groups significantly more than muscles of feet, though in both groups of muscles considerably increase in this indicator with the years. It reflects age increase in possibilities anaerobno-glikoliticheskogo an energy source. Thus, the general orientation of age development of power of muscles of hands as a

whole is similar to similar dynamics for muscles of feet. At the same time, both in dynamics processes, and in rates of development of power systems in muscles of hands there is a number of features. In prepubertate the period at boys of a muscle of hands morphofunctionale developments surpass muscles of feet in level of the. In puberty there are the most complicated reorganizations in power of muscles, and after its end of a muscle of feet appear more powerful and a little more hardy. As work in this series of researches was made "to the full", it was possible to expect that its labor input will be shown in dynamics of repayment pulse a debt. Before puberty at work as hands in both zones of capacity the smaller size of intensity of accumulation pulse a debt is observed, and after its end of size ИНПД at work as hands and feet are leveled or even become slightly more low at work as feet. It means that physiological labor input of work as hands before puberty more low, than at work as feet. Possibly, it is caused greet by degree morphofunctionale a maturity of muscles of hands at this age stage. Thus 5-10-кратная the difference in sizes of intensity of accumulation pulse a debt in zones of the big and submaximum capacity remains throughout all studied period ontogenese both at work as hands, and at work as feet. Received in process ergometric researches results have revealed serious qualitative distinctions in dynamics of development of power of muscles of the top and bottom extremities. The total volume of work executed in the test of in steps raising capacity before "refusal", at the age of 10 years at calculation on 1 kg of weight of muscles above when hands work. However in 16 years specific volume of work above at loading on muscles of feet. Thus, specific working capacity of muscles of hands during the period from 10 till 16 years decreases a little, and muscles of feet – practically doesn't change. The absolute size of critical capacity at which is registered МПК, during the period from 10 till 16 years increases approximately in 2 times as at work top, and the bottom extremities. Thus the specific size of critical capacity is almost identical to both groups of muscles and doesn't change almost with the years, making about 20 Vt/kg of weight of muscles. Such contrast of specific critical capacity can mean that the fabric mechanisms providing activity of an aerobic energy source, are developed approximately equally in the muscles belonging to different groups, and remain almost invariable during the period from 10 till 16 years. Apparently, the size of limiting capacity of weight of muscles of 20 Vt/kg can be considered as one of important biological constants of an organism. Specific size МПК for each of groups of muscles remains invariable from 10 till 16 years, but a difference between specific sizes МПК at work as feet and hands – more than double. From this it is possible to assume that size МПК depends not so much on weight of the muscles put into operation, how many from degree of participation of other fabrics in an oxidizing exchange in the course of muscular activity. It is important to underline that absolute size МПК at work as feet authentically above, than at work as hands. Specific capacity of loading at which it is reached anaerobic a threshold, for muscles of hands in 10 years in 1,8 times above, than for muscles of feet. This result korrespondire with very high size of factor "To" of Müller's equation at work as hands at 10-year-old age. Judging

by this data, during this age period aerobic possibilities of muscles of hands are well developed, whereas anaerobic are rather insignificant, what it is possible to judge, for example, on size of MUMS. By 16 years capacity АП for hands decreases almost twice, coming nearer to a similar indicator for muscles of feet. It is interesting that pulse characteristics АП are identical or very close at work as hands and feet. The analysis of dynamics of shock emission of heart at work as hands and feet have allowed to establish that capacity anaerobic a threshold is the top border of increase in shock emission of heart, and further at increase of intensity of loading this indicator either doesn't grow, or decreases. It is not excluded, what exactly restrictions from heart are one of the activation reasons anaerobic a metabolism in working muscles of extremities. Total expenses of energy have changed with the years more or less proportionally to volume of the performed work. As a result of EFFICIENCY of work from 10 till 16 years hasn't undergone authentic changes and remained essentially above at work as feet that speaks about smaller profitability of work as hands. Expansion anaerobic possibilities is more expressed with the years at work as hands if to judge it on size of the oxygen debt formed during performance of the test of in steps raising capacity to the full. Size ОКД at work as hands from 10 till 16 years has grown approximately in 5 times, whereas at work as feet – only in 3,3 times. Thus on absolute size ОКД after work as hands and feet it is almost identical. It can be illustrated by dynamics of repayment of an oxygen debt after work as hands and feet in the test of in steps accruing capacity before "refusal" at young men of 16 years. Structure OKD changes with the years unidirectionally both at work as hands, and at work as feet: basically the gain of volume ОКД is provided by increase in its slow fraction characterizing capacity anaerobnoglikoliticheskogo of an energy source. The share of fast fraction thus considerably decreases, especially at work as hands. The analysis of specific sizes of an oxygen debt hardly has strict physiological sense as the debt can't be recognized by function of actually skeletal muscles. About it tells practical equality of sizes ОКД at work as the top and bottom extremities both at boys of 10 years, and at young men of 16 years. Clearly that differing at least in 2 times on weight of group of muscles, having made about identical work on relative volume, couldn't influence a chemical compound of the internal environment of an organism with which restoration usually connect an oxygen debt equally. Hence oxygen debts and its repayment represent, apparently, system process at level of the whole organism, only in small degree depending on weight of the skeletal muscles directly participating in work. Given results allow to be convinced once again that parameters of capacity of power systems is defined, mainly, by a condition of fabric mechanisms, whereas capacity an essence the phenomenon, depending first of all from regulator possibilities of the systems providing maintenance of a homeostasis at level of cages, fabrics and the whole organism. If to accept that adequate characteristics of working capacity are capacitor indicators, from presented a conclusion: working capacity is the concept characterizing possibilities not of separate muscular groups, and an organism as a whole.

DEVELOPMENTAL CHANGES OF PHARMACOMECHANICAL AND ELECTROMECHANICAL COUPLING IN ARTERIAL SMOOTH MUSCLE

O.S. Tarasova[1,2], R. Schubert[3]

[1]M.V. Lomonosov Moscow State University, Leninskie Gory 1/12, 119234, Moscow, Russia

[2]SRC RF - Institute for Biomedical Problems RAS, Moscow, Russia

[3]Cardiovascular Physiology, Centre for Biomedicine and Medical Technology Mannheim, Ruprecht-Karls-University Heidelberg, Mannheim, Germany

Vascular smooth muscle (VSM) is the result of several consecutive steps: activation of receptors of the plasma membrane, influx of Ca^{2+} into the cytoplasm from the extracellular space and from intracellular stores and subsequent interaction of Ca^{2+} with the contractile machinery. Often, the contraction is simultaneously augmented as a result of sensitization of the contractile machinery to Ca^{2+} (Somlyo & Somlyo 2003). Mechanisms of smooth muscle contractions in vessels from fetal and/or neonates differ from those in vessels from adults. We have shown recently that maturation of VSM is associated with a growing role of Ca^{2+}-dependent mechanisms of contraction (Tarasova et al., 2009). Contrarily, in newborn animals VSM contraction during both receptor and non-receptor stimulation is mainly due to Ca^{2+}-sensitization of the contractile machinery and may occur on a background of an almost unchanged intracellular concentration of Ca^{2+} (Mochalov et al. 2008). This observation raises the question about the maturity of mechanisms regulating calcium homeostasis in VSM during early postnatal life. Special attention should be paid to L-type calcium channels as the major source of contractile Ca^{2+} in VSM (Thorneloe & Nelson 2005). The open state of these channels is regulated by membrane potential and can be modulated by intracellular signaling pathways that are activated, in particular, by α_1-adrenergic receptors. In this study we tested the hypothesis that the absence of a $[Ca^{2+}]_i$ change in newborns is due to the immaturity of mechanisms regulating membrane potential (MP), a main determinant of L-type calcium channel activity.

The experiments were performed on saphenous arteries of male Wistar rats aged 9-11 days ("newborn", n=8) and 2-3 months ("adult", n=6). The strong point of this study was the simultaneous recording of isometric artery contraction and MP at a precisely controlled degree of wall stretch. Wall stretch was set at the level where VSM contraction during the action of different regulatory stimuli was maximal. Passive and active wall tensions were recorded using wire myography (Mulvany, Halpern 1977). Intracellular recordings of MP were obtained by using sharp aluminosilicate glass, KCl-filled (3 M) microelectrodes with resistances in the range of 40–100 MOhm as previously described (Schubert et al. 1996). Input resistance was evaluated throughout the experiment by injecting 1-nA current pulses (25 ms) and measuring the subsequent potential change. An Ag-AgCl electrode in the organ bath was used as a reference electrode. The effects of methoxamine

(10^{-5} M), an agonist of α_1-adrenoceptors, and K^+-depolarization (42 mM) on wall tension and MP were investigated.

In the presence of Ca^{2+} (1.6 mM) in the extracellular solution resting MP in newborn rats (-43±3.0 mV) was more depolarized than in adults (-56±2.3 mV, $p<0.05$). This difference in MP level is much larger than observed earlier for non-stretched arteries (Sandow et al. 2004) and may be explained by a greater sensitivity of juvenile arteries to stretch.

The maximal contractile response (120 mM KCl + 10^{-5} M methoxamine) comprised 8.1±0.9 mN/mm in adult rats and 1.9±0.2 mN/mm in newborn rats ($p<0.05$). In response to methoxamine (10^{-5} M) the vessels of adult rats contracted to 89.3±7.7% of maximum (n=6), whereas in newborn rats the contraction was smaller: 54.3±6.5% of maximum (n=8) ($p<0.05$). Responses to VSM depolarization (K^+, 42 mM) were similar in the two experimental groups: 64.0±3.2% (n=6) and 70.3±4.2% (n=8) correspondingly.

Methoxamine induced depolarization of VSM was two-fold smaller in newborn (13±2.4 mV) than in adult arteries (26±1.6 mV, $p<0.05$). Noteworthy, this difference can not be explained by the more depolarized resting MP, since the depolarizing and contracting effects of high-K solution were not different in the two groups (28±3.3 mV and 23±1.9 mV, respectively). The smaller methoxamine-induced responses in newborn compared to adults rats despite similar K^+-induced responses suggest an immaturity in the part of the signalling pathway containing the receptor and the depolarizing ion channels.

VSM depolarization may result from opening of non-selective cation channels; the depolarizing influence of these channels is higher in Ca^{2+}-free solution (Wolfle et al., 2010). However, in our study VSM depolarization on transition from 1.6 mM to 0 mM of $[Ca^{2+}]_o$ was similar in adult and newborn rats (17±3.3 mV and 16±2.5 mV, $p>0.05$). Moreover, the depolarizing effect of methoxamine in Ca^{2+}-free solution was still larger in adult compared to newborn rats, whereas no difference was observed in response to treatment with high-K^+ solution. Therefore, mechanisms different from non-selective cation channel activation may contribute to the smaller sensitivity of MP to activation by α_1-adrenoceptors in VSM of newborn rats.

The results of our study show that both receptor and non-receptor activating stimuli are able to produce significant VSM depolarization in newborn rats. Therefore, the data obtained don't support our hypothesis that the smaller rise of the intracellular calcium concentration during physiological interventions in newborn rats is due to immaturity of MP control. It should be noted, however, that intracellular signaling pathways leading to Ca^{2+}-sensitisation of VSM contraction can be activated by membrane depolarization per se and that this effect is dissociated from the rise of intracellular Ca^{2+} (Yanagisawa, Okada, 1994). Such a signal transduction system from the sarcolemma regulating the Ca^{2+} sensitivity of contractile elements in accordance to the level of membrane potential may be responsible for contraction of VSM in newborn animals on a background of an unchanged intracellular concentration of Ca^{2+}.

Supported by the RFBR (grant 10-04-01723-a) and the DAAD fellowship.

References

1. Mochalov SV, Schubert R, Tarasova OS The role of Rho-kinase in regulation of Ca^{2+}-sensitivity of saphenous artery contraction in newborn and adults rats. Acta Physiol Scand 193(Suppl. 664): 90, 2008.
2. Mulvany MJ, Halpern W. Contractile properties of small arterial resistance vessels in spontaneously hypertensive and normotensive rats. Circ Res 41: 19–26, 1977.
3. Sandow SL, Goto K, Rummery NM, Hill CE. Developmental changes in myoendothelial gap junction mediated vasodilator activity in the rat saphenous artery. J Physiol. 556: 875-886, 2004.
4. Schubert R, Wesselman JP, Nilsson H, Mulvany MJ. Noradrenaline-induced depolarization is smaller in isobaric compared to isometric preparations of rat mesenteric small arteries. Pflugers Arch. 431:794-796, 1996.
5. Somlyo AP, Somlyo AV. Ca^{2+} sensitivity of smooth muscle and nonmuscle myosin II: modulated by G proteins, kinases, and myosin phosphatase. Physiol Rev. 83:1325-1358, 2003.
6. Tarasova OS, Puzdrova VA, Tarasova NV, Mochalov SV, Vorotnikov AV, Schubert R. Rapid contractile phenotype of vascular smooth muscle is controlled by trophic influence of sympathetic nerves. Auton Neuroscience: Basic and Clinical. 149:86-87, 2009.
7. Thorneloe KS, Nelson MT. Ion channels in smooth muscle: regulators of intracellular calcium and contractility. Can J Physiol Pharmacol. 83:215-242, 2005.
8. Wölfle SE, Navarro-Gonzalez MF, Grayson TH, Stricker C, Hill CE. Involvement of nonselective cation channels in the depolarisation initiating vasomotion. Clin Exp Pharmacol Physiol. 37:536-543, 2010.
9. Yanagisawa T, Okada Y. KCl depolarization increases Ca^{2+} sensitivity of contractile elements in coronary arterial smooth muscle. Am J Physiol. 267:H614-621, 1994.

ATP AS POSSIBLE CHANGES THE MECHANISMS OF CONTRACTILE FUNCTION OF SKELETAL MUSCLE *IN VITRO* BY EXPERIMENTAL ALLERGY

A.Y. Teplov[1], A.M. Farkhutdinov[1], M.M. Minnebaev[1], V.I. Torshin[2]

[1]Kazan State Medical University, Butlerova str., 49, R-420012 Kazan, Russia
[2]People's Friendship University,
Miklukho-Maklaya 6, Moscow, Russia, 117198
E-mail: AlikTeplov@mail.ru

The purpose of the work is to study the role of exogenous ATP in the change mechanisms of contractile function of mice isolated striated muscles at protein sensitization: "slow" – musculus soleus, "mixed" - muscle diaphragm and "fast" - musculus extensor digitorum longus – m. EDL.

The complex researches were performed to investigate this problem. The results of exogenous ATP affection on: 1) the rates of contraction muscles response, caused by agonist carbacholine (CCh) and 2) the rate of non-

quanta secretion of acetylcholine (ACh) in a zone of a trailer plate (H-effect) of non-sensitized and sensitized mice were compared.

Materials and methods. Experiments were conducted on both sexes mice weighing 17-22 g. Animals were twice albumin sensitize (OS) with gel hydrate aluminum (2 mkg of dry gel substance + 150 mkg ovalbuminum in 0,5 ml of a physiological solution, "Sigma", USA) parenteral. The second injection was made in 14 days after the first one. Animals were got into experiment on a pique of sensitization – 7-10 days after the second sensitization injections. Mechanomiographic researches were conducted on a preparation of an isolated muscle in terms of an isometry. Skeletal muscle was stretched during 20 minutes with force of 500 mg at a constant perfusion by a solution Krebs type to maintain isometric and temperature at 20-21 C^0. Contraction was recorded by the photoelectric converter. Agonist CCh was investigated at submaximal concentration: for m. Soleus – $5x10^{-4}$M, an m. Diaphragm – $2x10^{-4}$M, m.EDL – $7x10^{-4}$M. Contraction function was analyzed according muscles contraction parameters on CCh.

To study a condition of muscle fiber postsynaptic membrane in the zone of a trailer plate non quantum secretion of Ach was studied. It was measured by glass microelectrodes (with the resistance of 8-12 MΩ, filled with 2,5 M KCl). To determine its size armin action acetylcholinesteraze, then on a muscle was eliminated during 8-12 minutes application m-cholinergic receptors blockade d-tubocurarine (10^{-5}M). The rates difference of membrane potential before and after application d-TC corresponds to the rate of non-quanta secretion of ACh (H-effect). Effect on muscle ATP («Boehringer Mannheim Gmbh», Germany) was evaluated by comparing the reduction targets before and after 5 min perfusion of a solution containing ATP at a given molar concentration ($1x10^{-4}$M), while its effect on the muscle was determined by the duration of perfusion.

The results obtained were subjected to statistical analysis (BIOSTATISTICA, SA Glantz, McGraw Hill). Data are presented as means ± Sx; n represents the number of animals. Statistical differences were determined by Student's t test for comparison of two sample means ($P<0.05$ was considered statistically significant).

Results and discussion. The experimental data show that the protein sensitization changes the contractile function of diaphragm strips as well as mice isolated tibia skeletal muscles. Moreover, the nature of changes of the "fast" muscles on the one hand, and of the "mixed" and "slow" muscles on the other hand differ substantially. The reasons are the initial differences of the morpho-functional status of the objects and the change mechanisms in the process of allergic reorganization of the organism. It should be noted that mice do not have movement muscles, consisting of only "slow" muscle fibers. M.soleus contains 50-60% of "slow" muscle fibers, m.EDL consists of "fast" muscle fibers at 97-100%. Mouse m.diaphragma occupies an intermediate position, and contains 88.6% of fast myosin.

Changes that occur in muscle fibers at sensitization affect the surface membrane. We have confirmed previously observed fact, that the opposite direction of muscular contraction force changes: - of "fast" muscle - declines, of "slow" and "mixed" muscles increases. Such dynamics indicates that the differences in changes at protein sensitization of "fast" muscles on the one hand, and "mixed" and "slow" muscles on the other hand affect, primarily cholinoceptive processes of the muscle fibers excitation and are of multidirectional nature for it.

The ability of protein sensitization to affect the postsynaptic membrane excitation mechanisms in various ways of the different muscles is confirmed by comparing the dynamics of muscle contraction force on CCh with the rate change of non-quantum secretion of ACh in a zone of a trailer plate It was shown that the vector of force change of observed muscles at protein sensitization correlates with the level change of non-quantum secretion of ACh in a zone of a trailer plate. We can assume that the decrease of contractile force of “fast” muscles on the CCh is the result from the decrease of postsynapse sensibility to cholinomediate. The evidence of this fact comes from the increasing H-effect. Increase of non-quanta secretion of Ach in the zone of synapse contributes intensification of desensitization mechanisms of cholinergic receptors of postsynaptic membrane. Correspondingly, we observe reverse picture about “mixed” and “slow” muscles. Increase of contractile force on CCh results from increase of postsynapse sensibility to CCh. Decreasing H-effect reflects this process.

Thus, the allergic alteration of an organism causes change in the contractile function of mouse isolated striated muscle. Contraction force at CCh of "fast" muscle is reducing, of "mixed" and "slow" muscles - is increasing. This rate change occurs from the following. Decrease of contractile force of “fast” muscle results from decrease of postsynaptic membrane sensibility to CCh that is caused by increasing of non-quantal secretion of Ach in the zone of a trailer plate. “Mixed” and “slow” muscles show reverse dynamics of contractile force as well as of non-quanta secretion of ACh. Increase of contractile force of these muscles on CCh at protein sensitization results from increasing postsynaptic membrane sensibility to cholinomediate that is caused by decrease of non-quanta secretion of Ach in the zone of a trailer plate. Different changes of contraction function of skeletal muscles at protein sensitization are caused, primarily, by dynamics of cholinomediated processes of membrane excitement of muscle fibers.

Mechanisms of co-factors selection of synaptic transmission are supposed to cause observed variability of functional properties of studied muscles at protein sensitization. We suggested possible purine involvement in the process of striated muscles function change at protein sensitization proceeding from Tsai T.L. et al. data that show the role of ATP in immune response generating. This fact prompted us the idea to study the dynamics of observed muscles functional properties (strips m.Diaphragma, m.Soleus and m.EDL) of sensitized and intact mice before and after incubation with ATP within selected experimental models.

It should be mentioned that the question of exogenous ATP influence on various skeletal muscles is of great value itself, because their functions regulation mechanisms with purines participation are so poorly investigated, in contrast to the smooth and cardiac muscles.

We have shown that ATP increases the force of contraction to CCh of the strip m.Diaphragma and m.Soleus and reduces the rate at m.EDL. The level of non-quantum secretion ACh of m.Diaphragma and m.Soleus decreases, of m.EDL did not change. Vector of force and H-effect dynamics of m.Diaphragma and m.Soleus under ATP influence coincided with those at protein sensitization that suggested the sequence of events when force contraction increase is the result of the increase of postsynaptic membrane sensibility to cholinomediate. ATP effect on the dynamics of the above mentioned properties of m.Diaphragma and m.Soleus at sensitization demonstrates the same direction, indicating the lack of fundamental differences in the mechanisms of purines influence on the "slow" and "mixed" muscles of intact and sensitized mice.

However, m.Diaphragma contraction power of intact animals after ATP effect increased by 26,8%, while of sensitized animals - only by 15,1% ($p<0,05$). H-effect of this muscle of nonsensitized mice after ATP influence decreased to 28.8% from baseline, while of sensitized mice only to 54,5% ($p<0,05$). Less pronounced dynamics of m.Diaphragma functional properties, caused by ATP in sensitized mice compared with the control allows us to assume that it is involved in the mechanisms of functional changes of the respiratory muscles at protein sensitization.

The dynamics of "slow" muscle functional properties represents similar picture. If m.soleus contraction force of intact animals increased by 24,3%, while of sensitized is only by 12,2% ($p<0,05$). H-effect of this muscle of non sensitized mice after ATP influence decreased to 20% from baseline, while of sensitized mice - only to 67,7% ($p<0,05$). Less pronounced dynamics of m.soleus functional properties, caused by ATP in sensitized mice compared with the control allows us to assume that it is involved in the mechanisms of functional changes of "slow" muscles

In intact animals m.EDL contraction force decrease after ATP effect (to 72.6%) did not differ from that of sensitized animals (to 74.8%) ($p>0,05$). M.EDL H-effect after ATP effect did not change significantly either in intact or in sensitized mice. The absence of any difference in contraction force change and H-effect after ATP influence in both groups of animals indicates the fact that purines do not participate in changes mechanisms of contractile function of mouse "fast" muscle, caused by protein sensitization.

ATP effect on contractile function of all three observed mice muscles is similar to that of most other skeletal muscles and is carried out through P2-receptors. It is confirmed by published data and the results of our own research. Suramin, an antagonist of P2-receptors eliminated ATP effect in all experimental models. Besides, replacement of ATP by adenosine, that acts not via P2 but via P1 adenosine receptors, did not change neither parameters of K-induced muscle contraction, nor the rate of H-effect.

Possible ways of ATP effect in our experimental models are diverse and include direct action of purines on the contractile structures, the mediator secretion, the systems of intracellular intermediates and the work of ATP-dependent potassium channels. Besides, ATP participation can be suggested at some stages of the immune response generation. In particular, published data show that ATP is able to amplify a specific link of immunity increasing production of interleukin-1. Extra cellular ATP at immune response generation helps, which in its turn provides the secretion of biologically active form of interleukin-1. Over expression of the receptor R_2H_7 leads to mature interleukin-1ß secretion.

As an experimental model of allergy, OS of mice allows to study the mechanisms of both pathological and compensatory changes that occur in the lung and in striated muscle. We have shown that the sensitization of animals results in increase of contraction force on the CCh of a diaphragm strip. This fact, together with a smaller degree of variability of diaphragm functional properties caused by ATP in sensitized mice compared with control is a possible indication of development of resistance mechanisms, stability to external loads in the respiratory muscles, which should emerge with bronchospastik syndrome and bronchial asthma. Similar pattern of changes in functional properties at protein sensitization is also observed in "slow" muscle. We assume the participation of other non-ATP mechanisms in the change of contractile function of "fast" muscle at experimental allergy.

SELF-ASSOCIATES OF PHOSPHOLIPIDS DISPERSED IN AQUEOUS, AMPHIPHILE AND HYDROPHOBIC MEDIA

V.P. Topaly, E.E. Topaly

Institute of Theoretical and Experimental Biophysics of the Russian Academy of Sciences, Institutskaya 3, Pushchino, Moscow region, 142290, Russia

1. Introduction. There are some questions of fundamental importance concerning the lipid dispersions. First, the pioneering studies of K.-K. Fung and L. Stryer (1978) initiated a widespread adoption of fluorimetry for investigations of phospholipid (PL) dispersions. Authors proposed to use the Förster's (1949) resonance energy transfer (RET) theory applied by him to explain

Abbreviations: S, Φ, D, A – solute, fluorophore, donor, acceptor; {} – the nominal concentration; [S] – the concentration of S as molecules (monomers); true S solution – the dispersion of S under the condition [S] = {S}; PL – phospholipids; FPL – fluorescent PL; SA – self-associate; NBD-PE – N-(7-nitrobenz-2-oxa-1,3-diazol-4-yl) dioleoylphosphatidylethanolamine; Rh-PE – (N-(lissamine rhodamine B sulfonyl) dioleoylphosphatidylethanolamine; DOPE – dioleoylphosphatidilethanolamine; F – fluorescence; F_{max} – the fluorescence of Φ dispersion in the absence of interaction of Φ molecules with each other; r – the mean distance between neighbor Φ molecules; R_o – r at which $F = F_{max}/2$; F_{30nM} – the actual fluorescence related to {Φ} = 30 nM chosen arbitrarily but close to real {Φ} in our studies of PL dispersions; QYF – the quantum yield of the F; DMF – dimethylformamide; UL – unilamellar liposomes; CCS – critical concentration of spheroid formation.

the quenching of the fluorescence (F) of one compound (donor, D) by another compound (acceptor, A) in an organic solvent for determination of the surface density of PL molecules in liposome membranes. F of a series of PL dispersions with equal nominal concentrations {D} and different {A} served as the principal argument in favor of such application of the RET theory. D. K. Struck, D. Hoekstra and R.E. Pagano (1981) proceeded in the same way by using the D/A pair NBD-PE/Rh-PE which was later recommended by Methods in Enzymology (Hoekstra, Düzgüneş, 1993) for study of membrane fusion. Meanwhile the Förster's (1949) theory considers the content of D and A by the distance between their molecules only. Thus, it can be applied to equimolar dispersions only of a D and of an appropriate A. Moreover, for analysis of F values in the frame of the RET theory the maximal possible F (Fmax) must be known and it is recommended to be measured with the aid of detergents (Fung, Stryer, 1978; Hoekstra, Düzgüneş, 1993). But no evidence exists that Fmax is accurately measured in this way especially because both media and detergents can influence the quantum yield of the fluorescence (QYF). Second, many literature data show (Miyamoto, Stoeckenius, 1971; Lentz, Carpenter, Alford, 1987) that aqueous dispersions of PL monotonically change their properties in the course of many days but these dispersions are considered to be equilibrium systems. Third, it is considered that PL molecules spontaneously associate into liposomes containing closed bimolecular membranes as obligatory elements. One of numerous techniques to prepare liposomes (the injection method) consists in the simple dilution of an ethanolic solution of PL by water (Batzri, Korn, 1973; Kremer et al., 1977). But what the ethanolic solution does represent is not clear because even the usual notion "solution" is uncertain. In the range of definite concentrations any solute (S) is completely dispersed to molecules or ions (true solution) but the upper limit of this range is unknown. When Förster proposed his explanation of self-quenching of fluorophores (Φ) (Förster, 1948), then the quenching of one Φ (D) by another (A) (Förster, 1949), respective dispersions were regarded as true solutions in the whole range of {Φ} studied. Therefore, the decrease in the F with the increase of {Φ} was explained by RET between Φ molecules through the medium. But this fact can be alternatively explained by energy transfer between Φ molecules associated into different compounds. Owing to its high sensitivity the fluorimetry permits accurate measurements at low {Φ} and the data can serve to elucidate some of above questions. We propose to the attention of the reader a series of our data.

2. Materials and methods. NBD-PE and Rh-PE were purchased from Avanti Polar Lipids, Inc.; reduced Triton X-100 and DMF were from Sigma, the rest of solvents (chloroform, ethanol, decane) were of Russian production and each was redistilled before use. All dispersions were prepared by adding to the lipid thoroughly dried under deep vacuum the appropriate volume of the solvent, manual shaking and ultrasonication for 10 min in the presence of ice.

The fluorescence and scatterring of lipid dispersions in standard 1 cm x 1 cm quartz cuvettes were measured on a Perkin-Elmer 44B spectrofluorimeter at an angle of 90° to the direction of the exciting light beam. All measurements were carried out at 25 °C with *continuous agitation* of the cuvette content by a magnetic stirring rod. The excitation wavelength was 470 nm (the absorption maximum of NBD-PE) and the emission wavelength was 530 nm (the emission maximum of NBD-PE), both slits were 5 nm wide. All measurements were displayed on the monitor and recorded on a computer hard disc.

3. Results and discussion. The main postulate of the Förster's theory about the proportionality of the rate of RET to r^{-6} (r – the mean distance between neighbor Φ molecules) has been proved for usual reactions by authors of the mass action law. If the rest of postulates are applied, the theory predicts the RET

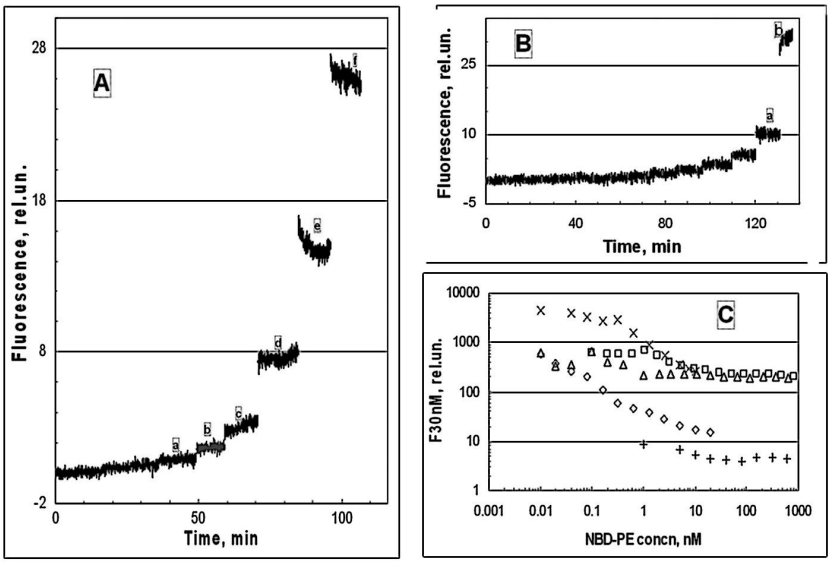

Fig. 1. Consecutive records of signals of detector at the dark, from the medium and after introduction into cuvette of NBD-PE up to different concentrations in the range1 – 602 nM (**A**) and 0.01 – 20 nM (**B**), and values of F_{30nM} calculated from them as function of {NBD-PE} (**C**, + and ◊). Measurements were taken under continuous agitation of the medium (decane in **A** and 100 mM NaCl, 10 mM Hepes, 0.1 mM EDTA, 1 mM sodium azide in **B**) by a magnetic stirring rod in the standard 1 cm x 1 cm quartz cuvette, λ_{ex} = 470 nm, λ_{em} = 530 nm, both slits are 5 nm. The temperature (thermostat) is 25 °C. Above conditions of measurements were applied also for experiments in ethanol **C**, x), chloroform (**C**, Δ) and DMF (**C**, □). {NBD-PE} shown were created in the cuvette by introducing appropriate volumes of 0.1 mkM and 1 mkM NBD-PE stock dispersions in respective solvents. The last record in **B** (b) is made after untroduction of the reduced Triton X-100 up to 2 mM. Records **A**a, **A**b, **A**c, **A**d, **B**b show the increase in F with time while **A**e, **A**f and **B**a, on the contrast, the decrease in F.

through medium at $r < 70$ Å. The experimentally found quenching of the fluorescence that has been explained by Förster (1948, 1949) occurs at $\{\Phi\} > 0.1$ mM, that is, exactly at $r < 70$ Å. But if at $\{\Phi\} > 0.1$ mM Φ molecules associate with each other, it is possible that the quenching results from the transfer of D exiting energy to unexited Φ molecules within associates. Thus, the Förster's explanation of the quenching can be a *single one* under the condition only that Φ dispersions were true solutions in the whole range of {Φ} investigated. Fluorescent PLs (FPLs) were found to quench each other at $\{\Phi\} << 0.1$ mM (Fung, Stryer, 1978) but in PL dispersions only. However if all lipids are associated into unilamellar liposomes (UL) only this quenching can be explained by RET at $r < 70$ Å as well. It is interesting that PL dispersions studied were prepared by the method of injection mentioned above. We show a series of data concerning dispersions of FPLs, which need new views on PL dispersions and F quenching.

Figs. 1A and B present the results of measurements taken in two experiments. Total signals were subtracted for dark and medium signals to calculate the F corresponding to each {NBD-PE}. The Fig. 1C (◊, +) shows these data, as well as those for other experiments, related to 30 nM NBD-PE (F30nM). 30 nM is chosen arbitrarily.

In all experiments shown in fig. 1 the single PL in the dispersion is NBD-PE which represents the fluorescently labeled DOPE. It is to note that under conditions of experiments the number of NBD-PE molecules in the cuvette only at {NBD-PE} > 100 nM is larger than the number of molecules necessary to fill the nanolayer (NL, on our opinion this is not a Langmuir monolayer (Topaly, 2010)) at the surface (air/liquid interface) of the dispersion ($n_{NL} \approx 10^{14}$), which PLs form spontaneously at any concentration. Of course, conditions for NL formation are unfavorable but, except for decane dispersion (see below), {NBD-PE} near the surface is most likely many times higher compared to average value of {NBD-PE}. This means that F_{30nM} in Fig. 1**C** are lower compared to equilibrium values the difference being the more pronounced the lower {NBD-PE}. But no reasons exist to assume that this factor is the single one, which determines the shape of curves in this figure. Indeed, records in any amphiphile medium are similar to those in water (Fig. 1**B**) and they show that at high {NBD-PE} only the fluorescence monotonically decreases with time (1**B**a) while at {NBD-PE} < 20 nM records in the limit of experimental error are horizontal straight lines. At the same time in decane records at {NBD-PE} 20, 40, 80 and 160 nM (1**A**a, b, c, d) show reliable increase in F with time and even at {NBD-PE} < 20 nM the increase is present but cannot be considered as reliable owing to noise. At {NBD-PE} > 160 nM, however, F also decreases with time (1**A**e and **A**f) as well as in the rest of media. These peculiar properties of records are caused by the absence of NL on the surface of decane. NL which represents a RBIPH (Fig. 2 and Topaly, 2010) cannot form in spite of hydrophobicity of its surface. RBIPHs at the interface and in the volume of decane are equally stable, thus, they are distributed homogeneously in the whole dispersion. Hence, the increase in F in decane (1**A**a, b, c, d) can be attributed to degradation only of associates introduced with the

probe of stock dispersion. The decrease in F starts when associates introduced are smaller compared to those at equilibrium in the cuvette, thus, they do not degrade but start to enlarge. Evidently, the dilution of stock dispersions by water or amphiphile solvents is also accompanied by degradation of FPL associates as long as at {NBD-PE} after dilution they are larger compared to those at equilibrium. But the increase in F is not seen because of simultaneous decrease in F owing to transfer of FPL from the volume to the interface. It is to note that the decrease in F in decane starts at {NBD-PE} > 160 nM (1**A**e and 1**A**f) while in water at {NBD-PE} ≥ 20 nM (Fig. 1**B**a), in chloroform at {NBD-PE} ≥ 360 nM (not shown) and in DMF at {NBD-PE} ≥ 260 nM (not shown). This is normal because the quantitative and even the qualitative composition of associates in respective stock dispersions are quite different.

Under equilibrium in the absence of any interaction of Φ molecules with each other, that is, in true solutions, F_{30nM} has the maximal possible value (F_{max}) and does not varies with {Φ}. For solutions with associated Φ molecules there are also two limit cases when F_{30nM} does not practically vary with {Φ} but is smaller than F_{max}. After dilution of such stock dispersion the number of associates changes slightly either because stability constants of associates are extremely large, thus, only a small portion of them degrade owing to equilibration, or because the equilibration is extremely slow.

Data in Fig. 1**C** show quenching of F but they cannot be understood in the frame of the Fung and Stryer's (1978) model, which postulates ULs as PL associates and accounts for the quenching of F by the RET between neighbor FPL molecules in UL membranes. In our case, *r* in these membranes and in BIHTs is so small (< 10 Å and < 14 Å, respectively, while 30 Å < R_o < 70 Å) that F would be by orders of magnitude smaller than measured F. So, the idea of ULs as PL associates is incompatible with the experimental data showing that dispersions of DOPE in any medium contain other types of associates (fig. 2), which form and degrade very slowly during equilibration. Fig. 2 presents schematically two PL molecules and a series of PL associates which can form spontaneously in the volume of liquid media according to our model of amphiphile dispersion. Earlier (Topaly, 2010) we have proposed amphiphile associates which can form at the interface air/water, between two air (soap bubble membrane) or aqueous media (black PL membrane). According to our model (see the caption to Fig.2) PLs cannot associate into ULs in the absence of a special molecular machine (liposomase) but accumulate both in aqueous and amphiphile media predominantly into spheroids which cannot be distinguished from Bangham's liposomes in electron microscope, although their structures are quite different. Associates formed by NBD-PE are very similar to those formed by any lecithin or cephalin but have some peculiarities. We think that DGM and BIHTs are retained within spheroids, as well as molecules within NBD-PE cylinders, owing to bonds between fluorophore groups (NBD) while in lecithin and cephalin spheroids by electrostatic bonds.

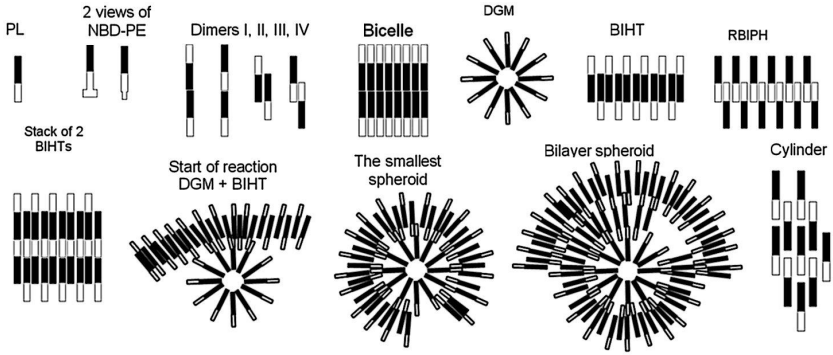

Fig. 2. Schematic picture of PL molecule, 2 views of NBD-PE and of some PL self-associates (SAs). The cylinder-like PL molecule consists of a hydrophobic (black) and a polar (white) parts. NBD-PE molecule differs from PL by the end of its polar part, which represents a plane structure with the thickness smaller than the diameter of cylinder and the surface larger than the surface of perpendicular section of cylinder. According to our model of PL dispersion based on estimation of the energy of interaction between PL molecules the *bicelle* is improbable as well as the *liposome* because neither can form spontaneously from PL molecules or other PL associates. In *water* the most probable SAs are *bicelles with interdigitated hydrophobic tails* (*BIHTs*) containing 2, 3, and so on up to any arbitrary large number of PL molecules. *Direct globular micelles* (*DGM*) are less probable SAs containing from 2 to a relatively not great number of PL molecules. Small *reverse bicelles with interdigitated polar haids* (*RBIPHs*) are also quite probable. All above structures except molecules are PL *complexes*. Two or more complexes can form more complicated associates, *aggregates*. The simplest aggregates are the *stack* of two BIHTs and the *spheroid* containing a DGM in its center and a BIHT around it. Both BIHTs and RBIPHs are disc-like particles with the thickness equal to about 1.5 lengths of PL molecule. Although cohesion of two BIHTs in the stack is stronger than that of a DGM and a BIHT in the smallest spheroid, the latter form more readily owing to large difference in energetic barriers, which must be overcome at association of these two pairs of complexes. The spheroid can associate a great number of larger and larger BIHTs and, as a result, the dispersion PL accumulates predominantly in these aggregates. In *amphiphile* media (ethanol, chloroform, DMF) PL SAs are similar to those in water but their average sizes are smaller at equilibrium. In *hydrophobic* media (decane) the most probable SAs are *cylinders*, which form by successive association of PL molecules and small complexes (predominantly dimers). The particles are at the same time discs but many times thicker than BIHTs and RBIPHs. Stability constants of almost any type of complexes and aggregates are very large and each increases with the size of respective associate. As a result, the equilibration of any PL dispersion occurs extremely slowly being limited by degradation of existing smallest or largest associates depending on the direction of equilibration. Any concentrated PL stock dispersion is most likely never equilibrated and the mean size of SAs in it always increases. This increase continues even after dilution of such dispersion. The pure PL contains predominantly spheroids or cylinders depending of the fluid medium where the lipid is dispersed and of the method used for drying.

As a result, all NBD-PE within spheroids except for that located on their surfaces becomes *unfluorescent*. Besides superficial NBD-PE molecules in spheroids only monomers and NBD-PE included in BIHTs fluoresce. Cylinders do not fluoresce practically at all but in decane a small portion of NBD-PE is present as BIHTs, stacks of BIHTs and maybe even as spheroids. We think that all our stock dispersions are not equilibrated and contain the lipid predominantly as spheroids which extremely slowly increase in size, thus, their F continuously decreases with time. Even after dilution of the stock dispersion F decreases if equilibrium size of associates is larger than the actual size of associates in the stock dispersion. This fact is reflected directly in the shape of records 1**A**e, 1**A**f, 1**B**a and indirectly in the decrease of F_{30nM} with the increase in {NBD-PE}, which is seen in all curves in Fig. 1**C**.

The bend in the curve 1C (x) shows that in the range 10 – 300 pM the portion of small FPL associates in the ethanol dispersion is significant and the decrease in F30nM occurs predominantly owing to transfer of the lipid from the volume into NL while at higher {FPL} a pronounced increase in the size of associates takes place. The curve 1C (◊) also has a weak bend. But the slope of the initial part of the curve is significantly larger. Thus, the aqueous dispersion contain larger than in ethanol FPL associates even at {FPL} ≈ 10 pM and their increase in size produces a more pronounced decrease in F30nM. We suppose that bending points in both curves show critical concentrations at which spheroids start to increase (CCS). Each event of association of a BIHT to a spheroid or even to a DGM is accompanied by quenching of many NBD-PE molecules, thus, the F starts to decrease quicker with the increase in {NBD-PE). Spheroids are introduced with the probe of stock dispersion, thus, are present in the whole range of {NBD-PE} but at {NBD-PE} < CCS they partially dissociate while at {NBD-PE} > CCS they enlarge. It is seen that these events occur at about 0.07 nM in water and at 0.3 nM in ethanol. If at {FPL} < CCS the whole lipid is present as molecules and complexes, the first spheroids seem to appear at lower {FPL}.

It seems that NBD-PE associates in chloroform (1**C**, Δ) and in DMF (1**C**, □) contain medium molecules as constituents and this makes them apparently more stable than in water in the whole range of {FPL} studied. The same seems to be true for ethanol dispersion at {FPL} > 10 nM. Owing to high stability of associates in chloroform and DMF even at lowest {FPL} the portion of NBD-PE as molecules is very small and NL forms very slowly. Because of this stability the enlargement of spheroids and even of BIHTs occurs extremely slowly too. As a result, NBD-PE associates in stock dispersions are always relatively small and remain practically intact after dilution of dispersions, thus, F_{30nM} practically does not depend on {NBD-PE}. FPL is contained predominantly in spheroids as well as in water but the concentration of them is higher, thus, F_{30nM} is also higher than in water because the portion of spheroid superficial FPL is significant (the total surfaces of spheroids is higher). Weak bends observed in the curves reflect the fact that spheroids are the most numerous fluorescent particles at any {NBD-PE} while in ethanol and even in water at {NBD-PE} < CCS the fluorescence comes predominantly from small associates and NBD-PE monomers.

The lowest F_{30nM} in decane (Fig. 1**C**, +) results from the fact that FPL is present as unfluorescent cylinders predominantly. Only a small portion of FPL is contained in fluorescent spheroids and other associates. But these compounds are also very stable and remain intact after dilution of the stock dispersion, thus, F_{30nM} practically does not change with {NBD-PE}.

The detergent sharply increases the F in water (Fig. 1**B**b), but F_{30nM} increases from 15 to 46 rel.un., while in the same medium at low {NBD-PE} $F_{30nM} \approx 580$ rel.un. (1**C**, ◊), and in ethanol exceeds 4000 rel.un. (1**C**, x). The presence of clear bend on the curve 1**C** (x), the increase (1**A**a, b, c, d, 1**B**a) or the decrease (1**A**e and f, 1**B**a) in F with time, close F_{30nM} values in three amphiphile media at {NBD-PE} > 10 nM (1C, x, □, Δ) permit to say that QYF weakly depends both on the medium and on the detergent. Hence, the detergent does not transform the PL dispersion into true PL solution as is believed and F_{max} of dispersions of fluorescently labeled PL was never measured. It is also to note that measurements of QYF presume the use of true solutions. Data presented show that FPL dispersions are not true solutions even at 10 pM, thus, all reports about QYF values of FPL, as well as the fluorescence in $\%F_{max}$ units, can be considered to be questionable.

As is seen all records in Fig. 1**A** and **B** contain a pronounced noise. It is interesting that amplitudes of the noise in the dark and in the absence of FPL under condition of F measurement are equal for any medium while in the presence of FPL the amplitude monotonically increases with {NBD-PE}. The increase in the amplitude averages ≈0.5 % of F measured in aqueous and amphiphile media, 2-3 % of F in decane and is practically independent of {NBD-PE} and {detergent}. The absence of the detergent effect on the fluctuation of F permits to suppose that the detergent stock dispersion also contain spheroids. Detergent spheroids introduced into cuvette quickly bind the majority of monomer FPL BIHTs. In itself this event does not influence the F at all but it sharply increases the rate of degradation of FPL spheroids. As a result, a significant quantity of small FPL associates appears and F sharply increases (Fig. 1**B**b). We suppose that so-named critical micellar concentration is in reality the CCS discussed above for PL dispersions. The fluctuation in F under discussion results, evidently, from the fluctuation in the number of fluorescent particles in the irradiated zone of the cuvette. It is easy to see that this effect cannot be understood in the frame of actual views concerning PL dispersions. Even supposing that fluorescent particles are multilayer liposomes the amplitude of F noise must be orders of magnitude smaller. The fact can be explained, however, in the frame of the model shown in Fig. 2. Indeed, the most stable FPL complex in any medium except for hydrocarbon is the BIHT, thus, the PL is accumulated in these particles, which are actively included into spheroids. But a small number of BIHTs remain in monomer form because of their large sizes which impede their association with spheroids. These are BIHTs whose diameters are more than twice as much as the diameter of largest spheroids. If F of these particles constitutes at least several percents of the total F, then fluctuation of their number results in the fluctuation of the total F.

Conclusions. 1) Dispersions of usual phospholipids (PL) in any medium are over a long period of time non-equilibrium systems at any PL concentration higher than 10 pM. However reactions of association/dissociation are so slow that any such dispersion looks like a stationary system. 2) The fluorescence of NBD-PE dispersion in any medium fluctuates. 3) A model of PL dispersion is proposed which allows the interpretation of experimental data presented.

References

Batzri S., Korn E.D. 1973. Single bilayer liposomes prepared without sonication. Biochim. Biophys. Acta, 298, 1015-1019.

Förster Th., 1948. Zwischenmolekulare Energiewanderung und Fluoreszenz. Annalen der Physik, 2, 55-75.

Förster Th. 1949. Experimentelle und theoretische untersuchung des zwischenmolekularen übergangs von elektronenanregungsenergie. Z. Naturforschung, 49, 321-327.

Fung K.-K., Stryer L. 1978. Surface density determination in membranes by fluorescence energy transfer. Biochemistry, 17, 5241-5248.

Hoekstra D., Düzgüneş N. 1993. Lipid mixing assays to determine fusion in liposome systems. Methods in Enzymology, 220, part A, 15-32.

Kremer J.M.H., Esker M.W.J., Pathmamanoharan C., Wiersma P.H. Vesicles of variable diameter prepared by a modified injection method. Biochemistry, 1977, 16, 3932-3935.

Lentz B.R., Carpenter T.J., Alford D.R. 1987. Spontaneous Fusion of Phosphatidylcholine Small Unilamellar Vesicles in the Fluid Phase. Biochemistry, 126, 5389-5397.

Miyamoto V.K., Stoeckenius W. 1971. Preparation and Characteristics of Lipid Vesicles. J. Membrane Biol. 4, 252-269.

Struck D. K., Hoekstra D., Pagano R. E. 1981. Use of resonance energy transfer to monitor membrane fusion. Biochemistry, 20, 4093-4099.

Topaly V.P. 2010. On the structure of phospholipid self-associates at air/water and hydrocarbon/water interfaces. Materials of the international symposium "Biological motility: from fundamental achievements to nanotechnologies", Pushchino, p. 293 – 299.

SEASONAL CHANGES OF TITIN ISOFORM COMPOSITION IN SKELETAL MUSCLES OF HIBERNATING GROUND SQUIRRELS (*SPERMOPHILUS UNDULATUS*)

K.O. Trapeznikova[1], I.M. Vikhlyantsev[2], Yu. M. Kokoz [2], A. D. Okuneva[2], V.V. Rogachevsky[2,3], S.S. Khutsyan[2,3], N.N. Salmov[2], Z. A. Podlubnaya[2,4]

[1]Belgorod State National Research University, Russia
[2]Institute of Theoretical and Experimental Biophysics, Russian Academy of Sciences, Pushchino, Moscow region, 142290 Russia
[3]Institute of Cell Biophysics, Russian Academy of Sciences, Pushchino, Moscow region, 142290 Russia
[4]Pushchino State Institute of Natural Science, Pushchino, Moscow region, Russia

It is known that the development of pathological (dilated cardiomyopathy, hypertrophy of the myocardium, myodystrophies, the Stiff-person syndrome) [1−6] and adaptational processes (adaptation to hibernation and

microgravity conditions [4, 7−9]) is accompanied by changes in the isoform composition of the giant sarcomere protein titin. In particular, it was shown that an increase in the content of the long N2BA isoform of titin in the myocardium of hibernating ground squirrels *Spermophilus undulatus* plays an adaptative role and consists in the enhancement of the contractile response of the myocardium aimed at the release of more viscous blood during hibernation [7]. Conversely, in the myocardium of the hibernating bear *Ursus arctos horribilis*, the content of the short N2B isoform of titin increases, which, in the opinion of the authors, is aimed at maintaining the systolic function of the myocardium during hibernation [10]. The studies of changes in the isoform composition of titin in slow (m. soleus) and fast (m. psoas) skeletal muscles of hibernating ground squirrels *Spermophilus undulatus* revealed a decrease in the content of the known N2A isoform of titin with the retention of the content of the higher-molecular isoform NT [11] of this protein during the winter hibernation [4, 7]. In the present work we studied changes in the isoform composition of titin in some skeletal muscles of the back and extremities of the hibernating ground squirrels *Spermophilus undulatus* in different periods of activity: summer activity, winter activity (5−6 h after the exit from hibernation), hibernation, and arousal to determine the contribution of these changes to adaptation of skeletal muscles to hibernation conditions.

The following skeletal muscles of the ground squirrel were used: *m. vastus lateralis, m. gastrocnemius, m. longissimus dorsi, m. psoas, m. soleus, m. triceps*. SDS PAGE was carried out by the method described in [11] with a content of agarose of 0.55% and polyacrylamide of 2.1−2.3%. The densitometry of gels was performed using the program Total Lab 1.11 [2]. The content of titin was estimated relative to the content of heavy myosin chains. The statistical processing was carried out using the nonparametric *U*-test of Mann−Whitney. Differences with a confidence level $p < 0.05$ were considered significant. The Western blotting of titin was carried out as described in [4] using monoclonal antibodies AB5 to the region of the titin molecule localized in the A disc of the sarcomere.

In all skeletal muscles of torpid ground squirrels, the relative content of the N2A isoform of titin was found to decrease ~1.3−1.5 times, whereas the relative content of the NT isoform of titin either remained unchanged or increased ~1.3−1.4 times. In this case, the content of the T2 fragment of titin decreased two times and more, and the total content of titin decreased by 20−30%.

During the exit of animals from hibernation, a high NT/N2A ratio of the titin isoforms was retained against the background of the decreased total content of titin. An increase in the content of titin, in particular N2A and T2 isoforms in skeletal muscles of winter-active ground squirrels was observed even two to three hours after the exit from hibernation. The content of titin was restored after 24 h of winter activity. In this case, the increased NT/N2A ratio of the titin isoforms was retained.

What are the mechanisms of the decrease in the content of titin, in particular N2A and T2 isoforms, in muscles of ground squirrels during hiberna-

tion? It is known that the translation process in different organs of the ground squirrel during hibernation is inhibited due to both the inactivation of initiation (eIF-2) and elongation (eEF-2) factors through reversible phosphorylation [12] and owing to a decrease in the fraction of polyribosomes [13]. These data agree with the results of in vivo study of the incorporation of labeled amino acids into proteins, which showed that the synthesis of the protein in the heart of ground squirrels during hibernation was strongly (more than 200 times) inhibited [14]. The proteolytic activity at the level of proteosomes is also inhibited during hibernation [15]. However, the development of atrophic processes in skeletal muscles of animals during hibernation [16] indicates that catabolic processes dominate in this period over anabolic processes. Considering that the half-life of titin is 72 h [17], it can be assumed that the ~1.3−1.5-fold decrease in the content of the N2A isoform of titin and the stronger decrease in the content of the T2 in muscles of hibernating ground squirrels result from the inhibited but not completely suppressed proteolysis of titin in the absence of the synthesis of this protein during the hibernation bout, which lasts for 7−14 days. Presumably, enzymes responsible for titin proteolysis are Ca^{2+}-dependent proteases calpaines [18].

What are possible consequences of the decrease in the content of titin in muscles of hibernating ground squirrels? It is known that a decrease in the content of the N2A isoforms of titin (T1) in fibers of rabbit skeletal muscles by the action of ionizing radiation led to disturbances of the ordered structure of sarcomeres (in particular, a displacement of A-discs to the Z line, the appearance of broader A-zones of the sarcomere with irregular edges) and a decrease in the force of muscle contraction [19]. Similar disturbances of the structure and functional properties were observed in glycerinated fibers of skeletal muscles of the frog after the proteolytic degradation of connectin (titin) [20]. There is evidence indicating that a twofold decrease in the content of the N2A isoform of titin in m. soleus of the rat after the 6-week immobilization of the hind limb was accompanied by abnormalities of sarcomeric ultrastructure and a decrease in the Ca^{2+}-sensitivity of muscle filaments during contraction [8]. Considering these data, a disturbance of the ordered sarcomere structure and a reduction in the contractile ability of skeletal muscles of hibernating ground squirrels due to a decrease in the content of the N2A isoforms of titin could be expected. However, the available literature data and the results of our electron microscopic examination of the sarcomeric structure do not confirm the occurrence of these disturbances in skeletal muscles of ground squirrels during hibernation. It should be noted that there is evidence indicating that, in the myocardium of torpid ground squirrels, too, no disturbances in the structural and functional characteristics occur ([23] and Yu. M. Kokoz, personal communication) despite an about 1.5-fold decrease in the content of the N2BA and N2B isoforms of titin with the retention in the content of the NT isoforms of this protein [7]. These results indicate that the main role in maintaining the structural and functional characteristics of striated muscles is played by higher-molecular-weight NT isoforms of titin

rather than its N2A, N2BA, and N2B isoforms the decrease in the content of which is not accompanied by the impairment of the above characteristics in cardiac and skeletal muscles of ground squirrels. This conclusion is confirmed by the results of our studies indicating that the decrease first of all in the content of the NT isoform of titin in human and rat m. soleus atrophied under microgravitation conditions is accompanied by considerable disturbances of the contractile characteristics of this muscle [4, 24].

Interestingly the increase in the relative content of the NT isoform of titin in skeletal muscles of ground squirrels was observed even in the period of autumn activity during the preparation of animals for the hibernation. These changes correlated with the increase in the content of the slow isoforms of MHC in skeletal muscles of ground squirrels in this period [25]. The results obtained indicate that the NT isoform of titin is predominantly synthesized in slow fibers of skeletal muscles. It should be noted that our results on the transformation of the phenotype of muscle fibers of skeletal muscles of ground squirrels during the autumn preparation for hibernation agree with the data of other authors indicating early adaptation changes in different systems of the organism of hibernators in this period [26, 27].

Thus, seasonal changes in the isoform composition of titin in skeletal muscles of ground squirrels *Spermophilus undulatus* are directed towards an increase in the content of the slow NT isoforms of titin during the autumn preparation for hibernation and the retention of their high content throughout the hibernation season, which is a necessary condition for the maintenance of the highly ordered sarcomere structure and the required level of contractile activity of skeletal muscles in all periods of hibernation.

This work was supported by the Russian Foundation for Basic Research (grants No. 10-04-00141, 11-04-01026) and a grant of the Federal Targeted Program “Scientific and Scientific-Pedagogical Personal of Innovative Russia”, State Contract No. 02.740.11.0710.

References

1. Matsumura K., Shimizu T., Sunada Y., Mannen T., Nonaka I., Kimura S., Maruyama K. // J. Neurol Sci. 1990. V. 98(2-3). P. 155-162.

2. Makarenko I., Opitz C.A., Leake M.C., Neagoe C., Kulke M., Gwathmey J.K., del Monte F., Hajjar R.J., Linke W.A. // Circ. Res. 2004. V. 95(7). P. 708-716.

3. Nagueh S.F., Shah G., Wu Y., Torre-Amione G., King N.M., Lahmers S., Witt C.C., Becker K., Labeit S., Granzier H.L. // Circulation. 2004. V. 110(2). P. 155-162.

4. Vikhlyantsev I.M., Podlubnaya Z.A. // Biofizika. 2008, V. 53(6). P. 1058-1065.

5.Warren C.M., Jordan M.C., Roos K.P., Krzesinski P.R., Greaser M.L. // Cardiovasc Res. 2003. V. 59(1). P. 86-94.

6.Karaduleva E.V., Vikhlyantsev I.M., Podlubnaya Z.A. // Biofizika. 2010. V. 55(4). P. 612-618.

7. Vikhlyantsev I.M., Karaduleva E.V., Podlubnaya Z.A // Biofizika. 2008. V. 53(6). P. 1066-1072.

8. Udaka J., Ohmori S., Terui T., Ohtsuki I., Ishiwata S., Kurihara S., Fukuda N. // J. Gen. Physiol. 2008. V. 131(1). P. 33-41.

9. Vikhlyantsev I.M., Okuneva A.D., Shpagina M.D., Shumilina Yu. V., Molochkov N.V., Salmov N.N., Podlubnaya Z.A. // Biochemistry (Moscow). 2011. V. 76(12).P. 1629-1639.
10. Nelson O.L., Robbins C.T., Wu Y., Granzier H. // Am. J. Physiol. Heart Circ. Physiol. 2008. V. 295(1). P. H366-371.
11. Vikhlyantsev I.M., Podlubnaya Z.A., Kozlovskaya I.B. // Doklady AN. 2004. V. 395(6). P. 828-831.
12. Chen Y., Matsushita M., Nairn A.C., Damuni Z., Cai D., Frerichs K.U., Hallenbeck J.M. // Biochem. 2001. V. 40. P. 11565–11570.
13. Knight J.E., Narus E.N., Martin S.L., Jacobson A., Barnes B.M., Boyer B.B. // Mol. Cell. Biol. 2000. V. 20(17). P. 6374-6379.
14. Zhegunov G.F., Mikulinsky Y.E., Kudokotseva E.V. // Cryo-Lett. 1988. V. 9. P. 236-245.
15. Velickovska V., Lloyd B.P., Safdar Qureshi, Frank van Breukelen // The Journal of Comparative Physiology B. 2005. V. 175. P. 329–335.
16. Wickler S.J., Horowitz B.A., Kott K.S. // J. Therm. Biol. 1987. V. 12. P. 163-166.
17. Isaacs W. B., Kim I. S., Struve A., Fulton A. B. // J. Cell. Biol. 1989. V. 109. P. 2189-2195.
18. Goll D.E., G. Neti, S.W. Mares, V.F. Thompson // J. Anim. Sci.V. 2008. 86 (E. Suppl.): E19-E35.
19. Horowits R., Kempner E.S., Bisher M.E., Podolsky R.J. // Nature. 1986. V. 323. P. 160-164.
20. Higuchi H. // J. Biochem. 1992. V. 111(3). P. 291-295.
21. Khromov A.S., Srebnickaya L.K., Rozdestvenskaya Z.E., Orlova A.A., Lednev V.V. // In book:“Mechanisms of hibernation“, 1987, Pushchino, ONTI, P. 95-101.
22. Steffen J.M., Li Y., Steele P.S., Klueber K.M., Milsom W.K. // In: “Life in the Cold. Ecological, physiological, and molecular mechanisms” (edited by C. Carey, G. Florant, B. Wunder, B. Horwitz), Westview Press, Boulder, San Francisco, Oxford, 1993. p. 511-518.
23. Wang S.Q., Lakatta E.G., Cheng H., Zhou Z. // J.. Exp. Biol. 2002. V. 205. P. 2957-2962.
24. Vikhlyantsev I.M., Podlubnaya Z.A., Shenkman B.S., Kozlovskaya I.B. // Dokl. Biochem Biophys. 2006. V. 407 (5). P. 88-90.
25. Lazareva M., Vikhlyantsev I., Bobylev A., Salmov N., Podlubnaya Z. // In book: 25. Biological Motility: Fundamental and Applied Science, 2012.
26. Semenova T.P., Medvinskaya N.I., Kolaeva S.G., Solomonov N.G. // Doklady AN. 1998. V. 363(4). P. 567-569.
27. Zakharova N.M., Nakipova O.V., Averin A.S., Tikhonov K.G., Solomonov N.G. // Doklady AN. 2009. V. 424(5). P. 696-699.

NEUROPHYSIOLOGICAL MECHANISM OF MOTOR AND MENTAL FUNCTIONS CORRECTION BY BIOFEEDBACK OF POSTURE STABILITY IN CHILDREN WITH ADHD

A.B. Trembach, G.A Grishina, O.V Gorbatova

Kuban State University of Physical Education, Sports and Tourism, Krasnodar, 350000, Russia

Background and Aims: Attention deficit and hyperactivity disorder (ADHD) is the common syndrome affecting 3-20% of children. In previous researches it was revealed, that electric brain activity increased at realization

of movements in range 5-7 Hz in frontal areas at children with ADHD in comparison with healthy children aged 6-7. High-frequency activity (25-35, 36-47, 48-60 Hz) in this experimental condition decreased in the cortex centers responsible for planning and the control of movements (Trembach et al, 2007). Training of standing posture by visual feedback satisfactory corrects ADHD brain dysfunction (Trembach et al, Gate & Mental Function, Amsterdam, 2008). The purpose of this investigation was to study dynamics of inattention, impulsivity and EEG during training of posture stability in children with ADHD and central mechanism of this correction.

Methods: By means of the test of continuous activity of continuous activity (Test of Variable of Attention, T.O.V.A) has been carried out testing 110 children of 6-7 years and is allocated group 23 children with the inattention and higher impulsivity. The patients underwent, beside clinical examination, Test of Variable of Attention, (T.O.V.A), electroencephalography, posturography test and video motion before and after training posture stability on computer stabiloanalyzer "Stabilan-01" by visual biological feedback of the center pressure according to a target on the screen in special computer games "Three balls" and "Building picture". Training had 14 sessions. Biomechanical parameters of postural sways (3D Video recordings «Statokin»), stance stability and electric activity of the cortex analyzed in conditions sitting with closed eyes, quiet upright stance and the ascent on tiptoe. Electroencephalogram (EEG) was recorded from 31 cortical areas to according modified 10-20 system by 32- channel EEG «Mitsar» in a frequency range of 0,5-105 Hz. EMG of M. Soleus was used for the indication of the movement. EEG spectrum power, event-related desynchronization (ERD) or event-related synchronization (ERS), wavelet transforms EEG and coherence between Fp1, C3, EMG of M. Soleus and all recorded areas were analyzed in ranges 4-7, 8-10, 14-24, 25-35, 36-47, 48-60 Hz in different experimental conditions by program Win EEG «Mitsar». The average topographic maps of EEG spectrum were compared among themselves in identical experimental conditions. Epoch of analysis was 1 s, amount of averages – 48. All procedure accords the Declaration of Helsinki.

Results: The results of computer games detected improved posture stability. After training posture stability by game "Three balls" amount of right answers increased from 21±1,3 at the beginning to 37±2,4 ($R< 0,05$) at the end of the motor learning. The amount mistakes decreased at the end of the training from 2,4±0,6 to 1,3±0,1 ($R< 0,05$). The similar dynamic was revealed during training "Building picture". After training posture stability under opened eyes improved. The spectral analysis of the longitudinal coordinate Y shoulder, articulation of hip and knee joint has allowed to reveal, that training posture stability improved control of body in space. Motions in these joints became synchronous, its amplitude increased from knee to shoulder joint. Attitude of the angle articulation hip to angle ankle joint increased. The training posture stability reduced the level to inattention (from 31,5 % to 19%) and impulsivity (from 18% to 8,5%). Thereby, motor learning, directed on shaping the new motor skill, perfected the motor functions child and its

cognition function (reduced the level of inattention and impulsivity). After training posture stability in children in position sitting with closed and open eyes was saved raised electric activity in cortex areas, which provide planning and realization of the motor acts. Revealed «remaining electric activity» of cortex in child can be morpho-functional base to correcting the syndrome of the deficit of attention with impulsivity by means of training posture stability. The comparative analysis of dynamics of significant changes spectrum and coherence EEG in children with ADHD at ascent on tiptoe in comparison with orthograde posture has shown, that training increased the spectrum and coherence (interhemispheric, intrahemispheric,) in gamma band EEG mainly in the central areas of cortex. After training event-desynchronizing EEG in low band and event-synchronizing EEG high band increased mainly in area, defining control of motion and checking level attention that serves the factor of activation these cortex structures (Pfrurtscheller, 2006). In connection with, that the electric activity increased only in M. Soleus after training posture stability, coherence between the spectrum EMG M. Soleus and the spectrum ЭЭГ investigated. It is revealed, that after training posture stability coherence between the spectrum EMG and the spectrum ЭЭГ increased mainly in the central areas, temporal and occipital areas of cortex. The analysis cognitive event-relations Go/NO GO potentials shown, that training optimizes mental functions. The amplitude positive potentials Go (P300) with localization in Pz and No/Go (P400) with localization in Cz raised. Such dynamics is caused by activation of activity of systems of involving and suppression of action and therefore inattention, impulsivity decreased.

Conclusion: Revealed increasing of activity cortex structures, which control voluntary movements and attention after training posture stability, can be basic of understanding mechanism of correction the level attention and impulsivity in children with ADHD.

STRUCTURAL PROPERTIES OF ACTIN-MYOSIN CROSS-BRIDGES IN CONTRACTING MUSCLE SUBJECTED TO STRETCH OR PRODUCING WORK

A.K. Tsaturyan[1], N.A. Koubassova[1], M.A. Ferenczi[2], S.Y. Bershitsky[3]

[1]Institute of Mechanics, Moscow University,
1 Mitchurinsky prosp., Moscow 119992 Russia;
[2]Imperial College London Exhibition Road, London SW7 2AZ, UK;
[3]Institute of Immunology and Physiology Ural branch RAS,
91 Pervomayskaya str. Yekaterinburg 620219 Russia

Although high resolution structure of actin [1] and globular myosin head [2] are available, structural properties of actin-myosin complex in contracting muscle are still unknown. Little is known about changes in its structure in muscle subjected to stretch or contracting under an intermediate load and producing mechanical work. To address these questions we determined changes in 2D x-ray diffraction pattern from small bundles of fibres with permeabilized membrane from rabbit fast skeletal muscle caused by transi-

tion from steady-state isometric contraction to ramp lengthening or shortening under nearly constant load. Direct modeling approach [3] was used for data analysis and interpretation.

Methods

Experiments were performed on the ID02 beamline at the European Synchrotron radiation source (ESRF, Grenoble, France). Main details of methods and apparatus were described recently [4]. Briefly, bundles were activated at 0-1°C with a saturating Ca-activating solution, suspended in cold wet atmosphere at 4-5°C and then subjected by a joule temperature jump (T-jump) to 31-34°C. When steady-state isometric tension was achieved an x-ray frame was recorded. Then muscle was stretched or shortened at a constant velocity and another x-ray frame was recorded at an approximately constant tension.

Results and Discussion

The time course of temperature, length change and tension in a ramp stretch experiment are shown in fig. 1*A* together with the timing of the x-ray frames. The meridional profiles of the meridional (reciprocal radius $R = \pm 0.018$ nm^{-1}) and off-meridional ($R = 0.018$-0.06 nm^{-1}) are plotted in fig. 1B.

The meridional myosin M3 intensity as well as off-meridional intensities of the inner myosin M1, M2 and actin A1, A2 layer lines decreased during forced lengthening of contracting muscle (fig. 1*B*). Control experiments with single muscle fibres show a 30-35% increase in instantaneous stiffness during stretch as was found earlier in intact frog muscle fibres [5, 6]. The stiffness rise together with the decrease in the intensities of myosin layer lines, M1 and M2(which mainly result from detached heads) indicate that stretch induces an increase in the fraction of actin-bound myosin heads, possibly due to fast binding of the second head of the same myosin molecule [6]. On the other hand,

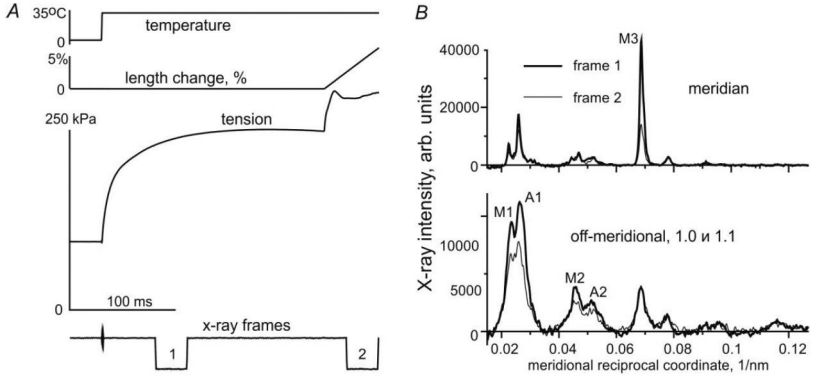

Fig. 1. Experimental protocol (A) and changes in the meridional and off-meridional x-ray intensities (B) in ramp stretch experiments. Data from 9 runs of the protocol in 5 bundles of muscle fibres, background is subtracted.

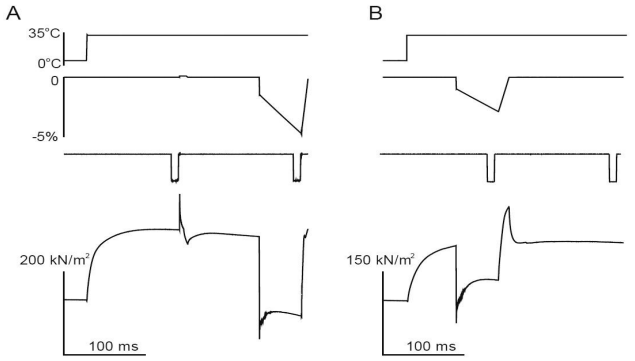

Fig. 2. Typical examples of experimental records for two series of experiments with steady shortening at low (*A*) and high (B) load. Records from top to bottom: temperature; changes in muscle fibre length (in % of its value at sarcomere length 2.45 □m); signal of opening of the fast x-ray shutter recorded with a pin diode (x-rayframes) and tension. Step stretches of 0.2% of muscle length completed in 0.14 ms were applied just after the end of the x-ray frames in *A* to measure instantaneous stiffness.

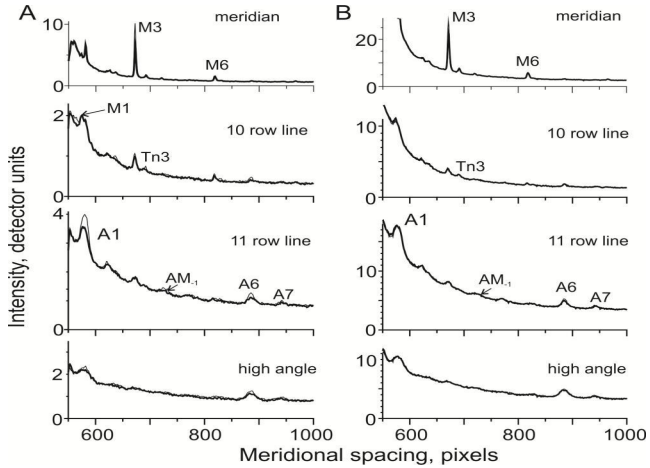

Fig. 3. Meridional profiles of the meridional and off-meridional x-ray intensities collected from two muscle samples presented in Fig. 2 (*A* and *B*, 7 and 20 runs of the protocol, respectively). Thin traces correspond to isometric contraction; thick ones were collected during steady shortening and then corrected for the change in the fibre volume exposed to the x-ray beam. From top to bottom: intensity profiles integrated on the meridian (radial spacing of 0-0.02 nm-1); the 10 row line (0.02-0.032 nm-1); the 11 row line (0.032-0.06 nm-1) and the high angle part of the patterns (0.06-0.09 nm-1). Some myosin (M) and tropomyosin (Tn) meridional reflections and actin (A) and actin-myosin beating (AM) layer lines are labeled.

the decrease in the A1 and A2 intensities at higher fraction of actin-attached heads (fig. 1*B*) show that during stretch the fraction of stereo-specifically bound heads decreases [2, 3]. We therefore conclude that stretch unlocks stereo-specifically bound myosin heads and possibly transforms them to a non-stereo-specifically attached state as suggested by the 'roll and lock' model [7].

In two other series of experiments 2D ray diffraction patterns during isometric contraction at elevated temperature was compared to those collected during near-steady shortening under load of ~0.3-04*P*0 or 0.61-0.68*P*0 where *P*0 is isometric tension. Typical experimental protocols are shown in fig. 2. The range of 0.3*P*0 to 0.7*P*0 corresponds to maximal work production of a skeletal muscle. From 2 to 20 runs of the protocol were performed with each of 14 samples until damage or isometric post-T-jump tension decreased by 15% compared to its value after the 1st run. In some experiments instantaneous stiffness was measured with fast (~0.14 ms long) step stretches applied during isometric contraction and at the end of ramp shortening just after the x-ray frames (fig. 2*A*). Both diffraction patterns were collected during 10 ms long exposures at near physiological temperature of 32-34°C achieved with a joule temperature jump (T-jump, top records in Fig. 2). Step shortening was applied before the ramps to accelerate the transient that precedes the steady-state shortening (fig. 2*A*).

Ramp shortening induced a decrease in the intensity of the M3 myosin meridional reflection and of all actin layer lines in the pattern, from A1 at ~(37 nm)-1 to A7 at ~(5.1 nm)-1. Also the intensity of the beating actin-myosin layer line at ~(10.3 nm)-1 decreased sharply (fig. 3). Changes in the intensities of the x-ray reflections caused by steady shortening at a ~*P*0/3 load were more pronounced than those at a ~2*P*0/3 load. A significant difference was found in the intensity of the actin layer lines which did not change much during shortening at the high load while decreased dramatically at the lower load (fig. 2). The reason for this striking difference is not clear. Further quantitative analysis and modeling [3, 4] are needed to draw more solid quantitative conclusions from the data.

References

1. Dominguez R., Holmes K.C. *Annu Rev Biophys.* 2011; 40:169-86.
2. Koubassova N.A., Tsaturyan A.K. *Biochemistry* (Mosc). 2011; 76(13):1484-506.
3. Koubassova N.A., Bershitsky S.Y., Ferenczi M.A., Tsaturyan A.K. *Biophys J.* 2008; 95(6):2880-94.
4. Tsaturyan A.K., Bershitsky S.Y., Koubassova N.A. *et al. Biophys J.* 2011; 101(2):404-10.
5. Lombardi V., Piazzesi G. *J. Physiol.* 1990; 431:141-71.
6. Brunello E., Reconditi M., Elangovan R. *et al. PNAS. USA.* 2007; 104(50):20114-9.
7. Ferenczi M.A., Bershitsky S.Y., Koubassova N. *et al. Structure.* 2005; 13(1):131-41.

MYELINATION DISORDERS IN MECHANISM OF HYPOGRAVITY MOTOR SYNDROME DEVELOPMENT

O.V. Tyapkina[1], L.F. Nurullin[1], P.N. Rezvyakov[2], E.E. Nikolskiy[1,2], R.R. Islamov[2]

Kazan Institute of biochemistry and biophysics of Russian Academy of Science, Lobachevski str., Kazan, 420111, Russia
Russia Kazan State Medical University, Butlerov str., Kazan, 420012, Russia

In the past decade has seen a significant increase in the amount of research devoted to studying the effects of weightlessness on living systems, both at the organism, and the molecular-cellular level. One manifestation of the effects of weightlessness on the human is hipogravity motor syndrome. The absence of functional load in conditions of weightlessness in space, as well as the simulation hypogravity on Earth, certainly leads to morphological changes (atrophy, distortion skeletomyscular phenotype) and function (decreased tone and strength, increased fatigue) properties of skeletal muscles. However, despite over 50 years of experience in human spaceflight, hypogravity influence on morphological characteristics of spinal cord that directly controls the innervation of skeletal muscle remain poorly understood. Previously, the model antiorthostatic hanging rats (hypogravity simulation on Earth of the Morey Holton, 2002), we found that the lumbar enlargement of spinal cord in the experimental rats became less pronounced, and the analysis of transverse serial sections of lumbar spinal cord revealed a decrease in their areas by the 7th day of experiment by 18%, which remained at this level up to 35 days. These results may indicate a decrease in the area of gray and / or white matter of the lumbar spinal cord of experimental rats. To clarify the spinal cord responsible for the decrease in lumbar enlargement in the experimental animals was carried out a differential analysis of the areas of white and gray matter cross sections in the lumbar and cervical regions of the control and experimental rats after antiorthostatic hanging for 7, 14 and 35 days. The analysis revealed a decrease in the area of white matter by 40% ($n = 4$, $p < 0.05$) by the 7th day of the experiment, 31% ($n = 4$, $p < 0.05$) - to 14-th day, and to 35 Day - 29% ($n = 4$, $p < 0.05$). The average values of the area of gray matter in the experimental rats remained unchanged. Also, the experimental animals revealed no change in the areas of white and gray matter in the cervical spinal cord. Thus, the decrease in the lumbar spinal cord of rats after antiorthostatic hanging due to a decrease in the area of white matter of the spinal cord. To identify possible mechanisms for the development of morphological changes in the spinal cord was performed by us fully genome study of gene expression in the lumbar spinal cord of mice after 30 days antiorthostatic hanging with the chip MouseRef-8 (Illumina).Statistically significant differences were documented in the expression of 38 genes, with the observed inhibition of expression of 37 genes and increased - a single gene. Of particular interest is the fact that reduction of mRNA expression of five genes encoding proteins of myelin (MPZ, PMP2, PMP22, C1orf130, PRX), which are responsible for the formation of the myelin sheath.

These data agree well with experimental rats revealed a decrease in the area of white matter in the lumbar spinal cord and give a good reason to think that the decrease in mRNA levels of genes encoding proteins of myelin, may be accompanied by a violation of myelinization in the CNS and is one of the factors underlying the development of hipogravity motor syndrome.

The study was supported by grants: Program for Basic Research Department of Biological Sciences of RAS, RFBR № 10-04-01423, Ministry of Education and Science of the Russian Federation, the federal program № 16.512.11.2101, the President of Russia NSh.

NITRIC OXIDE (II) DECREASES THE TRANSMITTER RELASE AT THE MOUSE NEUROMUSCULAR JUNCTION THROUGH CAMP AND CGMP-DEPENDENT SYSTEMS

F.F. Valiullina, E.V. Gerasimova, G.F. Sitdikova

Kazan Federal University, 18, Kremlevskii str., Kazan, 420008, Russia

Nitric oxide (II) (NO) has a broad spectrum of biological action. NO was first considered as a regulator of physiological processes after discovering of the nature of relaxing factor synthesized by endothelial cells of blood vessels. Subsequently it was shown that NO is a neurotransmitter and neuromodulators in many peripheral and central synapses, providing both inhibitory and activating effects on synaptic transmission [1]. In the peripheral nervous system has been shown that NO decreases the transmitter release from motor nerve terminal of frogs through cGMP-dependent and cGMP-independent mechanisms [3]. In the mammalian neuromuscular junction the effects of NO are not clear [2]. The aim of this study was to investigate the effects of NO on the neurotransmitter release in the neuromuscular synapse, mouse, and to identify of the role of second messengers (cAMP and cGMP) in the realization of these effects.

Methods

Experiments were conducted on isolated nerve-diaphragm muscle preparations of the laboratory white mice under conditions of constant perfusion of the standard Krebs solution. To eliminate the contraction of the muscles d-tubocurarine was added in the solution at concentration of 2-2.5 μM. Pharmacological agents from Sigma (USA) were used in the experiments. The end plate currents (EPCs) were registered using extracellular microelectrodes, filled with NaCl (2M). Stimulation of motor nerve was produced by rectangular electrical pulses of suprathreshold amplitude and duration of 0.16 ms with 0.2 Hz. Accumulation and averaging of the signals were produced by a personal computer using the original program «Elph» (author – PhD A. Zakharov). Statistical analysis of the obtained data was hold using the parametric Student's t-test.

Results

To study the effects of nitric oxide (II), we used an exogenous donor of NO - S-nitroso-N-acetylpenicillamine (SNAP) at a concentration of 100 μM. The addidtion of SNAP in the solution led to a decrease of the amplitude

of the EPCs to 71,6 ± 4,4% (n = 14, p <0.05) relative to controls by 30 minutes of its action (Fig. 1A). The substrate of NO synthesis - L-arginine at a concentration of 100 μM reduced the amplitude of the EPCs to 65,2 ± 6,8% (n=5, p<0,05) from control by 35 minutes of application (Fig. 1 B). Thus, the substrate of NO synthesis has the same effects as the donor, indicating that the endogenous synthesis of gas at the neuromuscular synapse Activation of soluble guanylyl cyclase (sGC) and the production of cGMP is the main target of NO action in many cells [1]. Inhibition of soluble guanylyl cyclase produced by selective blocker - 1H-[1,2,4]-oxadiazolo [4,3-a] quinoxalin-l-one (ODQ) at a concentration of 2.5 μM, completely prevented the decrease of transmitter release by SNAP, which indicated the participation of sGC in NO effects. To increase the intracellular levels of cAMP and cGMP, we used cell permeable analogs - 8BrcGMP and 8(4CPT) cAMP at a concentrations of 100 μM. In the blocking effect of SNAP guanylyl cyclase does not occur, and the 30-minute amplitude of EPCs was 102,9 ± 7,3% (n = 6, p> 0,05). In the presence of 8BrcGMP SNAP reduced the amplitude of the EPCs by 44,9 ± 4,0% (n = 6, p <0,05) compare to control, which indicated on cGMP-independent mechanism of NO action. In the presence of 8(4CPT) cAMP application of SNAP induced the increase of EPCs amplitude to 122,43 ± 12,3% (n = 6, p <0,05) by 20 min of its action.

The obtained date indicates that NO effects in mouse neuromuscular junction mediates by the activation of soluble guanylyl cyclase. At the same time the reduction of transmitter release by NO was not prevented by the increase of cGMP level but was completely prevented after the elevation of

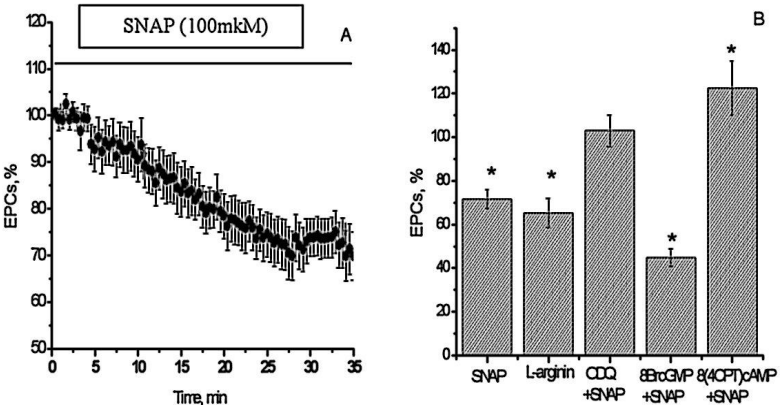

The effects and mechanisms of action of NO in transmitter release at the mouse neuromuscular junction. A – The effect of exogenous donor of NO - SNAP at a concentration of 100 μM on the amplitude of the EPCs; B - the amplitude of the EPCs during the exposure of SNAP in control, L-arginine, SNAP on the background of ODQ, 8BrcGMP and 8(4CPT)cAMP, respectively. * - p<0.05.

cAMP level, where we even observed the increase of transmitter release. It was suggested that cAMP- and cGMP-dependent mechanisms mediated the NO-action in mouse neuromuscular junction

Acknowledgement: This study was funded by RFBR and Leading Scientific School № SS-4670.2012.4.

References

1. Bredt, D.S. Nitric oxide, a novel neuronal messenger / D.S. Bredt, S.H. Snyder / / Neuron. - 1992.-V. Eight. № 1. - P.3-11.Two.
2. Nickels, T.J. Does nitric oxide modulate transmitter release at the mammalian neuromuscular junction? / T.J. Nickels, G.W. Reed // Journal of Physiology. – 2007. – V.32. – P. 318-326.
3. Yakovlev, AV Intracellular mechanisms of presynaptic effects of nitric oxide (II) in neuromuscular junction frog / A. Yakovlev, GF Sitdikova, AL Zefirov / / Neurochemistry. - 2005. - T. 22. Number 1. - S. 81-87.

MODELING TRANSMURAL ELECTRICAL AND MECHANICAL PROPERTIES OF CARDIOMYOCYTES FROM GUINEA PIG LEFT VENTRICLE

A.D. Vasilyeva[1], O.E. Solovyova[1,2]

[1]Institute of Immunology and Physiology Ural Branch of Russian Academy of Sciences, Pervomayskaya str. 106, Ekaterinburg, 620049, Russia
[2]Ural Federal University named after the first President of Russia B.N.Yeltsin, Mira str., 19, Ekaterinburg, 620002, Russia

It is shown that ventricular cardiomyocytes from the subepicardial, mid-myocardial, and subendocardial layers differ in their electrical and mechanical properties, heart rate dependence and pharmacologic sensitivity. In contrast to a number of papers addressing the electrophysiological heterogeneity of cardiomyocytes, much less is known about heterogeneity of the mechanical function. As to our knowledge, there are no detailed models, which take into account specific features of the mechanical behavior of cardiomyocytes from different regions of the ventricular wall.

We develop biophysically based mathematical models of cardiomyocytes from subEPI- and subENDO-cardial ventricular layers in guinea pig, that are based on our model of the electro-mechanical coupling in cardiomyocytes [1]. To develop EPI and ENDO models we used literature data on the differences in the electrophysiological parameters and in the mechanical characteristics of the molecular processes (different rates of bridge cycling, degree of cooperativity of calcium activation of contractile proteins, etc.) in the cells to simulate respective differences in the shape and duration of action potential, Ca^{2+} transient and contraction observed experimentally in the cells [2, 3].

The cellular models will be used within the tissue models of myocardium to explore the physiological effects of cellular heterogeneity in myocardium function.

Work is supported by Interdisciplinary project 12-M-14-2009 of Presidium of Ural Branch of Russian Academy of Sciences.

References

1. Sulman, T., Katsnelson, L. B., Solovyova, O. and Markhasin, V. S. (2008) Mathematical modeling of mechanically modulated rhythm disturbances in homogeneous and heterogeneous myocardium with attenuated activity of Na(+)-K(+) pump. Bull Math Biol 70 (3), 910-49.
2. Wan, X., Bryant, S., Hart, G. (2003). A topographical study of mechanical and electrical properties of single myocetes isolated from normal guinea-pig ventricular muscle. J Anat. 202. 525-536.
3. Aitmou, Y., Guennec, J., Mosca, E., Tombe, P., Cazorla, O. (2008). Differential contribution of cardiac sarcomeric proteins in the myofibrillar force response to stretch. Pflugers Arch. 457(1). 25-36.

COMPARATIVE ANALYSIS OF STRUCTURE OF CALIX[4]ARENEPHOSPHONIC ACIDS AND THEIR INHIBITORY PROPERTIES TOWARDS SMOOTH MUSCLE Na+,K+-ATPase

T. Veklich, A. Shkrabak, S. Kosterin

Palladin Institute of Biochemistry, National Academy of Sciences of Ukraine, Kyiv
e-mail: kinet@biochem.kiev.ua

Na^+,K^+-ATPase is an important plasma membrane enzyme of all tissues, which generates the concentration gradients of K^+ and Na^+ and takes part in different physiological processes. Taking into consideration the role of Na^+,K^+-ATPase in supplying of coupling of smooth muscles contractility, both for fundamental and practical viewpoint, search of new reversible effectors which would be able to make the direct influence on this enzymatic system has great significance.

Nowdays a great attention is paid to such synthetic compounds as calixarenes. It was shown that calixarenes can penetrate through plasma membrane in the cells and practically have no toxic action. Some of them posses bactericidal, antiviral, antitumoral, antithrombotic activity. So calixarenes are perspective for designing of compounds capable to influence on biochemical processes.

The aim of researches was to investigate the effects of the calix[4]arenes C-296, C-297, C-424, C-425, C-426, C-427, wich are structural similar to calix[4]arene C-99, on smooth muscle Na^+,K^+-ATPase activity.

In our previous investigation we found that calixarene C-99 (5,17-bis(dihydroxyphosphonylmethylol)-26,28-dihydroxy-25,27-dipropoxycalix[4]arene) effectively inhibited Na^+,K^+-ATPase and did not influence on activity of other membrane-bound ATPases. The calixarene C-99 inhibition coefficient $I_{0.5}$ was less than the same parameter of ouabain (98 ± 8 nM та 21 ± 5 μM respectivly). Trerefore calixarene C-99 much more effectively inhibits the enzymatic activity of sodium pump than ouabain does.

It was shown that calixarenes C-296 and C-297, which have two additional propoxygroups on the lower rim of macrocycle, were less effective inhibitors of Na^+,K^+-ATPase than calixarene C-99: the magnitudes of the inhibition coefficient $I_{0.5}$ of these calixarenes were 4.90 ± 0.31 and 15.21 ±

1.92 μM respectively. Trerefore additional propoxygroups on the lower rim of calixarenes C-296 and C-297 caused the decrease of effectivity of the Na^+,K^+-ATPase inhibition.

Calixarene C-424, which haes only two residues of carbonic acid on the upper rim, and calixarene C-426, which has ketomethylphosphonic residues on the upper rim instead of hydroxymethylphosphonic residues, almost did not influence on the Na^+,K^+-ATPase activity. The absence of inhibitory action of calixarene C-424 indicates that exactly phosphonate groups are crucial for effective interaction of calixarene C-99 with enzyme and its inhibition. Since calixarene C-426 has ketogroups on methylphosphonic residues instead of hydroxygroups of calixarene C-99, perhaps, these hydroxygroups form hydrogen bounds needed for creation inhibitory complex of calixaren C-99 with Na^+,K^+-ATPase. Besides, more inflexible conformation of calixarene C-426 probably cannot effectively interact with Na^+,K^+-ATPase.

Calixarenes C-425 and C-427, which have three and four phosphonate groups respectively on the upper rim of macrocycle, also inhibited Na^+,K^+-ATPase activity: the magnitudes of the inhibition coefficient $I_{0.5}$ of these calixarenes were 1.20 ± 0.10 and 2.80 ± 0.18 μM respectively, that indicated less effective inhibition relative to calixarene C-99. Obviously, the interaction of just two phosphonate groups with enzyme leads to effective inhibition of Na^+,K^+-ATPase.

Thus, comparing of the structural similar calix[4]arenes effects on uterus plasma membrane Na^+,K^+-ATPase let us determine certain chemical groups of molecule which cause their inhibitory properties relative to mentioned enzyme. Besides, using such analysis we can suppose the structures of new hypothetic calixarenes which could inhibit the Na^+,K^+-ATPase. In other words, the data of our work can be a foundation for further creation of effective inhibitors of Na^+,K^+-ATPase and muscle contractility.

We are thankful to corresponding member of NAS of Ukraine V.I. Kalchenko and his colleagues from Institute of organic chemistry of NAS of Ukraine for synthesis and kind giving of calixarenes for using in biochemical researches.

PHOTO-INDUCED CONFORMATIONAL MOTILITY OF PROTEINS

N.L. Vekshin

Institute of Cell Biophysycs of RAS, Pushchino, nvekshin@rambler.ru

Many researchers, who use tryptophan fluorescence as a method for indication of conformational dynamics of proteins, mean that this fluorescence reflects the spontaneous “thermal” dynamics. This assumption is fair only, if tryptophan residues are completely shipped in a water phase, i.e. when $\tau_{rel} << \tau$. Otherwise (for proteins with hidden tryptophan residues), the fluorescence analysis bears an information also about compelled dynamics, induced by photo-excitation. That is why theoretical estimations in the frames of spontaneous dynamics give low values of rotary mobility of tryptophan residues, but experimental fluorescence data, especially from depolarization of fluorescence – high ones.

In glycerol, ethanol, water and other polar solvents, the photo-excitation of a chromophore results in the compelled mobility of its solvate shell. Such mobility arises, first, owing to sharp increase in the dipole moment of chromophore at its excitation and, secondly, owing the expense of instant "heating" of solvated molecules by energy, liberated in a course of vibronic relaxation in the chromophore. For tryptophan in glycerol, substitution the values P_0 = 0,5, η = 10 poise, V = 30 Å^3, T = 294K, R = 8,3 J/mol × K and τ = 4,2 ns in the Levshin-Perrin equation gives P = 0,33. This value coincides with experimental P, received at excitation 300 nm and detection at 320 nm. Substitution τ = 5,4 ns gives P = 0,3, that is close to experimental value P at 380 nm. The change P along the emission spectrum of tryptophan molecules in glycerol is induced by increase in a turn angle of those molecules, which have greater life-time.

Proteins have three kinds of rotary mobility, which can depolarize their tryptophan fluorescence: a) own mobility of tryptophan residues; b) mobility of segments of protein; c) rotation of a protein globule as whole. For massive proteins (lactate dehydrogenase, peroxidase, membrane ATPase of sarcoplasmic reticulum and so on), the rotary mobility of globules as whole does not bring appreciable contribution to depolarization. For small proteins and polypeptides (for example, for glucagon), the globule rotation cannot be neglected. Changes in P along emission spectrum of proteins have the same main reason, as for tryptophan in glycerol, i.e. are caused by variations in rotary mobility.

One of the major reasons of inconstancy of P along emission spectra of probes (and labels also) is the increase of rotation angles of chromophores because of increase in their life-times. A similar situation takes place in proteins and peptides; photo-induced mobility arises in them. Spectral heterogeneity of tryptophan emission of proteins and peptides in many cases may be explaned like formation of exciplex photo-conformers.

The life-times and their amplitudes of three single-tryptophan proteins (with known spatial structure) are given in Table. The fluorescence decay of ribonuclease T1 at pH 5,5 is strict exponential (τ = 4 ns) and does not vary with emission wavelength. The tryptophan residue in this protein is hidden deep in globule and fixed enough rigidly. There are no polar groups (which capable to form different centers of emission) near this Trp. Therefore, there is no appearance a set of radiating centers upon photo-excitation, and there is only one emission center. Neither conformers or photo-conformers of this protein exist (at pH 5,5).

Fluorescence decay of the calcium form of parvalbumin is two-exponential. There is a change of τ along spectrum of emission (Table). Two types of radiating centers are detected at photo-excitation of parvalbumin. In "red" area, there is only one component (3,4 ns), belonging to exciplex of tryptophan with any protein polar group or molecule of water, penetrating into the protein globule after photo-excitation. The existence of the complex initially (before photo-excitation) is hardly possible, because of the tryptophan band in absorption spectrum of parvalbumin (Fig. 1) has precisely

expressed vibronic structure (it is characteristic for a gas-like phase). The protein initially has no conformers. Moreover, the emission spectrum (at 20°C) practically is deprived any vibronic structure. It is appreciably “smeared" (Fig. 2), i.e. very strong interactions in the excited state take place. They are

Life-times of tryptophan emission of ribonuclease T1, parvalbumin and phospholipase A2

Protein	λ_{em}, nm	τ_1, ns	τ_2, ns	τ_3, ns	a_1	a_2	a_3	τ, ns
Ribon]uclease	310	-	-	4,0	-	-	1,0	4,0
	320	-	-	4,0	-	-	1,0	4,0
	340	-	-	4,0	-	-	1,0	4,0
	375	-	-	4,0	-	-	1,0	4,0
Parvalbumin	310	-	1,1	3,4	-	0,15	0,85	2,7
	320	-	1,3	3,3	-	0,07	0,93	3,2
	340	-	1,7	3,3	-	0,05	0,95	3,3
	375	-	-	3,4	-	-	1,0	3,4
Phospholipase	320	0,6	2,1	5,3	0,71	0,24	0,05	1,2
	350	0,7	2,7	7,2	0,63	0,32	0,05	1,7
	385	0,7	2,7	6,5	0,61	0,33	0,06	1,7
Phospholipase in glycerol	320	0,4	2,1	5,6	0,40	0,43	0,17	2,0
	350	0,8	2,7	6,3	0,19	0,54	0,27	3,3
	385	-	-	4,0	-	-	1,0	4,0

Note: Excitation was 295 nm. Slits were 5 nm. RNAase T1 was in the 100 mM acetic buffer (pH 5,5). The calcium form of parvalbumin was used in the 25 mM Tris-HCl buffer with 1 mM CaCl2 (pH 8,2). Pork phospholipase A2 was in the 100 mM acetic buffer (pH 5,8) or 90 % glycerol. For detection of emission at 310 and 320 nm, mirror cuvettes were applied.

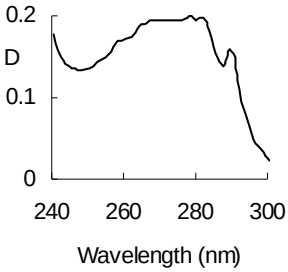

Fig. 1. Absorption spectrum of parvalbumin in 25 mM Tris-HCl (pH 8,3) at the presence of 1 mM calcium chloride.

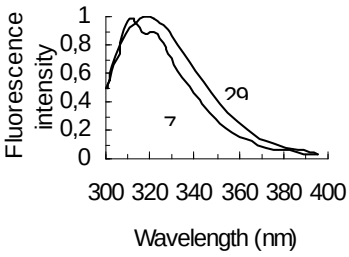

Fig. 2. Fluorescence spectrum of parvalbumin (the calcium form; the spectrum at low temperature was recorded by G.Deikus).

removed at low temperature (at 77 K): vibronic structure appears. So, at UV irradiation of the given protein at 20°C, the photo-conformers arise.

The fluorescence decay of phospholipase A_2 is three-exponential. Amplitudes of components rather poorly vary along the emission spectrum of given protein in aqueous solution. It is due to that the tryptophan residue in phospholipase places at a surface of the globule and contacts to water. This protein exists as a number of conformers. Vibronic relaxation in photo-excited tryptophan and solvated water molecules proceeds during picoseconds and, consequently, has not an effect in nanosecond range. Two components of the decay - 0,7 ns and 2,7 ns - are close to similar components for aqueous solutions of tryptophan or NATA. However, as against of tryptophan or NATA, the dominant is not second component, but first. The third component, having very small amplitude and very long life-time (~ 7 ns), belongs to exciplex of tryptophan with any polar group of protein, i.e. it reflects a little quantity of photo-conformers. In glycerol, the amplitude of long-lived components of the protein sharply grows and its value a little changes, especially in "red" area. Average life-time behaves here like in the case of tryptophan or NATA in glycerol solution: essentially grows from "dark blue" area to "red" one. And, in "red" region, there is only one component – long-lived. These data suggest about appearance the exciplexes between tryptophan residues of phospholipase and glycerol molecules.

The UV excitation of proteins induces both - own mobility of tryptophan and mobility of next groups. Energy (E), inducing such mobility, can be found as: $E = h\nu_{ex} - h\nu_{em.}$ For fluorescent tryptophan, the excitation at 290 nm and emission 340 nm gives E = 60 kJ/mol, that is enough to break 4 hydrogen bounds. For non-fluorescent tryptophan, E = 410 kJ/mol. It means that photo-conformational relaxation, translating a protein globule to a new steady conformation, can happen. Upon intensive UV illumination, the protein denaturation, accompanying by widening and long-wavelength shift of emission, occurs. For enzymes, it is equivalent as inactivation (Fig. 3). It is not surprised that UV photo-inactivation of enzymes takes place much faster, than photolysis of their tryptophan residues.

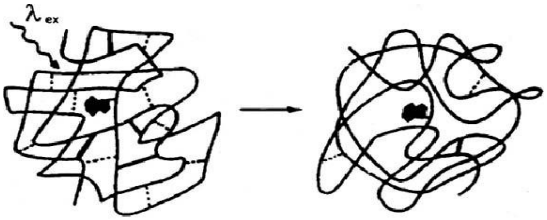

Fig. 3. Inactivation of an enzyme during photo-conformational relaxation upon UV illumination.

Reference

Vekshin N.L. Fluorescence Spectroscopy of Biomacromolecules. Photon-vek, 2009.

THE ISOLATION AND PURIFICATION OF HUMAN BLOOD PLASMA PROTEINS FORMED CHANNELS FOR POTASSIUM IN ARTIFICIAL BILAYER LIPID MEMBRANE

N. Venediktova[1], K. V. Kuznetsov[1], G.D. Mironova[1,2]

[1]*Institute of Theoretical and Experimental Biophysics, Russian Academy of Sciences, Pushchino, Moscow region, 142290, Russia*

[2]*Pushchino State Natural Science Institute, Pushchino, Moscow region, 142290, Russia*

It is known that the action of many drugs is related to their influence on the ion channel work. Generally these channels are localized in membranes of cells. Earlier from sport horse blood plasma using the methods of paper chromatography we have isolated a protein which capable to transport potassium across an artificial bilayer lipid membrane. The protein amount in the blood has varied depending on the animal functional state (M.Y. Alekseev et al., 1976).

In this work we report the purification of the blood plasma proteins and its structure and properties under reconstitution into bilayer lipid membrane (BLM).

The human blood plasma was extracted by 96% ethanol (-20°C). End concentration of alcohol extract was 50%. Extraction takes an hour at 4°C under constant stirring. The extract was separated by centrifugation at 5000×g for 1 hour at 4°C. The resulting pellet was resuspended carefully in the same volume of 50% ethanol (-20°C) followed by extraction for 30 min and centrifugation in the above described conditions. The supernatants were combined and evaporated to 20 ml under vacuum at 30°C. The lipids were removed from the extract by Folch method (J. Folch et al., 1956). Water-methanol phase was evaporated and was applied on G-15 Sephadex column volume 1350 ml. The elution was carried out with twice-distilled water at the rate of 45 ml/hr. The elution profile of the extract consists of four peaks.

The each peak content was evaporated to ~1 ml and was applied on the 1 ml DEAE sepharose column equilibrated with a buffer: 50 mM Tris-HCl, 1 mM EDTA, pH 7.4 and 0.05% β-mercaptoethanol. The sample was washed with the same buffer and eluted with step by step double gradient of 50, 100, 150, 200, 250 and 500 mM KCl at the rate of 5 ml/hr.

Composition of obtained protein fractions was examined by SDS/PAGE-electrophoresis. The fractions 50-150 mM KCl contained the proteins with m. m. about 50 kDa and 68-70 kDa proteins were detected in 250-300 mM KCl.

The ion-transporting properties of column effluent were tested using BLM formed from total brain lipids diluted in *n*-decane in a concentration 20 mg/ml (M. Montal and P. Mueller, 1972). The samples were reconstituted in artificial membrane and we found that the fraction of peak 2 eluated by 250 mM KCl had the most pronounced K^+-transporting activity in the presence of 100 mM KCl. The studied protein sample was added to the *trans* compartment. Incorporation of the potassium channel into the BLM was usually observed within a few

minutes. All measurements were carried out at 26 °C. The addition of the 250 mM KCl fraction resulted in the formation of transient channels in BLM with a minimum single-channel conductance about 3.4 pS. The average single-channel conductance was equal 5.4±0.9 pS. There were also the forming channels with higher conductance of about 6.6-7, 13.5-14, 25, 35 pS and others.

To obtain further information on the channel forming protein properties and structure the 250 mM KCl eluates of peak 2 were concentrated on the special filters (ultra-4 centrifugal filter unit, 30kDa) limited with molecular weight 30kDa. After addition of the concentrated fractions to the *trans* side of the artificial membrane in the presence of 100 mM KCl, we recorded the discrete current change. It was evidenced about the conductance channel formation (figure).

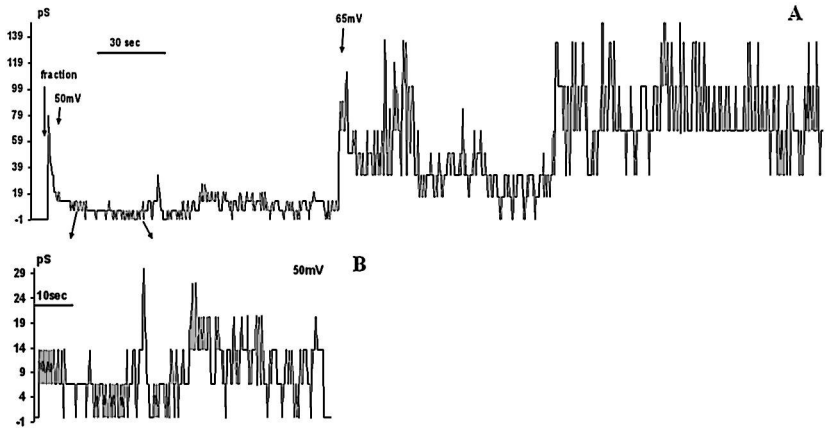

(A) current-time recordings in the presence of the concentrated fraction. (B) it is showed more detailed record of single channels. The chamber solution contained 20 mM Tris-HCl buffer, pH 7.4, and 100 mM KCl.

After the studied sample reconstruction in BLM the minimum single-channel conductance was 6.6-7 pS for set potential 25-65 mV. At incorporation of abundant channels into the lipid membrane we have registered conductance of 13.5-14, 27-28, 67, 135 pS.

The ion selectivity of the channel formed by the studied sample was carried out by zero-current membrane potential measurements in presence of KCl gradients. Using a threefold gradient of KCl (100 mM in *cis*- and 500 mM in *trans* side of lipid membrane) in the presence of fraction we recorded the potassium-selective potential balanced by voltage of - 29 mV. This value is very close to the theoretical Nernst potential in this case. This means that the examined ion channel is a cation-selective (A.G. Komarov et. al., 2004).

Channel forming activity of sample was observed only in the presence of cation K^+. In the absence of K^+, the permeability of the reconstituted

membrane was the same as that of the control membrane. No channel activity was recorded in the presence of calcium and sodium ions, until in medium K^+ was added to form the channel (table).

Effect of different cations on the permeability of the membrane modified with the studied protein component

Electrolyte	Concentration, мМ	Conductance
KCl	100	+
NaCl	100	-
$CaCl_2$	10	-

Using a 14% separating gel we detected in the concentrated fraction proteins with molecular weights of about 70, 57, 30 kDa. Their structure has studied with MS-MALDI-TOF/TOF analysis. Further information about the channel forming proteins consisted in the determination of homology to the sequences of known protein structures from the database NCBI. For this purpose electrophoresis of sample was carried out and proteins with molecular masses of 70, 57, 30 kDa were cut from the gel and analyzed MS-MALDI-TOF/TOF. According to data obtained with MS-MALDI-TOF/TOF and database NCBI 22% of amino acid sequence of protein №1 (m. m. ~ 70 kDa) was similar to the precursor protein of human serum albumin. Protein №2 having a molecular weight of approximately 57 kDa did not reveal any similarity with database proteins and was identified as an unnamed protein product/hypothetical protein/albumin-like protein. The molecular weight of the protein №3 (~ 30 kDa) was equal to 28061 Da, its 62% amino acid sequence was homologous to the chain A of human apolipoprotein A-I.

Thus, on the basis of MS-MALDI-TOF/TOF analysis we obtained three protein samples, which could form channels in the BLM. In order to exclude the involvement of albumin in the modification of the artificial membrane we tested the properties of the commercial serum albumin (SA). SA was subjected to the same procedures as the plasma, including Folch process, treatment with ethanol and purification by gel filtration and ion exchange chromatography. Albumin after the ion-exchange chromatography procedure was detected in the fractions eluted 100-200 mM KCl. No K^+-transporting activity was recorded in the presence eluates 100-200 mM KCl, as well as 250 and 500 mM KCl.

Thus, we could suggest that channel forming protein that modifies the lipid membrane is apolipoprotein A-I.

This work was supported by Department of the priority directions of science and technology №4.3010.2011 and by grant from Russian Foundation for Basic Research №10-04-00920-a.

References

1. M.Y. Alekseev, N.I. Fedotcheva, G.D. Mironova , M.N. Kondrashova. The potassium permeability activator and inhibitor of peroxidase in horses blood serum during exercise. Biological Sciences № 11, 1976, pp. 28-30.

2. J. Folch, M. Lees, and G.H. Sloane Stanley. A simple method for the isolation and purification of total lipids from animal tissues. J. Biol. Chem. 1957; 226(1): 497-509.
3. M. Montal and P. Mueller. Proc. Nat. Acad. Sci. USA. 1972, 69 (12), pp. 3561-3566.
4. Alexander G. Komarov, Brett H. Graham, William J. Craigen, and Marco Colombini. Biophysical Journal. 2004, 86, 152–162.

INVESTIGATION OF EC COUPLING IN ISCHAEMIC MYOCARDIUM USING A CONTINUOUS 1D MODEL OF A CARDIAC MUSCLE

N.A. Vikulova, L.B. Katsnelson, T.B. Sulman

Institute of Immunology and Physiology of the Ural Branch of the Russian Academy of Sciences, 106 Pervomayskaya st., Yekaterinburg, 620049, Russia

Modern researches of myocardial function in normal and pathological conditions extensively use mathematical models that describe both direct and feedback dependencies between mechanical, biochemical and electrical events in a heart on different levels of its organization.

In our investigation we aimed to study changes in electrical and mechanical function of cardiomyocytes during hypoxia and ischemia using a continuous 1D model of a cardiac muscle.

Ischemic heart disease is provoked by malfunction of blood flow in coronary arteries resulting in insufficient oxygen supply of cardiac tissue (hypoxic changes). Accumulation of metabolites as well as K^+, Ca^{2+} and Na^+ ions (ischemic changes) leads to myocardial damage up to cells' death. For instance, hypoxia results in intercellular ATP concentration decline ($[ATP]_i$), after that an increase of amplitude of ATP-dependent potassium current is seen affecting K^+ concentration in intra- and extracellular space. An increase in extracellular potassium concentration ($[K^+]_o$) tends to depolarize membrane of myocyte. During ischemia different changes in calcium membrane transport and calcium-regulatory proteins binding can be seen. Such ATP-dependent processes as crossbridges cycling and ion pumps activity could be modulated by $[ATP]_i$ decline, and thus essentially affect both mechanical and electrical behaviour of cardiomyocytes. As a result of changes on ionic and molecular levels contractile function of local segments and the whole myocardium is damaged (up to contracture). From the other hand, electrophysiological characteristics of myocardium are modified (e.g. the membrane rest potential becomes less negative, the action potential shortens, the refractory period becomes longer, the velocity of conduction could slow down) [1].

Common mathematical models studying hypoxic and ischemic influence on cardiac tissue properties focus on electrophysiological changes not taking into account biomechanical processes such as kinetics of calcium-troponin C complexes, rate properties of force generated crossbridges, etc. Since electrical and mechanical phenomena are closely linked, these models could not correctly describe electrophysiological changes during hypoxia and

ischemia because they don't consider the crosstalk between mechanical factors and electrical events in cardiac cells (for instance, [2]).

Our mathematical model of cardiac muscle fiber is based on continual description of cardiac tissue. On the one hand, myocardium is assumed to be a continuum, across which electrical waves of excitation and mechanical waves of deformation spread. From the other hand, each point of the continuum is matched by cardiomyocyte, which is described in detail by a mathematical model of electromechanical activity of a single ventricular cell. The mathematical description of a single cell consists of two interrelated parts. The first block is the electrophysiological model of a guinea-pig ventricular cardiomyocyte Noble'98, another one is our novel mathematical description of biomechanical processes in cardiac muscle. The mechanical part of the model describes passive and active myocardium mechanics including both viscous and active (contractile) components in rheological scheme [3]. Currently, we propose a model of 1D continuum which could be considered as a model of a single cardiac muscle fiber. The continual model of homogeneous cardiac fiber adequately demonstrates excitation wave spreading across a muscle and its velocity, resulting in mechanical interaction between adjacent cardiomyocytes. The 1D model correctly demonstrates shortening and lengthening of different fiber segments and sarcomeres of its cardiomyocytes; calcium activation of contraction; cellular ion concentration changes responsible for action potential generation and conduction; ion channel, pumps and exchangers activity depending on mechanical and electrical characteristics of virtual myocardium.

Now we could simulate different manifestation of hypoxia and ischemia by changing parameters of the model from "normal" to "pathological".

For instance, we increased K^+ concentration outside the cardiomyocytes from normal 4 mM to 12 mM as seen in hyperkalemia resulted from ischaemic changes of a myocardium. All experiments were made for isometrical conditions for 20 mm fiber stretched by preload. We used diffusion coefficient for electro-diffusion equation corresponding to 0.5 m/s velocity of ventricular depolarization. As a result of $[K^+]_o$ increase we obtained changes in both electrical and mechanical behaviour of the muscle. The rest potential and action potential plateau level of cardiomyocytes of muscle became less negative due to shift in potassium reversal potential. Action potential duration of cardiomyocytes decreased by ~20 ms across the whole fiber during modeled hyperkalemia. Dispersion of repolarization assessed as the difference between the timing of 90% repolarization of last and first activated end of the fiber is 38 ms during normal $[K^+]_o$ *vs* 31 ms during high $[K^+]_o$. Changes in mechanical activity is seen. First of all, during hyperkalemia active force amplitude fell by 14%. At high $[K^+]_o$ virtual fiber demonstrated earlier time to peak force and faster relaxation. This changes in biomechanical phenomena are not the direct influence of $[K^+]_o$ increase as sarcomere activation is not potassium- but calcium-dependent process. But during high $[K^+]_o$ action potential shift to more positive values changes an activity of calcium potential-dependent currents, which

brings less calcium during cycle. The less $[Ca^{2+}]_i$, the less calcium-troponin C complexes form, the less active force generates.

All these results are in good concordance with experimental data.

We have described only one experimental protocol and results for ischemia and hypoxia modeling. The research program includes different kinds of protocol in which one or several parameters of the model vary at different segments of the virtual muscle to simulate hypoxic and ischemic dysfunction heterogeneously distributed across myocardium.

This work is supported by Interdisciplinary Grants for Fundamental Research of the Ural Division of the Russian Academy of Sciences (12-M-14-2009, 12-П-4-1067). NV holds a Young Scientists Grant of the Ural Division of the Russian Academy of Sciences (11-4-НП-467).

References

1. Katz, A.M., *Physiology of the heart. Second edition.* 1992, New York: Raven Press. 687.
2. Shaw, R.M. and Y. Rudy, *Electrophysiologic effects of acute myocardial ischemia: a theoretical study of altered cell excitability and action potential duration.* Cardiovasc Res, 1997. **35**(2): p. 256-72.
3. Leonid Katsnelson, Tatiana Sulman, Olga Solovyova, Vladimir Markhasin. *Role of Myocardial Viscoelasticity in Disturbances of Electrical and Mechanical Activity in Calcium Overloaded Cardiomyocytes. Mathematical modeling* // Journal of Theoretical Biology. Volume 272, Issue 1, 7 March 2011, Pages 83-95.

INVESTIGATION OF EFFECTS OF CELL-PERMEANT PEPTIDE INHIBITORS OF THE MYOSIN LIGHT CHAIN KINASE ON ADHESION AND MIGRATION OF NEUTROPHILS

E.L. Vilitkevich, A.Yu. Khapchaev, O.A. Kazakova, M.V. Sidorova, V.N. Bushuev, Zh.D. Bespalova, V.P. Shirinsky

Institute of Experimental Cardiology, Russian Cardiology Research and Production Center, Moscow, 121552, Russia

Myosin light chain kinase (MLCK) activates the major molecular motor of eukaryotic cells - myosin II, which participates in adhesion of immune cells to endothelial cells and extracellular matrix as well as in extravasation and migration of these cells to the place of inflammation. Also, myosin activity is necessary for secretion and phagocytosis which is accomplished by activated immune cells. Cell-permeating peptide inhibitors of MLCK such as L-PIK, D-PIK and their analogs can theoretically exert a modulating effect on inflammation process by means of suppressing immune cell motile reactions.

In order to test this hypothesis, we synthesized two members of PIK peptide family, PIK2 and retroenantio-PIK, and assessed their effects on human neutrophil adhesion and chemokinesis in vitro. We established that both peptides are highly resistant to degradation by peptidases present in human blood plasma but have different MLCK inhibitory activity. PIK2 is the most potent MLCK inhibitor among PIK peptides produced to date. Surprisingly,

retroenantio-PIK turned out to have much lower inhibitory activity than L-PIK and PIK2 in spite of theoretical predictions that retroenantio-peptides have similar structure to corresponding L-amino acid peptides and, therefore exhibit similar functional features.

PIK2 and retroenantio-PIK used at concentration 10 microM and 100 microM prevented the adhesion of control neutrophils as well as neutrophils challenged with fMLP and IL-8 to fibronectin-coated plastic. Both peptides increased chemokinetic activity of fMLP-stimulated neutrophils apparently through a reduction of their attachment to the substrate along with preservation of cellular pseudopodial activity. We obtained preliminary results that PIK effects on neutrophils are due to both MLCK inhibition and to the modification of a fibronectin substrate. Standard in the field small organic MLCK inhibitor ML-7 also decreased the adhesion of neutrophils to fibronectin but did not lead to the increase in chemokinetic activity of cells. In the presence of ML-7 as in control the majority of neutrophils did not move over the substrate but exhibited unaffected pseudopodial activity. Thus, peptide inhibitors of MLCK reduce adhesive properties of neutrophils activated by proinflammatory agents. These molecules demonstrate potential for developent into the novel non-steriod anti-inflammatory drugs provided they also inhibit adhesion of neutrophils to vascular endothelium and extravasation.

Supported by RFBR grant 11-04-12143-ofi-m to VPS.

ADAPTATION TO PHYSICAL ACTIVITIES IN THE COURSE OF SPORTS TRAINING

N.I. Volkov, R.V. Tambovtseva

State university *physical training, sports of youth and tourism, parkway Serenevyj 4, Moscow, 105122, Russia*

Adaptation to influence of physical activities in the course of sports training is quantitatively described by dependence "dose-effect". As an indicator of reached effect the size of a gain of trained function during supervision serves, and the dose of influence of physical activity is set by product of intensity of power expenses of exercise for the period of action of loadings in which are summarised time of performance of exercise, the general time of pauses of rest between repetitions of exercise and time of the urgent restoration connected with payment of fast fraction of an oxygen debt. The absolute values of pulse rate usually used in practice of sports for an estimation of level of power expenses of exercise, find out linear dependence on level of allocation of energy in aerobic process only in the limited area of the physical activities which are not exceeding values of critical capacity where the maximum of consumption of oxygen is reached. Into a problem of the present research entered to study possibility of use of indicators pulse the sums and power cost of exercise for carrying out of the quantitative analysis and rationing of the training and competitive loadings applied by preparation of sportsmen of high qualification. In experiment from 18 till 24 years specialising in swimming, 26 sportsmen participated in run on average distances and in high-speed skating. Examinees have executed a series of unitary exercises on veloer-

gometr with limiting duration 10, 30, 60, 120 and 360 with. Besides all sportsmen have passed tests under the program of the standard laboratory tests which performance provided their complex estimation aerobic and anaerobic working capacity in critical modes of muscular activity: In the test of "step increase of loading" for definition of size of the maximum consumption of oxygen and critical capacity, in the test of "unitary limiting work" for definition of indicators anaerobic glicolitik capacities and capacities and in the test "maximum anaerobic capacities" for an establishment of indicators alactat anaerobic productivity. Exercises were carried out without preliminary warm-up. Measurements of gas volumes and structure of exhaled air carried out with use of monitor system "Sensormedics V-max 29C". With application of the special computer program counted values O2-прихода during exercise, sizes of an oxygen debt and oxygen inquiry, and also indicators of allocation of energy in aerobic and anaerobic processes. For definition of the maintenance of dairy acid in blood used a microphotometric method Lang. Measurements of indicators of oxygen-alkaline balance of blood carried out with microanalyzer use pH and gases of blood IL-213 of firm "Instrumentation Laboratory". Continuous registration of frequency of warm reductions in an operating time and in a current of 10 minutes of restoration made with use pulse the monitor "Team Polar". Record of pulse from the monitor entered into the computer via the infra-red interface.

The conducted researches have shown that parameters total pulse exercise costs quickly accrue in short-term exercises, but after a mark of the limiting time equal to 2 minutes, sharply reduce rates of the growth. In this range of limiting time rates of a gain pulse exercise costs are defined basically by changes pulse the work sums while in a range of short-term exercises of change pulse exercise costs basically are set by changes in values pulse the restoration sums. Level changes pulse costs are set mainly by changes in pulse to the sum of restoration reflecting the contribution anaerobic of sources in the general power of work. In a wide range of change of relative capacity of exercise indicators of level of oxygen inquiry and level pulse costs show linear increase together with increase in relative capacity of exercise. The greatest influence on change of indicators of level of oxygen inquiry and pulse costs of exercises at progressing increase of relative capacity render shifts in sphere anaerobic an exchange which are reflected in values of size of an oxygen debt and pulse the restoration sums. For more exact establishment of conformity of indicators pulse costs of exercise to values of power expenses at performance of exercises of various capacity and limiting duration us has been deduced regressione dependence for these indicators. As shows the regress schedule, indicators pulse to exercise cost change in rectilinear dependence on corresponding values of power expenses of exercise. Deduced regressione dependence can be used for an establishment of level of power expenses at known values pulse exercise costs. On the basis of this dependence there is possible a strict quantitative estimation of applied training loadings, and their so strict classification with use of the established values of indicators of power expenses and pulse the sums of exercise of critical modes of muscular activity. At the analysis and comparison among themselves indica-

tors of relative capacity, speed of accumulation of dairy acid in blood and pulse to exercise cost at work performance on veloergometre and on various distances of sports swimming by freestyle it is shown that despite identical to general views of exercises the rectilinear form of this dependence, increase in level O2-затрат and relative capacity in the conditions of sports swimming it is accompanied essentially by a large increase of indicators pulse costs of exercise because of less effective work on overcoming of hydrodynamic resistance of water and the considerable losses of energy connected with high heat conductivity in the water environment. It means that at practical appendices of a described method kvantification loadings in various sports it is necessary to identify strictly values pulse costs of exercises of the rather experimentally established values of indicators O2- request or speeds of formation of dairy acid in critical modes of muscular loadings. As show the data about changes of indicators of level pulse to cost on separate distances of swimming and at performance of repeated training loadings of the corresponding volume with various intervals of rest in various ranges of loadings to modes of repeated exercises there correspond considerably smaller on size level indicators pulse to exercise cost. As results of the spent researches, indicators pulse exercise costs testify can be used for the quantitative analysis and rationing of the training and competitive loadings used by preparation of sportsmen of high qualification. However wide introduction of these indicators in realization of physiological monitoring of process of sports preparation will demand creation of a corresponding databank for different sports taking into account the general orientation of training process in the selected kind of exercises. As an individual approach example to rationing of training loadings it is possible to submit data on changes of indicators of speed of accumulation of dairy acid in blood and level total pulse to cost, in various ranges of the loadings fixed at the master of sports "C". This data considerably differs from average group values of corresponding indicators. Even more strikingly these distinctions come to light, when the levels of power production established in critical modes of muscular work at sprinters, training on short distances of swimming, and the stayers, training on long distances, will be strictly identified on values of relative capacity of carried out physical activities corresponding to them. It is easy to notice that with transition from critical modes of loadings with low values of level of power expenses to modes with higher levels of power inputs, ranges of a variation of indicators of relative capacity at highly skilled swimmers of various specialization considerably extend. It means that at an establishment of specifications for loadings of various training influence, it is necessary kvantification applied exercises on values of indicators corresponding to them pulseand power cost differentially for sportsmen of various qualification and specialisation in the selected kind of exercises.

Thus, indicators pulse costs (pulse the sums of work, restoration and total pulse cost of exercise) rather precisely reproduce the basic dependences on parametres of relative capacity and the limiting operation time, established for indicators of oxygen inquiry and power cost of exercise. Calculation pulse allows cost of exercise with sufficient accuracy kvantification training load-

ings taking into account specific features of the sportsman. At rationing of training and competitive loadings with use of indicators pulse cost of exercises should consider the individual distinctions connected with character of specialisation in a certain mode of performance of selected training loadings.

HYDROGEN PEROXIDE IS A NEW SECOND MESSENGER IN RTK SIGNALING

A.V. Vorotnikov, P.A. Tyurin-Kuzmin, A.A. Sukhova, K.M. Agaronyan, E.A. Albert, V.A. Tkachuk

Faculty of Basic Medicine, Moscow State University,
31 Lomonosov Ave, bldg. 5, Moscow 119192, Russia
E-mail: vorotnikov@fbm.msu.ru

Hydrogen peroxide has emerged as a new second messenger in signaling cascades downstream of receptor tyrosine kinases (RTK). It conforms most of the criteria for candidate second messengers established somewhat 40 years ago by Earl Sutherland who won the 1971 Nobel Prize for cAMP:

(1) Hydrogen peroxide is produced, it acts and metabolizes inside cells.
(2) It mediates physiological cell responses to receptor activation.
(3) Receptor activation alters the hydrogen peroxide levels in cells.
(4) There is a molecular mechanism of hydrogen peroxide action.
(5) There are specific targets of hydrogen peroxide in cells.

We briefly discuss these properties of hydrogen peroxide and focus on few unresolved questions as to how long hydrogen peroxide signals persist within cells, where they localize and how couple to cell responses. In this context we determined that inhibition of plasma membrane NADPH-oxidase, an enzyme responsible for superoxide radical and H_2O_2 production, completely blocks growth factor-induced cell migration and proliferation. These effects of H_2O_2 were corroborated by increased phosphorylation and prolonged activation of RTKs and Akt/PKB effector kinase that is targeted by PI3-kinase downstream of RTK activation. As PI3-kinase activation is essential for eukaryotic cell chemotaxis, we followed H_2O_2 dynamics in living cells using genetically encoded biosensor for hydrogen peroxide HyPer. We found accordingly that the receptor-induced H_2O_2 dynamics are clearly distinct from that of external H_2O_2 diffusing into cells. Blocking the receptor-dependent NADPH assembly on plasma membrane prevented the intracelular peroxide responses to RTK activation. The latter were found associated with the endosome compartment and endocytosis of active RTKs. Consistent with this mechanism, inhibition of endocytosis completely blocked the receptor-induced cell migration. Using HyPer fused to different intracellular signaling molecules we found that hydrogen peroxide is selectively produced and localizes at the leading edge of migrating cells. Moreover, firboblasts moved along the direction of intracellular H_2O_2 gradients and re-oriented accordingly whenever they altered. Thus, we conclude that hydrogen peroxide is a novel critical regulator of the receptor-dependent signaling cascades and directed migration of fibroblasts.

Supported by the RFBR grant 11-04-01519a.

INFLUENCE OF NITRIC OXIDE DONOR ON THE PROCESSES OF EXO-AND ENDOCYTOSIS OF SYNAPTIC VESICLES IN THE MOTOR NERVE ENDING MOUSE

O.V. Yakovleva, M.U. Shafigullin, G.F. Sitdikova

Biology faculty, Kazan (Volga) federal university,
18 Kremlevskay st, Kazan, 420008, Russia
a-olay@yandex.ru

Nitric oxide (II) (NO) - gaseous mediator, whose function is fully investigated in various systems of the body [Sitdikova et al., 2006]. NO is involved the regulation of many physiological and pathophysiological processes, including synaptic transmission in the central and peripheral nervous system [Garthwait, 2008]. In motor nerve terminals of amphibian it was shown that NO reduced acetylcholine release [Thomas et al., 2001, Yakovlev et al., 2005], while data on the effect of NO on the release of neurotransmitter in the neuromuscular junction of mammals are contradictory. There is evidence that NO donors and substrate synthesis of NO - L-arginine induced both the increase and the inhibition of neurotransmitter release from motor nerve endings [Barroso et al., 2007]. In the rat diaphragm muscle the expression of constitutive endothelial and neuronal isoforms of NO-synthase, producing NO, which reduced the contractile function of muscle fibers was shown [Chaubourt et al., 2002]. In the central nervous system NO is involved in induction and maintaining of short-term and long-term synaptic plasticity, both by changes in the activity of second messenger systems, regulation of ion channels, and by the direct influence on the processes of transport and exo-, endocytosis of synaptic vesicles [Garthwaite, 2008]. The recycling of synaptic vesicles are the key process in the ensuring of neurotransmitters release [Zefirov et al. 2008]. The changing of the dynamics of these processes is the basis of presynaptic forms of plasticity, and vesicle cycle disturbances observed in many psychiatric and neurological diseases [Zefirov et al., 2008]. The aim of our work was to study the effects of NO donor on the processes of exo-and endocytosis of synaptic vesicles in mouse motor nerve ending using fluorescence and electrophysiological approaches.

Experiments were carried out on the mouse diaphragm muscle preparation. Animals were anesthetized with ether before being stunned and were pithed in accordance with the European Communities Council Directive (24th November 1986; 86/609/EEC) and the Russian Federation Public Health Ministry Directive (26th December 1987). Preparations were dissected and mounted to a recording chamber with Krebs solution: NaCl - 137.0; KCl - 5.0; $CaCl_2$ - 2.2; $MgCl_2$-1.0; NaH_2PO_4-1.0; $NaHCO_3$-16.0; glucose - 11.0; (t = 20 ° C, pH 7.2-7.4). SNAP was used at a concentration of 100 μM. All reagents were from Sigma-Aldrich (St. Louis, MO, USA), except FM 1-43, which was from Molecular Probes (Eugene, OR, USA). End-plate potentials (EPPs) were intracellular recorded with glass microelectrodes. Motor nerve stimulation produced by electrical impulses with a frequency of 0.2 and 20 Hz. Fluorescent styryl dye FM 1-43 (2-3 μM) was used to estimate the rate of exo-and endocytosis of synaptic vesicles. FM 1-43 reversibly binds to presynaptic membrane

and becomes trapped within recycled synaptic vesicles during endocytosis ("loading") [Betz et al., 1992]. Massive endocytosis leads to the appearance of bright fluorescent spots at the nerve terminals, which represent the clusters of synaptic vesicles, which underwent recycling [Betz et al., 1992]. To analyse the processes of endocytosis following protocol downloads was used: neuromuscular preparation was incubated in a solution containing FM 1-43 during the high-frequency stimulation (20 Hz for 30 seconds), after which washed from the dye with Krebs solution and after 40-45 min the bright fluorescent spots in the nerve terminals were recorded. The intensity of the staining was estimated in relative units (r.u.). To analyze the processes of exocytosis of synaptic vesicles the motor nerve was previously loaded with dye by stimulation for 3 minutes with a frequency of 20 Hz, FM 1-43 presented in the solution during stimulation, and within 7 minutes after the end of stimulation [Zefirov et al., 2008]. After this the motor nerve was re-stimulated with a frequency 20 Hz and the fluorescence intensity reduction was analyzed ("unloading" the dye). The preparations were viewed with the MIKMED-2 fluorescence microscope (LOMO, St. Petersburg). Only surface terminals of muscle fibers were studied. Images were captured with the AxioCam MRV (Carl Zeiss, Germany) camera and then stored and processed with a PC. The data are presented as the mean ± S.E.M. (n = number of synapses), with statistical significance assessed by Student's t-test. P value of less than 0.05 was accepted as indicative of a statistically significant difference.

SNAP in concentration 100 mkM decreased the amplitude of EPPs by 81.9% ± 2.5% compared to control (n = 9, $p < 0.05$) during single stimulation. The amplitude and frequency of the MEPPs was not significantly changed. In the frog motor nerve endings NO donors also decreased acetylcholine release and NO-synthase inhibitors had the opposite action [Thomas et al., 2001, Yakovlev et al., 2005]. At the neuromuscular synapse of mammals L-arginine and the NO donor, 3-morpho-linosydnonimine chloride (SIN-1), decreased [^{3}H]ACh release from stimulated rat phrenic nerve terminals [Barroso et al., 2007]. Another study demonstrated that NO donors and L-arginine had no effect on nerve-evoked transmitter release in the rat isolated phrenic nerve/hemidiaphragm preparation, however, induced a significant increase of acetylcholine release after the inhibition of the adenosine A1 receptor (Nickels et al. 2007).

High-frequency stimulation (20 Hz, 3 min) under control conditions resulted in the changes in the EPCs amplitude. We first observed a short period of facilitation, which was followed by the gradual reduction of the EPCs amplitude. By 15th sec of stimulation, EPCs amplitude was reduced to 45±1.5%, and by 30th sec - to 41±3% of the initial value. After 3 min stimulation, the EPCs amplitude was reduced to 20±2% (n = 13).In the presence of SNAP (100 mkM) we observed a short period of facilitation too. By 15th sec of stimulation, EPCs amplitude was reduced to 43±1.2%, and by 30th sec - to 37±3% of the initial value. After 3 min stimulation, the EPCs amplitude was reduced to 16±2% (n = 11). Thus, in the presence of nitric oxide donor was observed more pronounced depression of the amplitudes EPPs than in the controls.

It is known that in mouse nerve ending, there are several pools of synaptic vesicles, which are differ in size, in ability to exocytosis and recycling pathways. The initial rapid decline of the amplitude of EPPs for high-frequency stimulation is associated with the depletion of ready releasable pool. Then there is a stabilization of the EPPs amplitude, which reflects the process of replacement of the ready releasable pool when the rate of its depletion and replenishment are equal, that may be provided by the mobilization of vesicles in the area of the active zone [Rizzoli, Betz, 2005] and intense process of recycling of synaptic vesicles [Zefirov et al, 2008]. The secondary, slower decline in the amplitude reflects a further reduction of ready releasable pool [Zefirov et al, 2008].

To analyze the processes of endocytosis of synaptic vesicle the fluorescent dye FM 1-43 was added to solution within 30 sec during 20 Hz stimulation. Taking into account the high rate of recycling of synaptic vesicles in mammals [Zefirov et al, 2008], this scheme allows to minimize the unloading of dye-loaded vesicles during prolong stimulation. The fluorescence of terminals in was 94 ± 3 r.u. (n = 80). Pre-exposure of neuromuscular preparation with SNAP (100 uM) for 25 minutes led to a decrease in the intensity of luminescence by 78 ± 2 r.u. (n = 75, $p < 0.05$). These data suggested that NO decrease the process of endocytosis of synaptic vesicles during high-frequency stimulation.

To reveal the dynamics of synaptic vesicle exocytosis the decrease in intensity of fluorescence of pre-loaded nerve terminals during stimulation with a frequency of 20 Hz was recorded [Zefirov et al, 2008]. In the control, the intensity of fluorescent spots at the nerve terminals decreased to 76±0,4 % by 30 sec of stimulation, by the end of the first min of stimulation - to 66 ± 4%, and by the third minute - 50 ± 3% relative to the initial level (n = 8). SNAP increased the rate of destaining of nerve terminal to 69±1 % at the 30 sec of stimulation and by the end of the first minute of stimulation of luminescence was 46 ± 4%, and by the third minute - 34 ± 4% relative to the initial level (n = 6, $p < 0.05$).

Thus, at the mouse neuromuscular junction the donor of NO decreases the transmitter release during single stimulation and accelerates the depression of EPPs amplitude during high frequency stimulation, which may be associated with a reduction of the mobilization of synaptic vesicles to release sites and with the slower process of endocytosis of synaptic vesicle. The latter hypothesis was supported by the decrease of the capture of the dye during the brief high-frequency stimulation. It was suggested that NO participates in the regulation of high-frequency depression of neurotransmitter release, slowing down the process of recycling of synaptic vesicles.

The work was supported by the grants RFBR and "Leading scientific school".

References

1. Sitdikova G.F., Zefirov A.L. Gaseous mediators in nerve system // Russ. Physiol. J *2006.* Vol. 92(7), P 872-882.

2. Garthwaite J. Concepts of neural nitric oxide-mediated transmission.// Eur J Neurosci 2008. Vol. 27(11), P 2783-2802.
3. Thomas, S., Robitaille R. J. Differential frequency-dependent regulation of transmitter release by endogenous nitric oxide at the amphibian neuromuscular synapse. //Neuroscience 2001. Vol. 21(4), P 1087-1095
4. Yakovlev A.V., Sitdikova G.F., Zefirov A.L. Intracellular presynaptic mechanisms of effects of the nitric oxide (II) in the frog neuro-muscular junction.// Neurochemistry. 2005. Vol 22(1), P 81-87.
5. Barroso A., Oliveira L., Campesatto-Mella E., Silva C. et al. L-citrulline inhibits [3H]acetylcholine release from rat motor nerve terminals by increasing adenosine outflow and activation of A1 receptors. // British J Pharmacol 2007 Vol 151, P 541–550
6. Chaubourt E., Voisin V., Fossier P., Baux G., Israel M., De La Porte S. Muscular nitric oxide synthase (muNOS) and utrophin.// J. Physiology 2002 Vol 96, P 43–52
7. Zefirov A.L., Zaharov A.M., Mukhametzyanov R.D., Petrov A.M. Features of vesicular cycle in frog motor nerve endings, and mouse.// J Evol. Physiol. Biochem. 2008 Vol 44(6), P 603-612.
8. Betz W. J., Bewick G. S. Optical analysis of synaptic vesicle recycling at the frog neuromuscular junction. *Science.* 1992. Vol 255, P 200-203
9. Rizzoli S. O., Betz W. J. 2005 Synaptic vesicle pools Nature rev. Neurosci. 6, 57-69.

CHEMOTAXIS TO AMMONIUM AND NITRATE CHLAMYDOMONAS REINHARDTII: THE ROLE OF A NOVEL ANKYRIN-REPEAT PROTEIN

Zh. M. Zalutskaya, E.V. Ermilova

Laboratory of Adaptation in Microorganisms, Biological Research Institute of St. Petersburg University, Oranienbaumskoe schosse 2, Stary Peterhof, St. Petersburg, 198504, Russia

As many motile organisms, Chlamydomonas reinhardtii requires an efficient chemotactic system that allow cells to orient and migrate towards nutrients to ensure its survival. Since nitrogen is one of the macroelements that usually are limiting in many natural environments, chemotaxis to nitrogen sources appears to be an important property in vegetative cells of the alga (Ermilova, 2009). Ammonium and nitrate play important role in the nitrogen metabolism of most cells, including C. reinhardtii. The importance of ammonium and nitrate as nitrogen sources also means that Chlamydomonas vegetative cells have evolved an additional adaptation such as chemotaxis that allows them to move towards ammonium and nitrate. How flagellar motility is regulated during chemotactic behaviour is a challenging problem.

Chlamydomonas flagella have shown that outer arm dynein and inner arm dynein have strikingly different properties, and the inner arm dynein is particular important for producing proper flagellar waveforms. Flagellar movement in *C. reinhardtii* is in part regulated by phosphorylation of a 138 kDa intermediate chain (IC138) of inner arm dynein f (also called I1). Because of the functional importance of dynein f, its molecular composition has been extensively studied. A novel protein having ankyrin repeat motifs,

FAP120, functions in the regulatory process as part of a protein complex involving IC138 (Ikeda et al., 2009). This protein was missing or decreased in the axonemes of several alleles of *bop5*, a mutant deficient in the structural gene of IC138. Chemotaxis of vegetative cells to ammonium and nitrate in the *bop5* mutant has been analyzed. We found that the different alleles of bop5 lacking IC138 completely lack chemotaxis to both attractants.

The results showed that IC138 is essential for the *Chlamydomonas* cells to display chemotactic behaviour. A weak but stoichiometric interaction between FAP120 and IC138 has been suggested. We propose that FAP120 is involved in the control of chemotactic behaviour through its the regulation of IC138. (This work was supported by RFBR (10-04-00156).

References

Ermilova E. In: Cell Movement: New Research Trends, Editors: T. Abreu and G. Silva. Nova Science Publishers.2009. pp. 313-329.

Ikeda et al. (2009) Cell Mot. Cytoskel. 66:448-456.

MORPHOLOGICAL AND FUNCTIONAL CHANGES IN SKELETAL MUSCLES UNDER POSTTRAUMATIC CONDITIONS

D.O. Zavodovskiy[1], O.M. Motuzuk[2], O.V. Dolgopolov[3], O.U. Artemenko[1]

[1]Taras Shevchenko Kyiv National University, Department of Biophysics, Volodimirska Str., 64, 01033, Kyiv, Ukraine

[2]Lesia Ukrainka Volyn National University, 43025 Lutsk, Prospect Voli 13, Lutsk , Ukraine

[3]Institute of Traumatology and Orthopedics of Medical Sciences of Ukraine, Vorovskogo Str., 01601 Kyiv, Ukraine

Acute ischemia is one of the most harmful pathological conditions of skeletal muscles. Usually acute ischemia is induced by prolonged local interstitial pressure rising above normal level termed compartment syndrome. Several studies in this field showed that compartment syndrome and ischemia damage of skeletal muscles tissue leads to significant changes in force-lengths characteristics of muscles contraction process, yet little is known about morphofunctional transforming of skeletal muscles in posttraumatic ischemia conditions. This seriously complicates understanding of the pathological bases that underlies muscle function in acute compartment syndrome and ischemia conditions.

For experimental purposes 200-300g adult rats were used. Time of the full procedure was 8 hours, from which acute ischemia comprised 5 hours. Strain gauge studies were performed using the device engineered in the Laboratory of Excitable Systems of Biology faculty, Kiev National Taras Shevchenko University.

Light microscopy method.

Material was filled in homogenized mixture of paraffin (Histomix®). Slicing was performed on MC-2 sledge microtome. Samples blocs were cut in sagittal and frontal planes, with slices thickness of 5, 10 and 15 μm. JPEG microphotographs were obtained by using the SEO digital camera and the Axioscop microscope (Carl Zeiss). Photos were processed with the Adobe Photoshop 8.0 software.

Electron microscopy method.

Prepared skeletal muscles tissue was fixed in 2% glutaraldehyde cocodilate buffered (pH 7.4) water solution with prolonged osmium tetroxide postfixation for 0.5 hour. After dehydration in acetone concentration rising gradient samples were filled in epoxy resin (SPI-CHEM, USA). Cuts were performed parallel to muscle fibers: 1.2 μm thickness cuts were used for primal orientation in sample tissue using light microscopy. Best 20 nm slices were put on copper meshes and contrasted with lead citrate and uranyl acetate. Microphotographs was obtained on PEM-100 electron microscope, acceleration voltage 75 kV.

Severe necrotic degradation and fibrosis was noticed in undergoing microscopy studies. In posttraumatic state proportion of the contraction elements and connective tissue change (photo 1).

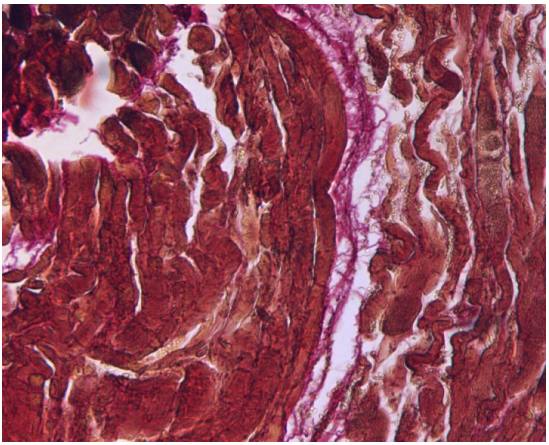

Photo 1. First steps in skeletal muscles necrotic changes and fibrosis. Lateral cut (x100 magnification).

The number of perforated muscles fibers is rising in parallel to necrosis evolution process. This results in degradation of most myocytes, at this step patients have problems with control of contraction process in damaged muscle (Photo 2).

Anoter characteristic property of necrotic muscle degradation is a large number of cell nuclei in intersticial space. It is impotent to conclude that the mechanism of pathological changes in single muscle cell can by divided in several main stages:

1) cell membrane integrity damage, perforations and projections,
2) nucleus escape into intersticial space through membrane breaks
3) myofibrils fragmentation, even if traumatized muscle is not used for work fragmentation continues
4) myofibrils substitution with collagen (Photo 3).

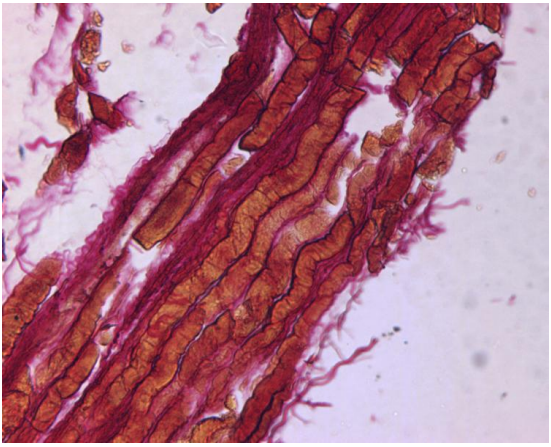

Photo 2. Ischemized muscle. Lateral cut (x100 magnification).

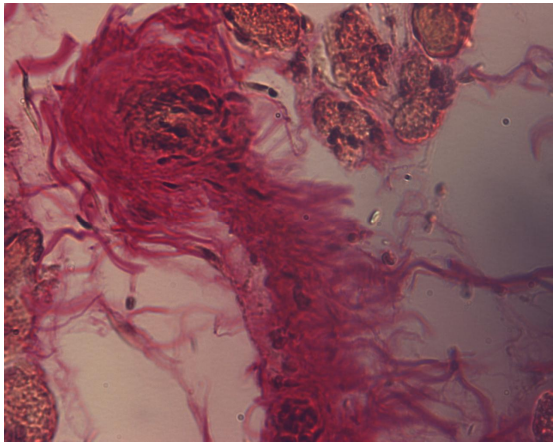

Photo 3. Ischemized muscle. Diametral cut (x100 magnification).

It is also important to note that in affected muscle fascia stays intact, connective tissue substitutes only interfascial contament. Single muscle can contain both healthy and damaged elements at the same time, but because of significant elevation of muscle stiffness it is impossible to properly regulate contraction.

Using greater magnification available in electron microscopy large obstructions have been detected at subcellular level, demonstrating changes in Z-disk organization. Z disk from the damaged myocytes lose they parallel orientation, and multiple fractures and deformations appear.

Changes in Z disk structure are thus an evidence of the degradation of thecontractile elements. This is the reason for muscle mechanical features

shift. This in our opinion may lead to future structural damage. On the other hand, breakage of Z disk parallel orientation can by provoked by functionality loses of structural proteins, such as titin.

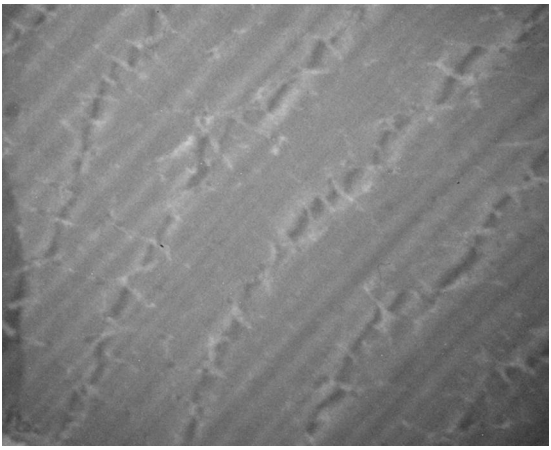

Photo 4. Pathological changes in Z disks (x6000 magnification)

These data allow as to conclude that acute muscle ischemia results in severe morphofunctional loses in single muscle filaments and with time will lead to full loss of the muscle ability to contract. Morphofunctional studies of ischemized muscles in parallel with contraction dynamics recordings can not only reveal the pathological status but also determine ischemia damage stage.

THE RENOPROTECTIVE EFFECTS OF STATINS: CASE STUDY OF MUSCLE DAMAGE RESULTING FROM EXPERIMENTAL CRASH SYNDROME

V.G. Zeleniuk, I.I. Zamorskii, and O.M. Goroshko

Bukovinian State Medical University,
2 Teatralna Sq., Chernovtsy, 58001, Ukraine

It is known that damage to striated muscle cells (rhabdomyolysis) may be caused by traumatic destructions of skeletal muscles, and also toxic effects of certain drugs. Specifically, rhabdomyolysis is closely associated with myoglobinuria that reduces renal blood flow, activates vasoconstrictive factors in kidneys, increases intratubular pressure, and also provokes the imbalances in prooxidant/antioxidant balance on the background of progressive of renal ischemia.

Rhabdomyolysis may be caused by different medicinal agents, including statins. As follows from routine medical practice, the number of cases of renal failure in the patients who received statins is low (no more than 0.3 – 0.6 cases per 1 million of prescriptions). Further, on the occasion of statin administration in permitted dosages, the reduced functions of kidneys and development of renal failure were significantly more often observed in pa-

tients who received placebo (0.8%) as compared to those treated with statins (0.5%). What is more, based on the results of 21 randomized clinical trials with statins, myopathy occurred in 5 and rhabdomyolysis in 1.6 cases per 100 thousand patients a year, respectively. The risks of rhabdomyolysis emergence depend significantly on the interactions between medicinal agents, especially, their effects on metabolism of cytochrome system and also binding with the glucuronic acid. The alternatives of statin myopathy include depletion of the mevalonic acid metabolites, reduced levels of ubiquinone level, the effects on chloride channels, high lipophilicity of certain statins and their easy penetration into myocyte membranes.

Notwithstanding a possibility for rhabdomyolysis, in has been found that statins had a positive effect on renal functions. Specifically, based on some experimental and clinical research studies its was found that on the occasions of postischemic and toxic acute renal failures (ARF) the statins were efficient to improve the renal functions of patients due to their effects on inflammatory mechanisms, the NO system, and also prooxidant and antioxidant systems.

Based on several current data available we may argue that statins do not cause direct nephrotoxic impact, and their administration, as a rule, is not a cause for any acute or chronic renal failure. Actually, as of today, we consider the cases of development of rhabdomyolysis as exceptions; however, it should be noted that the effects of statins on renal functions in myoglobinuric ARF are still not clearly understood.

Our research study was targeted at the examination of development of rhabdomyolytic ARF in rats; specifically, we initiated the appearance of ARF in its myoglobinuric form by injection of a 50% glycerol solution intramuscularly at a dose of 10 ml/kg, which is an experimental analogue of crash syndrome. Further, as a preventive measure, the statins (atorvastatin, lovastatin, and simvastatin) were introduced intragastrically at 10 mg/kg daily for 3 days before the ARF simulation. The renal functions were assessed 24 hrs after completion of ARF simulation.

As has been found in our experiments, 24 hrs after injection of 50% glycerol solution statin-treated rats featured improvements in the excretory functions of kidneys; the latter fact was demonstrated by an increased glomerular filtration rate and reduced proteinuria. Characteristically, the best results were found with lovastatin which caused an increase of diuresis, higher rates of glomerular filtration and levels of creatinine excretion.

Furthermore, we have found a number of favourable changes concerning the effects of studied medicinal agents on antioxidant/prooxidant system. To illustrate: the preventive administration of two statins (atorvastatin and simvastatin) at the 24th hour of the experiment has demonstrated considerably reduced levels of malonic dialdehyde in the tissues of kidneys and increased activity of glutathione peroxidase and higher levels of the SH-groups in blood plasma.

It should be emphasized that the renoprotective effects of statins compare well with those of the quercitin drugs (Zamorskii I.I., Goroshko O.M., 2010).

Relying on our data, we may conclude that under conditions of experimental rhabdomyolysis certain of studied statins (atorvastatin, lovastatin, and simvastatin) did not cause any aggravation of ARF. Quite the reverse, they have shown renoprotective properties, and they significantly reduced proteinuria. It is worthy of note that atorvastatin and simvastatin show rather high renoprotective properties due to improved prooxidant/antioxidant balances; alternatively, lovastatin improved the excretory function of kidneys.

REGULATION OF CENTROSOMAL PROTEINS BY PROTEIN KINASE LOSK

O.N. Zhapparova[1,2], E. N. Ryabkova[2], E. S. Nadezhdina[1,3]

[1] Belozersky Research Institute of Physico-Chemical Biology, Leninskiye Gory, 1, Moscow, 119899, Russia

[2] Lomonosov Moscow State Unversity, Biological Faculty, Leninskie Gory, 1-12, Moscow, 119991, Russia

[3] Institute of Protein Research, Institutskaya, 4 , Puschino, 142290, Russia

Microtubules in interphase cells provide tracks for intracellular transport, ensure proper interaction with the substrate and govern cell polarization and motility. Their radial organization is established as a result of nucleation and anchoring of microtubules at the centrosome. Dozens of centrosomal proteins can be divided into several groups according to their function: those that ensure structural integrity, nucleation, capping of microtubule minus-ends, attachment of microtubules to the pericentriolar material, delivery of all these proteins to the centrosome and regulation in response to signaling events. Protein kinase LOSK was shown to be required for maintenance of microtubule radial array. Here we report its direct and indirect targets among centrosomal proteins. We demonstrate that dynactin (cofactor of dynein motor protein) is phosphorylated by LOSK and targeted to the centrosome, where it is responsible for microtubule anchoring. We provide the first evidences that dynactin is involved in microtubule organization independently of its transport functions: phosphorylation by LOSK does not affect transport of other dynein-driven centrosomal proteins, but is ultimately required for microtubule anchoring. We also reveal a new target of LOSK - a structural protein of pericentriolar material called PCM-1. Its centrosomal location is disturbed in cells with inhibited LOSK. However, the observed effect is independent of dynactin phosphorylation. Overall, we assume that LOSK governs microtubule organization by a direct phosphorylation of dynactin and by modulation of PCM-1 localization. Thus, microtubule radial array results from a coordinated interplay between scaffolding, transport and regulatory proteins.

THE ROLE OF UNSATURATED FATTY ACIDS WITH 18 AND 20 CARBON ATOMS IN STABILITY OF PEA SEEDLING TO INSUFFICIENT MOISTERING

I. V. Zhigacheva, T. A. Misharina, M. B. Terenina, N. N. Krikunova, E. B. Burlakova

Emanuel Institute of Biochemical Physics, Russian Academy of Sciences, ul. Kosygina, 4, Moscow, 119334 Russia; e-mail: zhigacheva@mail.ru

One of the main ecological factors that are limiting the expansion of the areal and productivity of crops is the osmotic stress caused by drought. A water deficiency modifies cellular membranes as it affects their functions and cell metabolism [1]. Thereby, the fatty acid composition of membrane lipids alters: the relative content of saturated fatty acids increases and the content of unsaturated fatty acids decreases. The changes in the physicochemical composition of membranes result in changes in the protein–lipid ratios thereof and, consequently, in changes in the activity of membrane-bound enzymes, mainly enzymes of the electron-transport chains of mitochondria and chloroplasts [2].

It is well-known that plant growth and development regulators enhance the resistance of plants to the biotic and abiotic stresses, including a water deficiency [3]. One of such regulators is melafen – a melamine salt of bis(oxymethyl)-phosphine acid [4]. The aim of this work is to study the effect of insufficient moistening and melafen on the fatty acid composition of lipids of mitochondrial membrane of 5-day pea seedlings.

Materials and methods

Pea seeds were washed out with water with soap and an 0.01% $KMnO_4$ solution. The control group seeds were soaked in water; the experimental group, in a 3×10^{-12}M solution of melafen. The duration of soaking was 1 hour. Then the seeds were placed into closed cuvettes with periodically moistened filter paper and were allowed to stay for 24 hours. In 24 hours of stay, half of seeds of the control group and half of melafen-treated seeds were placed into open cuvettes on a dry filter paper and were allowed to stay there for two days. The second half of seeds of the control group remained in the closed cuvettes with periodically moistened filter paper for 5 days. In two days of “drought”, the seeds were placed into closed cuvettes with a periodically moistened filter paper and were allowed to stay there for the next two days. On the fifth day, mitochondria were isolated.

Isolation of mitochondria from the etiolated seedlings was performed by a differential centrifugation technique [5]. The medium for homogenizing the seedlings epicotyls contained 0.4 M sucrose, 5 mM EDTA, 20 mM KH_2PO_4 (pH 8.0), 10 mM KCl, 2 mM dithioerythtitol, and 0.1% bovine serum albumin (BSA) (free of fatty acids). The homogenate was centrifuged at 25000g for 5 min. The precipitate was resuspended in 8 ml of the washover medium and centrifuged at 3000g for 3 min. The supernatant was centrifuged at 11000g for 10 min to precipitate mitochondria. Then a precipitate was resuspended in 2 to 3 ml of the medium containing 0.4 M sucrose, 20 M

KH_2PO_4 (pH 7.4), 0.1% BSA, (free of fatty acids), and mitochondria were reprecipitated by centrifuging at 11000g for 10 min.

Respiration of mitochondria were recorded with a Clarke type oxygen electrode using an LP-7 polarograph (Czechia). The incubation medium contained 0.4 M sucrose, 20 mM HEPES-tris-buffer (pH 7.2), 5 mM KH_2PO_4, 4 mM $MgCl_2$, and 0.1% BSA (28°C).

Fatty acid methyl esters (FAME) were prepared by one-step methylation of fatty acids, without extracting the lipids [6]. The FAME were purified with a thin-layer chromatography technique on plates with silica gel. For a quantitative control of the methanolysis procedure, we used an internal standard – pentadecane. The FAME were extracted by hexane, the resulting solution was analyzed.

A quantitative analysis of FAME was performed on a "Kristall 2000M" chromatograph (Russia) equipped with a flame-ionization detector and a quartz capillary SPB–1 column (50 m × 0.32 mm, a nonpolar phase layer 0.25 μm). The analysis of FAME was performed at a programmed temperature of 120 to 270°C at a rate of 4°C/min. The temperature of the injector and the detector was 270^0C; the rate of the carrier gas – helium was 1.5 ml/min. The analysis was performed in 2 μl samples of hexane solutions. The FAME were identified by retention indices by comparing the values with the published [7] and our experimental data. The quantitative contents of FAME in the samples were calculated from the ratio of the peak area of the corresponding acid to the sum of peak areas of the identified FAME.

The Tables show average values ± standard deviations (M±m). The number of experiments: 8 (Table 1) and 10 (Table 2).

Results

Insufficient moistening resulted in an increase in the relative content of saturated fatty acids and a decrease in the content of unsaturated fatty acids in mitochondrial membrane lipids of pea seedlings. Thereby, the relative content of linoleic acid decreased by 11% and that of linolenic acid decreased by 29%. The content of stearic acid increased by 41% which resulted in decreasing the ratio of C18 unsaturated fatty acids to the stearic acid from 16.61±0.30 to 10.59±0.20 (Table 1). Similar data on the effect of the water deficiency on the fatty acid composition were obtained in mitochondrial membranes of corn, potato cell membranes, and leaf membranes of Arabidopsis thaliana and apricot [8,9]. The authors noted a considerable decrease in the content of linoleic and linolenic acids and an increase in the content of stearic acid in membranes.

Considerable changes were observed in the relative content of fatty acids having 20 carbon atoms. The pool of 20:2 ω6 is 2.7 times less; 20:1 ω 9 -1.4 times less; and 20:1 ω7- 1.3 times less. At the same time, the content of 20:0 increased more than twice. Thus, we noted decreasing the ratio of the pool of unsaturated fatty acids having 20 carbon atoms (20:1ω7+20:1 ω 9+20:2 ω6) to 20:0 from 3.8±0.03 to 1.22±0.16. The melafen treatment of seeds subjected to insufficient moistening (group IM + melafen) prevented changes in the fatty acid composition of the total lipid fraction of mitochondtrial membranes.

Table 1. Effect of insufficient moistening (IM) and melafen (MF) on the fatty acid composition of mitochondrial membranes of pea seedlings (relative %) (results of 8 experiments).

Acids	Control	Control+MF	IM	IM+MF
12:0	0.34 ± 0.03	0.34 ± 0.01	0.94 ± 0.30	0.34 ± 0.20
14:0	0.68 ± 0.03	0.64 ± 0.02	0.67 ± 0.20	0.69 ± 0.20
16:1ω7	0.36 ±0,03	0.36 ± 0.004	0.47 ± 0.13	.42 ± 0.005
16:0	18.64 ± 0.75	18.63 ± 0.05	20.74 ± 0.11	18.96 ± 0.50
17:0	0.45 ± 0.05	0.78 ± 0.12	0.66 ± 0.10	0.45 ± 0.16
18:2ω6	50.72 ± 0.80	50.74 ± 0.40	45.22 ± 0.10	50.65 ± 0.01
18:3ω3	11.3 ± 0.02	10.67 ± 0.01	9.18 ± 0.30	10.81 ± 0.09
18:1ω9	5.27 ± 0.40	5.25 ± 0.37	6.77 ± 0.20	5.22 ± 0.01
18:1ω7	0.81 ± 0.10	0.79 ± 0.24	0.61 ± 0.03	0.73 ± 0.05
18:0	4.10 ± 0.18	4.14 ± 0.32	5.83 ± 0.38	4.10 ± 0.15
20:2ω6	0.82 ± 0.01	0.80 ± 0.02	0.30 ±0.05	0.82 ± 0.10
20:1ω 9	2.22 ± 0.01	2.79 ± 0.01	1.57 ± 0.50	2.6 ± 0.30
20:1ω7	1.45 ± 0.01	1.14 ± 0.01	1.00 ± 0.10	1.52 ± 0.01
20:0	1.23 ± 0.03	1.20 ± 0.03	2.52 ± 0.20	1.30 ± 0.05
22:0	1.23 ± 0.11	1.20 ± 0.03	2.52 ± 0.20	1.04 ± 0.05
24:0	0.37 ± 0.02	0.55 ± 0.005	0.98 ± 0	0.35 ± 0.10

Table 2. Effect of insufficient moistening and melafen on the rate of oxidation of NAD-dependent substrates by mitochondria isolated from pea seedlings (results of 10 experiments).

Group	V_0	V_3	V_4	V_3/V_4	V_{FCCP}	V_{KCN}
Control	20,0±1,5	68,0±4.1	30,0±2.0	2,27±0,01	70,0±4.6	20,1±1.5
IM	12,0±2,0	48,6±3.0	40,2±1.0	1,70±0,02	48,9±3.2	18,3±2.0
IM+MF	19,8±3,0	66,0±2.4	27,5±1.3	2,40± 0,02	75,3±5.2	18,9±1.2

The incubation medium described in methods. Additives: malate + glutamate (10 mM), ADP (200 μM), FCCP (0.5 μM).

Changes in physicochemical properties of mitochondrial membranes may lead to changes in the lipid–protein interactions and, consequently, in the activity of membrane-bound enzymes, in particular enzymes of the mitochondrial respiratory chain: the rates of oxidation of malate+glutamate in the presence of ADP or FCCP were 29-30% lower than the control values (Table 2). Thus, the respiratory control rates (RCR) decreased. The melafen treatment of seeds prevented changes in the efficiency of oxidative phosphorylation and in the rates of oxidation of NAD-dependent substrates in the presence of ADP or FCCP.

Based on the data obtained, it is safe to suppose that increasing the content of unsaturated fatty acids, in particular C_{18} and C_{20} acids, in plant tissue membranes results in enhancement of the resistance of plants to insufficient moistening. Indeed, there was observed a correlation between the unsaturated coefficient of C_{18} fatty acids in mitochondrial membranes ($\sum$unsaturated C_{18} fatty acids/$C_{18:0}$) and the rates of oxidation of NAD-

dependent substrates in the presence of ADP or FCCP, the coefficient of correlation r =0.76489; an even higher correlation was observed for C_{20} fatty acids (r =0.96370). Melafen ehhances the content of unsaturated fatty acids having 18 and 20 carbon atoms and restores thereby the mitochondria energy disturbed by a temporary water deficiency. This is particularly important for germinating seeds, which require energy resources.

References

1. Boyer J.S. Science. 1982. V. 218. P. 443-448.
2 .Owen K. Atkin and David Macherel. Annals of Botany 2009 , V.103 .(4), 581-597
3. Zhirmunskaya N.M., Shapovalov A.A. Physiological aspects of using growth regulators to enhance the drought resistance of plants// Agrokhimiya. 1987(6), P. 5. 102-119
4. Zhigacheva I.V., Burlakova E.B., Shugaev A.G., Generozova I.P., Fattakhov S.G., Konovalov A.I. Organophosphorous plant growth regulator: resistance of plant and animal cells to stresses //Biological membranes 2008, 25, No. 3, 183-189.
5. Popov V.N., Ruge E.K., Starkov A.A. Biokhimiya 2003, Vol. 68 (7), P. 910-916.
6. J. Wang, H. Sunwoo, G. Cherian, I.S. Sim. Poultary science 2000, 8.V.79, P. 1168-1171.
7. R.V. Golovina, T.E. Kuzmenko Chromatog. 1977, 10 , 9, 545-546
8. M Olsson,, K. Nilsson, C. Liljenberg, G. A. F. Hendry. Physiologia Plantarum 1996, V 96 (4), P. 577-584
9. Selote DS, Bharti S, Khanna-Chopra R/ Biochem Biophys Res Commun. 2004, V. 314(3), P.724-729.

LOCALIZATION AND EXPRESSION OF CD97 IN HUMAN SLOW AND FAST MUSCLE FIBERS

T.Y. Zyryanova[1], G. Aust[2]

[1]Saint-Petersburg State University, 7/9 Universitetskaya nab., St.- Petersburg, 199034, Russia

[2]Leipzig University, 20 Liebigstrasse, Leipzig, 04103, Germany

CD97 belongs to a class B G-protein coupled receptor (GPCR) family with an unusual large N-terminal extracellular domain and a seven-transmembrane span (LNB-TM7) *(1)*. CD97 was firstly described as the founding member of a small subfamily, the EGF-TM7 receptors in 1994 *(2)*. This family is characterized by a variable number of N-terminally located EGF-domains, a long extracellular stalk, the TM7 and a short intracellular region. The proteins are self-cleaved in an α-chain and β-chain non-covalently bound at the cell surface *(3)*. Alternative splicing of the single mRNA results in different isoforms that contain in the case of CD97 either three, four or five EGF-domains *(4)*.

The restricted expression of most EGF-TM7 family members to leukocytes and the hybrid structure suggest dual adhesion and signaling function of these molecules within the immune system. The exception is CD97 shown to be present on various normal epithelial cells and found on several carci-

nomas *(5)*. Later CD97 was detected at smooth muscle cells of the lung, gastrointestinal tract, urinary bladder, uterus and veins but not arteries *(6)*.

Very recently, we detected CD97 to be present in human skeletal muscle. CD97 immunohistology revealed different staining intensities in single muscle fibers. *Cd97* knock-out mice showed i) a dilated sarcoplasmatic reticulum and changed triad structure in muscle cells and ii) a decreased running capacity in physiological tests. The physiologic function of CD97 in muscle cells is still unknown.

The aim of the study was to investigate the localization and expression of CD97 in human slow and fast-twitch fibers.

Materials and Methods

This research complied with the ethics guidelines of the University of Leipzig. We obtained ethics approval from the Ethics Committee of the Medical Faculty of the University of Leipzig (No111-2004) to analyze human muscle samples and written consent from all participants involved in this study. Biopsies of the *m. spinalis* from 6 patients were taken at the level L1 of lumbar spine during surgery. Biopsies of *m. vastus medialis* and were obtained from 7 patients after an *in vitro* contracture test to diagnose susceptibility to malignant hyperthermia. Samples of healthy *m. semitendinosus* were taken during reconstruction operation of *anterior cruciate ligament* (ACL) rupture by semitendinosus tendon autograft.

Fluorescence immunostaining. To localize CD97 in the muscle cryostat longitudinal and transversal sections were co-stained with antibodies to CD97 ($CD97^{stalk}$ 3D7) and desmin (clone D33), α-actinin (clone EA-53), ryanodine receptor type 1 (RyR1, clone C334), sarco(endo)plasmatic reticulum Ca^{2+} ATPase 2 (SERCA-1, clone VE121G9; SERCA-2, clone IID8) or dihydropyridine receptor (DHPR, clone 1A), myomesin (a kind gift from R. Schoenauer, Institute of Cell Biology, ETH Honeggerberg, Zürich).

To calculate the percentage of slow and fast-twitch fibers strongly expressing CD97 cryostat transversal sections were stained with antibodies to the myosin heavy chain (fast type, MHCfast; slow type, MHCslow) and ($CD97^{stalk}$ Mem-180). Sections were analyzed by laser-scanning microscopy (LSM5 Pascal, Carl Zeiss Jena, Germany). In the same areas of the each muscle section 1000 fibers of each muscle were analyzed.

Statistics. Unpaired Students's *t* test was applied. All statistical computations were performed using GraphPad Prism version 5.0 (San Diego, CA). *P* values less than 5% were considered as significant.

Results

CD97 is localized within the SR.

In cross sections we observed with the $CD97^{stalk}$ 3D7 mab a polygonal, honeycomb-like staining pattern throughout the myofiber which is typical for proteins within the SR or T-tubule. Double immunolabelling revealed co-localization of $CD97^{stalk}$ 3D7 and SERCA-2.

Longitutinal skeletal muscle sections labeled with CD97 antibodies revealed a striated pattern. CD97 did not show a dotted close double band

typical for RyR and DHPR staining thus excluding CD97 localization in T-tubules or in terminal cisternae of the SR. This result was confirmed by double labeling, CD97 was not co-localized with these receptors.

Instead, we found a good correlation of CD97 3D7 staining with proteins localized in or projecting to the Z-line as α-actinin, desmin, and Serca-2 but exclusion to myomesin, a constituent of the M-band. Our results confirmed the localization of CD97 in the SR which has been suggested from its transversal staining pattern.

Expression of CD97 in slow and fast-twitch fibers

Examination of transverse skeletal muscle sections labeled for CD97 showed that all fibers were CD97 positive. However, individual skeletal fibers displayed different intracellular CD97 staining intensities in both muscles. Two fiber types were discriminated: CD97 positive and strongly positive fibers.

MHCslow positive fibers showed stronger intracellular CD97 mem180 staining in both muscles compared to MHCfast fibers. Careful examination of the *m. vastus medialis* revealed that 95.5 ± 2.4 % of CD97 mem180 strongly positive fibers were slow-twitch, and 3.8 ± 1.9 % were fast-twitch fibers. In the *m. spinalis* 90.7 ± 4.4% of the CD97 mem180 strongly positive fibers were MHCslow positive and 8.3 ± 4.1 % were MHCfast positive. The results obtained with the CD97 3D7 antibody showed the same distribution of CD97 within the fibers.

In spine muscle 81.5 ± 8.6% of the CD97 3D7 strongly positive fibers were slow-twitch and 16.5 ± 8.1 % fast-twitch fibers. In *m. vastus medialis* the percentage of CD97 3D7 strongly positive slow fibers was 78.2 ± 2.0 % in slow twitch and 21.4 ± 1.7 % in fast twitch

In summary, our results showed that CD97 is localized within the SR. Especially the ultrastructural data suggest an essential but yet unknown role of CD97 in the maintenance of SR or T-tubule architecture, in EC-coupling or in ion transport regulation during contraction.

Furthermore, we showed that CD97 is expressed in both slow and fast-twitch fibers. Nearly all slow-twich fibers showed higher expression of CD97 compared to fast twitch fibers. This result did not depend on the muscle as well as the CD97 antibody used for staining.

The small percentage of CD97 strongly positive fast twitch fibers raises the question about the metabolic and physiologic subtype of these fibers.

References

1. J. Hamann *et al*., *Int. Immunol.* 12, 439 (2000).
2. W. Eichler, G. Aust, D. Hamann, *Scand. J. Immunol.* 39, 111 (1994).
3. M. J. Kwakkenbos *et al*., *Immunogenetics.* 55, 655 (2004).
4. J. X. Gray *et al., J. Immunol.* 157, 5438 (1996).
5. G. Aust *et al., Cancer Res.* 57, 1798 (1997).
6. G. Aust *et al., Cell Tissue Res.* 323, 1 (2006).

INDEX OF AUTHORS

TABLE OF CONTENTS

Научное издание

ООО «Фотон-век»
ИНН 5039008988
г. Пущино Московской обл.
тел. (4967)739432
beornot@rambler.ru

Подписано в печать 25.04.2012
Формат 60×90/16
Усл. печ. л. 18,4. Тираж 160 экз.